ADJOINT SENSITIVITY ANALYSIS OF THE TWO-PHASE TWO-FLUID MODEL BASED ON AN APPROXIMATE RIEMANN SOLVER

BY

GUOJUN HU

DISSERTATION

Submitted in partial fulfillment of the requirements
for the degree of Doctor of Philosophy in Nuclear, Plasma, and Radiological Engineering
in the Graduate College of the
University of Illinois at Urbana-Champaign, 2018

Urbana, Illinois

Doctoral Committee:

Associate Professor Tomasz Kozlowski, Chair
Assistant Professor Caleb Brooks
Dr. Brian F. Jewett
Professor James F. Stubbins
Professor Rizwan Uddin

Abstract

A new shock-capturing upwind numerical solver (i.e. forward solver) and an adjoint sensitivity analysis framework for the two-phase two-fluid model are developed and verified. Both the numerical solver and the adjoint sensitivity analysis framework are based on an analytical analysis of the two-phase two-fluid model.

The challenge (due to the arbitrary equation of state) in the analytical analysis of the two-phase system is overcome by introducing several new auxiliary variables. With the help of new auxiliary variables and thermodynamic transformations, the Jacobian matrix of the system can be simplified to a well-structured form, which is convenient for an analytical analysis. Approximate eigenvalues and eigenvectors are obtained using the difference in the thermodynamic properties of liquid and gas phases. The approximate eigenvalues and eigenvectors are essential for constructing the upwind numerical solver, because they provide correct upwind information of the system. Both the numerical solver and the adjoint sensitivity analysis framework are verified with several numerical tests.

For the forward tests, the results show that the solver is stable, accurate, and robust. Results from the new solver are in a very good agreement with either analytical solution or measurement data. The grid convergence study shows that the solver using a Roe-type numerical flux is first-order accurate in space and the solver using a WENO-type numerical flux is at least second-order accurate in space. For the adjoint tests, the results show that the adjoint sensitivity analysis framework works well for both steady-state problems and time-dependent problems. The adjoint sensitivities (with respect to initial conditions, boundary conditions, or physical model parameters) are verified by either analytical sensitivities or forward sensitivities.

A critical and unique feature of the new solver is that the formulation does not depend on the form of equation of state, which ensures that the solver is applicable to practical two-phase flow problems, such as a boiling pipe. The successful application of the solver to a boiling pipe is very encouraging, as it opens up the possibility of applying many other advanced methods to two-phase flow problems.

To my dear father and mother.

Acknowledgments

I want to thank Prof. Tomasz Kozlowski for making this thesis possible. In the spring of 2014, Prof. Kozlowski took me into his group and started to guide me into a research world. Since then, Prof. Kozlowski has been a wonderful mentor to me, both in research projects and this thesis. Prof. Kozlowski recommended working on developing a new two-phase flow solver and performing adjoint sensitivity analysis to two-phase systems. Without this recommendation, this thesis would not be possible.

I want to thank Prof. Caleb Brooks, Prof. James Stubbins, Prof. Rizwan Uddin, and Dr. Brian F. Jewett for being the committee members and guiding me in developing this thesis. Prof. Caleb Brooks was the instructor of one important course about the two-phase flow model. This course helped me a lot in understanding the two-phase flow and was one important basis of this thesis. Prof. Caleb Brooks is also one of the committee of this thesis and provides a lot of important comments and suggestion. Dr. Brian F. Jewett was the instructor of another important course about numerical fluid dynamics, from which I learned a lot on how to implement the mathematical derivations to a real code.

I want to thank Dr. William Wieselquist from Oak Ridge National Laboratory, Dr. Ling Zou, Dr. Haihua Zhao, and Dr. Hongbin Zhang from Idaho National Laboratory. Dr. Wieselquist was my mentor in the summer of 2015 when I was a summer intern at Oak Ridge National Laboratory. This internship is the starting point of obtaining professional programming experience. Dr. Ling Zou, Dr. Haihua Zhao, and Dr. Hongbin Zhang were my mentors in the summer of 2016 and 2017 when I was a summer intern at Idaho National Laboratory. From them, I learned a lot on the closure correlations for the two-phase two-fluid model. Without the help of Dr. Ling Zou on the development of a system code, this thesis would not be in the current status. I also want to thank the entire ARTS group at NPRE for their friendship and help: Dr. Rijan Shrestha, Dr. Rabie Abu Saleem, Dr. Xu Wu, Travis Mui, Guanfeng Gao, Chen Wang, Katarzyna Borowies, Majdi Radaideh, Daniel O' Grady, and many others. Special thanks go to all the supporting staffs, Becky Meline, Margaret Krause, Barbara Russel, and many others for the their help during the entire time in NPRE.

Table of Contents

List of Tables

List of Figures

List of Symbols

Scalars

α	Volume fraction.
p	Pressure.
u	One-dimensional velocity.
ρ, v	Density and specific volume.
T	Temperature.
$e, h, s, \mathfrak{g}$	Specific internal energy, enthalpy, entropy, and Gibbs free energy.
E	Specific total energy, including specific internal energy and kinetic energy.
H	Specific total enthalpy, including specific enthalpy and kinetic energy. H also represents the heat transfer coefficient.
a	Adiabatic speed of sound of water and steam. a also denotes the volumetric interfacial area concentration or the surface area in the closure correlations.
γ	Gamma coefficient or the ratio of compressibility in an isenthalpic process to the compressibility in an isentropic process.
C_p, μ, σ	Specific isobaric heat capacity, viscosity, and surface tension of water and steam.
k	Thermal conductivity of water and steam. k also denotes the wave number in the dispersion analysis. When used in the subscript, k denotes the k-phase of water and steam mixture.
Δt	Time step
Δx	Mesh size
f	Wall friction or interfacial friction. f also denotes the flux component in constructing the forward solver.
Q	Wall heat flux or interfacial heat flux.
G	Total mass flux.
Γ	Interfacial mass transfer rate.
D	Hydraulic diameter.
g	Gravitational constant.
λ	Eigenvalue or wave speed.

β	Auxiliary variables representing the coupling of the two phases.
δ_p	Correction to the interfacial averaged pressure for the hyperbolicity regularization
C_{vm}	Virtual mass for the hyperbolicity regulation.
R	Response function of interest.
q	Quantity of interest. q also denotes the heat flux in the closure correlations.
M	Phase indicator function.

Vectors

$\mathbf{W}$	Vector of primitive (physical) variables.
$\mathbf{U}$	Vector of conservative variables.
$\mathbf{F}$	Vector of fluxes.
$\mathbf{S}$	Vector of source terms.
$\mathbf{P}$	Vector of interfacial averaged pressure terms.
$\mathbf{K}$	Eigenvector or characteristic wave.
$\boldsymbol{\phi}$	Vector of Lagrange multipliers or adjoint solution. $\boldsymbol{\phi}$ also denotes the perturbation in the conservative variables in the dispersion analysis.
$\boldsymbol{\omega}$	Vector of parameters of interest for the sensitivity analysis.
$\mathbf{Q}$	Vector of source terms in the adjoint equation.
$\mathbf{v}$	Vector of 3D velocity field
$\mathbf{n}$	Normal vector of interface
$\mathbf{M}$	Vector of generalized drag force
$\mathbf{q}$	Vector of heat flux

Tensors and Matrices

$\mathbb{J}$	Efflux tensor.
$\mathbb{T}$	Stress tensor.
$\mathbb{A}$	Jacobian matrix. $\mathbb{A}$ also denotes the coefficient matrix in the adjoint equation.
$\mathbb{D}$	Eigenvalue matrix. The diagonal components of the eigenvalue matrix are the eigenvalues of the related Jacobian matrix.
$\mathbb{K}$	Eigenvector matrix. The columns of the eigenvector matrix are the eigenvectors of the related Jacobian matrix.

Subscripts

k	$k = l, g$ denotes the liquid-phase or gas-phase of the mixture.
w	Variables related to the wall transfer mechanism.

i	Variables relate to the the interfacial average. In the dispersion analysis, i also denotes the imaginary unit of a complex variables. In the spatial discretization, i also denotes the index of the cell center.
m	Index of the component in a vector or the index number in a summation. m also denotes the properties of the two-phase mixture.
c, nc	Variables related to the conservative or non-conservative part of the system.
x	Variables related to the x-direction partial directives.
t	Variables related to the time directives.
iso	Variables related to the isothermal system.

Superscripts

n	The n-th time step.
T	The transpose operator.
$+, -$	Variables related to the positive or negative direction.
ss	Values at steady-state.

Operators

$\overline{F}$	Time average of function F.
$\overline{\overline{F}}$	Phase average of function F.
$\widehat{F}$	Mass weighted average of function F.
$\langle F \rangle$	Area average of function F.
$\langle\langle F \rangle\rangle$	Void fraction weighted area average of function F.
$\langle F \rangle_x$	Integration in space of function F.
$\langle F \rangle_t$	Integration in time of function F.
$\langle F \rangle_{xt}$	Double integration in space and time of function F.

Chapter 1

INTRODUCTION

Two-phase flows are of great importance in reactor safety analysis. Development of appropriate mathematical models for two-phase flows is complicated because of the complex nature of two-phase flows, which originates from the existence of moving interfaces and significant discontinuities (in fluid properties) near the interface [1]. It is noted that many of two-phase systems have a common geometrical structure. Two-phase flows can be classified into different flow regimes according to the structure of interface, such as separated flow, mixed flow, and dispersed flow [1]. Mathematical models for two-phase flows depend on the flow regimes. For example, considering the flow of two phases, the velocity of one phase may be different from the other. For some systems, the liquid and vapor have comparable velocities; while in other systems, the liquid and vapor are completely separated. Various mathematical models have been derived, some with one momentum equation for the mixture while others with a separate momentum equation for each phase. In the mixture model, one momentum equation is used. In contrast, the two-fluid model treats the two phases separately, requiring two sets of governing equations. The more general model is the two-phase two-fluid model, which is proposed by averaging local field equations for each phase [1]. For transient two-phase flows, the two-fluid model offers a more general and detailed description than the mixture model. The focus of this thesis is the development of a new numerical solver and an adjoint sensitivity analysis framework for the two-phase two-fluid model.

This chapter gives a brief introduction to the motivation for developing a new numerical solver and an adjoint sensitivity analysis framework for the two-phase two-fluid model.

1.1 Existing numerical solvers

Several two-phase flow system codes, such as RELAP [2] and TRAC [3], were developed to simulate the two-phase flow problems in a nuclear power plant. The TRAC/RELAP Advanced Computational Engine (TRACE) [4] is the latest in a series of advanced systems codes developed by the U.S. Nuclear Regulatory Commission (NRC). It combines the capabilities of the NRC's four main system codes (TRAC-P, TRAC-B,

RELAP5, and RAMONA) into one modernized computational tool. Similarly, the RELAP5 series of codes has been developed at the Idaho National Laboratory (INL) under the sponsorship of the U.S. Department of Energy and U.S. NRC. RELAP5-3D [5] is the latest in the RELAP5 series of codes. TRACE and RELAP5-3D have a lot in common. Both codes use the same two-phase two-fluid model. Both codes employ the semi-implicit-based numerical methods to solve the partial differential equations with the Finite Volume Method (FVM). TRACE employs the so-called Stability Enhancing Two-Step (SETS) method [6], which avoids the Courant stability limit on the time step but has relatively high numerical diffusion. RELAP5-3D employs the so-called Semi-Implicit and Nearly-Implicit scheme. Semi-Implicit method is limited by the material Courant limit; while the Nearly-Implicit method is not limited by the Courant limit.

In these codes, the basic numerical method is the the first order donor cell differencing method on a staggered grid. Numerical dissipation and various degree of implicitness are necessary to stabilize the numerical method. Recently, there is a trend to solve the two-phase two-fluid model with a fully implicit method with the help of a Jacobian Free Newton Krylov (JFNK) solver. Abu Saleem [7] and Zou [8, 9] obtained encouraging success with this method.

Most of previous methods use a staggered grid. For numerical methods based on a staggered grid, scalar quantities (e.g. void fraction and pressure) are calculated at cell centers while vector quantities (e.g. velocity) are calculated at the cell boundaries. Because of this difference, the mass and energy equations are discretized differently than the momentum equations, which makes the notations for the discretized equations very complicated. Solving the two-phase two-fluid model with these methods is already very complicated; trying to develop an adjoint sensitivity analysis framework based on these methods is even more challenging. This is the main motivation for developing a new numerical solver, which is mathematically consistent, algebraically simpler, and numerically more accurate and stable than the existing solvers.

1.2 Adjoint sensitivity analysis

Analysis of uncertainty is critical for code Verification and Validation (V&V) [10]. V&V is usually defined as a primary means to assess the accuracy and reliability of simulations. Verification is separated into two different types: code verification and solution verification. The code verification assesses the reliability of software code, while the solution verification deals with the numerical accuracy of the computational model. In comparison, validation assesses the physical modeling accuracy of a computational simulation by comparing with the experimental data. Conceptually, verification is the process that ensures the physical models are correctly solved by the computer code, while validation is the process that ensures the physical

models are suitable for predicting desired phenomena.

The reliability of predictions of the system codes is closely related to the validation of their physical models. For example, the accuracy of void fraction prediction in a Boiling Water Reactor (BWR) is very important, because void fraction has a significant effect on the reactivity, pressure drop, critical heat flux, and many other phenomena which are relevant for reactor safety. The uncertainties of code predictions should be provided, which require an uncertainty analysis by propagating the input uncertainties to the output predictions.

An important step in uncertainty analysis is the sensitivity analysis of the response of interest to various uncertain input parameters. Common approach to calculate the sensitivity includes regression-based methods and variance-based methods [11, 12]. However, these methods require solving the system of interest (e.g. two-phase flow) multiple times, sometimes 100s of times, which is expensive in terms of computational time.

An alternative approach to compute sensitivities is the adjoint method. The use of adjoint method for computing sensitivities came up in nuclear science in the 1940s [13]. Later, the adjoint method was applied to fluid flow for the optimization of a wing design [14]. The cost of solving an adjoint equation is comparable to the cost of solving the original (forward) equation. However, once the adjoint solution is available, the sensitivity to an arbitrary number of input parameters can be calculated with little effort, which offers a powerful tool for calculating sensitivities to a large number of uncertain input parameters. However, to the author's best knowledge, successful application of adjoint sensitivity analysis to nuclear thermal-hydraulics simulations is rare, which is the main motivation for developing an adjoint sensitivity analysis framework in this thesis.

1.3 Overview of Organization

The organization of this thesis is as follows.

Chapter 2 presents a brief introduction to the basic two-phase two-fluid model. The first-half of this chapter presents the derivation of the one-dimensional two-phase two-fluid model. The second-half of this chapter introduces the models and closure correlations.

Chapter 3 presents the formulations for dealing with the arbitrary Equation Of State (EOS). Starting from the general relations between thermodynamic properties, new auxiliary variables are introduced to simplify the analysis. The International Association for the Properties of Water and Steam industrial formulation (IAPWS-IF97) [15], which is used to obtain the properties of water and steam, is implemented and verified. This chapter is essential for performing the analytic analysis to the two-phase two-fluid model

and for applying the new numerical solver to practical two-phase flow problems.

Chapter 4 presents the analytical analysis to the two-phase two-fluid model, including a characteristic analysis and a dispersion analysis. The characteristic analysis provides the essential basis for constructing the numerical solver.

Chapter 5 presents the details of constructing the numerical solver. The solver is tested with several benchmark problems, including a periodic pipe problem, a shock-tube problem, and a boiling pipe problem.

Chapter 6 presents the details of formulating the adjoint sensitivity analysis framework for the two-phase two-fluid model. The framework is tested with two problems: a time-dependent periodic problem and a steady-state boiling pipe problem.

Chapter 7 summarizes the research and recommends several possible improvements and extensions to the current work.

Chapter 2

TWO-PHASE TWO-FLUID MODEL

In this chapter, the details of the two-phase two-fluid governing equation are given. Starting from the general balance equation, the general three-dimensional (3D) two-phase two-fluid model is derived by performing a time average to the general balance equation; then, the 3D two-phase two-fluid model is simplified for one-dimensional (1D) problems by performing an area average in the transverse direction.

2.1 Introduction

The difficulty in modeling of the two-phase flow arises from the existence of moving and deforming interfaces between the two phases [1, 7]. Fluid properties near these interfaces are discontinuous and flow fields are complicated. The conceptual model for a single-phase flow is well established in terms of field equations describing the conservation laws of mass, momentum, and energy. The liquid and gas phase in a two-phase flow could be seen as single-phase continuum separated by the interface. The field equations for the single-phase flow could be applied to the liquid and gas continuum, which is the so-called local instant formulation. However, for most two-phase flow problems where many interfaces exist, the local instant formulation is not a realistic approach. A macroscopic formulation based on a proper averaging is necessary. In the following section, the derivation of the macroscopic formulation is presented. Note that the derivation and justification of the two-phase two-fluid model is not the focus of this thesis. Most of the concept and derivation given in **Sec. 2.2** are generalized from Ishii's original derivations [1].

2.2 Three-dimensional two-phase two-fluid model

2.2.1 General phasic balance equation

The general balance equation for phase k can be written by introducing the fluid density ρ_k, the efflux $\mathbb{J}_k$, and the body source ϕ_k of any quantity ψ_k defined for a unit mass. The general balance equation is

$$\frac{\partial \rho_k \psi_k}{\partial t} + \nabla \cdot (\rho_k \psi_k \mathbf{v}_k) = \nabla \cdot \mathbb{J}_k + \rho_k \phi_k \tag{2.1}$$

where the first term is the rate of the quantity (ψ_k), the second term is the rate of convection. The right-hand side terms represent the surface flux and the volume source. The conservation equations for phasic mass, momentum, and energy are

$$\frac{\partial \rho_k}{\partial t} + \nabla \cdot \big(\rho_k \mathbf{v}_k\big) = 0 \tag{2.2a}$$

$$\frac{\partial \rho_k \mathbf{v}_k}{\partial t} + \nabla \cdot \big(\rho_k \mathbf{v}_k \mathbf{v}_k\big) = -\nabla p_k + \nabla \cdot \mathbb{T}_k + \rho_k \mathbf{g} \tag{2.2b}$$

$$\frac{\partial \rho_k E_k}{\partial t} + \nabla \cdot \big(\rho_k E_k \mathbf{v}_k\big) = -\nabla \cdot \mathbf{q}_k - \nabla \cdot \big(p_k \mathbf{v}_k\big) + \nabla \cdot \big(\mathbb{T}_k \cdot \mathbf{v}_k\big) + \rho_k \mathbf{g} \cdot \mathbf{v}_k + \dot{q}_k \tag{2.2c}$$

where E_k is the specific total energy, $\mathbb{T}_k$ is the viscous stress tensor, $\mathbf{q}_k$ is the heat flux, and $\dot{q}_k$ is the body heating. In addition to the specific total energy (E_k), the specific internal energy (e_k), specific enthalpy (h_k), and specific total enthalpy (H_k) are also used in the following equations. These variables are related by

$$E_k \equiv e_k + \frac{\mathbf{v}_k^2}{2} \tag{2.3a}$$

$$H_k \equiv h_k + \frac{\mathbf{v}_k^2}{2} = e_k + \frac{p_k}{\rho_k} + \frac{\mathbf{v}_k^2}{2} \tag{2.3b}$$

2.2.2 Time average and weighted average

The general two-phase two-fluid field equations are obtained by performing a time average to the phasic balance law, Eq. (2.1). Throughout the derivations, the following definitions will be used.

Definition 2.1. The state density functions of the k-phase (M_k) and the interface (M_s) are defines as

$$M_k\big(\mathbf{x}, t\big) \equiv 1, M_s\big(\mathbf{x}, t\big) \equiv 0, \quad \text{If a point is occupied by the } k\text{-phase} \tag{2.4a}$$

$$M_k\big(\mathbf{x}, t\big) \equiv 0, M_s\big(\mathbf{x}, t\big) \equiv 1, \quad \text{If a point is occupied by the interface} \tag{2.4b}$$

Definition 2.2. A general function of the k-phase (F_k) at the averaging point ($\mathbf{x}_0$) is defined as

$$F_k(\mathbf{x}_0, t_0) \equiv M_k(\mathbf{x}_0, t_0) F \tag{2.5}$$

Definition 2.3. The Eulerian time average ($\overline{F}$) of the general function is defined as

$$\overline{F}(\mathbf{x}_0, t_0) \equiv \lim_{\delta \to 0} \frac{1}{\Delta t} \int_{\Delta t} F(\mathbf{x}_0, t) \mathrm{d}t \tag{2.6}$$

where δ is the thickness of the interface and Δt is a fixed time interval. As stated by Ishii: "Δt is taken to be large enough to smooth out the local variations of the properties yet small compared to the macroscopic time constant of the unsteadiness of the bulk flow" [1].

Definition 2.4. The local void fraction of k-phase (α_k) is defined as the time average of the phasic state density function

$$\alpha_k \equiv \lim_{\delta \to 0} \frac{1}{\Delta t} \int_{\Delta t} M_k(\mathbf{x}_0, t) \mathrm{d}t = \frac{\Delta t_k}{\Delta t} \tag{2.7}$$

where Δt_k is the time when the position is occupied by k-phase during the integration time interval (Δt). Physically, α_k represents a probability of finding k-phase in point ($\mathbf{x}_0$).

Definition 2.5. The phase average ($\overline{\overline{F}}_k$) of the general function is defined as

$$\overline{\overline{F}}_k(\mathbf{x}_0, t_0) \equiv \lim_{\delta \to 0} \frac{1}{\Delta t_k} \int_{\Delta t_k} F_k(\mathbf{x}_0, t) \mathrm{d}t = \frac{\Delta t}{\Delta t_k} \lim_{\delta \to 0} \frac{1}{\Delta t} \int_{\Delta t} F_k(\mathbf{x}_0, t_0) \mathrm{d}t = \frac{\overline{F}_k}{\alpha_k} \tag{2.8}$$

Definition 2.6. The mass weighted average ($\widehat{\psi}_k$) of a quantity is defined as

$$\widehat{\psi}_k \equiv \frac{\overline{\rho_k \psi_k}}{\overline{\rho}_k} = \frac{\overline{\overline{\rho_k \psi_k}}}{\overline{\overline{\rho}}_k} \tag{2.9}$$

Because of the difference between the time average of derivatives and the derivatives of time average, the time average of a quantity will produce several terms that represent the summation at the interface, i.e.

$$\overline{\frac{\partial F_k}{\partial t}} = \frac{\partial \overline{F}_k}{\partial t_0} - \frac{1}{\Delta t} \sum_j \frac{1}{v_{ni}} F_k \mathbf{n}_k \cdot \mathbf{v}_i \tag{2.10a}$$

$$\overline{\nabla F_k} = \nabla \overline{F}_k + \frac{1}{\Delta t} \sum_j \frac{1}{v_{ni}} \mathbf{n}_k F_k \tag{2.10b}$$

where $\mathbf{n}_k$ is the outward unit normal vector at the k-phase side of the interface and v_{ni} is the velocity in the normal direction. The summation is over all interfaces during the time interval Δt. A special case of the

above equation is for the derivative of the local void fraction, i.e.

$$\frac{\partial \alpha_k}{\partial t} = \frac{1}{\Delta t} \sum_j \frac{1}{v_{ni}} \mathbf{n}_k \cdot \mathbf{v}_i \tag{2.11a}$$

$$\nabla \alpha_k = -\frac{1}{\Delta t} \sum_j \frac{1}{v_{ni}} \mathbf{n}_k \tag{2.11b}$$

which will be used later in the interfacial mass, momentum, and energy transfer equation.

2.2.3 Time average of the general phasic balance law

The general two-phase two-fluid field equations are obtained by performing a time average to the phasic balance law, Eq. (2.1). The time average of Eq. (2.1) gives

$$\frac{\partial \overline{\rho_k \psi_k}}{\partial t} + \nabla \cdot \left(\overline{\rho_k \psi_k \mathbf{v}_k} \right) = -\nabla \cdot \overline{\mathbb{J}}_k + \overline{\rho_k \phi_k} + I_k \tag{2.12}$$

where I_k is the interfacial transfer term that represents the difference between time average of derivatives and the derivatives of time average,

$$I_k = \frac{1}{\Delta t} \sum_j \frac{1}{v_{ni}} \left[\mathbf{n}_k \cdot \rho_k \psi_k \left(\mathbf{v}_k - \mathbf{v}_i \right) + \mathbf{n}_k \cdot \mathbb{J}_k \right] \tag{2.13}$$

Using previous definitions for the phase average and mass weighted average, we obtain

$$\begin{aligned}
\overline{\rho_k \psi_k} &= \alpha_k \overline{\overline{\rho_k \psi_k}} = \alpha_k \overline{\rho}_k \widehat{\psi}_k \\
\overline{\rho_k \psi_k \mathbf{v}_k} &= \alpha_k \overline{\overline{\rho_k \psi_k \mathbf{v}_k}} = \alpha_k \overline{\rho}_k \widehat{\psi_k \mathbf{v}_k} = \alpha_k \overline{\rho}_k \widehat{\psi}_k \widehat{\mathbf{v}}_k + \alpha_k \mathbb{J}_k^T \\
\overline{\mathbb{J}}_k &= \alpha_k \overline{\overline{\mathbb{J}}}_k \\
\overline{\rho_k \phi_k} &= \alpha_k \overline{\overline{\rho_k \phi_k}} = \alpha_k \overline{\rho}_k \widehat{\phi}_k
\end{aligned} \tag{2.14}$$

where $\mathbb{J}_k^T$ represents the difference between the average of product and the product of average. It is defined as

$$\overline{\rho}_k \widehat{\psi_k \mathbf{v}_k} \equiv \overline{\rho}_k \widehat{\psi}_k \widehat{\mathbf{v}}_k + \mathbb{J}_k^T \tag{2.15}$$

Using Eq. (2.14), the time averaged balance law is written as

$$\frac{\partial \alpha_k \overline{\rho}_k \widehat{\psi}_k}{\partial t} + \nabla \cdot \left(\alpha_k \overline{\rho}_k \widehat{\psi}_k \widehat{\mathbf{v}_k} \right) = -\nabla \cdot \alpha_k \left(\overline{\overline{\mathbb{J}}}_k + \mathbb{J}_k^T \right) + \alpha_k \overline{\rho}_k \widehat{\phi}_k + I_k \tag{2.16}$$

The time averaged field equations for the two-phase two-fluid model are

$$\frac{\partial \alpha_k \overline{\overline{\rho}}_k}{\partial t} + \nabla \cdot \left(\alpha_k \overline{\overline{\rho}}_k \widehat{\mathbf{v}}_k\right) = I_{\rho,k} \tag{2.17a}$$

$$\frac{\partial \alpha_k \overline{\overline{\rho}}_k \widehat{\mathbf{v}}_k}{\partial t} + \nabla \cdot \left(\alpha_k \overline{\overline{\rho}}_k \widehat{\mathbf{v}}_k \widehat{\mathbf{v}}_k\right) = -\nabla\left(\alpha_k \overline{\overline{p}}_k\right) + \nabla \cdot \left[\alpha_k \left(\overline{\overline{\mathbb{T}}}_k + \mathbb{T}_k^T\right)\right] + \alpha_k \overline{\overline{\rho}}_k \mathbf{g} + \mathbf{I}_{\mathbf{v},k} \tag{2.17b}$$

$$\begin{aligned}\frac{\partial \alpha_k \overline{\overline{\rho}}_k \widehat{E}_k}{\partial t} + \nabla \cdot \left(\alpha_k \overline{\overline{\rho}}_k \widehat{E}_k \widehat{\mathbf{v}}_k\right) = &-\nabla \cdot \left(\alpha_k \overline{\overline{p}}_k \widehat{\mathbf{v}}_k\right) + \nabla \cdot \left[\alpha_k \left(\overline{\overline{\mathbb{T}}}_k + \mathbb{T}_k^T\right) \cdot \widehat{\mathbf{v}}_k\right] \\ &- \nabla \cdot \left[\alpha_k \left(\overline{\overline{\mathbf{q}}}_k + \mathbf{q}_k^T\right)\right] + \alpha_k \overline{\overline{\rho}}_k \mathbf{g} \cdot \widehat{\mathbf{v}}_k + I_{E,k}\end{aligned} \tag{2.17c}$$

where $I_{\rho,k}$, $\mathbf{I}_{\mathbf{v},k}$, and $I_{E,k}$ denote the interfacial transfer terms in mass, momentum, and energy equation, respectively. The internal heating $\dot{q}_k$ has been neglected because it is not important for most two-phase flow problems. In the momentum equation, $\mathbb{T}_k^T$ represents the turbulent flux tensor which is defined as

$$\mathbb{T}_k^T \equiv -\overline{\overline{\rho_k \mathbf{v}_k^{'} \mathbf{v}_k^{'}}}, \text{ with } \mathbf{v}_k^{'} \equiv \mathbf{v}_k - \widehat{\mathbf{v}}_k \tag{2.18}$$

In the energy equation, $\widehat{E}_k$ consists of the standard internal energy, kinetic energy, and the turbulent kinetic energy

$$\widehat{E}_k \equiv \widehat{e}_k + \frac{\widehat{\mathbf{v}}_k^2}{2} + \frac{\widehat{\left(\mathbf{v}_k^{'}\right)^2}}{2} \approx \widehat{e}_k + \frac{\widehat{\mathbf{v}}_k^2}{2} \tag{2.19}$$

where the approximation is made because the turbulent kinetic energy is relatively small compared to the internal energy. The $\mathbf{q}_k^T$ consists of the turbulent energy convection and the turbulent work

$$\mathbf{q}_k^T \equiv -\overline{\overline{\rho_k \left(e_k + \frac{\mathbf{v}_k^2}{2}\right) \mathbf{v}_k^{'}}} - \overline{\overline{\mathbb{T}_k \cdot \mathbf{v}_k^{'}}} + \overline{\overline{p_k \mathbf{v}_k^{'}}} \tag{2.20}$$

2.2.4 Interfacial transport

The interfacial transfer terms, $I_{\rho,k}$, $\mathbf{I}_{\mathbf{v},k}$, and $I_{E,k}$, in Eq. (2.17) are

$$\Gamma_k \equiv I_{\rho,k} = -\sum_j a_{ij} \dot{m}_k \tag{2.21a}$$

$$\mathbf{I}_{\mathbf{v},k} = -\sum_j a_{ij} \left(\dot{m}_k \mathbf{v}_k + p_k \mathbf{n}_k - \mathbf{n}_k \cdot \mathbb{T}_k\right) = \Gamma_k \widehat{\mathbf{v}}_{ki} + \overline{\overline{p}}_{ki} \nabla \alpha_k - \nabla \alpha_k \overline{\overline{\mathbb{T}}}_{ki} + \mathbf{M}_{ik} \tag{2.21b}$$

$$\begin{aligned}I_{E,k} &= -\sum_j a_{ij} \left[\dot{m}_k E_k - \mathbf{n}_k \cdot \left(p_k \mathbf{v}_k\right) + \mathbf{n}_k \cdot \left(\mathbb{T} \cdot \mathbf{v}_k\right) + \mathbf{n}_k \cdot \mathbf{q}_k\right] \\ &= \Gamma_k \left(\widehat{h}_{ki} + \widehat{\mathbf{v}}_{ki} \cdot \widehat{\mathbf{v}}_k - \frac{\widehat{\mathbf{v}}_k^2}{2}\right) - \overline{\overline{p}}_{ki} \frac{\partial \alpha_k}{\partial t} - \nabla \alpha_k \cdot \left(\overline{\overline{\mathbb{T}}}_{ki} \cdot \widehat{\mathbf{v}}_{ki}\right) + \mathbf{M}_{ik} \cdot \widehat{\mathbf{v}}_{ki} + a_i \overline{\overline{q}}_{ki}^{''} + W_{ki}^T\end{aligned} \tag{2.21c}$$

where W_{ki}^T is the turbulent flux of work due to drag force, which is often negligible. a_i is the volumetric interfacial area concentration and $\dot{m}_k$ is the rate of mass loss per interfacial area. They are defined as

$$a_i = \sum_j a_{ij}, \quad \text{with} \quad a_{ij} = \frac{1}{\Delta t}\frac{1}{v_{ni,j}} \tag{2.22}$$

$$\dot{m}_k = \mathbf{n}_k \cdot \rho_k\big(\mathbf{v}_k - \mathbf{v}_i\big) \tag{2.23}$$

$\mathbf{M}_{ik}$ is the total generalized drag force defined as

$$\mathbf{M}_{ik} \doteq \sum_j a_{ij}\big(\overline{\overline{p}}_{ki} - p_k\big)\mathbf{n}_k + \sum_j a_{ij}\mathbf{n}_k \cdot \big(\mathbb{T}_k - \overline{\overline{\mathbb{T}}}_{ki}\big) \tag{2.24}$$

where the variables with subscript ki represent the interfacial area averaged variables. The interfacial area average is defined as

$$\overline{\overline{F}}_{ki} \equiv \frac{\sum_j a_{ij}F_k}{\sum_j a_{ij}} \tag{2.25}$$

$$\widehat{F}_{ki} \equiv \frac{\sum_j a_{ij}\dot{m}_k F_k}{\sum_j a_{ij}\dot{m}_k} \tag{2.26}$$

Substituting Eq. (2.21) into Eq. (2.17), we obtain the field equations for the two-phase two-fluid model

$$\frac{\partial \alpha_k \overline{\overline{\rho}}_k}{\partial t} + \nabla \cdot \big(\alpha_k \overline{\overline{\rho}}_k \widehat{\mathbf{v}}_k\big) = \Gamma_k \tag{2.27a}$$

$$\begin{aligned}\frac{\partial \alpha_k \overline{\overline{\rho}}_k \widehat{\mathbf{v}}_k}{\partial t} + \nabla \cdot \big(\alpha_k \overline{\overline{\rho}}_k \widehat{\mathbf{v}}_k \widehat{\mathbf{v}}_k\big) =& -\nabla\big(\alpha_k \overline{\overline{p}}_k\big) + \nabla \cdot \big[\alpha_k\big(\overline{\overline{\mathbb{T}}}_k + \mathbb{T}_k^T\big)\big] + \alpha_k \overline{\overline{\rho}}_k \mathbf{g} \\ &+ \Gamma_k \widehat{\mathbf{v}}_{ki} + \overline{\overline{p}}_{ki}\nabla\alpha_k - \nabla\alpha_k \cdot \overline{\overline{\mathbb{T}}}_{ki} + \mathbf{M}_{ik}\end{aligned} \tag{2.27b}$$

$$\begin{aligned}\frac{\partial \alpha_k \overline{\overline{\rho}}_k \widehat{E}_k}{\partial t} + \nabla \cdot \big(\alpha_k \overline{\overline{\rho}}_k \widehat{E}_k \widehat{\mathbf{v}}_k\big) =& -\nabla \cdot \big(\alpha_k \overline{\overline{p}}_k \widehat{\mathbf{v}}_k\big) + \nabla \cdot \big[\alpha_k\big(\overline{\overline{\mathbb{T}}}_k + \mathbb{T}_k^T\big) \cdot \widehat{\mathbf{v}}_k\big] - \nabla \cdot \big[\alpha_k\big(\overline{\overline{\mathbf{q}}}_k + \mathbf{q}_k^T\big)\big] \\ &+ \alpha_k \overline{\overline{\rho}}_k \mathbf{g} \cdot \widehat{\mathbf{v}}_k + \Gamma_k\big(\widehat{h}_{ki} + \widehat{\mathbf{v}}_{ki} \cdot \widehat{\mathbf{v}}_k - \frac{\widehat{\mathbf{v}}_k^2}{2}\big) \\ &- \overline{\overline{p}}_{ki}\frac{\partial \alpha_k}{\partial t} - \nabla\alpha_k \cdot \big(\overline{\overline{\mathbb{T}}}_{ki} \cdot \widehat{\mathbf{v}}_{ki}\big) + \mathbf{M}_{ik} \cdot \widehat{\mathbf{v}}_{ki} + a_i \overline{\overline{q}}_{ki}^{''} + W_{ki}^T\end{aligned} \tag{2.27c}$$

Two more equations relating the phasic void fraction and physical pressure are required to close the system. They are

$$\alpha_l + \alpha_g = 1 \tag{2.28a}$$

$$f\big(\overline{\overline{p}}_l, \overline{\overline{p}}_g\big) = 0 \tag{2.28b}$$

where $f\left(\overline{\overline{p}}_l, \overline{\overline{p}}_g\right)$ is a general function relating the phasic pressure.

2.2.5 Determinism of two-phase two-fluid model

Let the unknown variables be

$$\mathbf{W} = \left[\alpha_k, \overline{\overline{p}}_k, \overline{\overline{T}}_k, \widehat{\mathbf{v}}_k\right], \quad \text{for} \quad k = l, g \tag{2.29}$$

where $\overline{\overline{T}}_k$ is the temperature of k-phase.

For each phase, the following unspecified variables are found in Eq. (2.27). For analysis purposes, we separate them into 3 groups:

- Thermodynamic properties: $\left[\overline{\overline{\rho}}_k, \widehat{e}_k, \widehat{h}_k\right]$
- Bulk average variables: $\left[\overline{\overline{\mathbb{T}}}_k, \mathbb{T}_k^T, \overline{\overline{\mathbf{q}}}_k, \mathbf{q}_k^T\right]$
- Interfacial average variables: $\left[\widehat{\mathbf{v}}_{ki}, \overline{\overline{p}}_{ki}, \overline{\overline{\rho}}_{ki}, \widehat{h}_{ki}, a_i, \Gamma_k, \overline{\overline{\mathbb{T}}}_{ki}, \mathbf{M}_{ik}, \overline{\overline{q}}_{ki}^{''}, W_{ki}^T\right]$

The thermodynamic properties, which are functions of the unknown variables, are specified by the EOS. In practice, the EOS is given by specifying the Gibbs free energy as a function of pressure and temperature, i.e.

$$\widehat{\mathfrak{g}}_k = \mathfrak{g}\left(\overline{\overline{p}}_k, \overline{\overline{T}}_k\right) \tag{2.30}$$

Then, the density, internal energy, and enthalpy of each phase are obtained by

$$\overline{\overline{\rho}}_k = \left[\frac{\partial \mathfrak{g}}{\partial p}\left(\overline{\overline{T}}_k, \overline{\overline{p}}_k\right)\right]^{-1} \tag{2.31a}$$

$$\widehat{e}_k = \widehat{\mathfrak{g}}_k - \overline{\overline{T}}_k \left[\frac{\partial \mathfrak{g}}{\partial T}\left(\overline{\overline{T}}_k, \overline{\overline{p}}_k\right)\right] - \overline{\overline{p}}_k \left[\frac{\partial \mathfrak{g}}{\partial p}\left(\overline{\overline{T}}_k, \overline{\overline{p}}_k\right)\right] \tag{2.31b}$$

$$\widehat{h}_k = \widehat{\mathfrak{g}}_k - \overline{\overline{T}}_k \left[\frac{\partial \mathfrak{g}}{\partial T}\left(\overline{\overline{T}}_k, \overline{\overline{p}}_k\right)\right] \tag{2.31c}$$

The bulk average variables and the interfacial average variables need to be modeled with closure correlations. Closure correlations for the general 3D two-phase two-fluid model are complicated, which are neglected in this thesis. The closure correlations will be given for the simplified 1D two-phase two-fluid model.

2.2.6 Transformation of two-phase two-fluid model

For analysis purposes, we separate the terms in Eq. (2.27) into the following groups:

- Arithmetic Function (AF) of unknown variables

$$\Big[\Gamma_k, \alpha_k\overline{\overline{\rho}}_k\mathbf{g}_k, \mathbf{M}_{ik}, \alpha_k\overline{\overline{\rho}}_k\mathbf{g}\cdot\widehat{v}_k, \Gamma_k\big(\widehat{h}_{ki}+\widehat{\mathbf{v}}_i\cdot\widehat{\mathbf{v}}_k-\frac{\widehat{\mathbf{v}}_k^2}{2}\big), \mathbf{M}_{ik}\cdot\widehat{\mathbf{v}}_i, a_i\widehat{q}_{ki}^{''}, W_{ki}^T\Big] \tag{2.32}$$

where we assume that $\big[\Gamma_k, \widehat{\mathbf{v}}_{ki}, \mathbf{M}_{ik}, \widehat{h}_{ki}, a_i\widehat{q}_{ki}^{''}, W_{ki}^{''}\big]$ could be modeled as arithmetic functions of the unknown variables.

- First-order Temporal Partial derivative (TP1) of unknown variables

$$\Big[\frac{\partial\alpha_k\overline{\overline{\rho}}_k}{\partial t}, \frac{\partial\alpha_k\overline{\overline{\rho}}_k\widehat{\mathbf{v}}_k}{\partial t}, \frac{\partial\alpha_k\overline{\overline{\rho}}_k\widehat{E}_k}{\partial t}, \overline{\overline{p}}_{ki}\frac{\partial\alpha_k}{\partial t}\Big] \tag{2.33}$$

- First-order Spatial Partial derivative (SP1) of unknown variables

$$\Big[\nabla\cdot\big(\alpha_k\overline{\overline{\rho}}_k\widehat{\mathbf{v}}_k\big), \nabla\cdot\big(\alpha_k\overline{\overline{\rho}}_k\widehat{\mathbf{v}}_k\widehat{\mathbf{v}}_k\big), \nabla\big(\alpha_k\overline{\overline{p}}_k\big), \overline{\overline{p}}_{ki}\nabla\alpha_k, \nabla\cdot\big(\alpha_k\overline{\overline{\rho}}_k\widehat{E}_k\widehat{\mathbf{v}}_k\big), \nabla\cdot\big(\alpha_k\overline{\overline{p}}_k\widehat{\mathbf{v}}_k\big)\Big] \tag{2.34}$$

- Second-order Spatial Partial derivative (SP2) of unknown variables

$$\Big\{\nabla\cdot\big[\alpha_k\big(\overline{\overline{\mathbb{T}}}_k+\mathbb{T}_k^T\big)\big], \nabla\cdot\big[\alpha_k\big(\overline{\overline{\mathbf{q}}}_k+\mathbf{q}_k^T\big)\big], \nabla\cdot\big[\alpha_k\big(\overline{\overline{\mathbb{T}}}_k+\mathbb{T}_k^T\big)\cdot\widehat{\mathbf{v}}_k\big]\Big\} \tag{2.35}$$

where we assume $\overline{\overline{\mathbb{T}}}_k$ and $\mathbb{T}_k^T$ are modeled as functions of velocity gradient, $\overline{\overline{\mathbf{q}}}_k$ and $\mathbf{q}_k^T$ are modeled as functions of temperature gradient.

- Mixed Spatial Partial derivative (M-SP1) of unknown variables

$$\Big[\nabla\alpha_k\cdot\overline{\overline{\mathbb{T}}}_{ki}, \big(\nabla\alpha_k\cdot\overline{\overline{\mathbb{T}}}_{ki}\big)\cdot\widehat{\mathbf{v}}_{ki}\Big] \tag{2.36}$$

In general, different discretization methods will be applied to terms in different groups. For now, we rewrite Eq. (2.27) by placing all SP1 and TP1 terms on the left-hand side and placing AF, SP2, and M-SP1

terms on the right-hand side, i.e.

$$\frac{\partial \alpha_k \overline{\overline{\rho}}_k}{\partial t} + \nabla \cdot \left(\alpha_k \overline{\overline{\rho}}_k \widehat{\mathbf{v}}_k\right) = \Gamma_k \tag{2.37a}$$

$$\begin{aligned}\frac{\partial \alpha_k \overline{\overline{\rho}}_k \widehat{\mathbf{v}}_k}{\partial t} + \nabla \cdot \left(\alpha_k \overline{\overline{\rho}}_k \widehat{\mathbf{v}}_k \widehat{\mathbf{v}}_k + \alpha_k \overline{\overline{p}}_k \mathbb{I}\right) - \overline{\overline{p}}_{ki} \nabla \alpha_k &= \nabla \cdot \left[\alpha_k \left(\overline{\overline{\mathbb{T}}}_k + \mathbb{T}_k^T\right)\right] + \alpha_k \overline{\overline{\rho}}_k \mathbf{g} \\ &\quad + \Gamma_k \widehat{\mathbf{v}}_{ki} - \nabla \alpha_k \cdot \overline{\overline{\mathbb{T}}}_{ki} + \mathbf{M}_{ik}\end{aligned} \tag{2.37b}$$

$$\begin{aligned}\frac{\partial \alpha_k \overline{\overline{\rho}}_k \widehat{E}_k}{\partial t} + \nabla \cdot \left(\alpha_k \overline{\overline{\rho}}_k \widehat{E}_k \widehat{\mathbf{v}}_k + \alpha_k \overline{\overline{p}}_k \widehat{\mathbf{v}}_k\right) + \overline{\overline{p}}_{ki} \frac{\partial \alpha_k}{\partial t} &= \nabla \cdot \left[\alpha_k \left(\overline{\overline{\mathbb{T}}}_k + \mathbb{T}_k^T\right) \cdot \widehat{\mathbf{v}}_k\right] - \nabla \cdot \left[\alpha_k \left(\overline{\overline{\mathbf{q}}}_k + \mathbf{q}_k^T\right)\right] \\ &\quad + \alpha_k \overline{\overline{\rho}}_k \mathbf{g} \cdot \widehat{\mathbf{v}}_k + \Gamma_k \left(\widehat{h}_{ki} + \widehat{\mathbf{v}}_{ki} \cdot \widehat{\mathbf{v}}_k - \frac{\widehat{\mathbf{v}}_k^2}{2}\right) \\ &\quad - \nabla \alpha_k \cdot \left(\overline{\overline{\mathbb{T}}}_{ki} \cdot \widehat{\mathbf{v}}_{ki}\right) + \mathbf{M}_{ik} \cdot \widehat{\mathbf{v}}_{ki} + a_i \overline{\overline{q}}_{ki}^{''} + W_{ki}^T\end{aligned} \tag{2.37c}$$

The two-phase two-fluid model is split into four parts:

- Conservative part with operator $\boldsymbol{\mathcal{C}}^\dagger$

$$\boldsymbol{\mathcal{C}}^\dagger \mathbf{W} = \begin{pmatrix} \frac{\partial \alpha_k \overline{\overline{\rho}}_k}{\partial t} + \nabla \cdot \left(\alpha_k \overline{\overline{\rho}}_k \widehat{\mathbf{v}}_k\right) \\ \frac{\partial \alpha_k \overline{\overline{\rho}}_k \widehat{\mathbf{v}}_k}{\partial t} + \nabla \cdot \left(\alpha_k \overline{\overline{\rho}}_k \widehat{\mathbf{v}}_k \widehat{\mathbf{v}}_k + \alpha_k \overline{\overline{p}}_k \mathbb{I}\right) \\ \frac{\partial \alpha_k \overline{\overline{\rho}}_k \widehat{E}_k}{\partial t} + \nabla \cdot \left(\alpha_k \overline{\overline{\rho}}_k \widehat{E}_k \widehat{\mathbf{v}}_k + \alpha_k \overline{\overline{p}}_k \widehat{\mathbf{v}}_k\right) \end{pmatrix} \tag{2.38}$$

  This part is conservative and can be written in the common form of a conservation law.

- Non-conservative part with operator $\boldsymbol{\mathcal{N}}^\dagger$

$$\boldsymbol{\mathcal{N}}^\dagger \mathbf{W} = \begin{pmatrix} 0 \\ -\overline{\overline{p}}_{ki} \nabla \alpha_k \\ \overline{\overline{p}}_{ki} \frac{\partial \alpha_k}{\partial t} \end{pmatrix} \tag{2.39}$$

  This part is non-conservative and can not be written in the common form of a conservation law.

- Second-order diffusive part with operator $\boldsymbol{\mathcal{D}}^\dagger$

$$\boldsymbol{\mathcal{D}}^\dagger \mathbf{W} = \begin{pmatrix} 0 \\ \nabla \cdot \left[\alpha_k \left(\overline{\overline{\mathbb{T}}}_k + \mathbb{T}_k^T\right)\right] \\ \nabla \cdot \left[\alpha_k \left(\overline{\overline{\mathbb{T}}}_k + \mathbb{T}_k^T\right) \cdot \widehat{\mathbf{v}}_k\right] - \nabla \cdot \left[\alpha_k \left(\overline{\overline{\mathbf{q}}}_k + \mathbf{q}_k^T\right)\right] \end{pmatrix} \tag{2.40}$$

- Arithmetic source part and mixed part with operator $\boldsymbol{\mathcal{A}}^{\dagger}$

$$\boldsymbol{\mathcal{A}}^{\dagger}\mathbf{W}=\begin{pmatrix}\Gamma_k\\ \alpha_k\overline{\overline{\rho}}_k\mathbf{g}+\Gamma_k\widehat{\mathbf{v}}_{ki}+\mathbf{M}_{ik}-\nabla\alpha_k\cdot\overline{\overline{\mathbb{T}}}_{ki}\\ \alpha_k\overline{\overline{\rho}}_k\mathbf{g}\cdot\widehat{\mathbf{v}}_k+\Gamma_k\big(\widehat{h}_{ki}+\widehat{\mathbf{v}}_{ki}\cdot\widehat{\mathbf{v}}_k-\frac{\widehat{\mathbf{v}}_k^2}{2}\big)+\big(\mathbf{M}_{ik}-\nabla\alpha_k\cdot\overline{\overline{\mathbb{T}}}_{ki}\big)\cdot\widehat{\mathbf{v}}_{ki}+a_i\overline{\overline{q}}_{ki}^{''}+W_{ki}^T\end{pmatrix} \tag{2.41}$$

Then, the two-phase two-fluid model is written as

$$\boldsymbol{\mathcal{G}}^{\dagger}\mathbf{W}=\boldsymbol{\mathcal{C}}^{\dagger}\mathbf{W}+\boldsymbol{\mathcal{N}}^{\dagger}\mathbf{W}-\boldsymbol{\mathcal{D}}^{\dagger}\mathbf{W}-\boldsymbol{\mathcal{A}}^{\dagger}\mathbf{W}=\mathbf{0} \tag{2.42}$$

where $\boldsymbol{\mathcal{G}}^{\dagger}$ is defined as the operator for the whole system.

2.3 One-dimensional two-phase two-fluid model

2.3.1 Area average and void fraction weighted area average

The 1D two-phase two-fluid model is obtained by performing an area average over the cross-section normal to the main flow direction, i.e. the x-direction in this thesis.

Definition 2.7. The area average of a general function is defined as

$$\big\langle F\big\rangle\equiv\frac{1}{A}\oint_A F\mathrm{d}S \tag{2.43}$$

where A is the area of the cross-section.

Definition 2.8. The void fraction weighted area average of a general function is defined as

$$\big\langle\big\langle F_k\big\rangle\big\rangle\equiv\frac{\big\langle\alpha_k F_k\big\rangle}{\big\langle\alpha_k\big\rangle} \tag{2.44}$$

During the area average, the phasic density in the cross-section is assumed to be uniform, i.e.

$$\rho_k=\overline{\overline{\rho}}_k\approx\big\langle\overline{\overline{\rho}}_k\big\rangle\approx\big\langle\big\langle\overline{\overline{\rho}}_k\big\rangle\big\rangle \tag{2.45}$$

This assumption is valid for most practical two-phase flow problems because the transverse pressure gradient within a channel is relatively small.

2.3.2 Area average of the two-phase two-fluid model

The transverse velocity components (v_k and w_k) are assumed to be negligible compared to the component (u_k) in the main flow direction. The area average of the conservative part gives

$$\left\langle \boldsymbol{\mathcal{C}}^{\dagger}\mathbf{W}\right\rangle \approx \begin{pmatrix} \frac{\partial\left\langle \alpha_k\right\rangle \rho_k}{\partial t}+\frac{\partial\left\langle \alpha_k\right\rangle \rho_k\left\langle\left\langle \widehat{u}_k\right\rangle\right\rangle}{\partial x} \\ \frac{\partial\left\langle \alpha_k\right\rangle \rho_k\left\langle\left\langle \widehat{u}_k\right\rangle\right\rangle}{\partial t}+\frac{\partial\left(C_{uk}\left\langle \alpha_k\right\rangle \rho_k\left\langle\left\langle \widehat{u}_k\right\rangle\right\rangle^2+\left\langle \alpha_k\right\rangle\left\langle\left\langle \overline{\overline{p}}_k\right\rangle\right\rangle\right)}{\partial x} \\ \frac{\partial\left\langle \alpha_k\right\rangle \rho_k\left\langle\left\langle \widehat{E}_k\right\rangle\right\rangle}{\partial t}+\frac{\partial C_{hk}\left\langle \alpha_k\right\rangle \rho_k\left\langle\left\langle \widehat{H}_k\right\rangle\right\rangle\left\langle\left\langle \widehat{u}_k\right\rangle\right\rangle}{\partial x} \end{pmatrix} \tag{2.46}$$

where C_{uk} and C_{hk} are the distribution parameters for the momentum flux and energy flux, respectively. C_{uk} represents the effect of the transverse void and velocity profiles on the area average of the momentum flux. C_{hk} represents the effect of the transverse void and enthalpy profile on the area average of the energy flux. Mathematically, these distribution parameters are important when the transverse velocity profile and enthalpy profile are not flat; in practice, C_{uk} and C_{hk} are assumed to be unity. This assumption is also used in TRACE and RELAP5-3D. Thus, these distribution parameters are dropped in the following analysis. In addition, the following approximations are made

$$\left\langle\left\langle \widehat{E}_k\right\rangle\right\rangle \approx \left\langle\left\langle \widehat{e}_k\right\rangle\right\rangle+\frac{\left\langle\left\langle \widehat{u}_k\right\rangle\right\rangle^2}{2} \tag{2.47a}$$

$$\left\langle\left\langle \widehat{H}_k\right\rangle\right\rangle \approx \left\langle\left\langle \widehat{e}_k\right\rangle\right\rangle+\frac{\left\langle\left\langle \widehat{u}_k\right\rangle\right\rangle^2}{2}+\frac{\left\langle\left\langle \overline{\overline{p}}_k\right\rangle\right\rangle}{\left\langle\left\langle \overline{\overline{\rho}}_k\right\rangle\right\rangle} \tag{2.47b}$$

The area average of the non-conservative part gives

$$\left\langle \boldsymbol{\mathcal{N}}^{\dagger}\mathbf{W}\right\rangle \approx \begin{pmatrix} 0 \\ -\left\langle\left\langle \overline{\overline{p}}_{ki}\right\rangle\right\rangle\frac{\partial\left\langle \alpha_k\right\rangle}{\partial x} \\ \left\langle\left\langle \overline{\overline{p}}_{ki}\right\rangle\right\rangle\frac{\partial\left\langle \alpha_k\right\rangle}{\partial t} \end{pmatrix} \tag{2.48}$$

The area average of the second-order diffusive part gives

$$\left\langle \boldsymbol{\mathcal{D}}^{\dagger}\mathbf{W}\right\rangle \approx \begin{pmatrix} 0 \\ \frac{\partial\left\langle \alpha_k\right\rangle\left\langle\left\langle \overline{\overline{\tau}}_{k,xx}+\tau^T_{k,xx}\right\rangle\right\rangle}{\partial x}-\frac{4\alpha_{kw}\overline{\overline{\tau}}_{kw}}{D} \\ -\frac{\partial\left\langle \alpha_k\right\rangle\left(\overline{\overline{q}}_{kx}+q^T_{kx}\right)}{\partial x}+\frac{\xi_h\alpha_{kw}\overline{\overline{q''_{kw}}}}{A}+\frac{\partial\left\langle \alpha_k\right\rangle\left\langle\left\langle \overline{\overline{\tau}}_{k,xx}+\tau^T_{k,xx}\right\rangle\right\rangle\left\langle\left\langle \widehat{u}_k\right\rangle\right\rangle}{\partial x}-\frac{4\alpha_{kw}\overline{\overline{\tau}}_{kw}\left\langle\left\langle \widehat{u}_k\right\rangle\right\rangle}{D} \end{pmatrix} \tag{2.49}$$

where τ_{kw} is the mean viscous stress near the wall, α_{kw} is the mean void fraction near the wall, D is the hydraulic diameter, ξ_h is the heated perimeter, $\overline{\overline{q''_{kw}}}$ is the wall heat flux, and A is the heated wall surface area.

The area average of the arithmetic part gives

$$\langle \boldsymbol{\mathcal{A}}^{\dagger}\mathbf{W}\rangle \approx \begin{pmatrix} \langle \Gamma_k \rangle \\ \langle \alpha_k \rangle \rho_k g_x + \langle \Gamma_k \rangle \langle\langle \widehat{u}_{ki} \rangle\rangle + \langle M_k^d \rangle \\ \langle \alpha_k \rangle \rho_k g_x \langle\langle \widehat{u}_k \rangle\rangle + \langle \Gamma_k \rangle \big(\langle\langle \widehat{h}_{ki} \rangle\rangle + \langle\langle \widehat{u}_{ki} \rangle\rangle \langle\langle \widehat{u}_k \rangle\rangle - \frac{\langle\langle \widehat{u}_k \rangle\rangle^2}{2} \big) + \langle a_i \overline{\overline{q_{ki}^{''}}} \rangle + \langle M_k^d \rangle \langle\langle u_k \rangle\rangle + \langle W_{ki}^T \rangle \end{pmatrix} \tag{2.50}$$

where $\langle M_k^d \rangle$ is the total interfacial shear force given by

$$\langle M_k^d \rangle = \langle \mathbf{M}_{ik} - \nabla \alpha_k \cdot \overline{\overline{\mathbb{T}}}_{ki} \rangle_x \tag{2.51}$$

The area average equations are closed with three more jump conditions [1],

$$\sum_{k=l,g} \langle \Gamma_k \rangle = 0 \tag{2.52a}$$

$$\sum_{k=l,g} \langle M_k^d \rangle = 0 \tag{2.52b}$$

$$\sum_{k=l,g} \big(\langle \Gamma_k \rangle \langle\langle \widehat{h}_{ki} \rangle\rangle + \langle a_i \overline{\overline{q_{ki}^{''}}} \rangle \big) = 0 \tag{2.52c}$$

2.3.3 One-dimensional two-phase two-fluid model

The average operators are dropped to simplify the expression of the 1D two-phase two-fluid model,

$$\begin{aligned} \langle \psi \rangle &\Rightarrow \psi, \quad \text{for} \quad \psi = \alpha_k, \Gamma_k \\ \langle\langle \overline{\psi} \rangle\rangle &\Rightarrow \psi, \quad \text{for} \quad \psi = p_k, p_{ki}, u_k, u_{ki}, e_k, h_k, h_{ki}, \tau_k, \tau_k^T, q_k, q_k^T \\ \langle\langle \widehat{\psi} \rangle\rangle &\Rightarrow \psi, \quad \text{for} \quad \psi = u_k, u_{ki}, e_k, h_k, h_{ki}, E_k, H_k \end{aligned} \tag{2.53}$$

The following variables are defined

$$f_{ik} \equiv \langle M_k^d \rangle \tag{2.54a}$$

$$f_{wk} \equiv \frac{4\alpha_{kw} \overline{\overline{\tau}}_{kw}}{D} \tag{2.54b}$$

$$Q_{ik} \equiv \langle a_i \overline{\overline{q_{ki}^{''}}} \rangle \tag{2.54c}$$

$$Q_{wk} \equiv \frac{\xi_h \alpha_{kw} \overline{\overline{q_{kw}^{''}}}}{A} \tag{2.54d}$$

The following approximations are made

$$C_{uk} \approx 1 \quad \text{and} \quad C_{hk} \approx 1 \tag{2.55a}$$

$$\langle W_{ki}^T \rangle \approx 0 \tag{2.55b}$$

Then, the 1D two-phase two-fluid model is simplified to

$$\frac{\partial \alpha_k \rho_k}{\partial t} + \frac{\partial \alpha_k \rho_k u_k}{\partial x} = \Gamma_k \tag{2.56a}$$

$$\frac{\partial \alpha_k \rho_k u_k}{\partial t} + \frac{\partial \big(\alpha_k \rho_k u_k^2 + \alpha_k p_k\big)}{\partial x} - p_{ki} \frac{\partial \alpha_k}{\partial x} = \frac{\partial \alpha_k \big(\tau_{k,xx} + \tau_{k,xx}^T\big)}{\partial x} + \alpha_k \rho_k g_x - f_{wk} + f_{ik} + \Gamma_k u_{ki} \tag{2.56b}$$

$$\begin{aligned} \frac{\partial \alpha_k \rho_k E_k}{\partial t} + \frac{\partial \big(\alpha_k \rho_k E_k u_k + \alpha_k p_k u_k\big)}{\partial x} + p_{ki} \frac{\partial \alpha_k}{\partial t} = & -\frac{\partial \alpha_k \big(q_{kx} + q_{kx}^T\big)}{\partial x} + \frac{\partial \alpha_k \big(\tau_{k,xx} + \tau_{k,xx}^T\big) u_k}{\partial x} \\ & + Q_{wk} + Q_{ik} + \alpha_k \rho_k g_x u_k - f_{wk} u_k + f_{ik} u_k \\ & + \Gamma_k \big(h_{ki} + u_{ki} u_k - \frac{u_k^2}{2}\big) \end{aligned} \tag{2.56c}$$

The spatial partial derivatives related to the normal viscous stress and heat flux are negligible compared to the other terms in the right-hand side. These terms will be dropped in the following analysis. This treatment is also used by TRACE and RELAP5-3D,

$$\frac{\partial \alpha_k \rho_k}{\partial t} + \frac{\partial \alpha_k \rho_k u_k}{\partial x} = \Gamma_k \tag{2.57a}$$

$$\frac{\partial \alpha_k \rho_k u_k}{\partial t} + \frac{\partial \big(\alpha_k \rho_k u_k^2 + \alpha_k p_k\big)}{\partial x} - p_{ki} \frac{\partial \alpha_k}{\partial x} = \alpha_k \rho_k g_x - f_{wk} + f_{ik} + \Gamma_k u_{ki} \tag{2.57b}$$

$$\begin{aligned} \frac{\partial \alpha_k \rho_k E_k}{\partial t} + \frac{\partial \big(\alpha_k \rho_k E_k u_k + \alpha_k p_k u_k\big)}{\partial x} + p_{ki} \frac{\partial \alpha_k}{\partial t} = & \; Q_{wk} + Q_{ik} + \Gamma_k h_{ki} \\ & + \big(f_{ik} - f_{wk} + \alpha_k \rho_k g_x + \Gamma_k u_{ki}\big) u_k - \Gamma_k \frac{u_k^2}{2} \end{aligned} \tag{2.57c}$$

The basic 1D two-phase two-fluid model assumes that all pressure terms are equal, i.e. $p_l = p_g = p_{li} = p_{gi}$.

Let p be the equal pressure, Eq. (2.57) is transformed into

$$\frac{\partial \alpha_l \rho_l}{\partial t} + \frac{\partial \alpha_l \rho_l u_l}{\partial x} = -\Gamma_g \tag{2.58a}$$

$$\frac{\partial \alpha_l \rho_l u_l}{\partial t} + \frac{\partial \left(\alpha_l \rho_l u_l^2 + \alpha_l p\right)}{\partial x} - p\frac{\partial \alpha_l}{\partial x} = \alpha_l \rho_l g_x - f_{wl} + f_i - \Gamma_g u_{li} \tag{2.58b}$$

$$\begin{aligned}\frac{\partial \alpha_l \rho_l E_l}{\partial t} + \frac{\partial \left(\alpha_l \rho_l E_l u_l + \alpha_l p u_l\right)}{\partial x} + p\frac{\partial \alpha_l}{\partial t} &= Q_{wl} + Q_{il} - \Gamma_g h_{li} \\ &\quad + \left(f_i - f_{wl} + \alpha_l \rho_l g_x - \Gamma_g u_{li}\right) u_l + \Gamma_g \frac{u_l^2}{2}\end{aligned} \tag{2.58c}$$

$$\frac{\partial \alpha_g \rho_g}{\partial t} + \frac{\partial \alpha_g \rho_g u_g}{\partial x} = \Gamma_g \tag{2.58d}$$

$$\frac{\partial \alpha_g \rho_g u_g}{\partial t} + \frac{\partial \left(\alpha_g \rho_g u_g^2 + \alpha_g p\right)}{\partial x} - p\frac{\partial \alpha_g}{\partial x} = \alpha_g \rho_g g_x - f_{wg} - f_i + \Gamma_g u_{gi} \tag{2.58e}$$

$$\begin{aligned}\frac{\partial \alpha_g \rho_g E_g}{\partial t} + \frac{\partial \left(\alpha_g \rho_g E_g u_g + \alpha_g p u_g\right)}{\partial x} + p\frac{\partial \alpha_g}{\partial t} &= Q_{wg} + Q_{ig} + \Gamma_g h_{gi} \\ &\quad + \left(-f_i - f_{wg} + \alpha_g \rho_g g_x + \Gamma_g u_{gi}\right) u_g - \Gamma_g \frac{u_g^2}{2}\end{aligned} \tag{2.58f}$$

In Eq. (2.58), Γ_l is replaced with $-\Gamma_g$, f_{il} is replaced with f_i, and f_{ig} is replaced with $-f_i$ because of the interface jump conditions

$$\Gamma_l + \Gamma_g = 0 \tag{2.59a}$$

$$f_{il} + f_{ig} = \left\langle M_l^d \right\rangle + \left\langle M_g^d \right\rangle = 0 \tag{2.59b}$$

The 1D two-phase two-fluid model, Eq. (2.58), can be written in a compact vector form as

$$\frac{\partial \mathbf{U}}{\partial t} + \frac{\partial \mathbf{F}}{\partial x} + \mathbf{P}_{ix}\frac{\partial \alpha_g}{\partial x} + \mathbf{P}_{it}\frac{\partial \alpha_g}{\partial t} = \mathbf{S} \tag{2.60}$$

where $\mathbf{U}$ is the vector of conservative variables, $\mathbf{F}$ is the vector of flux variables, $\mathbf{P}_{ix}$ and $\mathbf{P}_{it}$ are the vectors related to the interfacial average pressure terms, and $\mathbf{S}$ is the vector of source terms. They are defined as

$$\mathbf{U} \equiv \begin{pmatrix} \alpha_l \rho_l \\ \alpha_l \rho_l u_l \\ \alpha_l \rho_l E_l \\ \alpha_g \rho_g \\ \alpha_g \rho_g u_g \\ \alpha_g \rho_g E_g \end{pmatrix}, \mathbf{F} \equiv \begin{pmatrix} \alpha_l \rho_l u_l \\ \alpha_l \rho_l u_l^2 + \alpha_l p \\ \alpha_l \rho_l E_l u_l + \alpha_l p u_l \\ \alpha_g \rho_g u_g \\ \alpha_g \rho_g u_g^2 + \alpha_g p \\ \alpha_g \rho_g E_g u_g + \alpha_g p u_g \end{pmatrix}, \mathbf{P}_{ix} \equiv \begin{pmatrix} 0 \\ p \\ 0 \\ 0 \\ -p \\ 0 \end{pmatrix}, \mathbf{P}_{it} \equiv \begin{pmatrix} 0 \\ 0 \\ -p \\ 0 \\ 0 \\ p \end{pmatrix} \tag{2.61}$$

$$\mathbf{S} \equiv \begin{pmatrix} -\Gamma_g \\ \alpha_l \rho_l g_x - f_{wl} + f_i - \Gamma_g u_{li} \\ Q_{wl} + Q_{il} - \Gamma_g h_{li} + \big(f_i - f_{wl} + \alpha_l \rho_l g_x - \Gamma_g u_{li}\big) u_l + \Gamma_g \frac{u_l^2}{2} \\ \Gamma_g \\ \alpha_g \rho_g g_x - f_{wg} - f_i + \Gamma_g u_{gi} \\ Q_{wg} + Q_{ig} + \Gamma_g h_{gi} + \big(-f_i - f_{wg} + \alpha_g \rho_g g_x + \Gamma_g u_{gi}\big) u_g - \Gamma_g \frac{u_g^2}{2} \end{pmatrix} \tag{2.62}$$

In the following analysis, $\big(\partial \mathbf{U}/\partial t + \partial \mathbf{F}/\partial x\big)$ is called the conservative part. This part comes directly from the time average of instant phasic balance equation [1] and has the form of a conservation law. $\big(\mathbf{P}_{it}\partial\alpha_g/\partial t + \mathbf{P}_{ix}\partial\alpha_g/\partial x\big)$ is called the non-conservative part. This part comes from the interfacial transfer terms [1] and can not be written in the form of a conservation law. As was discussed by Dinh [16], the conservative part can also be written in an equivalent integral form, which admits a discontinuity solution in a weak sense. In the contrary, the non-conservative cannot be written in an integral form, which makes the construction of a weak solution to discontinuity questionable.

Eq. (2.60) will be the starting point of the work in this thesis. In the following chapters, the statement about "basic two-phase two-fluid model" is meant to Eq. (2.60).

2.3.4 Alternative form of the one-dimensional two-phase two-fluid model

Apart from the conservative form of the two-phase two-fluid model, Eq. (2.57), there are several important transformations. A good review of the transformed equations can be found in [1].

Equation of motion

By using the continuity equation, the momentum equation can be transformed into

$$\alpha_l \rho_l \frac{\partial u_l}{\partial t} + \alpha_l \rho_l u_l \frac{\partial u_l}{\partial x} = -\alpha_l \frac{\partial p_l}{\partial x} + \big(p_{li} - p_l\big)\frac{\partial \alpha_l}{\partial x} + \alpha_l \rho_l g_x + f_i - f_{wl} - \Gamma_g\big(u_{li} - u_l\big) \tag{2.63a}$$

$$\alpha_g \rho_g \frac{\partial u_g}{\partial t} + \alpha_g \rho_g u_g \frac{\partial u_g}{\partial x} = -\alpha_g \frac{\partial p_g}{\partial x} + \big(p_{gi} - p_g\big)\frac{\partial \alpha_g}{\partial x} + \alpha_g \rho_g g_x - f_i - f_{wg} + \Gamma_g\big(u_{gi} - u_g\big) \tag{2.63b}$$

This form of momentum equation is the preferred form for numerical solvers using a staggered grid, such as TRACE and RELAP5-3D. This form is not used in our numerical solver because it is difficult to construct a shock-capturing upwind solver with this form.

Internal energy equation

The kinetic energy can be subtracted from the total energy equation to obtain the so called internal energy equation

$$\frac{\partial \alpha_l \rho_l e_l}{\partial t} + \frac{\partial \alpha_l \rho_l e_l u_l}{\partial x} + p_{li}\frac{\partial \alpha_l}{\partial t} + p_l \frac{\partial \alpha_l u_l}{\partial x} = Q_{wl} + Q_{il} - \Gamma_g h_{li} \tag{2.64a}$$

$$\frac{\partial \alpha_g \rho_g e_g}{\partial t} + \frac{\partial \alpha_g \rho_g e_g u_g}{\partial x} + p_{gi}\frac{\partial \alpha_g}{\partial t} + p_g \frac{\partial \alpha_g u_g}{\partial x} = Q_{wg} + Q_{ig} + \Gamma_g h_{gi} \tag{2.64b}$$

This form of energy equation is also the preferred form for numerical solvers using a staggered grid, such as TRACE and RELAP5-3D. This form is not used in our numerical solver because the $p_k \partial \alpha_k u_k / \partial x$ term adds more difficulties to discretize the equation and construct appropriate numerical fluxes.

Enthalpy equation

Another form of the energy equation is the enthalpy equation

$$\frac{\partial \alpha_l \rho_l h_l}{\partial t} + \frac{\partial \alpha_l \rho_l h_l u_l}{\partial x} + \big(p_{li} - p_l\big)\frac{\partial \alpha_l}{\partial t} + \alpha_l \left(\frac{\partial p_l}{\partial t} + u_l \frac{\partial p_l}{\partial x}\right) = Q_{wl} + Q_{il} - \Gamma_g h_{li} \tag{2.65a}$$

$$\frac{\partial \alpha_g \rho_g h_g}{\partial t} + \frac{\partial \alpha_g \rho_g h_g u_g}{\partial x} + \big(p_{gi} - p_g\big)\frac{\partial \alpha_g}{\partial t} + \alpha_g \left(\frac{\partial p_g}{\partial t} + u_g \frac{\partial p_g}{\partial x}\right) = Q_{wg} + Q_{ig} + \Gamma_g h_{gi} \tag{2.65b}$$

This form is not used in our numerical solver because the $\partial p_k / \partial t + u_k \partial p_k / \partial x$ terms add more difficulties to discretize the equation and construct appropriate numerical fluxes.

Two-phase two-fluid model in RELAP5-3D and TRACE

The two-phase two-fluid six-equation model used by RELAP5-3D and TRACE is often written as

$$\frac{\partial \alpha_l \rho_l}{\partial t} + \frac{\partial \alpha_l \rho_l u_l}{\partial x} = -\Gamma_g \tag{2.66a}$$

$$\alpha_l \rho_l \frac{\partial u_l}{\partial t} + \alpha_l \rho_l u_l \frac{\partial u_l}{\partial x} + \alpha_l \frac{\partial p}{\partial x} = \alpha_l \rho_l g_x + f_i - f_{wl} - \Gamma_g \big(u_{li} - u_l\big) \tag{2.66b}$$

$$\frac{\partial \alpha_l \rho_l e_l}{\partial t} + \frac{\partial \alpha_l \rho_l e_l u_l}{\partial x} + p\frac{\partial \alpha_l}{\partial t} + p\frac{\partial \alpha_l u_l}{\partial x} = Q_{wl} + Q_{il} - \Gamma_w h_l^{'} - \Gamma_{ig} h_l^{*} \tag{2.66c}$$

$$\frac{\partial \alpha_g \rho_g}{\partial t} + \frac{\partial \alpha_g \rho_g u_g}{\partial x} = \Gamma_g \tag{2.66d}$$

$$\alpha_g \rho_g \frac{\partial u_g}{\partial t} + \alpha_g \rho_g u_g \frac{\partial u_g}{\partial x} + \alpha_g \frac{\partial p}{\partial x} = \alpha_g \rho_g g_x - f_i - f_{wg} + \Gamma_g \big(u_{gi} - u_g\big) \tag{2.66e}$$

$$\frac{\partial \alpha_g \rho_g e_g}{\partial t} + \frac{\partial \alpha_g \rho_g e_g u_g}{\partial x} + p\frac{\partial \alpha_g}{\partial t} + p\frac{\partial \alpha_g u_g}{\partial x} = Q_{wg} + Q_{ig} + \Gamma_w h_g^{'} + \Gamma_{ig} h_g^{*} \tag{2.66f}$$

where Γ_w, Γ_{ig}, $h_k^{'}$, and h_k^* are quantities related to vapor generation, which will be discussed later in **Sec. 2.4.2**. Eq. (2.66) is a convenient set of equations for RELAP5-3D and TRACE.

Discussion of different energy equations

Note that there are 3 sets of energy equations, i.e. internal energy equation Eq. (2.64), enthalpy equation Eq. (2.65), and total energy equation Eq. (2.58). These 3 sets of equations are mathematically equivalent but numerically different. The internal energy equation and enthalpy equation are convenient for RELAP5-3D and TRACE; however, the total energy equation, which is written in a conservative form, is preferred in our numerical solver. A conservative form is essential for constructing a shock-capturing upwind numerical solver. The advantages and disadvantages of the total energy equation (i.e. the conservative form) are listed below for future study.

Advantages:

1. The governing equation is in a conservative form. The numerical solver (if formulated appropriately) is inherently conservative even for problems with discontinuities. It is very difficult to construct a numerical solver that ensures the conservation of conservative variables using a non-conservative form.

2. For single-phase flows, the eigenvalues and eigenvectors of the conservative form are structured and well documented. For two-phase flows, the eigenvalues and eigenvectors are found to be very similar to that of single-phase flows, as will be seen in **Chapter 4**.

3. In the total energy equation, the non-conservative term, which is not included in the flux vector, is $p\partial\alpha_k/\partial t$. This non-conservative term is related to the temporal derivative instead of a spatial derivative. In general, the non-conservative spatial derivative is more difficult to handle numerically.

Disadvantages:

1. The total energy equation is not commonly solved in the existing system codes, e.g. RELAP5-3D and TRACE. The existing closure correlations for the internal energy equation or enthalpy equation might not be appropriate for the total energy equation. Because the closure correlations in this work are based on RELAP3-3D, the effect of the different energy equation to the solution is not known.

2. The additional mechanical energy in the total energy equation brings in uncertainties to the temperature of two phases. For problems where the wall and interfacial heat flux are much larger than the mechanical energy, this problem is not significant; however, for problems where the wall and interfacial heat transfer flux are small, the uncertainties in the additional terms (e.g. $f_i u_g$) would be propagated to the temperature of two phases.

2.4 One-dimensional models and correlations

This section gives a brief introduction to the models and correlations that are necessary for simulating real two-phase flow problems. The models and correlations are based on RELAP5-3D theory manual [5, 17, 18, 19]. The justifications and discussions to the models and correlations are not provided because they are not the main objective of this thesis. The general structure for modeling the source terms is summarized here to provide an overall picture and help understand the features and limitations of the two-phase two-fluid model.

2.4.1 Flow regime map

The vertical flow is the focus of this thesis. The flow regime map for a vertical flow is a three-dimensional function of the void fraction (α_g), average mixture velocity (u_m), and the wall superheat. In RELAP5-3D, the vertical flow regime map consists of bubbly (BBY), slug (SLG), annular mist (ANM), and dispersed/droplet mist (MPR) flows in the pre-CHF regime; inverted annular (IAN), inverted slug (ISL), and mist (MST) flows in post-dryout; and vertically stratified flow for sufficiently low mixture velocity. In this thesis, the flow regime map is a simplified version of the RELAP5-3D flow regime map, see page 3-9 of RELAP5-3D code manual [19].

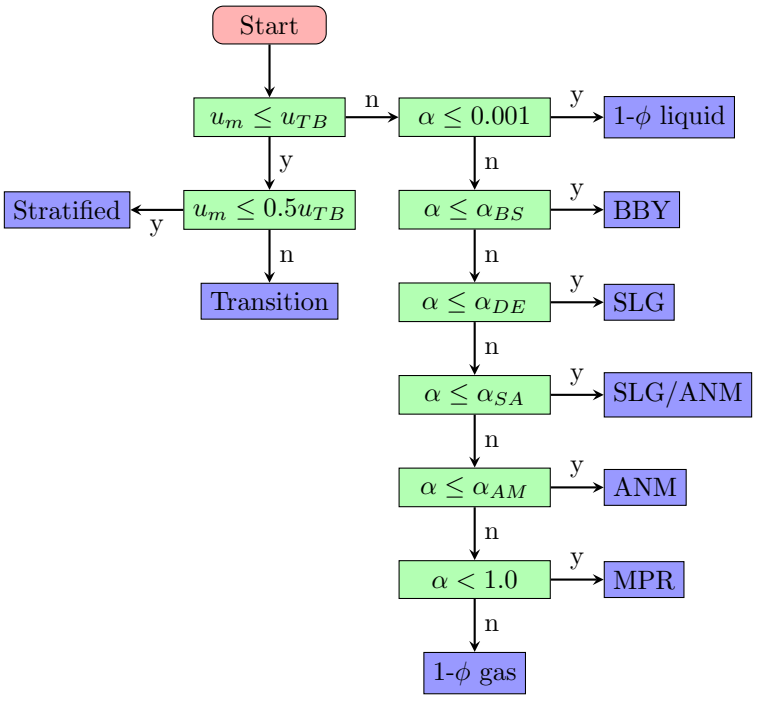

Figure 2.1: Flowchart for determining the vertical flow regime map for pre-CHF

Figure 2.1 shows the simplified flow regime map. It contains only vertical flow in pre-CHF conditions, which covers all test problems considered in this thesis. The average mixture velocity is defined as

$$u_m = \frac{G_m}{\rho_m} \tag{2.67}$$

where G_m is the mass flux of the mixture and ρ_m is the density of the mixture, they are defined as

$$G_m = \alpha_l \rho_l |u_l| + \alpha_g \rho_g |u_g| \tag{2.68a}$$

$$\rho_m = \alpha_l \rho_l + \alpha_g \rho_g \tag{2.68b}$$

The critical velocity determining if the flow is stratified is modeled as

$$u_{TB} = 0.35 \sqrt{\frac{gD\big(\rho_l - \rho_g\big)}{\rho_l}} \tag{2.69}$$

where g is the gravitational constant and D is the hydraulic diameter.

The void fraction plays an important role in determining the flow regime. The transition criteria are modeled as

$$\alpha_{BS} = \text{Interp}\big(G_m; 2000, 3000, \alpha^*_{BS}, 0.5\big) \tag{2.70a}$$

$$\alpha_{SA} = \max\big[\alpha^{\min}_{AM}, \min\big(\alpha^f_{crit}, \alpha^e_{crit}, \alpha^{\max}_{BS}\big)\big] \tag{2.70b}$$

$$\alpha_{DE} = \max\big(\alpha_{BS}, \alpha_{SA} - 0.05\big) \tag{2.70c}$$

$$\alpha_{AM} = 0.9999 \tag{2.70d}$$

where Interp() is an interpolation function which is defined as

$$\text{Interp}(\mathrm{x}; \mathrm{x}_1, \mathrm{x}_2, \mathrm{y}_1, \mathrm{y}_2) \equiv \begin{cases} y_1, & \text{if} \quad x \le x_1 \\ y_1 + \frac{y_2 - y_1}{x_2 - x_1}\big(x - x_1\big), & \text{if} \quad x_1 < x < x_2 \\ y_2, & \text{if} \quad x \ge x_2 \end{cases} \tag{2.71}$$

and the other parameters in Eq. (2.70) are modeled as

$$\alpha_{BS}^{*} = \max\left\{0.25\min\left[1.0,\left(0.045D\sqrt{\frac{g\left(\rho_l-\rho_g\right)}{\sigma}}\right)^{8}\right],10^{-3}\right\} \tag{2.72a}$$

$$\alpha_{crit}^{f} = \min\left\{\frac{1}{u_g}\sqrt{\frac{gD\left(\rho_l-\rho_g\right)}{\rho_g}},1.0\right\} \quad \text{for upflow} \tag{2.72b}$$

$$= 0.75 \quad \text{for downflow and countercurrent flow}$$

$$\alpha_{crit}^{e} = \min\left\{\frac{3.2}{u_g}\left[\sqrt{\frac{g\sigma\left(\rho_l-\rho_g\right)}{\rho_g^2}}\right]^{1/4},1.0\right\} \tag{2.72c}$$

$$\alpha_{AM}^{\min} = 0.5 \text{ (pipe) or } 0.8 \text{ (bundles)} \tag{2.72d}$$

$$\alpha_{BS}^{\max} = 0.9 \tag{2.72e}$$

where σ is the surface tension of the interface.

2.4.2 Interfacial mass transfer

The source vector for the two-phase two-fluid model is

$$\mathbf{S} = \begin{pmatrix} -\Gamma_g \\ \alpha_l\rho_l g_x - f_{wl} + f_i - \Gamma_g u_{li} \\ Q_{wl} + Q_{il} - \Gamma_g h_{li} + \left(f_i - f_{wl} + \alpha_l\rho_l g_x - \Gamma_g u_{li}\right)u_l + \Gamma_g\frac{u_l^2}{2} \\ \Gamma_g \\ \alpha_g\rho_g g_x - f_{wg} - f_i + \Gamma_g u_{gi} \\ Q_{wg} + Q_{ig} + \Gamma_g h_{gi} + \left(-f_i - f_{wg} + \alpha_g\rho_g g_x + \Gamma_g u_{gi}\right)u_g - \Gamma_g\frac{u_g^2}{2} \end{pmatrix} \tag{2.73}$$

where the following variables need to be specified with either models or correlations

- u_{ki}, h_{ki}: interfacial averaged velocity and specific enthalpy for k-phase
- Γ_g: net vapor generation rate
- f_i: interfacial friction between two phases
- f_{wk}: wall friction to k-phase
- Q_{ik}: interface to k-phase heat flux (interfacial heat flux)
- Q_{wk}: wall to k-phase heat flux (wall heat flux)

The vapor generation rate (or condensation) consists of two parts, vapor generation due to energy exchange (Γ_{ig}) and vapor generation due to the wall heat transfer effect (Γ_w). Each of the vapor generation (or condensation) processes involves interfacial heat transfer effect. Thus, in the phasic energy equation, the phasic enthalpy carried by the vapor generation term is also divided into two parts: (h_l^*, h_g^*) for the phasic enthalpy carried by Γ_{ig} and $(h_l^{'}, h_g^{'})$ for the phasic enthalpy carried by Γ_w. The vapor generation rate, phasic enthalpy, and the interfacial heat flux are related by

$$Q_{il} - \Gamma_g h_{li} = Q_{il} - \Gamma_w h_l^{'} - \Gamma_{ig} h_l^* \tag{2.74a}$$

$$Q_{ig} + \Gamma_g h_{gi} = Q_{ig} + \Gamma_w h_g^{'} + \Gamma_{ig} h_g^* \tag{2.74b}$$

The interfacial heat transfer terms (Q_{il} and Q_{ig}) include the heat transfer from the fluid states to the interface due to interface energy exchange in the bulk and in the thermal boundary layer near the wall. In practice, they are modeled as

$$Q_{il} = H_{il}\big(T_{sat} - T_l\big) - \Gamma_w\big(h_g^{'} - h_l^{'}\big) \tag{2.75a}$$

$$Q_{ig} = H_{ig}\big(T_{sat} - T_g\big) \tag{2.75b}$$

where H_{il} and H_{ig} are the volumetric interface-to-liquid and interface-to-gas heat transfer coefficients, respectively.

Γ_w is determined by the method proposed by Lahey [20], combined with Saha-Zuber correlation [21]. When the flow is in boiling conditions,

$$\Gamma_w = \mathrm{Mul} \cdot \frac{a_{wall} q_{wl}^{''}}{\max\big(h_g^{'} - h_l^{'}, 10^4 \mathrm{J/kg}\big)} \tag{2.76}$$

where $q_{wl}^{''}$ is the wall heat flux to the fluid, a_{wall} is the volumetric heated surface area, and Mul is the fraction of the wall heat flux that is accounting for the Γ_w term. The details of Mul are referred to page 4-193 of RELAP5-3D code manual [19]. The phasic enthalpies, $h_l^{'}$ and $h_g^{'}$, are modeled as

$$h_l^{'} = h_l, \quad h_g^{'} = h_{g,sat} \quad \text{for } \Gamma_w \geq 0 \tag{2.77a}$$

$$h_l^{'} = h_{l,sat}, \quad h_g^{'} = h_g \quad \text{for } \Gamma_w < 0 \tag{2.77b}$$

Γ_{ig} is determined by

$$\Gamma_{ig} = -\frac{H_{il}\big(T_{sat} - T_l\big) + H_{ig}\big(T_{sat} - T_g\big)}{h_g^* - h_l^*} \tag{2.78}$$

where the phasic enthalpies, h_l^* and h_g^*, are modeled as

$$h_l^* = h_l, \quad h_g^* = h_{g,sat} \quad \text{for } \Gamma_{ig} \geq 0 \tag{2.79a}$$

$$h_l^* = h_{l,sat}, \quad h_g^* = h_g \quad \text{for } \Gamma_{ig} < 0 \tag{2.79b}$$

In the momentum equation and energy equation, the interfacial averaged velocities, u_{li} and u_{gi}, are modeled as

$$u_i \equiv u_{gi} \approx u_{li} = \begin{cases} u_l, & \text{for } \Gamma_g \geq 0 \\ u_g, & \text{for } \Gamma_g < 0 \end{cases} \tag{2.80}$$

Finally, the source vector is written as

$$\mathbf{S} = \begin{pmatrix} -\Gamma_g \\ \alpha_l \rho_l g_x - f_{wl} + f_i - \Gamma_g u_i \\ Q_{wl} + Q_{il} - \Gamma_w h_l^{'} - \Gamma_{ig} h_l^* + \big(f_i - f_{wl} + \alpha_l \rho_l g_x - \Gamma_g u_i\big) u_l + \Gamma_g \frac{u_l^2}{2} \\ \Gamma_g \\ \alpha_g \rho_g g_x - f_{wg} - f_i + \Gamma_g u_i \\ Q_{wg} + Q_{ig} + \Gamma_w h_g^{'} + \Gamma_{ig} h_g^* + \big(-f_i - f_{wg} + \alpha_g \rho_g g_x + \Gamma_g u_i\big) u_g - \Gamma_g \frac{u_g^2}{2} \end{pmatrix} \tag{2.81}$$

2.4.3 Interfacial friction

Drift flux model

The drift flux approach is used to model the interfacial friction in bubbly and slug flow in a vertical flow. The interfacial friction between the two phases is modeled as

$$\begin{aligned} f_i &= C_i |u_R| u_R \\ C_i &= \frac{\alpha_g \alpha_l^3 \big(\rho_l - \rho_g\big) g \sin \phi_j}{|u_{gj}| u_{gj}} \\ u_R &= C_1 u_g - C_0 u_l \end{aligned} \tag{2.82}$$

where g is the gravitational constant, ϕ_j is the inclination angle of the flow, u_{gj} is the vapor/gas drift velocity, u_R is the relative velocity, and C_i is the friction coefficient. The relative velocity includes the effect of profile slip distribution by introducing two distribution coefficients, C_1 and C_0. These two coefficients account for the effect of a non-flat void fraction profile in the transverse cross-section and they are related

by

$$C_1 = \frac{1 - C_0 \alpha_g}{\alpha_l} \tag{2.83}$$

The remaining variables, the vapor/gas drift velocity and distribution coefficient C_0, are modeled with the EPRI correlation [22],

$$C_0 = \frac{L}{K_0 + \big(1 - K_0\big)\alpha_g^r} \tag{2.84a}$$

$$u_{gj} = 1.41 C \left[\frac{g\sigma\big(\rho_l - \rho_g\big)}{\rho_l^2} \right]^{1/4} \tag{2.84b}$$

where L, K_0, r, and C are parameters that requires additional correlations, see section 6.1 of RELAP5-3D code manual [19].

Drag coefficient model

The drag coefficient approach is used to model the interfacial friction in all flow regimes other than vertical bubbly and slug flows. The interfacial friction between the two phases is modeled as

$$\begin{aligned} f_i &= C_i |u_R| u_R \\ C_i &= \frac{1}{8} \rho_c S_F a_{lg} C_D \\ u_R &= u_g - u_l \end{aligned} \tag{2.85}$$

where ρ_c is the density of the continuous phase, C_D is the drag coefficient, a_{lg} is the volumetric interfacial area concentration, and S_F is the shape factor which is assumed to be unity. The drag coefficient (C_D) and the volumetric interfacial area concentration (a_{lg}) have different correlations depending on the flow regimes, see page 6-3 of RELAP5-3D code manual [19]. For a vertical annular mist flow (ANM), which is characterized by a liquid film along the wall and a vapor/gas core containing entrained liquid droplets, the friction coefficient contains two parts,

$$C_i^{\mathrm{ANM}} = \frac{1}{8} \rho_g a_{lg,ann} C_{D,ann} + \frac{1}{8} \rho_g a_{lg,drp} C_{D,drp} \tag{2.86}$$

For a vertical dispersed (droplet, mist) flow (MPR), which is characterized by continuous vapor with entrained liquid droplets, the friction coefficient is

$$C_i^{\mathrm{MPR}} = \frac{1}{8} \rho_g a_{lg,drp} C_{D,drp} \tag{2.87}$$

2.4.4 Wall friction

The wall friction terms account for the pressure loss due to the wall shear force. The two-phase multiplier approach is used to model the total friction. The phasic wall friction components are calculated by apportioning the total friction to the two phases using a technique derived from the Lockhart-Martinelli model, see page 3-177 of RELAP5-3D code manual [5]. Specifically, the two-phase multiplier approach models the two-phase pressure drop with

$$\left(\frac{\partial p}{\partial x}\right)_{2\phi} = \phi_l^2 \left(\frac{\partial p}{\partial x}\right)_l = \phi_g^2 \left(\frac{\partial p}{\partial x}\right)_g \tag{2.88}$$

where $(\partial p/\partial x)_l$ and $(\partial p/\partial x)_g$ are the liquid-alone and the gas-alone pressure drop; ϕ_l and ϕ_g are the liquid-alone and gas-alone two-phase friction multipliers. The liquid-alone and gas-alone pressure drop are modeled with the friction factor approach

$$\left(\frac{\partial p}{\partial x}\right)_l = \frac{1}{2D}\lambda_l^{'}\rho_l\alpha_l^2 u_l^2 \tag{2.89a}$$

$$\left(\frac{\partial p}{\partial x}\right)_g = \frac{1}{2D}\lambda_g^{'}\rho_g\alpha_g^2 u_g^2 \tag{2.89b}$$

where $\lambda_l^{'}$ and $\lambda_g^{'}$ are the friction factors modeled with,

$$\lambda_l^{'} = \text{FrictionFactor}\left(\frac{\alpha_l\rho_l D|u_l|}{\mu_l}\right) \tag{2.90a}$$

$$\lambda_g^{'} = \text{FrictionFactor}\left(\frac{\alpha_g\rho_g D|u_g|}{\mu_g}\right) \tag{2.90b}$$

where μ_l and μ_g are the viscosity of liquid and gas phase. The function 'FrictionFactor()' is used to calculate the friction factor with a given Reynolds number,

$$\text{FrictionFactor}\big(\text{Re}\big) \equiv \begin{cases} \frac{64}{\text{Re}}, & 0 \le \text{Re} \le 2200 \\ \big(3.75 - \frac{8250}{\text{Re}}\big)\big(\lambda_{3000} - \lambda_{2200}\big) + \lambda_{2200}, & 2200 < \text{Re} < 3000 \\ \left[-2.0\log_{10}\left(\frac{\varepsilon}{3.7D} + \frac{2.51}{\text{Re}\left[1.14 - 2.0\log_{10}\left(\frac{\varepsilon}{D} + \frac{21.25}{\text{Re}^{0.9}}\right)\right]}\right)\right]^{-2}, & \text{Re} \ge 3000 \end{cases} \tag{2.91}$$

where λ_{2200} and λ_{3000} are friction factors for $\text{Re} = 2200$ and $\text{Re} = 3000$, respectively.

The correlation between the two-phase friction multiplier is

$$\phi_l^2 = 1 + \frac{C}{\chi} + \frac{1}{\chi^2} \text{ and } \phi_g^2 = \chi^2 + C\chi + 1 \tag{2.92}$$

where C is the correlation coefficient and χ is the Lockhart-Martinelli ratio defined as

$$\phi_l^2 \equiv \frac{\left(\frac{\partial p}{\partial x}\right)_l}{\left(\frac{\partial p}{\partial x}\right)_g} = \frac{\phi_g^2}{\chi^2} \tag{2.93}$$

Combining Eq. (2.88), Eq. (2.89), and Eq. (2.92), the two-phase pressure drop is expressed as

$$\left(\frac{\partial p}{\partial x}\right)_{2\phi} = \frac{1}{2D}\left(\lambda_l^{'}\rho_l\alpha_l^2u_l^2 + \lambda_g^{'}\rho_g\alpha_g^2u_g^2 + C\sqrt{\lambda_l^{'}\rho_l\alpha_l^2u_l^2}\sqrt{\lambda_g^{'}\rho_g\alpha_g^2u_g^2}\right) \tag{2.94}$$

The two-phase pressure drop is then partitioned to each phase with

$$f_{wl} = \frac{\alpha_l Z_2}{\alpha_g + \alpha_l Z_2}\left(\frac{\partial p}{\partial x}\right)_{2\phi} \tag{2.95a}$$

$$f_{wg} = \frac{\alpha_g}{\alpha_g + \alpha_l Z_2}\left(\frac{\partial p}{\partial x}\right)_{2\phi} \tag{2.95b}$$

$$Z_2 = \frac{\lambda_l\rho_l u_l^2}{\lambda_l\rho_l u_l^2 + \lambda_g\rho_g u_g^2} \tag{2.95c}$$

where λ_l and λ_g are friction factors calculated with a different set of Reynolds number

$$\lambda_l = \text{FrictionFactor}\left(\frac{\rho_l D|u_l|}{\mu_l}\right) \tag{2.96a}$$

$$\lambda_g = \text{FrictionFactor}\left(\frac{\rho_g D|u_g|}{\mu_g}\right) \tag{2.96b}$$

2.4.5 Interfacial heat transfer

The interfacial heat transfer in the bulk fluid involves both heat and mass transfer. Temperature-gradient-driven bulk interfacial heat transfer is computed between each phase and the interface. The temperature of the interface is assigned at the saturation temperature. Heat transfer correlation for each side of the interface needs to be provided. Since both the superheated and the subcooled temperature are allowed, the heat transfer may be either into or away from the interface. All of the thermal energy transferred to the interface contributes to vaporization. Conversely, all of the thermal energy transferred away from the interface contributes to condensation. In other words, a superheated liquid and a superheated vapor/gas contribute to vaporization, while a subcooled liquid and a subcooled vapor/gas contribute to condensation. The net rate of mass transfer is determined by summing the contributions, positive and negative, from each side of the interface. Volumetric heat transfer coefficient (W/m^3K) is defined for four conditions: superheated liquid (SHL), subcooled liquid (SCL), superheated vapor/gas (SHG), and subcooled vapor/gas

(SCG) for each flow regime.

The volumetric heat transfer coefficient (H_{ik}) is modeled as

$$H_{ik} = a_{lg}\frac{k_k}{L}\mathrm{Nu} = a_{lg}h_{ik} \tag{2.97}$$

where

- H_{ik}: volumetric interfacial heat transfer coefficient for k-phase. [$\mathrm{W/(m^3 \cdot K)}$]
- k_k: thermal conductivity of k-phase. [$\mathrm{W/(m \cdot K)}$]
- L: characteristic length. [m]
- a_{lg}: volumetric interfacial area concentration. [$\mathrm{m^2/m^3}$]
- h_{ik}: interfacial heat transfer coefficient for k-phase. [$\mathrm{W/(m^2 \cdot K)}$]

The correlations for the volumetric interfacial area concentration and the interfacial heat transfer coefficient depend on flow regimes. The interfacial heat transfer in the transition regime is modeled through interpolation. The correlations for the interfacial heat transfer model are developed with two general guidelines: (a) the superheated liquid and subcooled vapor are not stable; (b) the vapor is assumed to be at the saturation temperature.

Bubbly flow

In a bubbly flow, the bubbles are viewed as spheres. The heat transfer coefficients are modeled as

$$H_{il} = \big(a_{lg}F_2F_3\big)\left\{\max\Big[-\frac{12k_l}{\pi d_b}\Delta T_{sl}\frac{\rho_l C_{p,l}}{\rho_g h_{lg}}\beta, \frac{k_l}{d_b}\big(2.0 + 0.74\mathrm{Re}_b^{0.5}\big)\Big] + 0.4|u_l|\rho_l C_{p,l}F_1\right\}, \text{ for SHL} \tag{2.98a}$$

$$H_{il} = \frac{F_3F_5h_{lg}\rho_l\rho_g\alpha_{bub}}{\rho_l - \rho_g}, \text{ for SCL} \tag{2.98b}$$

$$H_{ig} = h_{ig}a_{lg}F_6F_7, h_{ig} = 10^4\mathrm{W/m^2 \cdot K}, \text{ for SHG} \tag{2.98c}$$

$$H_{ig} = h_{ig}a_{lg}F_6F_7, h_{ig} = 10^4\mathrm{W/m^2 \cdot K}, \text{ for SCG} \tag{2.98d}$$

where F_1 to F_7 require additional sub-models, see 4-10 of RELAP5-3D code manual [19]. The specification of the volumetric heat transfer coefficients, H_{il} and H_{ig}, requires an estimate of the volumetric interfacial area concentration (a_{lg}). For a bubbly flow,

$$a_{lg} = \frac{3.6\alpha_g}{d_o} = 0.72\frac{\alpha_g\rho_l\big(u_g - u_l\big)^2}{\sigma} \tag{2.99}$$

Note that the heat transfer coefficient for SHG and SCG is made large to drive the vapor/gas temperature toward the saturation temperature.

Slug flow

In a slug flow, the interfacial heat transfer can be divided into two parts: (a) the heat transfer between the large Taylor bubbles and the liquid surrounding them, and (b) the heat transfer between the small bubbles in the liquid slug and their host liquid. The heat transfer contains the effect of these two parts. The total bulk heat transfer coefficient is

$$H_{ik} = H_{ik,Tb} + H_{ik,bub} \tag{2.100}$$

the correlations for different states are

$$H_{il} = 3.0 \times 10^6 a^*_{lg,Tb}\alpha_{Tb} + H_{il,bub}, \text{ for SHL} \tag{2.101a}$$

$$H_{il} = 1.18942\mathrm{Re}_l^{0.5}\mathrm{Pr}_l^{0.5}\frac{k_l}{D}a^*_{lg,Tb}\alpha_{Tb} + H_{il,bub}, \text{ for SCL} \tag{2.101b}$$

$$H_{ig} = \big(2.2 + 0.82\mathrm{Re}_g^{0.5}\big)\frac{k_g}{D}a^*_{lg,Tb}\alpha_{Tb} + h_{ig}F_6\big(1-\alpha_{Tb}\big)a_{lg,bub}, \text{ for SHG} \tag{2.101c}$$

$$H_{ig} = h_{ig}F_6 a^*_{lg,Tb}\alpha_{Tb} + h_{ig}F_6\big(1-\alpha_{Tb}\big)a_{lg,bub}, \text{ for SCG} \tag{2.101d}$$

where α_{Tb} is the average void fraction and $a^*_{lg,Tb}$ is the average volumetric interfacial area concentration for the Taylor bubble. The details for modeling α_{Tb} and $a^*_{lg,Tb}$ are given in page 4-15 of RELAP5-3D code manual [19]. The correlations for the contribution of bubbles in the liquid slug are based on those for a bubbly flow. Note that the heat transfer coefficient for SHL and SCG is made large to drive the temperature quickly toward the saturation temperature.

Annular mist flow

For an annular mist flow, the interfacial heat transfer results from two sources: (a) the heat transfer between the annular liquid film and vapor/gas core, and (b) the heat transfer between the vapor/gas core and the entrained liquid droplets. The overall volumetric heat transfer coefficient is

$$H_{ik} = H_{ik,ann} + H_{ik,drp} \tag{2.102}$$

the correlations for different states are

$$H_{il} = 3.0 \times 10^6 a_{lg,ann} F_{10} + \frac{k_l}{d_d} a_{lg,drp} F_{12} F_{13}, \text{ for SHL} \tag{2.103a}$$

$$H_{il} = 10^{-3} \rho_l C_{p,l} |u_l| a_{lg,ann} F_{10} + \frac{k_l}{d_d} a_{lg,drp} F_{13}, \text{ for SCL} \tag{2.103b}$$

$$H_{ig} = 0.023 \frac{k_g}{D} \mathrm{Re}_g^{0.8} a_{lg,ann} F_{10} + \frac{k_g}{d_d} \left(2.0 + 0.5 \mathrm{Re}_d^{0.5}\right) a_{lg,drp}, \text{ for SHG} \tag{2.103c}$$

$$H_{ig} = h_{ig} a_{lg,ann} F_{10} F_6 + h_{ig} a_{lg,drp} F_6, \text{ for SCG} \tag{2.103d}$$

where d_d is the characteristic droplet diameter, $a_{lg,ann}$ is the average interfacial area in the annular liquid film region, and $a_{lg,drp}$ is the average interfacial area in the entrained liquid droplets region. The details for modeling d_d, $a_{lg,ann}$, and $a_{lg,drp}$ are on page 4-22 of RELAP5-3D code manual [19]. Similarly, the correlations for SHL and SCG are developed to drive the superheated liquid and the subcooled vapor/gas to saturation temperature.

Dispersed (droplet, mist) flow

In a dispersed (droplet, mist) flow, the droplets are viewed as spheres. The interfacial heat transfer is from the entrained droplets to the surrounding vapor/gas. The correlations for different states are

$$H_{il} = \frac{k_l}{d_d} a_{lg} F_{12} F_{13} F_{23}, \text{ for SHL} \tag{2.104a}$$

$$H_{il} = \frac{k_l}{d_d} a_{lg} F_{13} F_{23}, \text{ for SCL} \tag{2.104b}$$

$$H_{ig} = \frac{k_g}{d_d} \left(2.0 + 0.5 \mathrm{Re}_d^{0.5}\right) a_{lg} F_{24}, \text{ for SHG} \tag{2.104c}$$

$$H_{ig} = h_{ig} a_{lg} F_6 F_{24}, \text{ for SCG} \tag{2.104d}$$

where a_{lg} is the interfacial area for the entrained droplets and d_d is the characteristic droplet diameter. The details for modeling a_{lg} and d_d are given in page 4-44 of RELAP5-3D code manual [19].

2.4.6 Wall heat transfer

When the solid surface has a convective boundary condition, the wall heat flux must be calculated. Experimentally, the wall heat transfer coefficient is determined by obtaining the experimental heat flux and dividing it by a wall-to-reference-temperature difference. The general expression for the total wall heat flux

is

$$q''_{wall} = h_{wg,g}\left(T_w - T_g\right) + h_{wg,spt}\left(T_w - T_{spt}\right) + h_{wg,spp}\left(T_w - T_{spp}\right) + h_{wl,l}\left(T_w - T_l\right) + h_{wl,spt}\left(T_w - T_{spt}\right) \quad (2.105)$$

where

- $h_{wg,g}$: heat transfer coefficient to vapor/gas, with the vapor/gas temperature as the reference temperature (W/m^2K).
- $h_{wg,spt}$: heat transfer coefficient to vapor/gas, with the saturation temperature at total pressure as the reference temperature (W/m^2K). Since we do not consider the non-condensable gas, the total pressure is the same as the vapor partial pressure, which is also the local pressure.
- $h_{wg,spp}$: heat transfer coefficient to vapor/gas, with the saturation temperature at vapor partial pressure as the reference temperature (W/m^2K). Since we do not consider the non-condensable gas, the total pressure is the same as the vapor partial pressure, which is also the local pressure.
- $h_{wl,l}$: heat transfer coefficient to liquid, with the liquid temperature as the reference temperature (W/m^2K).
- $h_{wl,spt}$: heat transfer coefficient to liquid, with the saturation temperature at total pressure as the reference temperature (W/m^2K).

Note that only one or two of the heat transfer coefficients are nonzero in most flow regimes. For example, during nucleate boiling, $h_{wl,l}$ and $h_{wl,spt}$ are nonzero, all other terms are zero. The exception is at high void fraction where $h_{wg,g}$ has a value to smooth the transition to vapor/gas cooling, see page 4-72 of RELAP5-3D code manual [19]. In this thesis, T_{sat} is used to denote the saturation temperature. The difference between the total pressure and vapor partial pressure is ignored since there is no non-condensable gas.

A boiling curve is used to govern the selection of heat transfer correlations for heat transfer from the wall to the fluid, see page 4-76 of RELAP5-3D code manual [19]. Figure 2.2 is the simplified version of the boiling curve logic. As is seen, much of the boiling curve logic is based on void fraction, liquid temperature, and wall surface temperature. Unlike RELAP5-3D which has many more modes to cover different geometries and system conditions, we only provide heat transfer modes relevant to a vertical flow in a pipe

- M2: Single-phase liquid convection
- M3/M4: Subcooled/saturated nucleate boiling
- M5/M6: Subcooled/saturated transition boiling

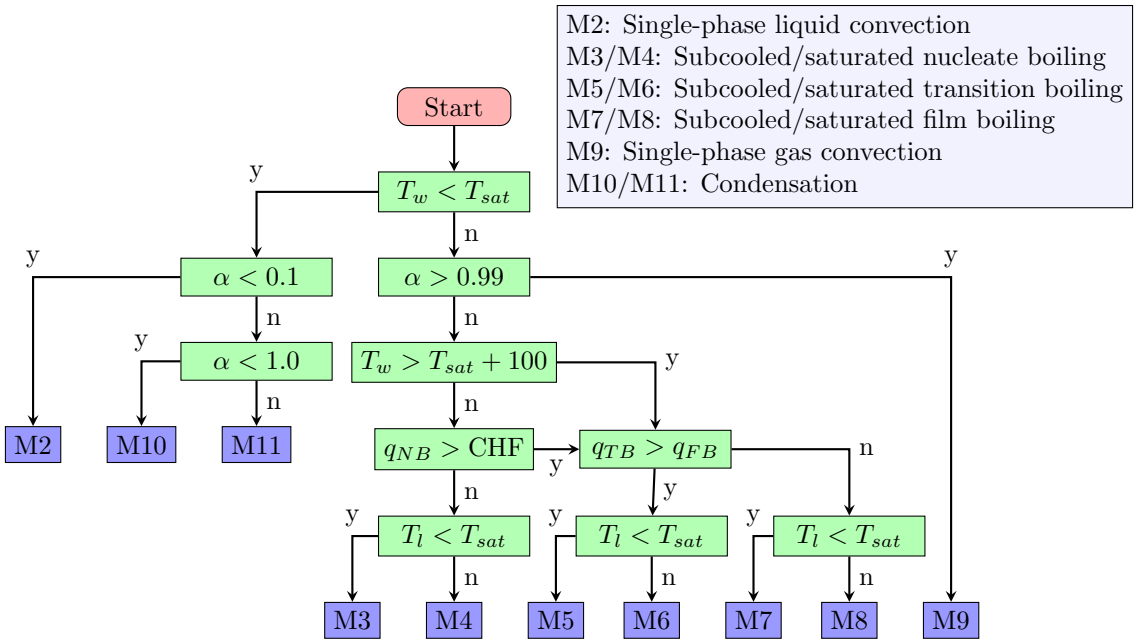

Figure 2.2: Flowchart for determining the wall heat transfer mechanism

- M7/M8: Subcooled/saturated film boiling
- M9: Single-phase gas convection
- M10/M11: Condensation

For simplifications, for problems where the wall temperature is not of interest and the flow is in pre-CHF region, the wall heat transfer correlations are not enabled. In this case, all wall heat flux is assumed to be transferred to the liquid phase, i.e.

$$Q_{wl} = a_{wall} q''_{wall}, \text{ and } Q_{wg} = 0 \tag{2.106}$$

where a_{wall} is the volumetric heated surface area and q''_{wall} is the total wall heat flux, which is determined by the heating power.

Convection

For the single-phase liquid (M2) and single-phase gas (M9) mode, the classical single-phase convection models are used. Correlations for forced turbulent convection, forced laminar convection, and natural convection are provided. The maximum heat transfer coefficient from these three correlations is used to ensure a smooth

transition, i.e.

$$\mathrm{Nu} \equiv \frac{hD}{k} = \max \begin{cases} 4.36, & \text{for forced laminar convection} \\ 0.023\mathrm{Re}^{0.8}\mathrm{Pr}^{0.4}, & \text{for forced turbulent convection} \\ \left[0.825 + \frac{0.387\left(\mathrm{Ra}_L\right)^{1/8}}{1+\left(\frac{0.492}{\mathrm{Pr}}\right)^{9/16}}\right]^{8/27}, & \text{for natural convection} \end{cases} \tag{2.107}$$

where the correlation for the forced turbulent convection is the classical Dittus-Boelter correlation, which is also used in other heat transfer modes; Re, Pr, and Ra are the Reynolds number, Prandtl number, and Rayleigh number, respectively. The dimensionless numbers used in the correlations are evaluated with either liquid or gas properties depending on the heat transfer mode, see page 4-76 of RELAP5-3D code manual [19].

Subcooled/saturated nucleate boiling

The Chen correlation is used for the subcooled and the saturated nucleate boiling (M3 and M4). The nucleate boiling correlation considers a macroscopic convection term and a microscopic boiling term. Though the correlation was based on the saturated liquid, it is also used for the subcooled liquid by using the bulk liquid temperature as the reference temperature for the convective part of the correlation.

$$q''_{wall} = h_{mac}\left(T_w - T_l\right)F + h_{mic}\left(T_w - T_{sat}\right)S, \quad \text{for subcooled nucleate boiling} \tag{2.108a}$$

$$q''_{wall} = h_{mac}\left(T_w - T_{sat}\right)F + h_{mic}\left(T_w - T_{sat}\right)S, \quad \text{for saturated nucleate boiling} \tag{2.108b}$$

where F is the Reynolds number factor and S is suppression factor. Details about F and S are given in page 4-96 of RELAP5-3D code manual [19]. h_{mac} accounts for the convective part that is modeled with the Ditus-Boelter correlation, and h_{mic} accounts for the microscopic boiling which is modeled with the Foster-Zuber correlation

$$h_{mic} = 0.00122\left(\frac{k_l^{0.79}C_{p,l}^{0.45}\rho_l^{0.49}g_c^{0.25}}{\sigma^{0.5}\mu_l^{0.29}h_{lg}^{0.24}\rho_g^{0.24}}\right)\left(\Delta T_w\right)^{0.24}\left(\Delta p\right)^{0.75} \tag{2.109}$$

where g_c is the gravitational conversion factor that equals to unity in SI units, h_{lg} is the enthalpy difference between the liquid and gas phase, and

$$\Delta T_w = T_w(\text{wall temperature}) - T_{sat}(\text{saturation temperature based on total pressure}) \tag{2.110a}$$

$$\Delta p = p_{sat}(\text{saturation pressure based on wall temperature}) - p(\text{local total pressure}) \tag{2.110b}$$

Subcooled/saturated transition boiling

For the transition boiling (M5 and M6), the same correlation is applied to both the subcooled and the saturated flow. The calculated heat flux for transition boiling is applied to post-CHF heat transfer. The total wall heat flux is obtained from components describing the wall-to-liquid heat flux and wall-to-vapor/gas heat flux,

$$q''_{wall} = q''_{\mathrm{CHF}} A_l M_l + h_{wg,g}\big(T_w - T_g\big)\big(1 - A_l M_l\big) \tag{2.111}$$

where q''_{CHF} is the critical heat flux, $h_{wg,g}$ is the heat transfer coefficient to vapor/gas obtained with Dittus-Bolter correlation, A_l is the fraction of wetted surface area, and M_l is the vertical stratification and mixture tracking model multipliers. Details of q''_{CHF}, A_l, and M_l are given in page 4-100 of RELAP5-3D code manual [19].

Subcooled/saturated film boiling

The film boiling (M7 and M8) is described by heat transfer mechanisms that occur in an inverted annular flow, slug flow, and dispersed flow. The wall-to-fluid heat transfer mechanisms are conduction across a vapor/gas film blanket next to a heated wall, convection to flowing vapor/gas and between the liquid droplets, and radiation across the film to a continuous liquid blanket or dispersed mixture of liquid droplets and vapor/gas. Details are given in page 4-103 of RELAP5-3D code manual [19].

Critical heat flux

RELAP5-3D uses the 1986 AECL-UO Critical Heat Flux Lookup Table [23] to evaluate the critical heat flux. The table was made based on tube data normalized to a tube with an inside diameter of 0.008 m. Correction factors are used to allow its use in other sized tubes and in rod bundles. The AECL-UO table is a three-dimensional table covering 15 pressures from 0.1 to 20.0 MPa, 14 values of mass flux from 0.0 to 7500.0 kg/m^{2}s, and 21 equilibrium qualities from -0.5 to 1.0.

2.5 Conclusion

In this chapter, the general 3D two-phase two-fluid model is derived from the instant balance law for each phase. Then, an area average to the 3D two-phase two-fluid model is performed to obtain the 1D two-phase two-fluid model, which will be used in the following chapters. Different forms of the 1D two-phase two-fluid model are explained and the conservative form is chosen as the starting point for constructing the numerical

solver in the following chapters. A brief introduction to the physical models and correlations is included in the second-half of this chapter.

Chapter 3

EQUATION OF STATE

A major challenge in simulating realistic two-phase flow problems is the complex properties of real water and steam. In practice, the properties of water and steam are formulated as complicated functions of pressure and temperature. There is not a simple form of EOS that can to be used for realistic two-phase flow problems. Because of the complexity in the EOS, analytical analysis to the two-phase two-fluid model is either rare or mathematically very complicated. In this chapter, we will try to overcome this challenge and provide formulations for the analytical analysis in the following chapters.

3.1 Introduction

As was already seen in Eq. (2.57), the two-phase two-fluid model requires explicitly the density, specific internal energy, and specific enthalpy. Choosing the phasic pressure and temperature as unknown variables, we need to provide formulations to calculate the density, specific internal energy, and specific enthalpy with given pressure and temperature. Choosing the phasic pressure and temperature as unknown variables and expanding the temporal partial derivative terms in continuity equation and energy equation, we obtain

$$\frac{\partial \alpha_l \rho_l}{\partial t} = \rho_l \frac{\partial \alpha_l}{\partial t} + \alpha_l \left[\left(\frac{\partial \rho_l}{\partial T_l} \right)_{p_l} \frac{\partial T_l}{\partial t} + \left(\frac{\partial \rho_l}{\partial p_l} \right)_{T_l} \frac{\partial p_l}{\partial t} \right] \tag{3.1a}$$

$$\frac{\partial \alpha_g \rho_g}{\partial t} = \rho_g \frac{\partial \alpha_g}{\partial t} + \alpha_g \left[\left(\frac{\partial \rho_g}{\partial T_g} \right)_{p_g} \frac{\partial T_g}{\partial t} + \left(\frac{\partial \rho_g}{\partial p_g} \right)_{T_g} \frac{\partial p_g}{\partial t} \right] \tag{3.1b}$$

$$\frac{\partial \alpha_l \rho_l e_l}{\partial t} = e_l \frac{\partial \alpha_l \rho_l}{\partial t} + \alpha_l \rho_l \left[\left(\frac{\partial e_l}{\partial T_l} \right)_{p_l} \frac{\partial T_l}{\partial t} + \left(\frac{\partial e_l}{\partial p_l} \right)_{T_l} \frac{\partial p_l}{\partial t} \right] \tag{3.1c}$$

$$\frac{\partial \alpha_g \rho_g e_g}{\partial t} = e_g \frac{\partial \alpha_g \rho_g}{\partial t} + \alpha_g \rho_g \left[\left(\frac{\partial e_g}{\partial T_g} \right)_{p_g} \frac{\partial T_g}{\partial t} + \left(\frac{\partial e_g}{\partial p_g} \right)_{T_g} \frac{\partial p_g}{\partial t} \right] \tag{3.1d}$$

Thus, 8 more partial derivatives are needed to solve for the phasic pressure and temperature. These 8 partial derivatives are

$$x_{11} \equiv \left(\frac{\partial \rho_l}{\partial T_l}\right)_{p_l}, \quad x_{12} \equiv \left(\frac{\partial \rho_l}{\partial p_l}\right)_{T_l} \tag{3.2a}$$

$$x_{21} \equiv \left(\frac{\partial \rho_g}{\partial T_g}\right)_{p_g}, \quad x_{22} \equiv \left(\frac{\partial \rho_g}{\partial p_g}\right)_{T_g} \tag{3.2b}$$

$$y_{11} \equiv \left(\frac{\partial e_l}{\partial T_l}\right)_{p_l}, \quad y_{12} \equiv \left(\frac{\partial e_l}{\partial p_l}\right)_{T_l} \tag{3.2c}$$

$$y_{21} \equiv \left(\frac{\partial e_g}{\partial T_g}\right)_{p_g}, \quad y_{22} \equiv \left(\frac{\partial e_g}{\partial p_g}\right)_{T_g} \tag{3.2d}$$

where 8 new variables are defined for brevity. Note that notation x and y here has no relation to the spatial position. As will be seen in the following sections, more similar variables will show up, which requires appropriate thermodynamic relations for simplification purposes.

3.2 Thermodynamic relations

3.2.1 Thermodynamic potential

A thermodynamic potential is a scalar quantity that is used to represent the thermodynamic state of a system [24]. The main thermodynamic potential that has a physical interpretation is the internal energy. For brevity reasons, the subscript k in the following derivations is ignored. The relations given in the following sections are valid for both liquid and gas phases. The standard form of the fundamental equation of state is given by relating the specific internal energy (e) to the specific entropy (s) and the specific volume (v)

$$e = e\big(s, v\big) \tag{3.3}$$

Note that the specific volume is the inverse of the density, i.e. $v = 1/\rho$. Then, the temperature and pressure are defined as

$$T = \left(\frac{\partial e}{\partial s}\right)_v, \quad p = -\left(\frac{\partial e}{\partial v}\right)_s \tag{3.4}$$

Two other thermodynamic potentials are used in this thesis: the specific enthalpy (h) and the specific Gibbs free energy ($\mathfrak{g}$). These two potentials are obtained by the following Legendre transformations

$$h = e + pv \tag{3.5a}$$

$$\mathfrak{g} = e - Ts + pv \tag{3.5b}$$

The specific internal energy (e), specific enthalpy (h), specific Gibbs free energy ($\mathfrak{g}$), specific entropy (s), and specific volume (v) are called extensive variables. The pressure (p) and temperature (T) are called intensive variables. The physical importance of these three thermodynamic potentials are reflected in the following processes [24]:

- When the entropy and volume of a closed system are held constant, the internal energy decreases and reaches a minimum value at equilibrium.
- When the pressure and volume of a closed system are held constant, the enthalpy decreases and reaches a minimum value at equilibrium.
- When the temperature and pressure of a closed system are held constant, the Gibbs free energy decreases and reaches a minimum value at equilibrium.

The variables that are held constant in these processes are called the natural variables of that potential, e.g. entropy and volume are the natural variables of internal energy. In short, the specific internal energy, specific enthalpy, and the specific Gibbs free energy are expressed as

$$e = e(s, v) \tag{3.6a}$$

$$h = h(p, v) \tag{3.6b}$$

$$\mathfrak{g} = \mathfrak{g}(T, p) \tag{3.6c}$$

The natural variables are important because if a thermodynamic potential is given as a function of its natural variables, all other thermodynamic properties of the system can be found from partial derivatives of that potential with respect to its natural variables.

3.2.2 Mathematics of thermodynamics

Consider a function $z(x, y)$, which defines a relation between x, y, and z. Then,

$$\left(\frac{\partial x}{\partial y}\right)_z = -\left(\frac{\partial x}{\partial z}\right)_y \cdot \left(\frac{\partial z}{\partial y}\right)_x = -\frac{\left(\frac{\partial z}{\partial y}\right)_x}{\left(\frac{\partial z}{\partial x}\right)_y} \tag{3.7}$$

This equation will be used extensively in the following transformations. For example, applying Eq. (3.7) to the functions $e(s, v)$, $h(p, v)$, and $\mathfrak{g}(p, T)$, we obtain

$$\left(\frac{\partial s}{\partial v}\right)_e = -\left(\frac{\partial e}{\partial v}\right)_s \cdot \left(\frac{\partial s}{\partial e}\right)_v \tag{3.8a}$$

$$\left(\frac{\partial p}{\partial v}\right)_h = -\left(\frac{\partial h}{\partial v}\right)_p \cdot \left(\frac{\partial p}{\partial h}\right)_v \tag{3.8b}$$

$$\left(\frac{\partial p}{\partial T}\right)_\mathfrak{g} = -\left(\frac{\partial \mathfrak{g}}{\partial T}\right)_p \cdot \left(\frac{\partial p}{\partial \mathfrak{g}}\right)_T \tag{3.8c}$$

Now, let's consider the 1D two-phase two-fluid model without the source term, i.e.

$$\frac{\partial \mathbf{U}}{\partial t} + \frac{\partial \mathbf{F}}{\partial x} + \mathbf{P}_{ix}\frac{\partial \alpha_g}{\partial x} + \mathbf{P}_{it}\frac{\partial \alpha_g}{\partial t} = \mathbf{0} \tag{3.9}$$

Eq. (3.9) contains explicitly the density, specific internal energy, specific enthalpy, and the pressure; but, Eq. (3.9) does not contain explicitly the specific entropy and the temperature. Thus, the specific enthalpy is a more natural thermodynamic potential for analysis purposes rather than specific internal energy or specific Gibbs free energy.

Taking p and v (or ρ) as independent variables, Eq. (3.9) involves the following partial derivatives

$$\left(\frac{\partial e}{\partial p}\right)_v, \quad \left(\frac{\partial e}{\partial v}\right)_p, \quad \left(\frac{\partial h}{\partial p}\right)_v, \quad \left(\frac{\partial h}{\partial v}\right)_p \tag{3.10a}$$

$$\left(\frac{\partial e}{\partial p}\right)_\rho, \quad \left(\frac{\partial e}{\partial \rho}\right)_p, \quad \left(\frac{\partial h}{\partial p}\right)_\rho, \quad \left(\frac{\partial h}{\partial \rho}\right)_p \tag{3.10b}$$

Note that these partial derivatives are not very informative. Without appropriate transformations, these partial derivatives make the analytical analysis in the following chapter very complicated. Using the relation

$h = e + pv$, $v = 1/\rho$, and the mathematical identity in Eq. (3.7), we can obtain

$$\left(\frac{\partial p}{\partial e}\right)_{\rho} = -\frac{\left(\frac{\partial \rho}{\partial h}\right)_{p}}{\left(\frac{\partial \rho}{\partial p}\right)_{h} + \frac{1}{\rho}\left(\frac{\partial \rho}{\partial h}\right)_{p}} \tag{3.11a}$$

$$\left(\frac{\partial p}{\partial \rho}\right)_{e} = \frac{1 + \frac{p}{\rho^2}\left(\frac{\partial \rho}{\partial h}\right)_{p}}{\left(\frac{\partial \rho}{\partial p}\right)_{h} + \frac{1}{\rho}\left(\frac{\partial \rho}{\partial h}\right)_{p}} \tag{3.11b}$$

The following two new auxiliary variables are defined to relate the partial derivatives in Eq. (3.10)

$$\gamma \equiv \frac{\left(\frac{\partial \rho}{\partial p}\right)_{h}}{\left(\frac{\partial \rho}{\partial p}\right)_{h} + \frac{1}{\rho}\left(\frac{\partial \rho}{\partial h}\right)_{p}} \tag{3.12a}$$

$$a^2 \equiv \frac{1}{\left(\frac{\partial \rho}{\partial p}\right)_{h} + \frac{1}{\rho}\left(\frac{\partial \rho}{\partial h}\right)_{p}} \tag{3.12b}$$

We can check that the partial derivative in Eq. (3.10) can be related through a and γ, i.e.

$$\left(\frac{\partial p}{\partial h}\right)_{\rho} = \frac{\rho(\gamma - 1)}{\gamma} \tag{3.13a}$$

$$\left(\frac{\partial p}{\partial \rho}\right)_{h} = \frac{a^2}{\gamma} \tag{3.13b}$$

$$\left(\frac{\partial p}{\partial e}\right)_{\rho} = \rho(\gamma - 1) \tag{3.13c}$$

$$\left(\frac{\partial p}{\partial \rho}\right)_{e} = a^2 - \frac{p}{\rho}(\gamma - 1) = \frac{p}{\rho} + \frac{\rho a^2 - \gamma p}{\rho} \tag{3.13d}$$

Eq. (3.13) is important, because it tells that all partial derivatives, excluding these related to temperature, can be expressed as simple functions of two auxiliary variables, a and γ. Of great importance is the physical meaning of a and γ. Through similar thermodynamic transformations, we obtain the following relations

$$a^2 \equiv \frac{1}{\left(\frac{\partial \rho}{\partial p}\right)_{h} + \frac{1}{\rho}\left(\frac{\partial \rho}{\partial h}\right)_{p}} = \frac{1}{\left(\frac{\partial \rho}{\partial p}\right)_{s}} \tag{3.14a}$$

$$\gamma \equiv \frac{\left(\frac{\partial \rho}{\partial p}\right)_{h}}{\left(\frac{\partial \rho}{\partial p}\right)_{h} + \frac{1}{\rho}\left(\frac{\partial \rho}{\partial h}\right)_{p}} = \frac{\left(\frac{\partial \rho}{\partial p}\right)_{h}}{\left(\frac{\partial \rho}{\partial p}\right)_{s}} \tag{3.14b}$$

Eq. (3.14a) shows that a is the isentropic speed of sound. Eq. (3.14b) shows that γ is the ratio of compressibility in an isenthalpic process (or throttling process) to the compressibility in an isentropic process. If the material is an ideal gas, γ is equal to the ratio of specific heat capacity. However, for a real gas, γ is

in general different than the ratio of specific heat capacity. For real water and steam, Figure 3.4 shows the behavior of a and γ for different pressure and temperature.

For further simplifications, we will define the following dimensionless variable

$$\varepsilon = \frac{\rho a^2 - \gamma p}{p} \tag{3.15}$$

For an ideal gas, we find that $\varepsilon_g = 0$ and for a real gas, e.g. steam, ε_g is a small number close to zero. ε_l is in general a large positive number. For real water and steam, Figure 3.4 shows the behavior of ε_l and ε_g for different pressure and temperature. Using Eq. (3.15), Eq. (3.13c) and Eq. (3.13d) are transformed into

$$\left(\frac{\partial p}{\partial e}\right)_{\rho} = \rho(\gamma - 1), \quad \left(\frac{\partial p}{\partial \rho}\right)_{e} = \frac{p}{\rho}(1 + \varepsilon) \tag{3.16}$$

The importance of these new auxiliary variables (especially, a, γ, and ε) is that they simplify significantly the Jacobian matrix in the following chapter. The application of these new auxiliary variables are given in **Appendix A**.

3.3 Properties of water and steam

In this thesis, the liquid and gas phases are taken to be water and steam, respectively. In the two-phase two-fluid model, because the right-hand side source terms are modeled as functions of the temperature, we choose the Gibbs free energy as the thermodynamic potential to specify the EOS. All partial derivatives shown in **Sec. 3.2** can be obtained through thermodynamic transformations with respect to the Gibbs free energy. Table 3.1 lists the thermodynamic properties and mechanical properties of water and steam that are needed. These properties are obtained with the International Association for the Properties of Water and Steam (IAPWS-IF97) industrial formulation [15].

3.3.1 IAPWS: Thermodynamic properties of water and steam

The IAPWS-IF97 consists of a set of equations for different regions, including the subcooled water region (region 1), the superheated steam region (region 2, 5), the saturation line (region 4), and the critical region (region 3). These regions are shown in Figure 3.1. In this thesis, we implemented the region in the red box which covers part of region 1, region 2, and region 4, i.e.

$$273.15\text{K} \leq T \leq 1073.15\text{K}, \quad 611.675\text{Pa} \leq p \leq 16.529\text{MPa} \tag{3.17}$$

Table 3.1: Thermodynamic and mechanical properties of water and steam

Variable	Property name	Variable	Property name
T	Temperature	C_p	Specific isobaric heat capacity
p	Pressure	$\left(\frac{\partial \rho}{\partial T}\right)_p$	–
v	Specific volume	$\left(\frac{\partial \rho}{\partial p}\right)_T$	–
ρ	Density	$\left(\frac{\partial e}{\partial T}\right)_p$	–
e	Specific internal energy	$\left(\frac{\partial e}{\partial p}\right)_T$	–
h	Specific enthalpy	k	Thermal conductivity
s	Specific entropy	μ	Viscosity
$\mathfrak{g}$	Specific Gibbs free energy	σ	Surface tension
a	Adiabatic speed of sound		
γ	Gamma coefficient		

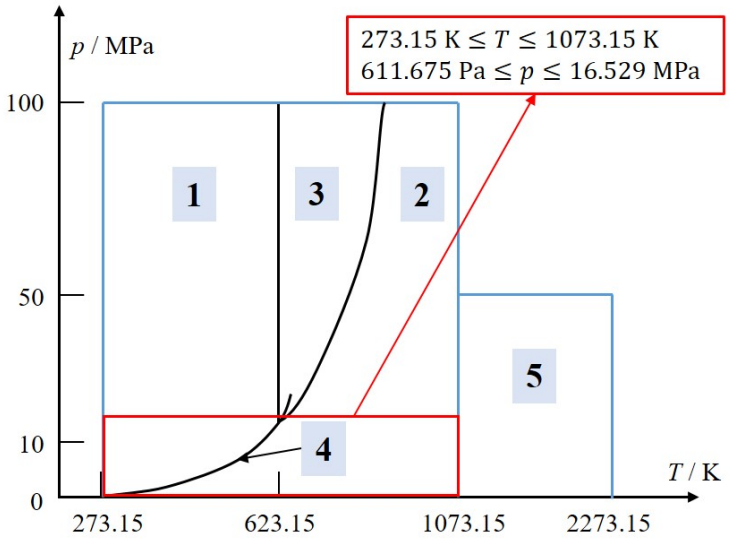

Figure 3.1: Schematic of IAPWS-IF97 for the thermodynamic properties of water and steam

This selected region covers the normal conditions in nuclear reactor thermal-hydraulic simulations.

The EOS in region 1 and region 2 is specified by the specific Gibbs free energy, which is implemented as a function of pressure and temperature, i.e.

$$\mathfrak{g} = \mathfrak{g}(T, p) \tag{3.18}$$

All other thermodynamic properties are derived from this equation using appropriate combination of the specific Gibbs free energy and its derivatives. For brevity, we will define the following variables

$$\mathfrak{g}_1 \equiv \left(\frac{\partial \mathfrak{g}}{\partial T}\right)_p, \mathfrak{g}_2 \equiv \left(\frac{\partial \mathfrak{g}}{\partial p}\right)_T, \mathfrak{g}_{11} \equiv \left(\frac{\partial^2 \mathfrak{g}}{\partial T^2}\right)_p, \mathfrak{g}_{22} \equiv \left(\frac{\partial^2 \mathfrak{g}}{\partial p^2}\right)_T, \mathfrak{g}_{12} \equiv \left(\frac{\partial^2 \mathfrak{g}}{\partial T \partial p}\right) \tag{3.19}$$

Relations between the relevant thermodynamic properties and the specific Gibbs free energy are

$$v = \rho^{-1} = \mathfrak{g}_2 \tag{3.20a}$$

$$e = \mathfrak{g} - T\mathfrak{g}_1 - p\mathfrak{g}_2, \quad h = \mathfrak{g} - T\mathfrak{g}_1 \tag{3.20b}$$

$$a^2 = \frac{Tv^2\mathfrak{g}_{11}}{T\mathfrak{g}_{12}^2 - T\mathfrak{g}_{11}\mathfrak{g}_{22}}, \quad \gamma = \frac{T\mathfrak{g}_{12}^2 - T\mathfrak{g}_{11}\mathfrak{g}_{22} - v\mathfrak{g}_{12}}{T\mathfrak{g}_{12}^2 - T\mathfrak{g}_{11}\mathfrak{g}_{22}} \tag{3.20c}$$

$$C_p = -T\mathfrak{g}_{11} \tag{3.20d}$$

$$\left(\frac{\partial \rho}{\partial T}\right)_p = -\frac{1}{v^2}\mathfrak{g}_{12}, \quad \left(\frac{\partial \rho}{\partial p}\right)_T = -\frac{1}{v^2}\mathfrak{g}_{22} \tag{3.20e}$$

$$\left(\frac{\partial e}{\partial T}\right)_p = -T\mathfrak{g}_{11} - p\mathfrak{g}_{12}, \quad \left(\frac{\partial \rho}{\partial T}\right)_p = -T\mathfrak{g}_{12} - p\mathfrak{g}_{22} \tag{3.20f}$$

The region 4 (saturation line) specifies the boundary between region 1 (subcooled water) and region 2 (superheated steam). The saturation line is given by an implicit quadratic function of the saturation pressure (p_{sat}) and the saturation temperature (T_{sat}),

$$x^2y^2 + n_1x^2y + n_2x^2 + n_3xy^2 + n_4xy + n_5x + n_6y^2 + n_7y + n_8 = 0 \tag{3.21}$$

where

$$x = \left(\frac{p_{sat}}{p^*}\right)^{1/4}, \quad y = \frac{T_{sat}}{T^*} + \frac{n_9}{T_{sat}/T^* - n_{10}} \tag{3.22}$$

where $p^* = 1\text{MPa}$ and $T^* = 1\text{K}$; the coefficients n_1 to n_{10} are given in IAPWS-IF97 [15].

3.3.2 IAPWS: Viscosity of ordinary water substance

The correlating equation for the shear viscosity of pure water substance is represented as

$$\bar{\mu} = \bar{\mu}_0(\bar{T}) \times \bar{\mu}_1(\bar{T}, \bar{\rho}) \times \bar{\mu}_2(\bar{T}, \bar{\rho}) \tag{3.23}$$

where the first factor $\bar{\mu}_0$ represents the viscosity in the dilute-gas limit, the second factor $\bar{\mu}_1$ represents the contribution to viscosity due to finite density, and the third factor $\bar{\mu}_2$ represents the critical enhancement of the viscosity. Details of these three factors are specified in IAPWS-IF97 [15]. The IAPWS-IF97 is used to determine the density when the state point is specified by the temperature and pressure or other state variables. The dimensionless variables in Eq. (3.23) are defined as

$$\bar{T} = T/T^*, \quad \text{with} \quad T^* = 647.096\text{K} \tag{3.24a}$$

$$\bar{\rho} = \rho/\rho^*, \quad \text{with} \quad \rho^* = 322.0\text{kg} \cdot \text{m}^{-3} \tag{3.24b}$$

$$\bar{\mu} = \mu/\mu^*, \quad \text{with} \quad \mu^* = 1.00 \times 10^{-6}\text{Pa} \cdot \text{s} \tag{3.24c}$$

Eq. (3.23) is valid in the following ranges

$$0 < p < p_t \quad \text{and} \quad 273.16\text{K} \leq T \leq 1173.15\text{K} \tag{3.25a}$$

$$p_t < p < 300 \text{ MPa} \quad \text{and} \quad T_m(p) \leq T \leq 1173.15\text{K} \tag{3.25b}$$

where T_m is the pressure-dependent melting temperature and p_t is the triple-point pressure.

3.3.3 IAPWS: Surface tension of ordinary water substance

The correlating equation for the surface tension of pure water substance is represented as

$$\sigma = 235.8 \cdot \tau^{1.26}(1 - 0.625\tau) \quad [\text{mN/m}] \tag{3.26}$$

where

$$\tau = 1 - T/T_c, \quad \text{with} \quad T_c = 647.096 \text{ K} \tag{3.27}$$

This correlating equation is valid for temperature between the triple point (0.01 °C) and the reference temperature T_c. The correlating equation for the surface tension depends only on the temperature. In practice, this temperature is the saturation temperature of water and steam. When the pressure is specified

as input to obtain surface tension, a saturation temperature corresponding to the given pressure is calculated at first with IAPWS-IF97.

3.3.4 IAPWS: Thermal conductivity of ordinary water substance

The correlating equation for the thermal conductivity of pure water substance is represented as

$$\bar{k} = \bar{k}_0\big(\bar{T}\big) \times \bar{k}_1\big(\bar{T}, \bar{\rho}\big) + \bar{k}_2\big(\bar{T}, \bar{\rho}\big) \tag{3.28}$$

where the first factor $\bar{k}_0$ represents the thermal conductivity in the dilute-gas limit, the second factor $\bar{k}_1$ represents the contribution to thermal conductivity due to finite density, and the third additive contribution $\bar{k}_2$ represents the critical enhancement of the thermal conductivity. Details of these three factors are specified in [15]. The IAPWS-IF97 is used to determine the density when the state point is specified by the temperature and pressure or other state variables. The dimensionless variables in Eq. (3.28) are defined as

$$\bar{T} = T/T^*, \quad \text{with} \quad T^* = 647.096\text{K} \tag{3.29a}$$

$$\bar{\rho} = \rho/\rho^*, \quad \text{with} \quad \rho^* = 322.0\text{kg} \cdot \text{m}^{-3} \tag{3.29b}$$

$$\bar{k} = k/k^*, \quad \text{with} \quad k^* = 1.00 \times 10^{-3}\text{W} \cdot \text{K}^{-1} \cdot \text{m}^{-1} \tag{3.29c}$$

Eq. (3.28) is valid in the following ranges

$$0 < p < p_t \quad \text{and} \quad 273.16\text{K} \leq T \leq 1173.15\text{K} \tag{3.30a}$$

$$p_t < p < 100 \text{ MPa} \quad \text{and} \quad T_m\big(p\big) \leq T \leq 1173.15\text{K} \tag{3.30b}$$

where T_m is the pressure-dependent melting temperature and p_t is the triple-point pressure.

3.4 Implementation and computer program verification

The C++ programming language is used to implement the correlating equations discussed in previous sections. First, we implement the correlating equations in a continuous form, which we call IAPWS-C. Because the correlating equations have to be evaluated extensively in the numerical solver, we implement a tabulated version of the correlating equations, which we call IAPWS-T. For the tabulated version IAPWS-T, the properties of water and steam are pre-calculated with IAPWS-C at a set of design points $\big(T_i, p_j\big)$ and then a bi-linear interpolation scheme is used to interpolate values at other states. For the range specified

Table 3.2: Program verification table for thermodynamic properties of water and steam with IAPWS-C

Variable	$T = 300\text{K}, p = 3\text{MPa}$		$T = 500\text{K}, p = 3\text{MPa}$	
	Reference	IAPWS-C	Reference	IAPWS-C
$v : \text{m}^3/\text{kg}$	1.00215168 E-03	1.00215167(97) E-03	1.20241800E-03	1.20241800(34) E-03
$h : \text{kJ/kg}$	1.15331273 E+02	1.15331273(02) E+02	9.75542239E+02	9.75542239(10) E+02
$e : \text{kJ/kg}$	1.12324818 E+02	1.12324817(98) E+02	9.71934985E+02	9.71934985(09) E+02
$s : \text{kJ/kg}$	3.92294792 E-01	3.92294792(40) E-01	2.58041912	2.58041912(01)
$a : \text{m/s}$	1.50773921 E+03	1.50773920(97) E+03	1.24071337E+02	1.24071337(31) E+03
$C_p : \text{kJ/(kg K)}$	4.17301218	4.17301218(41)	4.65580682	4.65580682(21)

in Eq. (3.17), 545 design points are used for temperature and 565 design points are used for pressure. Verification of both IAPWS-C and IAPWS-T is performed. The results of IAPWS-C are compared with the reference values given in the specification [15]. The results of IAPWS-T are compared with the results of IAPWS-C.

Table 3.3: Program verification table for the viscosity of water and steam with IAPWS-C

T (K)	$\rho : \text{kg/m}^3$	Reference $\mu : \mu\text{Pa} \cdot \text{s}$	IAPWS-C $\mu : \mu\text{Pa} \cdot \text{s}$
298.15	998.0	889.735100	889.735100(15)
298.15	1200.0	1437.649467	1437.649466(69)
373.15	1000.0	307.883622	307.883622(34)
433.15	1.0	14.538324	14.538324(48)
433.15	1000.0	217.685358	217.685358(26)
873.15	1.0	32.619287	32.619286(97)
873.15	100.0	35.802262	35.802261(72)
873.15	600.0	77.430195	77.430195(23)

Table 3.4: Program verification table for the surface tension of water and steam with IAPWS-C

T (K)	Reference $\sigma : \text{mN/m}$	IAPWS-C $\sigma : \text{mN/m}$
273.16	75.65	75.64(61)
323.15	67.94	67.94(39)
373.15	58.91	58.91(19)
423.15	48.74	48.74(13)
473.15	37.67	37.67(45)
523.15	26.04	26.04(30)
573.15	14.36	14.35(96)

Table 3.5: Program verification table for the thermal conductivity of water and steam with IAPWS-C

T (K)	$\rho : \text{kg/m}^3$	Reference $k : \text{mW/(m} \cdot \text{K)}$	IAPWS-C $k : \text{mW/(m} \cdot \text{K)}$
298.15	0.0	18.4341883	18.4341883(50)
298.15	998.0	607.712868	607.712867(59)
298.15	1200.0	799.038144	799.038143(56)

Table 3.2, Table 3.3, Table 3.4, and Table 3.5 show the verification of IAPWS-C for thermodynamic properties, viscosity, surface tension, and thermal conductivity, respectively. As expected, the results from

Table 3.6: Program verification table for properties of water and steam with IAPWS-C and IAPWS-T

Variable	IAPWS-C	IAPWS-T	IAPWS-C	IAPWS-T
	$T = 325.17\text{K}, p = 1.2525\text{MPa}$		$T = 583.87\text{K}, p = 1.2525\text{MPa}$	
ρ : kg/m^3	9.876168(69) E+02	9.876163(90) E+02	4.786684(19)	4.786688(78)
e : kJ/kg	2.176144(42) E+02	2.176144(88) E+02	2.806656(19) E+03	2.806655(77) E+03
h : kJ/kg	2.188826(47) E+02	2.188826(46) E+02	3.068319(58) E+03	3.068319(51) E+03
a : m/s	1.549400(03) E+03	1.549395(74) E+03	5.822827(13) E+02	5.822826(61) E+02
γ	1.270658(07)	1.270654(55)	1.299694(80)	1.299694(89)
C_p : kJ/(kg K)	4.177399(70)	4.177401(58)	2.171046(63)	2.171048(08)
k : mN/m	6.434786(66) E+02	6.433170(15) E+02	4.661400(94) E+01	4.590544(58) E+01
μ : μPa s	5.286551(92) E+02	5.289837(78) E+02	2.063717(08) E+01	2.061687(93) E+01
	$T = 345.08\text{K}, p = 5.2525\text{MPa}$		$T = 648.24\text{K}, p = 5.2525\text{MPa}$	
ρ : kg/m^3	9.789240(94) E+02	9.789239(03) E+02	1.920055(78) E+01	1.920068(78) E+01
e : kJ/kg	3.000020(02) E+02	3.000020(20) E+02	2.855556(45) E+03	2.855554(70) E+03
h : kJ/kg	3.053675(86) E+02	3.053676(27) E+02	3.129116(21) E+03	3.129114(38) E+03
a : m/s	1.567040(62) E+03	1.567039(13) E+03	5.929655(29) E+02	5.929644(71) E+02
γ	1.347295(17)	1.347293(89)	1.296541(03)	1.296540(37)
C_p : kJ/(kg K)	4.178251(62)	4.178251(99)	2.571846(38)	2.571881(52)
k : mN/m	6.640030(48) E+02	6.638393(08) E+02	5.881207(16) E+01	5.747597(16) E+01
μ : μPa s	3.944396(02) E+02	3.947377(60) E+02	2.329529(93) E+01	2.325797(22) E+01

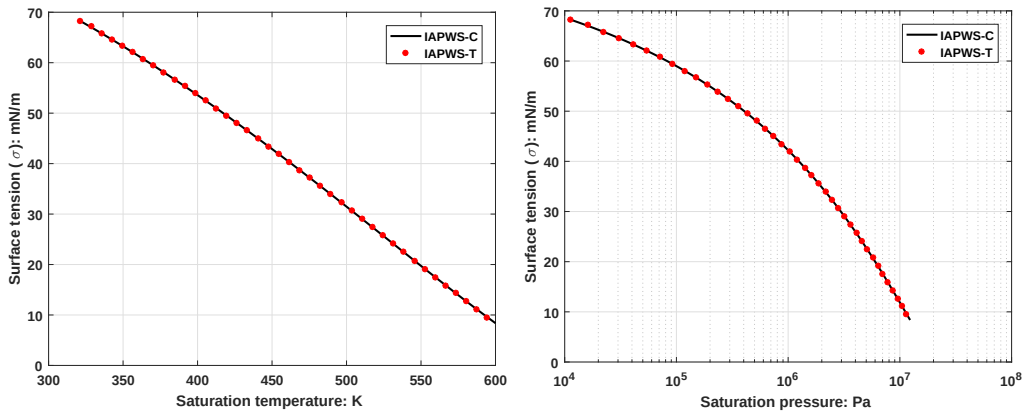

(a) (b)

Figure 3.2: IAPWS-C: Surface tension of water/steam in saturation conditions

IAPWS-C are consistent with the reference values.

Table 3.6 shows the verification of IAPWS-T. Results from IAPWS-T are compared with results from IAPWS-C. Figure 3.2 also shows the comparison of IAPWS-C and IAPWS-T surface tension at saturation conditions. As expected, the results from IAPWS-T are consistent with the results from IAPWS-C. For reference, Figure 3.3, Figure 3.4, and Figure 3.5 show the properties of water and steam at different states.

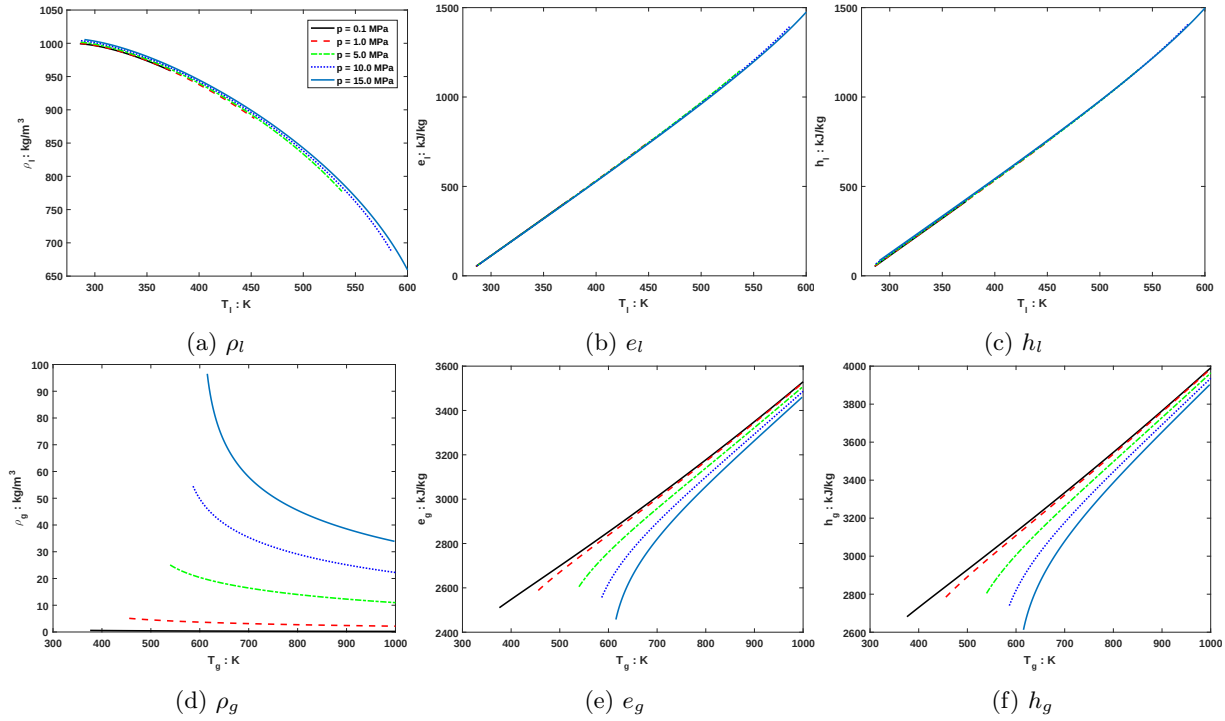

(a) ρ_l (b) e_l (c) h_l

(d) ρ_g (e) e_g (f) h_g

Figure 3.3: IAPWS-C: properties of water and steam I.

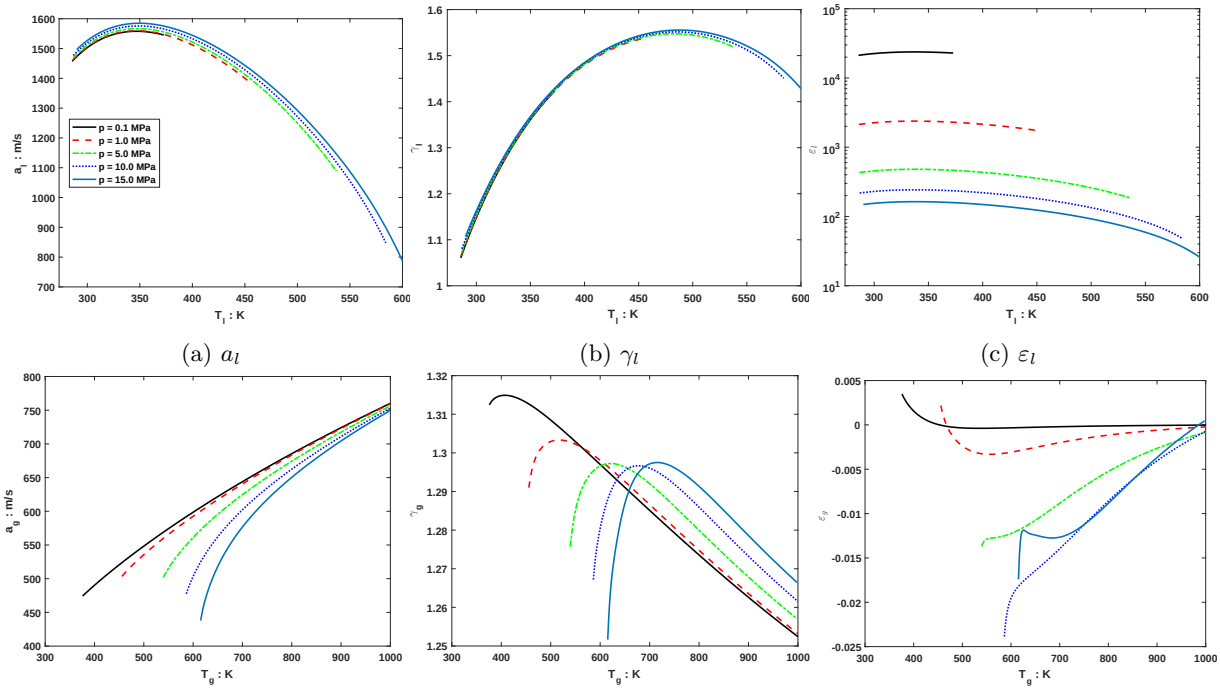

(a) a_l (b) γ_l (c) ε_l

(d) a_g (e) γ_g (f) ε_g

Figure 3.4: IAPWS-C: properties of water and steam II.

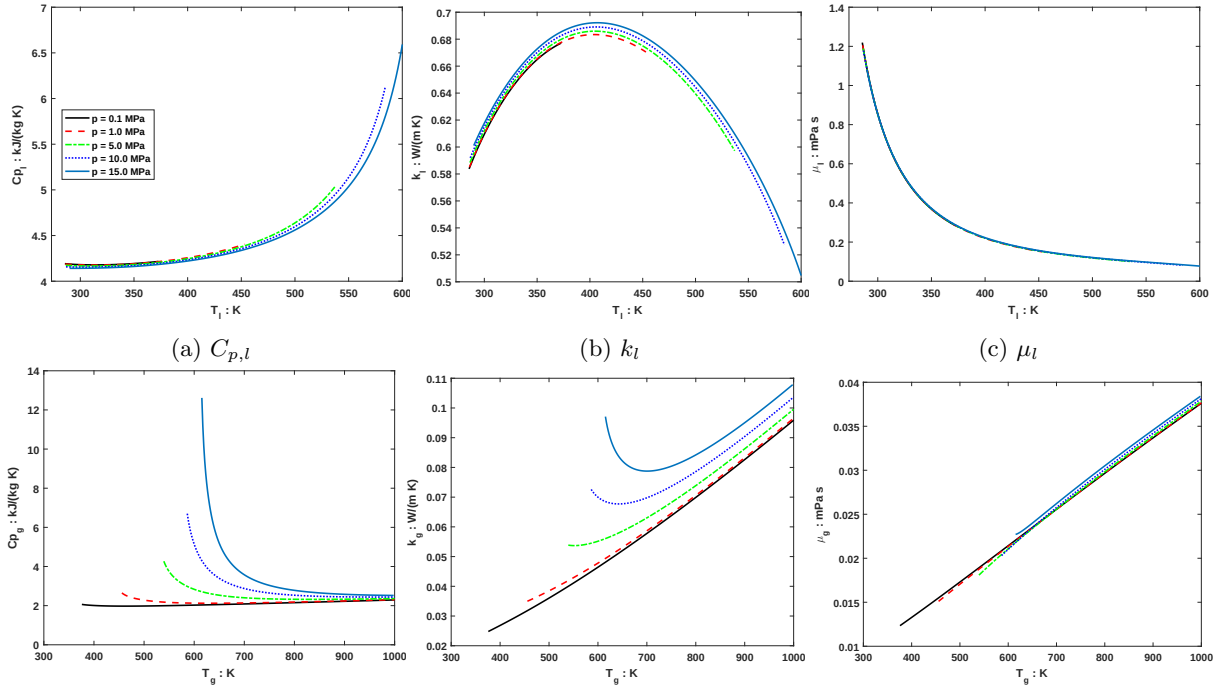

(a) $C_{p,l}$ (b) k_l (c) μ_l

(d) $C_{p,g}$ (e) k_g (f) μ_g

Figure 3.5: IAPWS-C: properties of water and steam III

3.5 Conclusion

In this chapter, a few new auxiliary variables are introduced to overcome the challenge in analyzing the two-phase two-fluid model with a complex EOS. Through thermodynamic transformations, it is found that the partial derivatives related to the two-phase two-fluid model can be replaced by simple algebraic functions of these new auxiliary variables. These new auxiliary variables are critical for simplifying the Jacobian matrix of the two-phase two-fluid model in the following chapter.

The EOS and the properties of water and steam are implemented with the help of the specific Gibbs free energy. Once the specific Gibbs free energy and its partial derivatives (with respect to pressure and temperature) are given, it is shown that all thermodynamic properties of water and steam can be written as functions of the specific Gibbs free energy and its partial derivatives. The EOS is implemented for practical application in nuclear reactor thermal-hydraulic simulations and verified.

Chapter 4

ANALYTIC ANALYSIS

4.1 Introduction

The two-phase two-fluid model originates from the conservation laws for phasic mass, momentum, and energy. The governing equation has the form of a hyperbolic Partial Differential Equation (PDE). Analytical analysis, especially the characteristic analysis, of the PDE is essential for understanding the behavior of the system and constructing a stable solver. From the mathematical point of view, an analytical analysis to the system provides the dynamic behavior of the system under different conditions; from the numerical point of view, an analytical analysis provides the upwind information of the system, which is essential to construct a stable and accurate numerical solver.

This chapter presents a detailed characteristic analysis and dispersion analysis of the two-phase two-fluid model with the help of EOS formulations given in **Chapter 3**.

4.2 Review of notions

4.2.1 Quasi-linear system

The 1D two-phase two-fluid model belongs to a general systems of first-order partial differential equations of the form [25]

$$\frac{\partial u_i}{\partial t} + \sum_{j=1}^{m} a_{ij}\big(u_1, \cdots, u_m; x, t\big)\frac{\partial u_j}{\partial x} + s_i\big(u_1, \cdots, u_m; x, t\big) = 0, \quad \text{for } i = 1, \cdots, m \tag{4.1}$$

which is a system of m equations with m unknowns (u_i) that depends on space (x) and time (t). System (4.1) can be written in a matrix form

$$\frac{\partial \mathbf{U}}{\partial t} + \mathbb{A}\frac{\partial \mathbf{U}}{\partial x} + \mathbf{S} = \mathbf{0} \tag{4.2}$$

where

$$\mathbf{U} = \begin{pmatrix} u_1 \\ u_2 \\ \vdots \\ u_m \end{pmatrix}, \mathbb{A} = \begin{pmatrix} a_{11} & \cdots & a_{1m} \\ a_{21} & \cdots & a_{2m} \\ \vdots & \vdots & \vdots \\ a_{m1} & \cdots & a_{mm} \end{pmatrix}, \mathbf{S} = \begin{pmatrix} s_1 \\ s_2 \\ \vdots \\ s_m \end{pmatrix} \tag{4.3}$$

System (4.2) is linear when entries of coefficient matrix $\mathbb{A}$ and vector $\mathbf{S}$ do not depends on unknown vector $\mathbf{U}$; system (4.2) is called quasi-linear [25] when the coefficient matrix $\mathbb{A}$ is a function of the unknown vector $\mathbf{U}$, i.e. $\mathbb{A} = \mathbb{A}\big(\mathbf{U}\big)$. The quasi-linear system is in general a system of non-linear equations. Two simplest examples of system (4.2) are the linear advection equation

$$\frac{\partial u}{\partial t} + a\frac{\partial u}{\partial x} = 0 \tag{4.4}$$

and the inviscid Burgers equation

$$\frac{\partial u}{\partial t} + u\frac{\partial u}{\partial x} = 0 \tag{4.5}$$

Definition 4.1. Conservation laws. Conservation laws are partial differential equations that can be written into the form

$$\frac{\partial \mathbf{U}}{\partial t} + \frac{\partial \mathbf{F}\big(\mathbf{U}\big)}{\partial x} = \mathbf{S} \tag{4.6}$$

where $\mathbf{U}$ is the vector of conserved variables, $\mathbf{S}$ is the vector of source terms, and $\mathbf{F}\big(\mathbf{U}\big)$ is the vector of fluxes

$$\mathbf{U} = \begin{pmatrix} u_1 \\ u_2 \\ \vdots \\ u_m \end{pmatrix}, \mathbf{F} = \begin{pmatrix} f_1 \\ f_2 \\ \vdots \\ f_m \end{pmatrix} = \begin{pmatrix} f_1\big(u_1, \cdots, u_m\big) \\ f_2\big(u_1, \cdots, u_m\big) \\ \vdots \\ f_m\big(u_1, \cdots, u_m\big) \end{pmatrix} \tag{4.7}$$

An example of the conservation law is the one-dimensional Euler equation for single-phase gas

$$\frac{\partial \rho}{\partial t} + \frac{\partial \rho u}{\partial x} = 0 \tag{4.8a}$$

$$\frac{\partial \rho u}{\partial t} + \frac{\partial \big(\rho u^2 + p\big)}{\partial x} = 0 \tag{4.8b}$$

$$\frac{\partial \rho E}{\partial t} + \frac{\partial \big(\rho u E + p u\big)}{\partial x} = 0 \tag{4.8c}$$

where ρ is the density, u is the velocity, p is the pressure, and $E = e + u^2/2$ is the specific total energy. In a

vector form,

$$\mathbf{U}_{\text{Euler}} = \begin{pmatrix} \rho \\ \rho u \\ \rho E \end{pmatrix}, \mathbf{F}_{\text{Euler}} = \begin{pmatrix} \rho u \\ \rho u^2 + p \\ \rho u E + p u \end{pmatrix} \tag{4.9}$$

Definition 4.2. Jacobian matrix. The Jacobian matrix of the flux function $\mathbf{F}\big(\mathbf{U}\big)$ is the matrix $\mathbb{A}\big(\mathbf{U}\big)$ defined as

$$\mathbb{A}\big(\mathbf{U}\big) \equiv \frac{\partial \mathbf{F}}{\partial \mathbf{U}} = \begin{pmatrix} \partial f_1/\partial u_1 & \cdots & \partial f_1/\partial u_m \\ \partial f_2/\partial u_1 & \cdots & \partial f_2/\partial u_m \\ \vdots & \vdots & \vdots \\ \partial f_m/\partial u_1 & \cdots & \partial f_m/\partial u_m \end{pmatrix} \tag{4.10}$$

For example, the Jacobian matrix of the Euler equation is

$$\mathbb{A}_{\text{Euler}} = \begin{pmatrix} 0 & 1 & 0 \\ -u^2 + \big[a^2 + \big(\gamma - 1\big)\big(u^2 - H\big)\big] & 2u - \big(\gamma - 1\big)u & \gamma - 1 \\ -uH + u\big[a^2 + \big(\gamma - 1\big)\big(u^2 - H\big)\big] & H - \big(\gamma - 1\big)u^2 & u + \big(\gamma - 1\big)u \end{pmatrix} \tag{4.11}$$

where $H = E + p/\rho$ is the specific total enthalpy. We omit the derivation of this Jacobian matrix, because it is a straightforward simplification of the Jacobian matrix for a two-phase system, which will be derived later. Two auxiliary variables, a and γ, are defined by Eq. (3.12) of **Chapter 3**.

The conservation laws can be written in a quasi-linear form

$$\frac{\partial \mathbf{U}}{\partial t} + \frac{\partial \mathbf{F}}{\partial x} = \frac{\partial \mathbf{U}}{\partial t} + \mathbb{A}\frac{\partial \mathbf{U}}{\partial x} = \mathbf{S} \tag{4.12}$$

Definition 4.3. Eigenvalues/eigenvectors. The eigenvalues λ_i and right eigenvectors $\mathbf{K}_i$ of a matrix $\mathbb{A}$ are defined by

$$\mathbb{A}\mathbf{K}_i = \lambda_i \mathbf{K}_i \tag{4.13}$$

For example, the eigenvalues and eigenvectors of the Jacobian matrix Eq. (4.11) are

$$\lambda_1 = u - a, \lambda_2 = u, \lambda_3 = u + a \tag{4.14}$$

$$\mathbf{K}_1 = \begin{pmatrix} 1 \\ u - a \\ H - ua \end{pmatrix}, \mathbf{K}_2 = \begin{pmatrix} 1 \\ u \\ H - \gamma^* a^2 \end{pmatrix}, \mathbf{K}_3 = \begin{pmatrix} 1 \\ u + a \\ H + ua \end{pmatrix}, \tag{4.15}$$

where $\gamma^* = 1/(\gamma - 1)$.

Definition 4.4. Hyperbolic system. A system is said to be hyperbolic if the Jacobian matrix $\mathbb{A}$ has m real eigenvalues, $\lambda_1, \cdots, \lambda_m$, and a set of m linearly independent right eigenvectors, $\mathbf{K}_1, \cdots, \mathbf{K}_m$. The system is said to be strictly hyperbolic if the eigenvalues are all distinct [25]. The strict hyperbolicity implies hyperbolicity, because real and distinct eigenvalues ensure the existence of a set of linearly independent eigenvectors. Conversely, if the Jacobian matrix has imaginary eigenvalue(s), the system is said to be non-hyperbolic. For example, the one-dimensional Euler equation is strictly hyperbolic because all three eigenvalues are real and distinct.

Definition 4.5. Diagonalizable system. A matrix $\mathbb{A}$ is said to be diagonalizable if $\mathbb{A}$ can be decomposed to

$$\mathbb{A} = \mathbb{K}\mathbb{D}\mathbb{K}^{-1} \tag{4.16}$$

where

$$\mathbb{D} = \mathrm{Diag}(\lambda_1, \cdots, \lambda_m) \tag{4.17a}$$

$$\mathbb{K} = \begin{pmatrix} \mathbf{K}_1 & \dots & \mathbf{K}_m \end{pmatrix} \tag{4.17b}$$

where 'Diag' is an operator that forms a diagonal matrix with a given vector. The diagonal elements of $\mathbf{D}$ are the eigenvalues of $\mathbb{A}$ and the columns of $\mathbb{K}$ are the right eigenvectors of $\mathbb{A}$. A system is said to be diagonalizable if the Jacobian matrix $\mathbb{A}$ is diagonalizable. For example, the one-dimensional Euler equation is diagonalizable with

$$\mathbb{D} = \begin{pmatrix} u-a & 0 & 0 \\ 0 & u & 0 \\ 0 & 0 & u+a \end{pmatrix}, \mathbb{K} = \begin{pmatrix} 1 & 1 & 1 \\ u-a & u & u+a \\ H-ua & H-\gamma^* a^2 & H+ua \end{pmatrix}, \tag{4.18}$$

Note that $\mathbb{K}$ is invertible because the three column vectors are linearly independent.

4.2.2 General Fourier analysis

Now, we start the analytical analysis of the 1D two-phase two-fluid model. Recall that the 1D two-phase two-fluid model in a vector form is

$$\frac{\partial \mathbf{U}}{\partial t} + \frac{\partial \mathbf{F}}{\partial x} + \mathbf{P}_{ix}\frac{\partial \alpha_g}{\partial x} + \mathbf{P}_{it}\frac{\partial \alpha_g}{\partial t} = \mathbf{S} \tag{4.19}$$

where $\mathbf{U}$, $\mathbf{F}$, $\mathbf{P}_{ix}$, $\mathbf{P}_{it}$, and $\mathbf{S}$ are given in Eq. (2.61) of **Chapter 2**. In general, $\mathbf{U}$ is a function of space (x) and time (t); $\mathbf{F}$, $\mathbf{P}_{ix}$, and $\mathbf{P}_{it}$ are explicit functions of $\mathbf{U}$, but do not depend explicitly on x and t; $\mathbf{S}$ is a function of $\mathbf{U}$ and might depend explicitly on x and t. Thus, we obtain

$$\mathbf{U} = \mathbf{U}\big(x,t\big), \mathbf{F} = \mathbf{F}\big(\mathbf{U}\big), \mathbf{P}_{ix} = \mathbf{P}_{ix}\big(\mathbf{U}\big), \mathbf{P}_{it} = \mathbf{P}_{it}\big(\mathbf{U}\big), \mathbf{S} = \mathbf{S}\big(\mathbf{U};x,t\big) \tag{4.20}$$

Assuming all unknown variables are smooth enough to obtain partial derivatives, we transform the equation into a quasi-linear form

$$\big(\mathbb{I} + \mathbb{A}_{it,nc}\big)\frac{\partial \mathbf{U}}{\partial t} + \big(\mathbb{A}_c + \mathbb{A}_{ix,nc}\big)\frac{\partial \mathbf{U}}{\partial x} = \mathbf{S} \tag{4.21}$$

where

$$\mathbb{A}_c \equiv \frac{\partial \mathbf{F}}{\partial \mathbf{U}}, \mathbb{A}_{ix,nc} \equiv \mathbf{P}_{ix}\frac{\partial \alpha_g}{\partial \mathbf{U}}, \mathbb{A}_{ix,nc} \equiv \mathbf{P}_{it}\frac{\partial \alpha_g}{\partial \mathbf{U}} \tag{4.22}$$

where $\mathbb{A}_c$ is the matrix from the conservative part of the system; $\mathbb{A}_{ix,nc}$ and $\mathbb{A}_{it,nc}$ are the matrices from the non-conservative part of the system. As will be seen later, $\big(\mathbb{I} + \mathbb{A}_{it,nc}\big)$ is in general invertible, so we transform the quasi-linear equation into

$$\frac{\partial \mathbf{U}}{\partial t} + \mathbb{A}\frac{\partial \mathbf{U}}{\partial x} = \mathbf{S}^* \tag{4.23}$$

where $\mathbb{A}$ is the Jacobian matrix of the system and $\mathbf{S}^*$ is the new source vector

$$\mathbb{A} = \big(\mathbb{I} + \mathbb{A}_{it,nc}\big)^{-1}\big(\mathbb{A}_c + \mathbb{A}_{ix,nc}\big), \mathbf{S}^* = \big(\mathbb{I} + \mathbb{A}_{it,nc}\big)^{-1}\mathbf{S} \tag{4.24}$$

We will perform a dispersion analysis to study the dynamic character of the two-phase two-fluid model. The dispersion relationship is obtained by linearizing the system about an initial state and using a general Fourier representation for each solution component [26]. The local linear dynamic character of Eq. (4.23) can be investigated by this method for a known state $\mathbf{U}_0$. The linear differential equation for the behavior of the perturbation, $\boldsymbol{\phi} = \mathbf{U} - \mathbf{U}_0$, is

$$\frac{\partial\big(\mathbf{U}_0 + \boldsymbol{\phi}\big)}{\partial t} + \mathbb{A}_0\frac{\partial\big(\mathbf{U}_0 + \boldsymbol{\phi}\big)}{\partial x} = \mathbf{S}^*\big(\mathbf{U}_0 + \boldsymbol{\phi};x,t\big) \tag{4.25}$$

which gives

$$\frac{\partial \mathbf{U}_0}{\partial t} + \mathbb{A}_0\frac{\partial \mathbf{U}_0}{\partial x} + \frac{\partial \boldsymbol{\phi}}{\partial t} + \mathbb{A}_0\frac{\partial \boldsymbol{\phi}}{\partial x} = \mathbf{S}_0^* + \mathbb{S}_0\boldsymbol{\phi} \tag{4.26}$$

where $\mathbb{S}_0 = \left(\mathbb{I} + \mathbb{A}_{it,nc}\right)_0^{-1}\left(\partial\mathbf{S}/\partial\mathbf{U}\right)_0$. Since $\mathbf{U}_0$ is a known state of the system, we have

$$\frac{\partial \mathbf{U}_0}{\partial t} + \mathbb{A}_0 \frac{\partial \mathbf{U}_0}{\partial x} = \mathbf{S}_0^* \tag{4.27}$$

Subtracting Eq. (4.27) from Eq. (4.26), the equation for the perturbation is

$$\frac{\partial \boldsymbol{\phi}}{\partial t} + \mathbb{A}_0 \frac{\partial \boldsymbol{\phi}}{\partial x} = \mathbb{S}_0 \boldsymbol{\phi} \tag{4.28}$$

Assuming the perturbation has a solution in the form of a traveling wave [26], i.e.

$$\boldsymbol{\phi} = \boldsymbol{\phi}_0 \exp\left[i\left(kx - \omega t\right)\right] \tag{4.29}$$

where k is the wave number, ω is the frequency, and $\boldsymbol{\phi}_0$ is the initial amplitude of the perturbation. Substituting Eq. (4.29) into Eq. (4.28), we obtain

$$-i\omega\boldsymbol{\phi}_0 + ik\mathbb{A}_0\boldsymbol{\phi}_0 = \mathbb{S}_0\boldsymbol{\phi}_0 \tag{4.30}$$

Assuming k is non-zero, we change Eq. (4.30) to the following form

$$\left(\mathbb{A}_0 + \frac{i}{k}\mathbb{S}_0 - \frac{\omega}{k}\mathbb{I}\right)\boldsymbol{\phi}_0 = 0 \tag{4.31}$$

Eq. (4.31) is a homogeneous linear system of equations. The condition for $\boldsymbol{\phi}_0$ to have a non-trivial solution is that the determinant of the coefficient matrix is zero, i.e.

$$\det\left(\mathbb{A}_0 + \frac{i}{k}\mathbb{S}_0 - \frac{\omega}{k}\mathbb{I}\right) = 0 \tag{4.32}$$

Let $\lambda = \omega/k$, we see that λ is the eigenvalue of $\mathbb{A}_0 + i/k\mathbb{S}_0$. For each non-zero value of k, Eq. (4.32) gives a corresponding value of ω and λ. Let

$$\omega = \omega_R + i\omega_I \tag{4.33a}$$

$$\lambda = \lambda_R + i\lambda_I \tag{4.33b}$$

where the subscript R and I denote the real and imaginary part. For ω and λ, the imaginary part governs growth or decay of the Fourier component (depending on its sign) and the real part governs the speed

of propagation of the Fourier component. For finite λ in the $k \to \infty$ limit, Eq. (4.32) reduces to the characteristic equation and λ reduces to the characteristic eigenvalue of the system. For finite value of k, the imaginary part of λ and ω are in general non-zero. The analytical analysis starts with the characteristic analysis for $k \to \infty$.

4.3 Characteristic analysis

The characteristic analysis corresponds to $k \to \infty$ or $\mathbb{S}_0 = 0$. To ensure the system is well-posed, the eigenvalues of the system are required to be real. The eigenvalues are determined by

$$\det\left(\mathbb{A} - \lambda \mathbb{I}\right) = 0 \tag{4.34}$$

The key issue in the characteristic analysis is deriving and simplifying the matrices, $\mathbb{A}_c$, $\mathbb{A}_{ix,nc}$, and $\mathbb{A}_{it,nc}$, such that analytical eigenvalue/eigenvectors can be derived.

4.3.1 Characteristic analysis: Jacobian matrix

The Jacobian matrix of the system is defined as

$$\mathbb{A} = \left(\mathbb{I} + \mathbb{A}_{it,nc}\right)^{-1}\left(\mathbb{A}_c + \mathbb{A}_{ix,nc}\right) \tag{4.35}$$

Following the derivation and simplification given in the **Appendix A**, we obtain the matrixes $\mathbb{A}_c$, $\mathbb{A}_{ix,nc}$, and $\mathbb{A}_{it,nc}$, they are

$$\mathbb{A}_c = \begin{pmatrix} 0 & 1 & 0 & 0 & 0 & 0 \\ -u_l^2 + \beta_l c_l^h & 2u_l - \beta_l c_l^u & \beta_l c_l^1 & \sigma_l c_g^h & -\sigma_l c_g^u & \sigma_l c_g^1 \\ -u_l H_l + u_l \beta_l c_l^h & H_l - u_l \beta_l c_l^u & u_l + u_l \beta_l c_l^1 & \sigma_l u_l c_g^h & -\sigma_l u_l c_g^u & \sigma_l u_l c_g^1 \\ 0 & 0 & 0 & 0 & 1 & 0 \\ \sigma_g c_l^h & -\sigma_g c_l^u & \sigma_g c_l^1 & -u_g^2 + \beta_g c_g^h & 2u_g - \beta_g c_g^u & \beta_g c_g^1 \\ \sigma_g u_g c_l^h & -\sigma_g u_g c_l^u & \sigma_g u_g c_l^1 & -u_g H_g + u_g \beta_g c_g^h & H_g - u_g \beta_g c_g^u & u_g + u_g \beta_g c_g^1 \end{pmatrix} \tag{4.36}$$

$$\mathbb{A}_{ix,nc} = \begin{pmatrix} 0 & 0 & 0 & 0 & 0 & 0 \\ -\alpha_g\tau_l c_l^h & \alpha_g\tau_l c_l^u & -\alpha_g\tau_l c_l^1 & \alpha_l\tau_g c_g^h & -\alpha_l\tau_g c_g^u & \alpha_l\tau_g c_g^1 \\ 0 & 0 & 0 & 0 & 0 & 0 \\ 0 & 0 & 0 & 0 & 0 & 0 \\ \alpha_g\tau_l c_l^h & -\alpha_g\tau_l c_l^u & \alpha_g\tau_l c_l^1 & -\alpha_l\tau_g c_g^h & \alpha_l\tau_g c_g^u & -\alpha_l\tau_g c_g^1 \\ 0 & 0 & 0 & 0 & 0 & 0 \end{pmatrix} \tag{4.37}$$

$$\mathbb{A}_{it,nc} = \begin{pmatrix} 0 & 0 & 0 & 0 & 0 & 0 \\ 0 & 0 & 0 & 0 & 0 & 0 \\ \alpha_g\tau_l c_l^h & -\alpha_g\tau_l c_l^u & \alpha_g\tau_l c_l^1 & -\alpha_l\tau_g c_g^h & \alpha_l\tau_g c_g^u & -\alpha_l\tau_g c_g^1 \\ 0 & 0 & 0 & 0 & 0 & 0 \\ 0 & 0 & 0 & 0 & 0 & 0 \\ -\alpha_g\tau_l c_l^h & \alpha_g\tau_l c_l^u & -\alpha_g\tau_l c_l^1 & \alpha_l\tau_g c_g^h & -\alpha_l\tau_g c_g^u & \alpha_l\tau_g c_g^1 \end{pmatrix} \tag{4.38}$$

where we used the following auxiliary variables

$$c_l^h \equiv a_l^2 + \big(\gamma_l - 1\big)\big(u_l^2 - H_l\big); \quad c_g^h \equiv a_g^2 + \big(\gamma_g - 1\big)\big(u_g^2 - H_g\big) \tag{4.39a}$$

$$c_l^u \equiv \big(\gamma_l - 1\big)u_l; \quad c_g^u \equiv \big(\gamma_g - 1\big)u_g \tag{4.39b}$$

$$c_l^1 \equiv \gamma_l - 1; \quad c_g^1 \equiv \gamma_g - 1 \tag{4.39c}$$

$$\beta_l \equiv \frac{1 + \alpha_l\varepsilon_g}{1 + \alpha_g\varepsilon_l + \alpha_l\varepsilon_g}; \quad \beta_g \equiv \frac{1 + \alpha_g\varepsilon_l}{1 + \alpha_g\varepsilon_l + \alpha_l\varepsilon_g} \tag{4.39d}$$

$$\sigma_l \equiv \frac{\alpha_l\varepsilon_l}{1 + \alpha_g\varepsilon_l + \alpha_l\varepsilon_g}; \quad \sigma_g \equiv \frac{\alpha_g\varepsilon_g}{1 + \alpha_g\varepsilon_l + \alpha_l\varepsilon_g} \tag{4.39e}$$

$$\tau_l \equiv \frac{1}{1 + \alpha_g\varepsilon_l + \alpha_l\varepsilon_g}; \quad \tau_g \equiv \frac{1}{1 + \alpha_g\varepsilon_l + \alpha_l\varepsilon_g} \tag{4.39f}$$

where a_l, a_g, γ_l, γ_g, ε_l, and ε_g are defined in Eq. (3.12) and Eq. (3.15) of **Chapter 3**.

4.3.2 Characteristic analysis: conservative part

We start the analysis with the matrix $\mathbb{A}_c$, which represents the conservative part of the governing equation. Let λ_c and $\mathbf{K}_c$ be the eigenvalue and right eigenvector of $\mathbb{A}_c$. Note that λ_c and $\mathbf{K}_c$ are not the eigenvalue and eigenvector of the complete system, because the non-conservative part is missing, see Eq. (4.35) and Eq. (4.36). The eigenvalue analysis is performed with the symbolic calculation software Mathematica [27].

The characteristic polynomial of $\mathbb{A}_c$ given by Mathematica is

$$P_c(\lambda_c) = (\lambda_c - u_l)(\lambda_c - u_g)\Big\{\Big[(\lambda_c - u_l)^2 - \beta_l a_l^2\Big]\Big[(\lambda_c - u_g)^2 - \beta_g a_g^2\Big] - \sigma_l\sigma_g a_l^2 a_g^2\Big\} \tag{4.40}$$

where the subscript c denotes that the characteristic polynomial is derived for the matrix $\mathbb{A}_c$. This characteristic polynomial is surprisingly simple because of the algebraic transformations we made to the Jacobian matrix with the help of auxiliary variables, including a_k, γ_k, β_k, and σ_k.

$P_c(\lambda_c)$ has two simple eigenvalues, u_l and u_g, which represent the convection of liquid- and gas-phase enthalpy; however, the other four eigenvalues are more complicated. Fortunately, we can obtain accurate approximation by taking into account the different thermodynamic properties of liquid- and gas-phase, especially ε_l and ε_g. For water and steam, ε_g is a small value close to zero while ε_l is a large positive value, see Figure 3.4. Another special example is the ideal gas, for which $\varepsilon_g = 0$ in any conditions. Thus, we obtain the following approximation

$$\left.\begin{array}{l}\varepsilon_g \approx 0\\ \varepsilon_l \gg 1\end{array}\right\} \Rightarrow \sigma_g = \frac{\alpha_g\varepsilon_g}{1 + \alpha_g\varepsilon_l + \alpha_l\varepsilon_g} \approx 0 \tag{4.41}$$

This approximation means that, in matrix $\mathbb{A}_c$, the coupling effect of the lower triangular block containing σ_g is not significant. Substituting $\sigma_g \approx 0$ into Eq. (4.36), we find that the eigenvalues are

$$\lambda_{c,1} \approx u_l - \sqrt{\beta_l}a_l; \lambda_{c,2} = u_l; \lambda_{c,3} \approx u_l + \sqrt{\beta_l}a_l \tag{4.42a}$$

$$\lambda_{c,4} \approx u_g - \sqrt{\beta_g}a_g; \lambda_{c,5} = u_g; \lambda_{c,6} \approx u_g + \sqrt{\beta_g}a_g \tag{4.42b}$$

and the right eigenvectors are

$$\mathbf{K}_{1,c} \approx \begin{pmatrix} 1 \\ u_l - \sqrt{\beta_l} a_l \\ H_l - \sqrt{\beta_l} a_l u_l \\ 0 \\ 0 \\ 0 \end{pmatrix}, \mathbf{K}_{2,c} \approx \begin{pmatrix} 1 \\ u_l \\ H_l - \gamma_l^* a_l^2 \\ 0 \\ 0 \\ 0 \end{pmatrix}, \mathbf{K}_{3,c} \approx \begin{pmatrix} 1 \\ u_l + \sqrt{\beta_l} a_l \\ H_l + \sqrt{\beta_l} a_l u_l \\ 0 \\ 0 \\ 0 \end{pmatrix}$$
$$\mathbf{K}_{4,c} \approx \begin{pmatrix} q_4 \\ q_4 \lambda_{c,4} \\ q_4 \big[H_l - u_l^2 + u_l \lambda_{c,4} \big] \\ 1 \\ u_g - \sqrt{\beta_g} a_g \\ H_g - \sqrt{\beta_g} a_g u_g \end{pmatrix}, \mathbf{K}_{5,c} \approx \begin{pmatrix} 0 \\ 0 \\ 0 \\ 1 \\ u_g \\ H_g - \gamma_g^* a_g^2 \end{pmatrix}, \mathbf{K}_{6,c} \approx \begin{pmatrix} q_6 \\ q_6 \lambda_{c,6} \\ q_6 \big[H_l - u_l^2 + u_l \lambda_{c,6} \big] \\ 1 \\ u_g + \sqrt{\beta_g} a_g \\ H_g + \sqrt{\beta_g} a_g u_g \end{pmatrix} \tag{4.43}$$

where $\gamma_l^* = 1/\big(\gamma_l - 1\big)$ and $\gamma_g^* = 1/\big(\gamma_g - 1\big)$. q_4 and q_6 are two auxiliary variables defined as

$$q_4 \equiv \frac{\sigma_l a_g^2}{\big(\lambda_{c,4} - \lambda_{c,1}\big)\big(\lambda_{c,4} - \lambda_{c,3}\big)}; \quad q_6 \equiv \frac{\sigma_l a_g^2}{\big(\lambda_{c,6} - \lambda_{c,1}\big)\big(\lambda_{c,6} - \lambda_{c,3}\big)} \tag{4.44}$$

The right eigenvector matrix can thus be approximated as

$$\mathbb{K}_c \approx \begin{pmatrix} \mathbf{K}_{1,c} & \mathbf{K}_{2,c} & \mathbf{K}_{3,c} & \mathbf{K}_{4,c} & \mathbf{K}_{5,c} & \mathbf{K}_{6,c} \end{pmatrix} \tag{4.45}$$

Note that though $\mathbb{K}_c$ is neither the exact eigenvector matrix of $\mathbb{A}_c$ nor the exact eigenvector matrix of the system, it provides very accurate upwind information of the system.

A series of numerical tests are performed to verify the approximations by comparing the exact eigenvalues calculated with Eq. (4.40) with the approximate eigenvalues calculated with Eq. (4.42). Table 4.1 lists the test conditions for the verification. The test matrix covers a wide range of void fraction, pressure (in MPa), temperature (in K), and density (in kg/m^3). The liquid velocity and gas velocity are kept constant in all cases, i.e. $u_l = 2.0$ m/s and $u_g = 5.0$ m/s. For test case 1 to 5, the liquid is a subcooled water and the gas is a superheated steam; for test case 6 to 10, the liquid and the gas are at saturation temperature. Table 4.2, Table 4.3, and Table 4.4 show the comparison of exact eigenvalues ($\lambda_{c,i}^e, i = 1, 3, 4, 6$) to the approximate eigenvalues ($\lambda_{c,i}^a, i = 1, 3, 4, 6$) for $\alpha_g = 0.001$, $\alpha_g = 0.2$, and $\alpha_g = 0.999$, respectively. We see that the

approximate eigenvalues are very close to the exact eigenvalues for all test cases. At low void fraction, the maximum relative eigenvalue difference is 0.4%, most of the eigenvalues are within 0.2%; at intermediate void fraction, the maximum relative eigenvalue difference is 1.4%, most of the eigenvalues are within 0.2%; at high void fraction, the maximum relative eigenvalue difference is less than 0.1%. This confirms that approximation given in Eq. (4.41) is valid.

Table 4.1: Verification of approximate eigenvalues of $\mathbb{A}_c$: test matrix

Case	p	T_l	T_g	ρ_l	ρ_g	a_l	a_g	γ_l	γ_g	ε_l	ε_g
1	0.1	300.0	500.0	996.56	0.44	1503.13	548.30	1.148	1.308	2.25E+04	-3.41E-04
2	0.5	300.0	500.0	996.74	2.21	1503.76	542.92	1.149	1.306	4.51E+03	-1.43E-03
3	1.0	300.0	500.0	996.96	4.53	1504.56	535.67	1.149	1.303	2.26E+03	-2.38E-03
4	5.0	300.0	600.0	998.74	20.39	1510.93	561.17	1.153	1.297	4.55E+02	-1.22E-02
5	10.0	300.0	600.0	1000.95	49.77	1518.93	503.35	1.158	1.280	2.30E+02	-1.95E-02
6	0.1	372.8	372.8	958.64	0.59	1545.45	472.05	1.424	1.312	2.29E+04	3.90E-03
7	0.5	425.0	425.0	915.28	2.67	1461.95	493.80	1.514	1.297	3.91E+03	4.53E-03
8	1.0	453.0	453.0	887.13	5.15	1391.64	500.89	1.537	1.288	1.72E+03	3.00E-03
9	5.0	537.1	537.1	777.36	25.35	1088.43	498.18	1.519	1.273	1.83E+02	-1.41E-02
10	10.0	584.1	584.1	688.41	55.45	847.74	472.46	1.451	1.263	4.80E+01	-2.57E-02

Table 4.2: Verification of approximate eigenvalues of $\mathbb{A}_c$: exact vs approximate eigenvalues for $\alpha_g = 0.001$

Case	$\lambda^e_{c,1}$	$\lambda^a_{c,1}$	$\lambda^e_{c,3}$	$\lambda^a_{c,3}$	$\lambda^e_{c,4}$	$\lambda^a_{c,4}$	$\lambda^e_{c,6}$	$\lambda^a_{c,6}$
1	-308.00	-307.92	312.00	311.92	-543.26	-543.31	553.26	553.31
2	-313.66	-314.75	317.70	318.75	-467.75	-467.02	477.71	477.02
3	-539.10	-537.99	549.17	547.99	-637.51	-638.44	641.44	642.44
4	-486.61	-488.57	496.55	498.57	-660.34	-658.89	664.40	662.89
5	-531.61	-530.86	541.62	540.86	-830.68	-831.16	834.67	835.16
6	-494.89	-495.62	504.89	505.62	-843.57	-843.14	847.58	847.14
7	-559.91	-558.54	569.91	568.54	-1247.63	-1248.24	1251.62	1252.24
8	-496.93	-496.19	506.93	506.19	-997.38	-997.75	1001.37	1001.75
9	-503.48	-502.39	513.49	512.39	-1364.75	-1365.16	1368.75	1369.16
10	-473.78	-473.34	483.78	483.34	-825.34	-825.59	829.34	829.59

Table 4.3: Verification of approximate eigenvalues of $\mathbb{A}_c$: exact vs approximate eigenvalues for $\alpha_g = 0.2$

Case	$\lambda^e_{c,1}$	$\lambda^a_{c,1}$	$\lambda^e_{c,3}$	$\lambda^a_{c,3}$	$\lambda^e_{c,4}$	$\lambda^a_{c,4}$	$\lambda^e_{c,6}$	$\lambda^a_{c,6}$
1	-20.40	-20.39	24.40	24.39	-543.30	-543.30	553.30	553.30
2	-48.06	-48.03	52.06	52.03	-537.92	-537.92	547.92	547.92
3	-68.76	-68.69	72.76	72.69	-530.66	-530.67	540.66	540.67
4	-155.62	-154.79	159.61	158.79	-555.96	-556.20	565.97	566.20
5	-220.09	-217.96	224.06	221.96	-497.49	-498.43	507.52	508.43
6	-20.84	-20.87	24.84	24.87	-467.06	-467.05	477.06	477.05
7	-50.24	-50.33	54.24	54.33	-488.81	-488.79	498.80	498.79
8	-73.00	-73.09	77.00	77.09	-495.91	-495.89	505.91	505.89
9	-175.81	-174.68	179.80	178.68	-492.85	-493.26	502.86	503.26
10	-259.43	-255.89	263.36	259.89	-465.96	-467.92	476.03	477.92

Table 4.4: Verification of approximate eigenvalues of $\mathbb{A}_c$: exact vs approximate eigenvalues for $\alpha_g = 0.999$

Case	$\lambda^e_{c,1}$	$\lambda^a_{c,1}$	$\lambda^e_{c,3}$	$\lambda^a_{c,3}$	$\lambda^e_{c,4}$	$\lambda^a_{c,4}$	$\lambda^e_{c,6}$	$\lambda^a_{c,6}$
1	-8.02	-8.02	12.02	12.02	-543.30	-543.30	553.30	553.30
2	-8.22	-8.22	12.22	12.22	-467.05	-467.05	477.05	477.05
3	-20.41	-20.41	24.41	24.41	-537.92	-537.92	547.92	547.92
4	-21.39	-21.39	25.39	25.39	-488.80	-488.80	498.80	498.80
5	-29.69	-29.69	33.69	33.69	-530.67	-530.67	540.67	540.67
6	-31.60	-31.60	35.60	35.60	-495.89	-495.89	505.89	505.89
7	-68.80	-68.80	72.80	72.80	-556.17	-556.17	566.17	566.17
8	-78.35	-78.35	82.35	82.35	-493.18	-493.18	503.18	503.18
9	-98.04	-98.04	102.04	102.04	-498.35	-498.35	508.35	508.35
10	-119.14	-119.14	123.14	123.14	-467.46	-467.46	477.46	477.46

4.3.3 Characteristic analysis: system

Basic two-phase two-fluid model

Recall that the Jacobian matrix of the system is

$$\mathbb{A} = \big(\mathbb{I} + \mathbb{A}_{it,nc}\big)^{-1}\big(\mathbb{A}_c + \mathbb{A}_{ix,nc}\big) \tag{4.46}$$

The derivation of $\mathbb{A}$ is complicated, it is shown in **Appendix A**. However, we find that the characteristic polynomial of $\mathbb{A}$ can be simplified to a convenient form. Let λ and $\mathbf{K}$ be the eigenvalue and eigenvector of $\mathbb{A}$. The eigenvalue analysis is performed with the symbolic calculation software Mathematica. The characteristic polynomial of $\mathbb{A}$ given by Mathematica is

$$P(\lambda) = (\lambda - u_l)(\lambda - u_g)\left\{\left[(\lambda - u_l)^2 - \beta_l^* a_l^2\right]\left[(\lambda - u_g)^2 - \beta_g^* a_g^2\right] - \beta_l^*\beta_g^* a_l^2 a_g^2\right\} \tag{4.47}$$

where

$$\beta_l^* = \frac{\alpha_l\rho_g a_g^2}{\alpha_l\rho_g a_g^2 + \alpha_g\rho_l a_l^2}, \beta_g^* = \frac{\alpha_g\rho_l a_l^2}{\alpha_l\rho_g a_g^2 + \alpha_g\rho_l a_l^2} \tag{4.48}$$

To study the eigenvalues, we define the following 4^{th}-order polynomial

$$P_4(\lambda) = (\lambda - \lambda_l^-)(\lambda - \lambda_l^+)(\lambda - \lambda_g^-)(\lambda - \lambda_g^+) - \beta_l^*\beta_g^* a_l^2 a_g^2 \tag{4.49}$$

where

$$\begin{aligned} \lambda_l^- &= u_l - \sqrt{\beta_l^*}a_l; \quad \lambda_l^+ = u_l + \sqrt{\beta_l^*}a_l \\ \lambda_g^- &= u_g - \sqrt{\beta_g^*}a_g; \quad \lambda_g^+ = u_g + \sqrt{\beta_g^*}a_g \end{aligned} \tag{4.50}$$

The features of this polynomial are

- If $\alpha_g = 0$, then $\beta_g^* = 0$ and $\beta_l^* = 1$; the system degenerates to single-phase liquid and $P_4(\lambda)$ has two meaningful roots, $u_l - a_l$ and $u_l + a_l$.

- If $\alpha_g = 1$, then $\beta_g^* = 1$ and $\beta_l^* = 0$; the system degenerates to single-phase gas and $P_4(\lambda)$ has two meaningful roots, $u_g - a_g$ and $u_g + a_g$.

- If $0 < \alpha_g < 1$, then $0 < \beta_g^* < 1$ and $0 < \beta_l^* < 1$; the system is mixed with two phases and the characteristic polynomial is a general 4^{th}-order polynomial, see Figure 4.1. For analysis purposes, let u_1, u_2, u_3, and u_4 denote the increasing order of λ_g^-, λ_l^-, λ_l^+, and λ_g^+

$$u_1 \leq u_2 \leq u_3 \leq u_4 \tag{4.51}$$

For problems where α_g is non-negligible and the relative velocity is small, we have in fact that $\lambda_g^- \leq \lambda_l^- \leq \lambda_l^+ \leq \lambda_g^+$. Because β_l^* and β_g^* are non-zero, λ_g^-, λ_l^-, λ_l^+, and λ_g^+ are not roots of $P_4(\lambda)$. $P_4(\lambda)$ always has two real roots: one in $(-\infty, u_1)$ and the other one in $(u_4, +\infty)$. Because

$$\begin{aligned} P_4(\lambda = u_2) &= -\beta_l^* \beta_g^* a_l^2 a_g^2 < 0 \\ P_4(\lambda = u_3) &= -\beta_l^* \beta_g^* a_l^2 a_g^2 < 0 \end{aligned} \tag{4.52}$$

depending on the sign of the local maximum value in (u_2, u_3), $P_4(\lambda)$ may have another two real roots, two equal real roots, or two complex roots. The sign of the local maximum value is determined by the relative velocity. Let $P_4^{\max}$ be the local maximum value in (u_2, u_3)

$$P_4^{\max} = \max_{\lambda \in (u_2, u_3)} P_4(\lambda) \tag{4.53}$$

we can check that

$$\begin{aligned} P_4^{\max} &= 0, \quad \text{for} \quad |u_g - u_l| = 0 \\ &< 0, \quad \text{for} \quad 0 < |u_g - u_l| \leq \sqrt{\beta_l^*} a_l + \sqrt{\beta_g^*} a_g \end{aligned} \tag{4.54}$$

which means that the remaining two roots are either two equal real values for $u_g = u_l$ or two complex values for $0 < |u_g - u_l| \leq \sqrt{\beta_l^*} a_l + \sqrt{\beta_g^*} a_g$. For larger relative velocity, the two roots transition from two complex roots, to two equal real roots, and finally to two distinct real roots. For example, we can

check that if $|u_g - u_l| \geq \sqrt{\beta_l^*}a_l + \sqrt{\beta_g^*}a_g + \sqrt[4]{\beta_l^*\beta_g^* a_l^2 a_g^2}$, we have

$$P_4^{\max} \geq P_4\left(\lambda = \frac{u_2+u_3}{2}\right) = \frac{\sqrt{\beta_l^*}\sqrt{\beta_g^*}a_l a_g}{16}\left[\beta_l^*\beta_g^* a_l a_g + 4\sqrt[4]{\beta_l^*\beta_g^* a_l^2 a_g^2}\left(\sqrt{\beta_l^*}a_l + \sqrt{\beta_g^*}a_g\right)\right] > 0 \tag{4.55}$$

which means there are two real roots in interval (u_2, u_3).

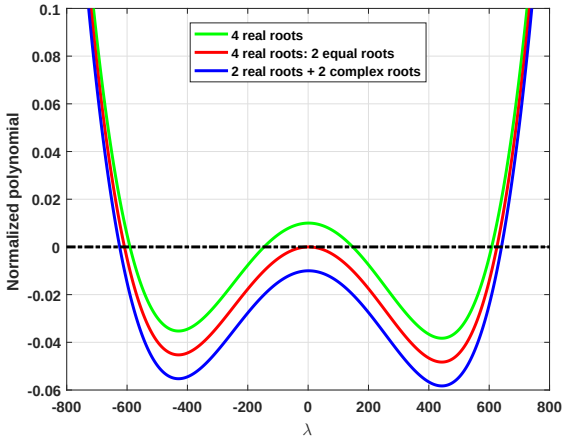

Figure 4.1: Characteristic polynomial of the basic two-phase two-fluid model

Thus, we obtain the following well-known facts [28, 16] about the basic two-phase two-fluid model

- If $\alpha_g = 0$ or $\alpha_g = 1$, the system degenerates to single-phase liquid or single-phase gas. The system is hyperbolic.
- If $0 < \alpha_g < 1$ and $u_l = u_g$, the system has 6 real eigenvalues and is hyperbolic.
- If $0 < \alpha_g < 1$, $u_l \neq u_g$, and $|u_g - u_l| \leq \sqrt{\beta_l^*}a_l + \sqrt{\beta_g^*}a_g$, the system has 4 real eigenvalues and two complex eigenvalues. The system is non-hyperbolic.
- If $0 < \alpha_g < 1$, $u_l \neq u_g$, and $|u_g - u_l| > \sqrt{\beta_l^*}a_l + \sqrt{\beta_g^*}a_g$, the system transitions from having 4 real eigenvalues to 6 real eigenvalues.

Isothermal case

In previous characteristic analysis found in the literature, most researchers ignore the energy equation because the energy equation does not affect the dynamic character of the two-phase flow equations [26], i.e. its hyperbolicity. As a special case of our previous analysis, we also provide the analysis without the energy equation, which is called the isothermal case. For the isothermal case, the phase change is ignored and the

governing equation is

$$\frac{\partial \alpha_l \rho_l}{\partial t} + \frac{\partial \alpha_l \rho_l u_l}{\partial x} = 0 \tag{4.56a}$$

$$\frac{\partial \alpha_l \rho_l u_l}{\partial t} + \frac{\partial \big(\alpha_l \rho_l u_l^2 + \alpha_l p\big)}{\partial x} - p\frac{\partial \alpha_l}{\partial x} = \alpha_l \rho_l g_x - f_{wl} + f_i \tag{4.56b}$$

$$\frac{\partial \alpha_g \rho_g}{\partial t} + \frac{\partial \alpha_g \rho_g u_g}{\partial x} = 0 \tag{4.56c}$$

$$\frac{\partial \alpha_g \rho_g u_g}{\partial t} + \frac{\partial \big(\alpha_g \rho_g u_g^2 + \alpha_g p\big)}{\partial x} - p\frac{\partial \alpha_g}{\partial x} = \alpha_g \rho_g g_x - f_{wg} - f_i \tag{4.56d}$$

The phasic density is determined by $\rho_k = \rho_k\big(p\big)$. Following a similar derivation given in **Appendix A**, the Jacobian matrix of the system is found to be

$$\mathbb{A}_{iso} = \begin{pmatrix} 0 & 1 & 0 & 0 \\ -u_l^2 + \beta_l^* a_l^2 & 2u_l & \sigma_l^* a_g^2 & 0 \\ 0 & 0 & 1 & 0 \\ \sigma_g^* a_l^2 & 0 & -u_g^2 + \beta_g^* a_g^2 & 2u_g \end{pmatrix} \tag{4.57}$$

where a_l and a_g are isothermal speed of sound defined as

$$a_l^2 \equiv \left(\frac{\partial \rho_l}{\partial p}\right)^{-1}; \quad a_g^2 \equiv \left(\frac{\partial \rho_g}{\partial p}\right)^{-1} \tag{4.58}$$

and

$$\beta_l^* \equiv \frac{\alpha_l \rho_g a_g^2}{\alpha_l \rho_g a_g^2 + \alpha_g \rho_l a_l^2}; \quad \beta_g^* \equiv \frac{\alpha_g \rho_l a_l^2}{\alpha_l \rho_g a_g^2 + \alpha_g \rho_l a_l^2} \tag{4.59a}$$

$$\sigma_l^* \equiv \frac{\alpha_l \rho_l a_l^2}{\alpha_l \rho_g a_g^2 + \alpha_g \rho_l a_l^2}; \quad \sigma_g^* \equiv \frac{\alpha_g \rho_g a_g^2}{\alpha_l \rho_g a_g^2 + \alpha_g \rho_l a_l^2} \tag{4.59b}$$

Let λ be the eigenvalue. The characteristic polynomial for the isothermal case is found to be

$$P_{iso}\big(\lambda\big) = \Big[\big(\lambda - u_l\big)^2 - \beta_l^* a_l^2\Big]\Big[\big(\lambda - u_g\big)^2 - \beta_g^* a_g^2\Big] - \beta_l^* \beta_g^* a_l^2 a_g^2 \tag{4.60}$$

Note the $P_{iso}\big(\lambda\big)$ in Eq. (4.60) has the same form as $P_4\big(\lambda\big)$ in Eq. (4.47). From this analysis, we see that the characteristic polynomial for the isothermal case is very similar to the general case, though the definition of speed of sound is different. The analysis performed for the general case can be applied exactly to the isothermal case.

4.3.4 Characteristic analysis: hyperbolicity regularization

There are two common methods to hyperbolize the basic two-phase two-fluid model: interfacial pressure correction [29] and virtual mass force [30]. These two methods can be written in a general form as

$$\frac{\partial \alpha_l \rho_l}{\partial t} + \frac{\partial \alpha_l \rho_l u_l}{\partial x} = S_l^c \tag{4.61a}$$

$$\frac{\partial \alpha_l \rho_l u_l}{\partial t} + \frac{\partial \big(\alpha_l \rho_l u_l^2 + \alpha_l p\big)}{\partial x} - p\frac{\partial \alpha_l}{\partial x} - F_\delta = S_l^m \tag{4.61b}$$

$$\frac{\partial \alpha_l \rho_l e_l}{\partial t} + \frac{\partial \alpha_l \rho_l e_l u_l}{\partial x} + p\frac{\partial \alpha_l}{\partial t} + p\frac{\partial \alpha_l u_l}{\partial x} = S_l^e \tag{4.61c}$$

$$\frac{\partial \alpha_g \rho_g}{\partial t} + \frac{\partial \alpha_g \rho_g u_g}{\partial x} = S_g^c \tag{4.61d}$$

$$\frac{\partial \alpha_g \rho_g u_g}{\partial t} + \frac{\partial \big(\alpha_g \rho_g u_g^2 + \alpha_g p\big)}{\partial x} - p\frac{\partial \alpha_g}{\partial x} + F_\delta = S_g^m \tag{4.61e}$$

$$\frac{\partial \alpha_g \rho_g e_g}{\partial t} + \frac{\partial \alpha_g \rho_g e_g u_g}{\partial x} + p\frac{\partial \alpha_g}{\partial t} + p\frac{\partial \alpha_g u_g}{\partial x} = S_g^e \tag{4.61f}$$

Note that we always add/remove the same amount of force from the liquid-phase momentum equation and remove/add the same amount to the gas-phase momentum equation. This ensures that we get the correct mixture equation when the two momentum equations are added. The interfacial pressure correction and virtual mass force are

$$F_\delta = \delta_p \frac{\partial \alpha_g}{\partial x}, \quad \text{for interfacial pressure correction} \tag{4.62a}$$

$$F_\delta = C_{vm}\left[\frac{\partial \big(u_g - u_l\big)}{\partial t} + u_l\frac{\partial u_g}{\partial x} - u_g\frac{\partial u_l}{\partial x}\right], \quad \text{for virtual mass force} \tag{4.62b}$$

In Eq. (4.62), δ_p is the interfacial pressure correction that has the dimension of pressure and C_{vm} is the virtual mass that has the dimension of density.

Interfacial pressure correction

The first common method to hyperbolize the system is the interfacial pressure correction, used in CATHARE code [29]. With Eq. (4.61) and Eq. (4.62a), following the derivation given in **Appendix A**, the characteristic polynomial of the system is found to be

$$P\big(\lambda\big) = \big(\lambda - u_l\big)\big(\lambda - u_g\big)\left\{\left[\big(\lambda - u_l\big)^2 - \beta_l^* a_l^2\right]\left[\big(\lambda - u_g\big)^2 - \beta_g^* a_g^2\right] - \beta_l^*\beta_g^* a_l^2 a_g^2 + f\big(\delta_p\big)a_l^2 a_g^2\right\} \tag{4.63}$$

where

$$\beta_l^* = \frac{\alpha_l\left[\rho_g a_g^2 - \left(\gamma_g - 1\right)\delta_p\right] + \alpha_g\delta_p}{\alpha_l\left[\rho_g a_g^2 - \left(\gamma_g - 1\right)\delta_p\right] + \alpha_g\left[\rho_l a_l^2 - \left(\gamma_l - 1\right)\delta_p\right]} \tag{4.64a}$$

$$\beta_g^* = \frac{\alpha_g\left[\rho_l a_l^2 - \left(\gamma_l - 1\right)\delta_p\right] + \alpha_l\delta_p}{\alpha_l\left[\rho_g a_g^2 - \left(\gamma_g - 1\right)\delta_p\right] + \alpha_g\left[\rho_l a_l^2 - \left(\gamma_l - 1\right)\delta_p\right]} \tag{4.64b}$$

$$f\left(\delta_p\right) = \frac{\delta_p}{\alpha_l\left[\rho_g a_g^2 - \left(\gamma_g - 1\right)\delta_p\right] + \alpha_g\left[\rho_l a_l^2 - \left(\gamma_l - 1\right)\delta_p\right]} \tag{4.64c}$$

Extensive algebraic transformations are performed to obtain Eq. (4.63). We define the following 4^{th}-order polynomial to study the eigenvalues

$$P_4\left(\lambda;\delta_p\right) = P_4^0\left(\lambda;\delta_p\right) + f\left(\delta_p\right) \tag{4.65}$$

where

$$P_4^0\left(\lambda;\delta_p\right) = \frac{1}{a_l^2 a_g^2}\left(\lambda - \lambda_l^-\right)\left(\lambda - \lambda_l^+\right)\left(\lambda - \lambda_g^-\right)\left(\lambda - \lambda_g^+\right) \tag{4.66}$$

The behavior of $P_4\left(\lambda;\delta_p\right)$ is shown on Figure 4.2. It contains two parts: the first part $P_4^0\left(\lambda;\delta_p\right)$ determines the shape of the characteristic polynomial; the second part $f\left(\delta_p\right)$ is the perturbation to the characteristic polynomial. When δ_p is small, $f\left(\delta_p\right)$ is approximately a linear function of δ_p.

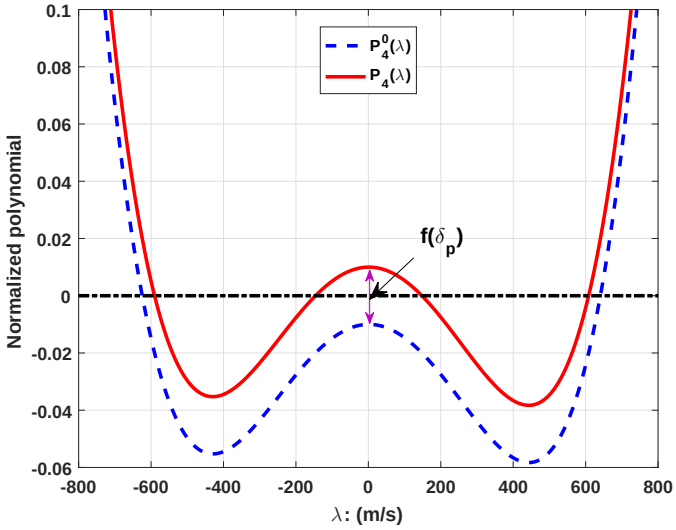

Figure 4.2: Characteristic polynomial of the system with interfacial pressure correction

If the interfacial pressure correction δ_p is to be used for regularization purpose, we would require that δ_p is large enough to ensure the characteristic polynomial has all real eigenvalues. The condition is: the local

maximum value of $P_4(\lambda;\delta_p)$ in interval (u_2,u_3) is non-negative, i.e.

$$P_4^{\max}(\delta_p) = \max_{\lambda\in(u_2,u_3)} P_4(\lambda;\delta_p) \geq 0 \tag{4.67}$$

Let δ_p^{cr} be the critical value of the correction that satisfy

$$P_4^{\max}(\delta_p^{cr}) = \max_{\lambda\in(u_2,u_3)} P_4(\lambda;\delta_p^{cr}) = 0 \tag{4.68}$$

Finding the local maximum value and δ_p^{cr} analytically is complicated; however, δ_p^{cr} can be found numerically with little computational effort.

For problems where $|u_g - u_l|$ is much smaller than the phasic speed of sound, the interfacial pressure correction is much smaller than phasic pressure and such correction is physically realistic. When $|u_g - u_l|$ is comparable to the phasic speed of sound, interfacial pressure correction is on the order of the phasic pressure, which is difficult to justify.

Using Eq. (4.68), we can study the behavior of the interfacial pressure correction at different physical conditions. Among all possible variables, the void fraction and the relative velocity are important. In the following numerical tests, we keep the liquid velocity at 0 and change the gas velocity through a relative Mach number (Mr), which is defined as

$$\text{Mr} = \frac{|u_g - u_l|}{\sqrt{\beta_l^*}a_l + \sqrt{\beta_g^*}a_g} \tag{4.69}$$

Table 4.5 lists the physical conditions for the numerical tests.

Table 4.5: Physical conditions for studying δ_p^{cr}

Primary variables		Auxiliary variables	
Pressure (MPa)	15.	ε_l	154.76
Liquid velocity (m/s)	0.	ε_g	-0.012664
Liquid temperature (K)	300.	a_l (m/s)	1526.9
Gas temperature (K)	700.	a_g (m/s)	576.66
Liquid density (kg/m^3)	1003.1	γ_l	1.1629
Gas density (kg/m^3)	57.941	γ_g	1.2971

Regardless of the validity of the interfacial pressure correction, Figure 4.3a shows δ_p^{cr} as a function of void fraction and relative Mach number. The value of δ_p^{cr} in the figure is normalized by the phasic pressure. As a function of void fraction, δ_p^{cr} is zero in the single-phase limit; δ_p^{cr} is non-zero for two-phase system when the relative velocity is non-zero. As a function of Mr, δ_p^{cr} increases with Mr until it reaches the phasic pressure. When Mr is larger than 1, δ_p^{cr} decreases with Mr until it reaches 0.

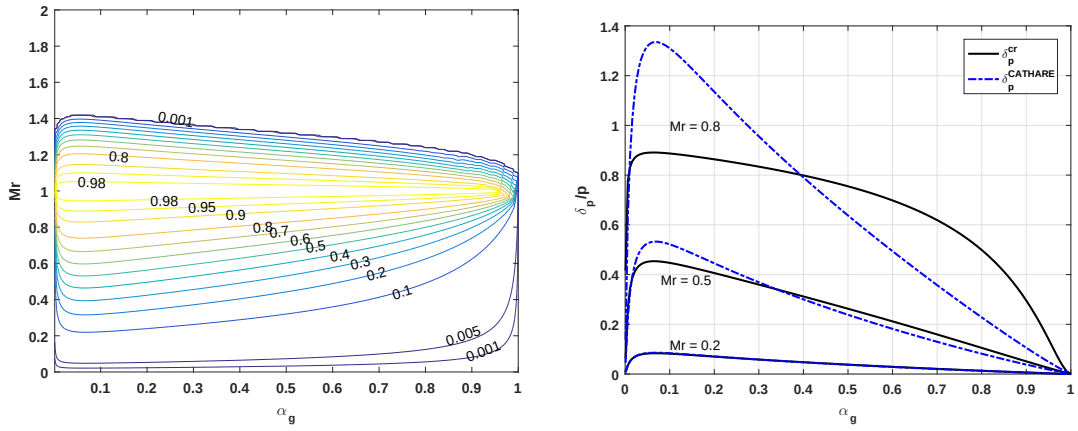

(a) (b)

Figure 4.3: Normalized interfacial pressure correction δ_p^{cr} as a function of void fraction and relative Mach number. The interfacial pressure correction is normalized by the phasic pressure.

Table 4.6: Eigenvalues of the system with/without interfacial pressure correction

Case	$\lvert u_g - u_l \rvert$	α_g	δ_p	λ_4	λ_6	λ_1	λ_3
1	10.	0.01	0	-1107.80	1110.78	8.51 -3.56i	8.51 +3.56i
2	10.	0.01	δ_p^{cr}	-1107.80	1110.78	8.51	8.51
3	10.	0.10	0	-679.41	692.57	3.42 -4.74i	3.42 +4.74i
4	10.	0.10	δ_p^{cr}	-679.40	692.56	3.42	3.42
5	10.	0.50	0	-581.21	600.12	0.55 -2.27i	0.55 +2.27i
6	10.	0.50	δ_p^{cr}	-581.21	600.12	0.55	0.54
7	10.	0.99	0	-566.81	586.80	0.01 -0.24i	0.01 +0.24i
8	10.	0.99	δ_p^{cr}	-566.81	586.80	0.01	0.00
9	100.	0.01	0	-1095.97	1126.03	84.97 -35.59i	84.97 +35.59i
10	100.	0.01	δ_p^{cr}	-1095.43	1125.47	84.99	84.98
11	100.	0.10	0	-625.33	756.34	34.50 -47.04i	34.50 +47.04i
12	100.	0.10	δ_p^{cr}	-623.51	755.00	34.25	34.25
13	100.	0.50	0	-497.74	686.28	5.73 -22.91i	5.73 +22.91i
14	100.	0.50	δ_p^{cr}	-497.41	686.11	5.65	5.65
15	100.	0.99	0	-476.88	676.76	0.06 -2.45i	0.06 +2.45i
16	100.	0.99	δ_p^{cr}	-476.88	676.76	0.06	0.06
17	500.	0.01	0	-1064.01	1247.90	408.06 -175.19i	408.06 +175.19i
18	500.	0.01	δ_p^{cr}	-1051.16	1235.58	407.80	407.79
19	500.	0.10	0	-485.95	1097.75	194.10 -194.29i	194.10 +194.29i
20	500.	0.10	δ_p^{cr}	-443.18	1087.98	177.60	177.59
21	500.	0.50	0	-225.75	1079.06	73.35 -119.05i	73.35 +119.05i
22	500.	0.50	δ_p^{cr}	-205.21	1077.78	63.72	63.71
23	500.	0.99	0	-84.61	1076.68	3.96 -22.73i	3.96 +22.73i
24	500.	0.99	δ_p^{cr}	-84.90	1076.68	4.11	4.11

We compare the interfacial pressure correction obtained from Eq. (4.68) with the correction used in CATHARE code

$$\delta_p^{\text{CATHARE}} = \frac{\alpha_l \alpha_g \rho_l \rho_g}{\alpha_l \rho_g + \alpha_g \rho_l} \big(u_g - u_l\big)^2 \tag{4.70}$$

The comparison is shown in Figure 4.3b. We see that $\delta_p^{\text{CATHARE}}$ is not large enough at high void fraction and is larger than the phasic pressure when the relative Mach number is high.

Table 4.6 lists the eigenvalues of the system calculated with Eq. (4.47) and with the interfacial pressure correction. The eigenvalues of the system are calculated with different combinations of void fraction and relative velocity. For the odd cases, $\delta_p = 0$, which reduces to the basic two-phase two-fluid model; for the even cases, $\delta_p = \delta_p^{cr}$. We see from the table that the interfacial pressure correction works as expected to bring the two complex eigenvalues (λ_1 and λ_3) to real values. The two real eigenvalues (λ_4 and λ_6) stay real.

Virtual mass force

Another common method to make the system hyperbolic is adding a virtual mass force to the phasic momentum equations. For simplicity, we will show analysis and results for the isothermal case. Combining Eq. (4.61) and Eq. (4.62b), following the derivation given in **Appendix A**, the Jacobian matrix for the isothermal system is found to be

$$\mathbb{A}_{iso,vm} = \big(\mathbb{I} + \mathbb{A}_{vmt}\big)^{-1} \mathbb{A}_{iso} \tag{4.71}$$

where $\mathbb{A}_{vmt}$ accounts for the effect of time derivatives in the virtual mass force. We obtain

$$\big(\mathbb{I} + \mathbb{A}_{vmt}\big)^{-1} = \begin{pmatrix} 1 & 0 & 0 & 0 \\ \frac{\eta_l u_l}{1+\eta_l+\eta_g} & \frac{1+\eta_g}{1+\eta_l+\eta_g} & -\frac{\eta_g u_g}{1+\eta_l+\eta_g} & \frac{\eta_g}{1+\eta_l+\eta_g} \\ 0 & 0 & 1 & 0 \\ -\frac{\eta_l u_l}{1+\eta_l+\eta_g} & \frac{\eta_l}{1+\eta_l+\eta_g} & \frac{\eta_g u_g}{1+\eta_l+\eta_g} & \frac{1+\eta_l}{1+\eta_l+\eta_g} \end{pmatrix} \tag{4.72}$$

Performing the matrix-matrix multiplication, we obtain the Jacobian matrix of the system

$$\mathbb{A}_{iso,vm} = \begin{pmatrix} 0 & 1 & 0 & 0 \\ -u_l^2 + \beta_l^v a_l^2 - \kappa_l^v u_l u_R & 2u_l + \kappa_l^v u_R & \sigma_l^v a_g^2 - \kappa_g^v u_g u_R & \kappa_g^v u_R \\ 0 & 0 & 1 & 0 \\ \sigma_g^v a_l^2 + \kappa_l^v u_l u_R & -\kappa_l^v u_R & -u_g^2 + \beta_g^v a_g^2 + \kappa_g^v u_g u_R & 2u_g - \kappa_g^v u_R \end{pmatrix} \tag{4.73}$$

Eq. (4.72) and Eq. (4.73) use the following auxiliary variables

$$\kappa_l^v \equiv \frac{\eta_l}{1+\eta_l+\eta_g}, \quad \kappa_g^v \equiv \frac{\eta_g}{1+\eta_l+\eta_g} \tag{4.74a}$$

$$\beta_l^v \equiv \frac{\beta_l^* + (\beta_l^* + \sigma_g^*)\eta_g}{1+\eta_l+\eta_g}, \quad \beta_g^v \equiv \frac{\beta_g^* + (\beta_g^* + \sigma_l^*)\eta_l}{1+\eta_l+\eta_g} \tag{4.74b}$$

$$\sigma_l^v \equiv \frac{\sigma_l^* + (\beta_g^* + \sigma_l^*)\eta_g}{1+\eta_l+\eta_g}, \quad \sigma_g^v \equiv \frac{\sigma_g^* + (\beta_l^* + \sigma_g^*)\eta_l}{1+\eta_l+\eta_g} \tag{4.74c}$$

where β_l^*, β_g^*, σ_l^*, and σ_g^* are auxiliary variables defined in Eq. (4.59). η_l, η_g, and u_R are additional auxiliary variables defined as

$$\eta_l \equiv \frac{C_{vm}}{\alpha_l \rho_l}, \quad \eta_g \equiv \frac{C_{vm}}{\alpha_g \rho_g}, \quad u_R \equiv u_g - u_l \tag{4.75}$$

Let λ be the eigenvalue. The characteristic polynomial is found with Mathematica

$$P_{iso,vm}(\lambda; C_{vm}) = \left[(\lambda - u_l)^2 - \beta_l^v a_l^2\right]\left[(\lambda - u_g)^2 - \beta_g^v a_g^2\right] - \sigma_l^v \sigma_g^v a_l^2 a_g^2 + f(\lambda; C_{vm}) \tag{4.76}$$

where

$$f(\lambda; C_{vm}) = u_R\left\{\kappa_g^v(\lambda - u_g)\left[(\lambda - u_l)^2 - (\beta_l^v + \sigma_g^v)a_l^2\right] - \kappa_l^v(\lambda - u_l)\left[(\lambda - u_g)^2 - (\beta_g^v + \sigma_l^v)a_g^2\right]\right\} \tag{4.77}$$

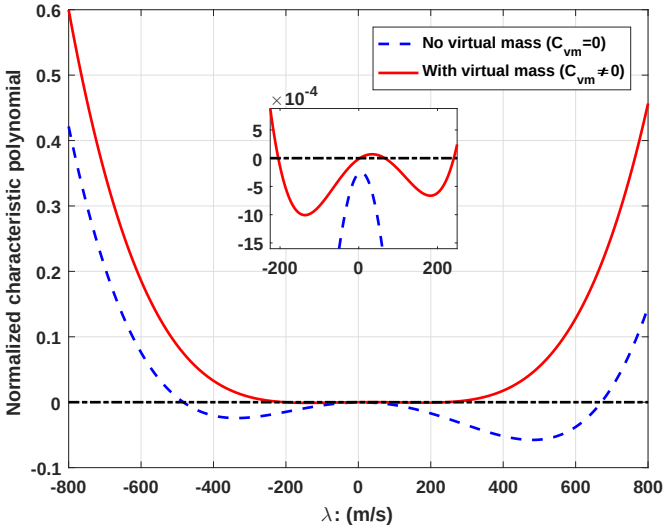

Figure 4.4: Behavior of characteristic polynomial $P_{iso,vm}(\lambda; C_{vm})$ with and without virtual mass

Figure 4.4 shows the behavior of $P_{iso,vm}(\lambda; C_{vm})$. For the case without the virtual mass force, the characteristic polynomial might have two complex roots; for the case with the virtual mass force, the

characteristic polynomial has 4 reals roots if the virtual mass is large enough. The following analysis gives the condition for C_{vm} to ensure the characteristic polynomial has 4 real roots.

Assuming that the virtual mass is positive, we can check that

$$P_{iso,vm}\big(u_l; C_{vm}\big) = -\frac{\alpha_l\rho_g a_g^2 a_l^2\big(u_g-u_l\big)^2}{\big(\alpha_l\rho_g a_g^2+\alpha_g\rho_l a_l^2\big)\big(1+\eta_l+\eta_g\big)} \le 0 \tag{4.78a}$$

$$P_{iso,vm}\big(u_g; C_{vm}\big) = -\frac{\alpha_g\rho_l a_l^2 a_g^2\big(u_g-u_l\big)^2}{\big(\alpha_l\rho_g a_g^2+\alpha_g\rho_l a_l^2\big)\big(1+\eta_l+\eta_g\big)} \le 0 \tag{4.78b}$$

For analysis purposes, we denote $u_1 = \min\big(u_l, u_g\big)$ and $u_2 = \max\big(u_l, u_g\big)$. Eq. (4.78) shows that $P_{iso,vm}\big(\lambda; C_{vm}\big)$ has at least two reals roots: one in interval $\big(-\infty, u_1\big)$ and the other one in interval $(u_2, +\infty)$. The other two roots, if they are real, they should be in the interval (u_1, u_2). Because of Eq. (4.78), we know that if the local maximum value of $P_{iso,vm}\big(\lambda; C_{vm}\big)$ in (u_1, u_2) is non-negative, then there are two real roots in (u_1, u_2), which gives the condition

$$\max_{\lambda\in(u_1,u_2)} P_{iso,vm}\left(\lambda; C_{vm}\right) \ge 0 \tag{4.79}$$

We obtain the critical value C_{vm}^{cr} when Eq. (4.79) is satisfied. Finding C_{vm}^{cr} analytically from Eq. (4.79) is complicated. However, we find that Toumi [30] gave a good approximation to C_{vm}^{cr}. The approximation is

$$C_{vm}^{\text{Toumi}} = 2\alpha_l\alpha_g\sqrt{\alpha_l\alpha_g\rho_l\rho_g} \tag{4.80}$$

We can prove that C_{vm}^{Toumi} is sufficient. Let

$$\begin{aligned} u_0 &= \frac{u_l+u_g}{2} + \frac{u_g-u_l}{2}\frac{\rho_0}{\rho_0+2\rho_s}\left(1-2\frac{\alpha_g\rho_l}{\rho_0}\right) \\ &= \frac{u_l+u_g}{2} + \frac{u_g-u_l}{2}\frac{\alpha_l\rho_g-\alpha_g\rho_l}{\rho_0+2\rho_s} \end{aligned} \tag{4.81}$$

We can check that $u_0 \in (u_1, u_2)$. Evaluating $P_{iso,vm}\big(\lambda; C_{vm}\big)$ with $\lambda = u_0$ and $C_{vm} = C_{vm}^{\text{Toumi}}$, we obtain

$$P_{iso,vm}\big(u_0; C_{vm}^{\text{Toumi}}\big) = \frac{\rho_0^2+4\big(\rho_s^2+\rho_0\rho_s\big)}{\big(\rho_0+2\rho_s\big)^4\big(\rho_l\rho_g+2\rho_m\rho_s\big)}\big(\alpha_l-\alpha_g\big)^2\alpha_l\alpha_g\rho_l^2\rho_g^2\big(u_g-u_l\big)^4 \ge 0 \tag{4.82}$$

where

$$\rho_0 = \alpha_l\rho_g + \alpha_g\rho_l \tag{4.83a}$$

$$\rho_m = \alpha_l\rho_l + \alpha_g\rho_g \tag{4.83b}$$

$$\rho_s = \sqrt{\alpha_l\alpha_g\rho_l\rho_g} \tag{4.83c}$$

Combining Eq. (4.78) with Eq. (4.82), we know that if $C_{vm} = C_{vm}^{\text{Toumi}}$, then there are two real roots on interval (u_1, u_2), one in (u_1, u_0) and another one in (u_0, u_2). Eq. (4.80) shows that the critical virtual mass does not depend on the relative velocity, which is different than the interfacial pressure correction that increases greatly with the relative velocity.

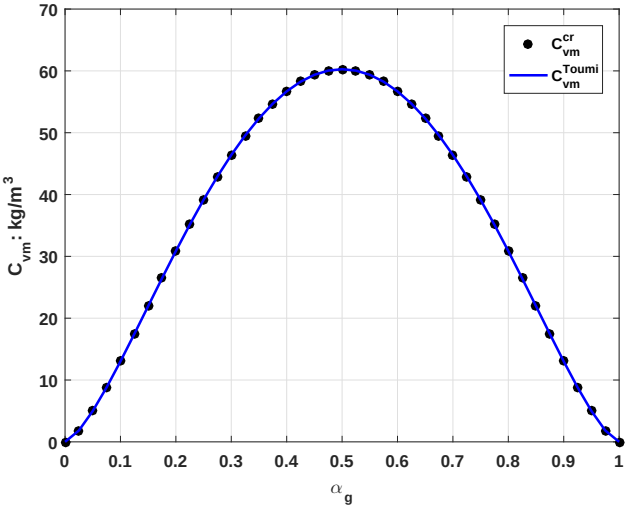

Figure 4.5: Critical virtual mass as a function of void fraction

Figure 4.5 shows the comparison of critical virtual mass calculated with Eq. (4.79) and Eq. (4.80). It is interesting to note that C_{vm}^{Toumi} is very close to the critical value C_{vm}^{cr}. Though we prove that C_{vm}^{Toumi} is sufficient, it is difficult to prove that C_{vm}^{Toumi} is also necessary.

Based on the previous analysis, we know that Eq. (4.79) is guaranteed to make the system hyperbolic. However, virtual mass force has a major drawback: the eigenvalues of the system are significantly shifted, which can be seen in Figure 4.4. Addition of virtual mass force changes the shape of characteristic polynomial (due to change in β_l^v and β_g^v), and the two real eigenvalues (related to the speed of sound) are shifted toward the phasic velocity. This drawback is shown in the following numerical tests.

Table 4.7 lists the eigenvalues of the isothermal system calculated with Eq. (4.76) and with the virtual mass force. The test conditions are shown in Table 4.5. The virtual mass force is not enabled in the odd cases, which correspond to the basic two-phase two-fluid model; the virtual mass force is added to the system in the even cases. From the table, we see that the virtual mass force works as expected to make the two complex eigenvalues (λ_1 and λ_3) real. The two real eigenvalues (λ_4 and λ_6) remain real but are shifted by the virtual mass force (sometimes significantly). Because the virtual mass is larger for the cases when void fraction is close to 0.5, we see that the shift in these two eigenvalues is very large for cases 3-6, 11-14, and 19-22. The two complex eigenvalues (λ_1 and λ_3) are made real except for case 10 and case 18. For these two cases, λ_1 and λ_3 are still complex but with very small imaginary parts. This is because of the numerical

Table 4.7: Eigenvalues of the system with and without virtual mass force: eigenvalues

Case	$\lvert u_g - u_l \rvert$	α_g	C_{vm}	λ_4	λ_6	λ_1	λ_3
1	10.	0.01	0	-1107.80	1110.78	8.51 -3.56i	8.51 +3.56i
2	10.	0.01	C_{vm}^{cr}	-1075.07	1076.47	7.05	7.06
3	10.	0.10	0	-679.41	692.57	3.42 -4.74i	3.42 +4.74i
4	10.	0.10	C_{vm}^{cr}	-527.89	532.66	4.19	4.19
5	10.	0.50	0	-581.21	600.12	0.55 -2.27i	0.55 +2.27i
6	10.	0.50	C_{vm}^{cr}	-393.21	403.21	1.92	1.95
7	10.	0.99	0	-566.81	586.80	0.01 -0.24i	0.01 +0.24i
8	10.	0.99	C_{vm}^{cr}	-564.85	584.75	0.23	0.24
9	100.	0.01	0	-1095.97	1126.03	84.97 -35.59i	84.97 +35.59i
10	100.	0.01	C_{vm}^{cr}	-1069.39	1083.45	70.44 -0.08i	70.44 +0.08i
11	100.	0.10	0	-625.33	756.34	34.50 -47.04i	34.50 +47.04i
12	100.	0.10	C_{vm}^{cr}	-509.02	557.16	41.33	42.00
13	100.	0.50	0	-497.74	686.28	5.73 -22.91i	5.73 +22.91i
14	100.	0.50	C_{vm}^{cr}	-352.25	452.20	17.74	21.07
15	100.	0.99	0	-476.88	676.76	0.06 -2.45i	0.06 +2.45i
16	100.	0.99	C_{vm}^{cr}	-476.17	675.01	1.89	3.03
17	500.	0.01	0	-1064.01	1247.90	408.06 -175.19i	408.06 +175.19i
18	500.	0.01	C_{vm}^{cr}	-1052.51	1135.58	342.38 -1.96i	342.38 +1.96i
19	500.	0.10	0	-485.95	1097.75	194.10 -194.29i	194.10 +194.29i
20	500.	0.10	C_{vm}^{cr}	-460.69	739.64	176.72	194.10
21	500.	0.50	0	-225.75	1079.06	73.35 -119.05i	73.35 +119.05i
22	500.	0.50	C_{vm}^{cr}	-240.40	737.32	62.48	134.36
23	500.	0.99	0	-84.61	1076.68	3.96 -22.73i	3.96 +22.73i
24	500.	0.99	C_{vm}^{cr}	-145.93	1095.00	3.55	78.00

error in calculating the C_{vm}^{cr} and the eigenvalues.

4.4 Dispersion analysis

In previous sections, the characteristic analysis is performed for the 1D two-phase two-fluid model. As is well known, the basic two-phase two-fluid model is in general ill-posed with complex eigenvalues. Two common hyperbolicity regularization methods, interfacial pressure correction and virtual mass force, are studied analytically. Regardless of the physical validity of these two methods, we see that both methods are capable of making the system hyperbolic. However, both methods have drawbacks: the interfacial pressure correction is very large for large relative velocity; the virtual mass force depends weakly on the relative velocity, but it changes significantly the shape of the characteristic polynomial and the magnitude of the two real eigenvalues, especially for the case where the void fraction is close to 0.5. It is very difficult to justify the regularization methods.

The characteristic analysis corresponds to the case where the wave number $k \to \infty$ or $\mathbb{S}_0 = \mathbf{0}$. For the case with finite wave number and non-trivial source, we need to perform a dispersion analysis. This allows to study the effect of algebraic source terms on the stability of the system. Unlike the characteristic analysis where we can perform analytical analysis, it is very difficult to perform the dispersion analysis analytically because of two reasons: 1) the source terms are in general problem-dependent and are complicated non-linear functions of the unknown variables; 2) the dispersion analysis requires finding roots of a complex characteristic polynomial. Thus, we will derive the dispersion relation analytically as much as possible and then solve it numerically. As mentioned earlier, the energy equation does not affect the dynamic character of the two-phase system, we will perform the dispersion analysis for the isothermal system.

Recall that the governing equation for the isothermal system is

$$\frac{\partial \alpha_l \rho_l}{\partial t} + \frac{\partial \alpha_l \rho_l u_l}{\partial x} = 0 \tag{4.84a}$$

$$\frac{\partial \alpha_l \rho_l u_l}{\partial t} + \frac{\partial \left(\alpha_l \rho_l u_l^2 + \alpha_l p\right)}{\partial x} - p\frac{\partial \alpha_l}{\partial x} = \alpha_l \rho_l g_x - f_{wl} + f_i \tag{4.84b}$$

$$\frac{\partial \alpha_g \rho_g}{\partial t} + \frac{\partial \alpha_g \rho_g u_g}{\partial x} = 0 \tag{4.84c}$$

$$\frac{\partial \alpha_g \rho_g u_g}{\partial t} + \frac{\partial \left(\alpha_g \rho_g u_g^2 + \alpha_g p\right)}{\partial x} - p\frac{\partial \alpha_g}{\partial x} = \alpha_g \rho_g g_x - f_{wg} - f_i \tag{4.84d}$$

which is in general ill-posed due to the complex eigenvalues discussed before. The isothermal system with the mathematical hyperbolicity regularization, e.g. interfacial pressure correction or virtual mass force, is

generalized to

$$\frac{\partial \alpha_l \rho_l}{\partial t} + \frac{\partial \alpha_l \rho_l u_l}{\partial x} = 0 \tag{4.85a}$$

$$\frac{\partial \alpha_l \rho_l u_l}{\partial t} + \frac{\partial \big(\alpha_l \rho_l u_l^2 + \alpha_l p\big)}{\partial x} - p\frac{\partial \alpha_l}{\partial x} - F_\delta = \alpha_l \rho_l g_x - f_{wl} + f_i \tag{4.85b}$$

$$\frac{\partial \alpha_g \rho_g}{\partial t} + \frac{\partial \alpha_g \rho_g u_g}{\partial x} = 0 \tag{4.85c}$$

$$\frac{\partial \alpha_g \rho_g u_g}{\partial t} + \frac{\partial \big(\alpha_g \rho_g u_g^2 + \alpha_g p\big)}{\partial x} - p\frac{\partial \alpha_g}{\partial x} + F_\delta = \alpha_g \rho_g g_x - f_{wg} - f_i \tag{4.85d}$$

For the following analysis, the regularization force F_δ is controlled by

$$F_\delta = \phi_{vm} C_{vm}^{cr} \left[\frac{\partial \big(u_g - u_l\big)}{\partial t} + u_l \frac{\partial u_g}{\partial x} - u_g \frac{\partial u_l}{\partial x} \right] + \phi_p \delta_p^{cr} \frac{\partial \alpha_g}{\partial x} \tag{4.86}$$

where ϕ_p and ϕ_{vm} are two dimensionless variables. Depending on the values of ϕ_p and ϕ_{vm}, we have the following 4 cases that are important to study

- $\phi_p = 0$ and $\phi_{vm} = 0$. No correction is added to the basic two-phase two-fluid model.
- $\phi_p > 0$ and $\phi_{vm} = 0$. Interfacial pressure correction is added to the to the basic two-phase two-fluid model.
- $\phi_p = 0$ and $\phi_{vm} > 0$. Virtual mass force is added to the basic two-phase two-fluid model.
- $\phi_p > 0$ and $\phi_{vm} > 0$. Both interfacial pressure correction and virtual mass force are added to the basic two-phase two-fluid model.

4.4.1 Dispersion analysis: interfacial and wall friction models

The starting point for the dispersion analysis is

$$\det\left(\mathbb{A}_0 + \frac{i}{k}\mathbb{S}_0 - \frac{\omega}{k}\mathbb{I} \right) = 0 \tag{4.87}$$

In this case, $\mathbb{A}_0$ is the matrix derived in Eq. (4.73) and $\mathbb{S}_0$ is

$$\mathbb{S}_0 = \big(\mathbb{I} + \mathbb{A}_{vmt}\big)_0^{-1} \left(\frac{\partial \mathbf{S}}{\partial \mathbf{U}} \right)_0 \tag{4.88}$$

where $\big(\mathbb{I} + \mathbb{A}_{vmt}\big)^{-1}$ is shown in Eq. (4.72). To proceed, we have to provide the source vector $\mathbf{S}$, which requires models for the interfacial friction and wall friction. We will use the models discussed in **Chapter**

2. For simplicity, the drag coefficient model is used for the interfacial friction

$$f_i = \frac{1}{8}\rho_c a_{lg} C_D |u_R| u_R \tag{4.89}$$

where u_R is the relative velocity, ρ_c is the density of continuous phase, a_{lg} is the volumetric interfacial area concentration, and C_D is the drag coefficient. For this dispersion analysis, we take

$$\rho_c = \rho_l, \quad a_{lg} = \frac{3.6\alpha_g}{d_o} \tag{4.90}$$

where d_o is the characteristic diameter, which we will set to a constant value. Finally, the interfacial friction is

$$f_i = K_i \alpha_g \rho_l |u_R| u_R, \quad \text{where } K_i = \frac{3.6}{8 d_o} C_D \tag{4.91}$$

For simplicity, we simplify the wall friction to

$$f_{wl} = \frac{1}{2D}\alpha_l \Big(\lambda_l \alpha_l \rho_l u_l^2 + \lambda_g \alpha_g \rho_g u_g^2 \Big) \tag{4.92a}$$

$$f_{wg} = \frac{1}{2D}\alpha_g \Big(\lambda_l \alpha_l \rho_l u_l^2 + \lambda_g \alpha_g \rho_g u_g^2 \Big) \tag{4.92b}$$

We take λ_l, λ_g, and D as constants. Finally, the wall friction to use is

$$f_{wl} = \alpha_l \Big(K_{wl} \alpha_l \rho_l u_l^2 + K_{wg} \alpha_g \rho_g u_g^2 \Big), \quad \text{where } K_{wl} = \frac{\lambda_l}{2D} \tag{4.93a}$$

$$f_{wg} = \alpha_g \Big(K_{wl} \alpha_l \rho_l u_l^2 + K_{wg} \alpha_g \rho_g u_g^2 \Big), \quad \text{where } K_{wg} = \frac{\lambda_g}{2D} \tag{4.93b}$$

Combining Eq. (4.89) and Eq. (4.93), we obtain

$$\frac{\partial \mathbf{S}}{\partial \mathbf{U}} = \begin{pmatrix} 0 & 0 & 0 & 0 \\ s_{21} & s_{22} & s_{23} & s_{24} \\ 0 & 0 & 0 & 0 \\ s_{41} & s_{42} & s_{43} & s_{44} \end{pmatrix} \tag{4.94}$$

where

$$s_{21} = g_x + \alpha_l K_{wl} u_l^2 + K_i \frac{\alpha_g}{\alpha_l}\big(u_g - u_l\big)\big(u_g + u_l\big) - c_0 \alpha_g a_l^2 \tag{4.95a}$$

$$s_{22} = -2\alpha_l K_{wl} u_l - 2K_i \frac{\alpha_g}{\alpha_l}\big(u_g - u_l\big) \tag{4.95b}$$

$$s_{23} = \alpha_l K_{wg} u_g^2 - 2K_i \frac{\rho_l}{\rho_g}\big(u_g - u_l\big)u_g + c_0 \alpha_l a_g^2 \tag{4.95c}$$

$$s_{24} = -2\alpha_l K_{wg} u_g + 2K_i \frac{\rho_l}{\rho_g}\big(u_g - u_l\big) \tag{4.95d}$$

$$s_{41} = \alpha_g K_{wl} u_l^2 - K_i \frac{\alpha_g}{\alpha_l}\big(u_g - u_l\big)\big(u_g + u_l\big) + c_0 \alpha_g a_l^2 \tag{4.95e}$$

$$s_{42} = -2\alpha_g K_{wl} u_l + 2K_i \frac{\alpha_g}{\alpha_l}\big(u_g - u_l\big) \tag{4.95f}$$

$$s_{43} = g_x + \alpha_g K_{wg} u_g^2 + 2K_i \frac{\rho_l}{\rho_g}\big(u_g - u_l\big)u_g - c_0 \alpha_l a_g^2 \tag{4.95g}$$

$$s_{44} = -2\alpha_g K_{wg} u_g - 2K_i \frac{\rho_l}{\rho_g}\big(u_g - u_l\big) \tag{4.95h}$$

where c_0 is an auxiliary variable

$$c_0 = \frac{\alpha_l\Big(K_{wl}\alpha_l\rho_l u_l^2 + K_{wg}\alpha_g\rho_g u_g^2\Big) + K_i\rho_l\big(u_g - u_l\big)^2}{\alpha_l\big(\alpha_l\rho_g a_g^2 + \alpha_g\rho_l a_l^2\big)} \tag{4.96}$$

Now we are ready to proceed with the numerical analysis.

4.4.2 Dispersion analysis: results

We are interested in the imaginary part of ω, denoted by ω_I, as a function of wave number k. Table 4.8 lists

Table 4.8: Physical conditions for the dispersion analysis

Variable	Value	Variable	Value
α_g	0.2	p: (MPa)	5.52
ρ_l: (kg/m^3)	788.47	ρ_g: (kg/m^3)	28.168
u_l: (m/s)	2.0	u_g: (m/s)	3.0
a_l: (m/s)	1121.6	a_g: (m/s)	496.14
K_{wl}	0.77485	K_{wg}	0.80268
K_i	317.68	C_D	0.47655

the test conditions for this analysis. The values of these variables are taken from a boiling pipe experiment, which will be discussed in the following chapter. Figure 4.6 and Figure 4.7 show the behavior of the growth factor (ω_I). The system has 4 eigenvalues for each wave number k, the maximum value of the imaginary

parts is taken to be the growth factor, that is

$$\omega_I = \max\left(\omega_{1,I}, \omega_{2,I}, \omega_{3,I}, \omega_{4,I}\right) \tag{4.97}$$

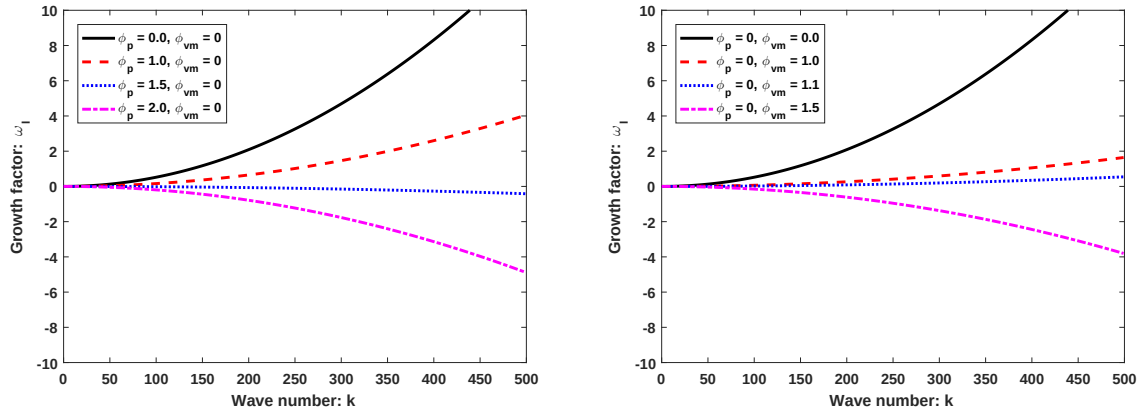

(a) Interfacial pressure correction (b) Virtual mass force

Figure 4.6: Effect of interfacial pressure correction (a) and virtual mass force (b) on the growth factor

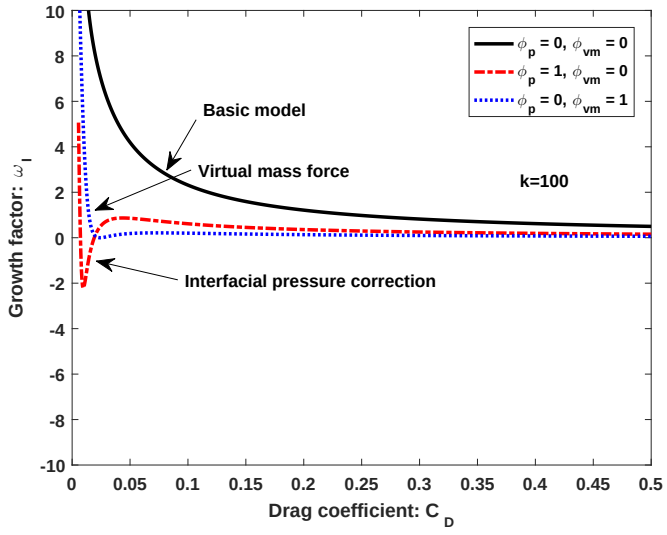

Figure 4.7: Effect of interfacial friction on the growth factor. Wall friction and gravity force are kept constant.

Figure 4.6 shows the effect of interfacial pressure correction and virtual mass force on the growth factor. As expected, the basic two-phase two-fluid model has positive growth factor and the growth factor increases with the wave number, which means that the system does not represent the short-wavelength phenomena [26], such as the dissipative viscous effect. When the interfacial pressure correction or virtual mass is

sufficiently large, we find that the growth factor becomes negative values, meaning the system is stable with short-wavelength phenomena. However, because the growth factor depends on the problem-dependent source terms, it is very difficult to specify how large the interfacial pressure correction or virtual mass is sufficient.

Numerical tests show that the interfacial friction helps reduce the growth factor. Figure 4.7 shows the growth factor as a function of the interfacial friction. When increasing the drag coefficient, the growth factor with interfacial pressure correction and virtual mass force has an interesting behavior. The growth factor decrease to a minimum as the drag coefficient is small, then increase to a maximum, and finally decrease gradually. It is worth mentioning that Pokharna [26] performed a similar dispersion analysis of the isothermal system. Our results are consistent with their results.

4.5 Conclusion

In this chapter, the Jacobian matrix of the two-phase two-fluid model is derived. The Jacobian matrix is simplified to a well-structured form with the help of a few auxiliary variables defined in **Chapter 3**. The derivation and simplification are general for arbitrary EOS. Based on the simplified Jacobian matrix, an analytical characteristic analysis and dispersion analysis to the two-phase two-fluid model are performed.

The characteristic analysis starts with the conservative part of the model. Analytical eigenvalues and eigenvectors of the conservative part are obtained with a reasonable approximation to the Jacobian matrix. Verification shows that the approximation is acceptable. The characteristic analysis to the complete model shows that the model is in general non-hyperbolic when the relative velocity is non-zero. Hyperbolicity regularization using the interfacial pressure correction and the virtual mass force is studied analytically. The minimum interfacial pressure correction and virtual mass force to ensure hyperbolicity is studied analytically and numerically. A dispersion analysis is performed for the two-phase two-fluid model using the physical conditions of a boiling pipe problem. The dispersion analysis shows that the basic two-phase two-fluid model gives positive growth factor for waves of all wavelength. Regardless of the validity of the interfacial pressure correction or virtual mass force, the dispersion analysis shows that both the interfacial pressure correction and the virtual mass force help reduce the growth factor. When the interfacial pressure correction or virtual mass force are large enough, the growth factor could be reduced to negative values, which means the system is stable for waves of all wavelength. However, the physical justification for the interfacial pressure correction or virtual mass force is difficult.

Chapter 5

FORWARD SOLVER

5.1 Introduction

A numerical method based on the first order donor cell differencing and a staggered grid is used in most two-phase flow system codes, such as RELAP [2], TRAC [3], and CATHARE [31]. In these system codes, inherent numerical dissipation and various degree of implicitness are necessary to stabilize the method. As is discussed in previous chapters, notations and discretization for these solvers are very complicated.

The development of shock-capturing upwind schemes started in early 1980s for single-phase hyperbolic systems (Euler equation of gas dynamics) by many pioneering researchers, such as Godunov [32], Roe [33], van Leer [34], and Osher [35]. The research and applications of shock-capturing upwind schemes were mainly in the aeronautical industry and in the Computational Fluid Dynamics (CFD) field. Exact or approximate Riemann solver is at the heart of most shock-capturing upwind schemes. Among different approximate Riemann solvers, the Roe-type approximate Riemann solver is the most popular one. The advanced discretization methods in CFD field include Weighted Essentially-Non-Oscillatory (WENO) [36, 37, 38, 39] and Discontinuous Galerkin Finite Element Method (DG-FEM) [40, 41, 42]. Among these advanced methods, the WENO-type method is both mathematically and numerically simple. The extension of shock-capturing upwind methods, especially the Roe-type method and the WENO-type method, to the two-phase two-fluid model is the focus of this chapter.

The challenge in constructing a shock-capturing upwind solver for the two-phase system is that the eigenvalue analysis is difficult because of the coupling between the two phases and the complex EOS. Several shock-capturing upwind schemes have been proposed for the two-phase two-fluid six-equation model. Toumi [30] proposed an approximate Riemann solver using Roe's approach assuming the liquid being non-compressible; Yeom [43] also proposed a stable upwind scheme based on the Harten, Lax, and van Leer (HLL) Riemann solver using the stiffened EOS; Chang [44] proposed the Advection Upwind Splitting Method (AUSM) method using stiffened EOS. Many of these schemes were based on a specific form of EOS, especially the stiffened EOS. However, the stiffened EOS is not general enough for practical two-phase problems,

e.g. a boiling pipe, and applications of these solvers to practical two-phase problems are not seen in the literature. In this chapter, we are going to develop a new scheme, based on a Roe-type and a WENO-type numerical flux, for the two-phase two-fluid model using arbitrary EOS.

5.2 Review of numerical methods for conservation law

This section gives a review of numerical methods for solving a conservation law. The numerical methods for single-phase Euler equation are used as examples.

5.2.1 Discretization

For 1D problems, the spatial discretization is shown in Figure 5.1. In this thesis, we consider uniform spatial discretization. The physical domain is divided into N cells. The cell center is denoted with an index i and the cell boundaries are denoted with $i \pm 1/2$, for $i = 1, \cdots, N$. All unknown variables are stored in the cell center (collocated mesh). On each side of the physical domain, ghosts cells are used to deal with boundary conditions.

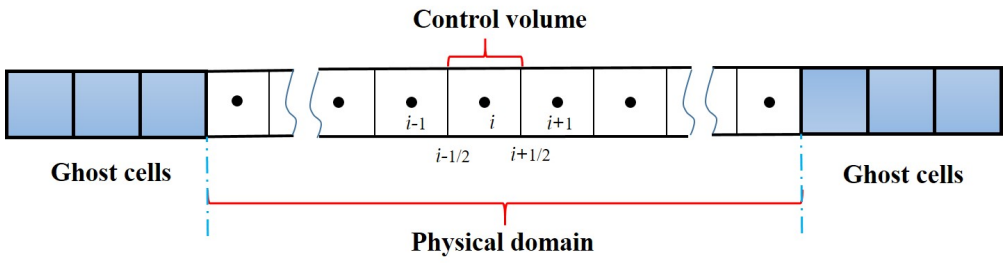

Figure 5.1: Schematic of the 1D spatial discretization

In time domain, the time step is denoted with $n = 0, 1, 2, \cdots$. The time step is determined by the Courant-Friedrichs and Lewy (CFL) condition

$$\Delta t = \mathrm{CFL} \frac{\Delta x}{\lambda_{\max}} \tag{5.1}$$

where $0 < \mathrm{CFL} \leq 1$ is a predetermined number and $\lambda_{\max}$ is the maximum wave speed (or eigenvalue) at the current time step.

5.2.2 Conservative method

The one-dimensional conservation law (without source) is

$$\frac{\partial \mathbf{U}}{\partial t} + \frac{\partial \mathbf{F}}{\partial x} = \mathbf{0} \tag{5.2}$$

where $\mathbf{U}$ is the vector of conservative variables and $\mathbf{F}$ is the vector of fluxes. To distinguish the conservative variables with the physical variables, i.e. $\big(\alpha_g, p, T_l, T_g, u_l, u_g\big)$, we will use $\mathbf{W}$ to denote the vector of physical variables. In this thesis, we will focus on conservative methods.

Definition 5.1. Conservative method. A conservative method for the conservation law, Eq. (5.2), is a numerical method of the form

$$\mathbf{U}_i^{n+1} = \mathbf{U}_i^n - \frac{\Delta t}{\Delta x}\Big[\hat{\mathbf{F}}_{i+\frac{1}{2}} - \hat{\mathbf{F}}_{i-\frac{1}{2}}\Big] \tag{5.3}$$

where

$$\hat{\mathbf{F}}_{i+\frac{1}{2}} = \mathbf{F}_{i+\frac{1}{2}}\big(\mathbf{U}_{i-l_L}^n, \cdots, \mathbf{U}_{i+l_R}^n\big) \tag{5.4}$$

where l_L and l_R are two non-negative integers. $\hat{\mathbf{F}}_{i\pm 1/2}$ is the numerical flux, which is an approximation to the exact flux. For a conservative method, a fundamental requirement on the numerical flux is the consistency condition

$$\mathbf{F}_{i+\frac{1}{2}}\big(\mathbf{U}, \cdots, \mathbf{U}\big) = \mathbf{F}\big(\mathbf{U}\big) \tag{5.5}$$

For example, the numerical flux of the Lax-Friedrichs method is given by

$$\hat{\mathbf{F}}_{i+\frac{1}{2}}^{\mathrm{LF}} = \frac{1}{2}\big(\mathbf{F}_i^n + \mathbf{F}_{i+1}^n\big) - \frac{1}{2}\lambda_{\max}\big(\mathbf{U}_{i+1}^n - \mathbf{U}_i^n\big) \tag{5.6}$$

In this thesis, two type of numerical flux are constructed: a Roe-type low-order numerical flux and a WENO-type high-order numerical flux, denoted by $\hat{\mathbf{F}}_{i+1/2}^{\mathrm{Roe}}$ and $\hat{\mathbf{F}}_{i+1/2}^{\mathrm{WENO}}$, respectively. We take the single-phase Euler equation as an example to explain the concept in these two numerical fluxes.

5.2.3 Roe-type numerical flux

The governing equation and the associated Jacobian matrix of Euler equation are given in Eq. (4.8) and Eq. (4.10) of **Chapter 4**. Let $\mathbb{A}$ be the Jacobian matrix, $\mathbb{D}$ be the diagonal matrix containing the eigenvalues,

and $\mathbb{K}$ be the right eigenvector matrix whose columns are the eigenvectors. Recall that

$$\mathbb{D} = \begin{pmatrix} u-a & 0 & 0 \\ 0 & u & 0 \\ 0 & 0 & u+a \end{pmatrix}, \mathbb{K} = \begin{pmatrix} 1 & 1 & 1 \\ u-a & u & u+a \\ H-ua & H-\gamma^* a^2 & H+ua \end{pmatrix} \tag{5.7}$$

where $\gamma^* = \big(\gamma - 1\big)^{-1}$ and

$$\mathbb{A} = \mathbb{K}\mathbb{D}\mathbb{K}^{-1} \tag{5.8}$$

In the expression of the Roe-type numerical flux, the following matrix $|\mathbb{A}|$ is commonly used

$$|\mathbb{A}| = \mathbb{K}|\mathbb{D}|\mathbb{K}^{-1}, \text{ with } |\mathbb{D}| = \begin{pmatrix} |u-a| & 0 & 0 \\ 0 & |u| & 0 \\ 0 & 0 & |u+a| \end{pmatrix} \tag{5.9}$$

The Roe-type numerical flux is constructed by

$$\hat{\mathbf{F}}^{\text{Roe}}_{i+\frac{1}{2}} = \frac{1}{2}\big(\mathbf{F}^n_i + \mathbf{F}^n_{i+1}\big) - \frac{1}{2}|\tilde{\mathbb{A}}|\big(\mathbf{U}^n_{i+1} - \mathbf{U}^n_i\big) \tag{5.10}$$

where $\tilde{\mathbb{A}}$ is the Jacobian matrix evaluated at an intermediate state $\tilde{\mathbf{U}}$ (or $\tilde{\mathbf{W}}$). The Roe-type numerical flux contains two parts: the first part $\big(\mathbf{F}^n_i + \mathbf{F}^n_{i+1}\big)/2$ is the classical central flux, which is unconditionally unstable even for linear advection problems; the second part, $|\tilde{\mathbb{A}}|\big(\mathbf{U}^n_{i+1} - \mathbf{U}^n_i\big)/2$, gives the correction to the central flux by removing characteristic waves moving in the wrong direction.

The remaining task is to find an appropriate intermediate state for evaluating $\tilde{\mathbb{A}}$. The intermediate state is often found with the Roe-Pike method [25, 45], which requires the intermediate state satisfying

$$\mathbf{U}^n_{i+1} - \mathbf{U}^n_i = \sum_{m=1}^{3} \tilde{c}_m \tilde{\mathbf{K}}_m \tag{5.11a}$$

$$\mathbf{F}^n_{i+1} - \mathbf{F}^n_i = \sum_{m=1}^{3} \tilde{c}_m \tilde{\lambda}_m \tilde{\mathbf{K}}_m \tag{5.11b}$$

where $\tilde{c}_m$ are the coefficients when decomposing $\mathbf{U}^n_{i+1} - \mathbf{U}^n_i$ to the eigenvectors. Note that $\tilde{c}_m$, $\tilde{\lambda}_m$, and $\tilde{\mathbf{K}}_m$ are all evaluated at the intermediate state. For the cell boundary where $\mathbf{U}_i$ and $\mathbf{U}_{i+1}$ are not close, finding the intermediate state is in fact non-trivial for an arbitrary EOS [45]. For brevity, we leave the derivation

in **Appendix B**. The conclusion is that by taking the following intermediate state

$$\tilde{\rho} = \sqrt{\rho_i \rho_{i+1}} \tag{5.12a}$$

$$\tilde{u} = \omega_i u_i + \omega_{i+1} u_{i+1} \tag{5.12b}$$

$$\tilde{H} = \omega_i H_i + \omega_{i+1} H_{i+1} \tag{5.12c}$$

$$\tilde{h} = \omega_i h_i + \omega_{i+1} h_{i+1} \tag{5.12d}$$

$$\tilde{\gamma} = \omega_i \gamma_i + \omega_{i+1} \gamma_{i+1} \tag{5.12e}$$

$$\tilde{a} = \omega_i a_i + \omega_{i+1} a_{i+1}, \qquad \text{if} \quad \Delta p = 0 \text{ and } \Delta h = 0 \tag{5.12f}$$

$$= \left[\frac{\Delta \rho}{\tilde{\gamma} \Delta p - \big(\tilde{\gamma} - 1\big) \tilde{\rho} \Delta h} \right]^{-1/2}, \quad \text{otherwise}$$

where ω_i and ω_{i+1} are weights defined as

$$\omega_i = \frac{\sqrt{\rho_i}}{\sqrt{\rho_i} + \sqrt{\rho_{i+1}}}, \quad \omega_{i+1} = \frac{\sqrt{\rho_{i+1}}}{\sqrt{\rho_i} + \sqrt{\rho_{i+1}}} \tag{5.13}$$

we can show that Eq. (5.11a) and Eq. (5.11b) are satisfied with the following coefficients

$$\tilde{c}_1 = \frac{1}{2\tilde{a}^2} \big(\Delta p - \tilde{\rho} \tilde{a} \Delta u \big) \tag{5.14a}$$

$$\tilde{c}_2 = \Delta \rho - \Delta p / \tilde{a}^2 \tag{5.14b}$$

$$\tilde{c}_3 = \frac{1}{2\tilde{a}^2} \big(\Delta p + \tilde{\rho} \tilde{a} \Delta u \big) \tag{5.14c}$$

where $\Delta \rho = \rho_{i+1} - \rho_i$, $\Delta u = u_{i+1} - u_i$, and $\Delta p = p_{i+1} - p_i$.

Once the intermediate state and the coefficients $\tilde{c}_m$ are found, the Roe-numerical flux can be transformed into

$$\hat{\mathbf{F}}^{\text{Roe}}_{i+\frac{1}{2}} = \frac{1}{2} \big(\mathbf{F}^n_i + \mathbf{F}^n_{i+1} \big) - \frac{1}{2} \sum_{m=1}^{3} \tilde{c}_m |\tilde{\lambda}_m| \tilde{\mathbf{K}}_m \tag{5.15}$$

Eq. (5.15) is preferable to Eq. (5.10) because it avoids constructing the eigenvector matrix, constructing the inverse of eigenvector matrix, and performing the matrix-vector product required by Eq. (5.10).

5.2.4 WENO-type numerical flux

The WENO scheme [36, 37, 38, 39] is based on the ENO (essentially non-oscillatory) scheme [46]. The key idea of the ENO scheme is to use the smoothest stencil among several candidates to approximate the fluxes at cell boundaries to obtain a high order accuracy and avoid spurious oscillations. The cell-average version

of the ENO scheme involves a procedure of reconstructing points values from cell averages. Later, Shu and Osher [36] developed the flux version of the ENO scheme. The WENO scheme of Liu, Osher, and Chan [47] is another way to obtain a high order accuracy. The idea of WENO scheme is that a convex combination of all the candidate stencils is used to approximate the numerical flux instead of using only the smoothest one. Each of the candidate stencils is assigned a weight to achieve the high-order accuracy in smooth regions and to avoid oscillations near discontinuities. Like ENO schemes, there are two versions of WENO schemes [38, 48, 49]: cell-average version and flux version. We will formulate our numerical flux based on the flux version of WENO schemes, because it requires fewer EOS evaluations than the cell-average version.

WENO reconstruction procedure

The WENO scheme is based on a WENO reconstruction procedure, see Figure 5.2. The WENO scheme uses a convex combination of three candidate stencils, i.e. $S_0 = \big(x_{i-2}, x_{i-1}, x_i\big)$, $S_1 = \big(x_{i-1}, x_i, x_{i+1}\big)$, and $S_2 = \big(x_i, x_{i+1}, x_{i+2}\big)$, to approximate the numerical flux at the cell boundary $x_{i+1/2}$.

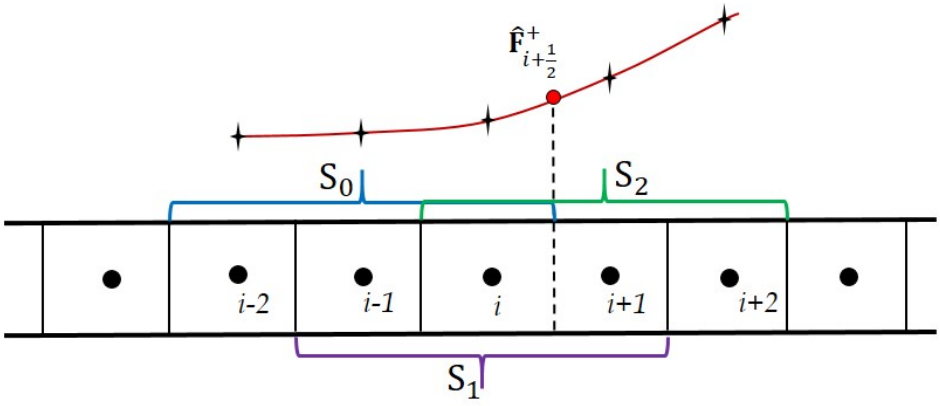

Figure 5.2: Schematic of the WENO reconstruction procedure

Let f be a scalar flux function. The approximate numerical flux at the cell boundary $x_{i+1/2}$ from WENO reconstruction procedure is

$$\hat{f}_{i+\frac{1}{2}} = \text{WenoRS}\big(f_{i-2}, f_{i-1}, f_i, f_{i+1}, f_{i+2}\big) = \sum_{k=0}^{2} \omega_k q_k\big(f_{i+k-2}, f_{i+k-1}, f_{i+k}\big) \tag{5.16}$$

where $\text{WenoRS}\big()$ is the reconstruction function. q_k is the interpolation function and ω_k is the weight of k-th stencil. q_k is defined by

$$q_k\big(g_0, g_1, g_2\big) = \sum_{m=0}^{2} a_{km} g_m \tag{5.17}$$

where a_{km} for $k, m = 0, 1, 2$ are constant coefficients given by Jiang [38]. Table 5.1 lists the coefficients a_{km}.

Table 5.1: Constant coefficients a_{km} used in the WENO reconstruction procedure

a_{km}	$m=0$	$m=1$	$m=2$
$k=0$	1/3	-7/6	11/6
$k=2$	-1/6	5/6	1/3
$k=3$	1/3	5/6	-1/6

The weight ω_k is

$$\omega_k = \frac{\theta_k}{\theta_0+\theta_1+\theta_2}, \quad \text{with} \quad \theta_k = \frac{C_k}{\big(\epsilon + \mathrm{IS}_k\big)^2} \tag{5.18}$$

where C_k is the optimal weight. In [38], $C_0 = 1/10$, $C_1 = 6/10$, and $C_2 = 3/10$ are used. $\epsilon = 10^{-6}$ is a positive real number to avoid the denominator becoming zero. IS_k is the smoothness measurement of the flux function in the k-th candidate stencil,

$$\mathrm{IS}_0 = \frac{13}{12}\big(f_{i-2} - 2f_{i-1} + f_i\big)^2 + \frac{1}{4}\big(f_{i-2} - 4f_{i-1} + 3f_i\big)^2 \tag{5.19a}$$

$$\mathrm{IS}_1 = \frac{13}{12}\big(f_{i-1} - 2f_i + f_{i+1}\big)^2 + \frac{1}{4}\big(f_{i-1} - f_{i+1}\big)^2 \tag{5.19b}$$

$$\mathrm{IS}_2 = \frac{13}{12}\big(f_i - 2f_{i+1} + f_{i+2}\big)^2 + \frac{1}{4}\big(3f_i - 4f_{i+1} + f_{i+2}\big)^2 \tag{5.19c}$$

The details of defining the weights of the stencils are referred to [38]. The key idea is: for each stencil, the weight is assigned a very small positive value if a discontinuity is detected in that stencil; if no discontinuities are detected in all three stencils, the weights are assigned to achieve optimal accuracy. The WENO reconstruction procedure is problem independent and works like a interpolation procedure for any scalar functions.

WENO-type numerical flux for a non-linear system

We take the Euler equation as an example to explain the procedure for constructing a WENO-type numerical flux for a non-linear system. The WENO reconstruction procedure does not take into account the upwind information, which is however required by the numerical flux. To account for the upwind information, Jiang [38] suggest using the flux vector splitting approach. At first, the flux in the cell center is split into positive and negative parts

$$\mathbf{F}_i = \mathbf{F}_i^+ + \mathbf{F}_i^-, \quad \text{for each } i \tag{5.20}$$

The flux should be split such that $\mathbf{F}_i^+$ contains waves moving in the positive direction and $\mathbf{F}_i^-$ contains waves moving in the negative direction. Then, the WENO reconstruction procedure is applied to the two parts to

give $\hat{\mathbf{F}}^{+}_{i+1/2}$ and $\hat{\mathbf{F}}^{-}_{i+1/2}$. Finally, the numerical flux is obtained with

$$\mathbf{F}^{\text{WENO}}_{i+\frac{1}{2}} = \hat{\mathbf{F}}^{+}_{i+\frac{1}{2}} + \hat{\mathbf{F}}^{-}_{i+\frac{1}{2}} \tag{5.21}$$

In practice, the most common flux splitting approach is the Lax-Friedrichs flux splitting

$$\mathbf{F}^{\pm}_{i} = \frac{1}{2}\big(\mathbf{F}_i \pm \lambda_{\max}\mathbf{U}_i\big), \quad \text{for each } i \tag{5.22}$$

where $\lambda_{\max}$ is the maximum wave speed or eigenvalue at a time level.

The WENO reconstruction procedure works for a scalar flux function, the natural approach in constructing $\hat{\mathbf{F}}^{+}_{i+1/2}$ and $\hat{\mathbf{F}}^{-}_{i+1/2}$ would be the component-by-component reconstruction. However, for problems that contain strong discontinuities, the component-by-component reconstruction is not effective in the sense that spurious solutions exist near the discontinuities. In this case, Jiang [38] suggest applying the reconstruction in characteristic space. The reconstruction in characteristic space will be used in this thesis.

We take the positive part as an example to explain the reconstruction process. The procedure for the negative part is analogous. Let $\tilde{\mathbb{K}}$ be the intermediate eigenvector matrix used in the Roe-type numerical flux, the reconstruction has three steps. First, the split flux vector is projected into the characteristic space by

$$\big(\boldsymbol{\mathcal{F}}^{+}_{i-2}, \boldsymbol{\mathcal{F}}^{+}_{i-1}, \boldsymbol{\mathcal{F}}^{+}_{i}, \boldsymbol{\mathcal{F}}^{+}_{i+1}, \boldsymbol{\mathcal{F}}^{+}_{i+2}\big) = \tilde{\mathbb{K}}^{-1} \cdot \big(\mathbf{F}^{+}_{i-2}, \mathbf{F}^{+}_{i-1}, \mathbf{F}^{+}_{i}, \mathbf{F}^{+}_{i+1}, \mathbf{F}^{+}_{i+2}\big) \tag{5.23}$$

Second, in the characteristic space, the WENO reconstruction procedure is applied component-by-component to get the flux at the cell boundary, i.e.

$$\boldsymbol{\mathcal{F}}^{+}_{i+\frac{1}{2},m} = \text{WenoRS}\big(\boldsymbol{\mathcal{F}}^{+}_{i-2,m}, \boldsymbol{\mathcal{F}}^{+}_{i-1,m}, \boldsymbol{\mathcal{F}}^{+}_{i,m}, \boldsymbol{\mathcal{F}}^{+}_{i+1,m}, \boldsymbol{\mathcal{F}}^{+}_{i+2,m}\big), \quad \text{for} \quad m = 1, 2, 3 \tag{5.24}$$

Third, the flux at the cell boundary is projected back to the normal space by

$$\mathbf{F}^{+}_{i+\frac{1}{2}} = \tilde{\mathbb{K}} \cdot \boldsymbol{\mathcal{F}}^{+}_{i+\frac{1}{2}} \tag{5.25}$$

$\mathbf{F}^{+}_{i+1/2}$ is then used in Eq. (5.21).

5.2.5 Third-order Total Variation Diminishing Runge-Kutta method

The third-order Total Variation Diminishing (TVD) Runge-Kutta (RK3) method is often used with the WENO-type numerical flux to integrate the system of ordinary equations in time. For ease of notations, we

suppose the system is written as

$$\frac{\partial \mathbf{U}}{\partial t} = \boldsymbol{\mathcal{L}}^{\dagger}(\mathbf{U}) \tag{5.26}$$

where $\boldsymbol{\mathcal{L}}^{\dagger}$ contains the spatial differential operator and the source vector. The RK3 method is given by

$$\mathbf{U}^{*} = \mathbf{U}^{n} + \Delta t \boldsymbol{\mathcal{L}}^{\dagger}(\mathbf{U}^{n}) \tag{5.27a}$$

$$\mathbf{U}^{**} = \frac{3}{4}\mathbf{U}^{n} + \frac{1}{4}\mathbf{U}^{*} + \frac{1}{4}\Delta t \boldsymbol{\mathcal{L}}^{\dagger}(\mathbf{U}^{*}) \tag{5.27b}$$

$$\mathbf{U}^{n+1} = \frac{1}{3}\mathbf{U}^{n} + \frac{2}{3}\mathbf{U}^{**} + \frac{2}{3}\Delta t \boldsymbol{\mathcal{L}}^{\dagger}(\mathbf{U}^{**}) \tag{5.27c}$$

where $\mathbf{U}^{*}$ and $\mathbf{U}^{**}$ are conservative vectors at two intermediate steps.

5.3 Numerical solver for two-phase two-fluid model

In previous sections, we introduced two numerical flux for solving the 1D conservation law for single-phase problems: the Roe-type numerical flux and the WENO-type numerical flux. In this section, we extend these two numerical flux to the 1D two-phase two-fluid model.

Recall that the one-dimensional two-phase two-fluid model is

$$\underbrace{\frac{\partial \mathbf{U}}{\partial t} + \frac{\partial \mathbf{F}}{\partial x}}_{\text{Conservative parts}} \underbrace{+ \mathbf{P}_{ix}\frac{\partial \alpha_g}{\partial x} + \mathbf{P}_{it}\frac{\partial \alpha_g}{\partial t}}_{\text{Non-conservative parts}} = \underbrace{\mathbf{S}}_{\text{Source}} \tag{5.28}$$

where $\mathbf{U}$ is the vector of conservative variables. In practice, we need to solve for the physical variables, denoted by $\mathbf{W}$. For the two-phase two-fluid model, the physical variables are

$$\mathbf{W} = \begin{pmatrix} \alpha_g & p & T_l & T_g & u_l & u_g \end{pmatrix}^{T} \tag{5.29}$$

where the superscript T denote the transpose operator. Note that we assume the pressure of liquid and gas phases are equal.

The RK3 method is used to integrate the system in time. Here, we take the first step in RK3 method as an example to explain the process. After discretizing the equation in time and space, we get

$$\boldsymbol{\mathcal{L}}^{\dagger}(\mathbf{U}_i^n) = -\frac{\hat{\mathbf{F}}_{i+\frac{1}{2}} - \hat{\mathbf{F}}_{i-\frac{1}{2}}}{\Delta x} - \mathbf{P}_{ix,i}^{n}\frac{\alpha_{g,i+1}^{n} - \alpha_{g,i-1}^{n}}{2\Delta x} - \mathbf{P}_{it,i}^{n}\frac{\alpha_{g,i}^{n} - \alpha_{g,i}^{n-1}}{\Delta t} + \mathbf{S}_i^{n} \tag{5.30}$$

where $\hat{\mathbf{F}}_{i+1/2}$ and $\hat{\mathbf{F}}_{i-1/2}$ are the numerical fluxes, a Roe-type or a WENO-type numerical flux.

Note that we approximate the non-conservative part with a simple finite difference approximation. This approximation inherently requires the void fraction being smooth. For problems where the void fraction contains discontinuities, this approximation will cause issues on a very fine mesh. In other words, because the $p\partial\alpha_g/\partial x$ part is non-conservative, constructing a weak solution to a discontinuity is problematic [16].

In our numerical tests, we observe that it is possible to approximate the $\partial\alpha_g/\partial x$ with a high-order central or one-side finite difference scheme when the WENO-type numerical flux is used. However, the difficulties in determining the ghost cell quantities make high-order finite difference schemes less preferable, because inappropriate ghost cell quantities could easily corrupt the solutions in the physical domain. Applying the central second-order approximation to $\partial\alpha_g/\partial x$ will eventually degrade the WENO-type scheme to second-order accurate in space.

After each time step, we need to transform the conservative variables ($\mathbf{U}$) into physical variables ($\mathbf{W}$). This transformation is non-linear because of the complicated EOS. In this thesis, the transformation is handled by

$$\mathbf{U}_i^{n+1} - \mathbf{U}_i^n = (\mathbb{A}_{\mathrm{w}})_i^n \left(\mathbf{W}_i^{n+1} - \mathbf{W}_i^n\right) \tag{5.31}$$

where $\mathbb{A}_{\mathrm{w}} = \partial\mathbf{U}/\partial\mathbf{W}$. Then, we obtain

$$\mathbf{W}_i^{n+1} = \mathbf{W}_i^n + \left(\mathbb{A}_{\mathrm{w}}^{-1}\right)_i^n \left(\mathbf{U}_i^{n+1} - \mathbf{U}_i^n\right) \tag{5.32}$$

The details of $\mathbb{A}_{\mathrm{w}}$ and $\mathbb{A}_{\mathrm{w}}^{-1}$ are given in **Appendix D**.

The remaining task is to construct the numerical flux at the cell boundaries. We constructed two types of numerical flux: a Roe-type flux and a WENO-type flux.

5.3.1 Roe-type numerical flux

The conservative part matrix $\mathbb{A}_c$ of the two-phase two-fluid model is given in Eq. (4.36) of **Chapter 4**. Like the numerical flux for the Euler equation, the Roe-type numerical flux for the two-phase system is constructed with

$$\hat{\mathbf{F}}_{i+\frac{1}{2}}^{\mathrm{Roe}} = \frac{1}{2}\left(\mathbf{F}_i^n + \mathbf{F}_{i+1}^n\right) - \frac{1}{2}|\tilde{\mathbb{A}}_c|\left(\mathbf{U}_{i+1}^n - \mathbf{U}_i^n\right) \tag{5.33}$$

or equivalently,

$$\hat{\mathbf{F}}_{i+\frac{1}{2}}^{\mathrm{Roe}} = \frac{1}{2}\left(\mathbf{F}_i^n + \mathbf{F}_{i+1}^n\right) - \frac{1}{2}\sum_{m=1}^{6} \tilde{c}_m|\tilde{\lambda}_{c,m}|\tilde{\mathbf{K}}_{c,m} \tag{5.34}$$

where $\lambda_{c,m}$ and $\mathbf{K}_{c,m}$ are the m-th eigenvalue and eigenvector of the matrix $\mathbb{A}_c$. As was discussed in **Sec. 4.3**, we are not able to obtain the exact eigenvalues and eigenvectors of $\mathbb{A}_c$. In practice, we use the approximation

made in Eq. (4.42) and Eq. (4.43), i.e.

$$\lambda_{c,1} \approx u_l - \sqrt{\beta_l} a_l; \lambda_{c,2} = u_l; \lambda_{c,3} \approx u_l + \sqrt{\beta_l} a_l \tag{5.35a}$$

$$\lambda_{c,4} \approx u_g - \sqrt{\beta_g} a_g; \lambda_{c,5} = u_g; \lambda_{c,6} \approx u_g + \sqrt{\beta_g} a_g \tag{5.35b}$$

and the right eigenvectors are approximated as

$$\begin{gathered}
\mathbf{K}_{1,c} \approx \begin{pmatrix} 1 \\ u_l - \sqrt{\beta_l} a_l \\ H_l - \sqrt{\beta_l} a_l u_l \\ 0 \\ 0 \\ 0 \end{pmatrix}, \mathbf{K}_{2,c} \approx \begin{pmatrix} 1 \\ u_l \\ H_l - \gamma_l^* a_l^2 \\ 0 \\ 0 \\ 0 \end{pmatrix}, \mathbf{K}_{3,c} \approx \begin{pmatrix} 1 \\ u_l + \sqrt{\beta_l} a_l \\ H_l + \sqrt{\beta_l} a_l u_l \\ 0 \\ 0 \\ 0 \end{pmatrix} \\
\mathbf{K}_{4,c} \approx \begin{pmatrix} q_4 \\ q_4 \lambda_{c,4} \\ q_4 \left[H_l - u_l^2 + u_l \lambda_{c,4} \right] \\ 1 \\ u_g - \sqrt{\beta_g} a_g \\ H_g - \sqrt{\beta_g} a_g u_g \end{pmatrix}, \mathbf{K}_{5,c} \approx \begin{pmatrix} 0 \\ 0 \\ 0 \\ 1 \\ u_g \\ H_g - \gamma_g^* a_g^2 \end{pmatrix}, \mathbf{K}_{6,c} \approx \begin{pmatrix} q_6 \\ q_6 \lambda_{c,6} \\ q_6 \left[H_l - u_l^2 + u_l \lambda_{c,6} \right] \\ 1 \\ u_g + \sqrt{\beta_g} a_g \\ H_g + \sqrt{\beta_g} a_g u_g \end{pmatrix}
\end{gathered} \tag{5.36}$$

where $\gamma_l^* = 1/\big(\gamma_l - 1\big)$ and $\gamma_g^* = 1/\big(\gamma_g - 1\big)$. q_4 and q_6 are two auxiliary variables defined as

$$q_4 \equiv \frac{\sigma_l a_g^2}{\big(\lambda_{c,4} - \lambda_{c,1}\big)\big(\lambda_{c,4} - \lambda_{c,3}\big)}; \quad q_6 \equiv \frac{\sigma_l a_g^2}{\big(\lambda_{c,6} - \lambda_{c,1}\big)\big(\lambda_{c,6} - \lambda_{c,3}\big)} \tag{5.37}$$

The right eigenvector matrix can thus be approximated as

$$\mathbb{K}_c \approx \begin{pmatrix} \mathbf{K}_{1,c} & \mathbf{K}_{2,c} & \mathbf{K}_{3,c} & \mathbf{K}_{4,c} & \mathbf{K}_{5,c} & \mathbf{K}_{6,c} \end{pmatrix} \tag{5.38}$$

Like what is done for the Euler equation, the variables, $\tilde{c}_m$, $\tilde{\lambda}_{c,m}$, and $\tilde{\mathbf{K}}_{c,m}$, are evaluated at an appro-

priate intermediate state. Following the Roe-Pike's method, the intermediate state should satisfy

$$\mathbf{U}_{i+1}^n - \mathbf{U}_i^n = \sum_{m=1}^{6} \tilde{c}_m \tilde{\mathbf{K}}_{c,m} \tag{5.39a}$$

$$\mathbf{F}_{i+1}^n - \mathbf{F}_i^n = \sum_{m=1}^{6} \tilde{c}_m \tilde{\lambda}_{c,m} \tilde{\mathbf{K}}_{c,m} \tag{5.39b}$$

However, because of the complexity of the two-phase two-fluid model, it is very complicated to find the exact intermediate state. In addition, because the eigenvalues and eigenvectors are approximate, finding the exact intermediate state will not improve the numerical solution much. Based on the similarity of λ_c and $\mathbb{K}_c$ to that of the Euler equation, we propose to use the following intermediate variables

$$\tilde{\phi}_k = \omega_{k,i}\phi_{k,i} + \omega_{k,i+1}\phi_{k,i+1}, \text{ for } \phi = u, H, h, a, \gamma, \sigma, \beta \text{ and } k = l, g \tag{5.40}$$

where $\omega_{k,i}$ and $\omega_{k,i+1}$ are the weights defined by

$$\omega_{k,i} = \frac{\sqrt{\alpha_{k,i}\rho_{k,i}}}{\sqrt{\alpha_{k,i}\rho_{k,i}} + \sqrt{\alpha_{k,i+1}\rho_{k,i+1}}}, \quad \omega_{k,i+1} = \frac{\sqrt{\alpha_{k,i+1}\rho_{k,i+1}}}{\sqrt{\alpha_{k,i}\rho_{k,i}} + \sqrt{\alpha_{k,i+1}\rho_{k,i+1}}} \tag{5.41}$$

After specifying the intermediate variables, the coefficients $\tilde{c}_m$ are found by solving Eq. (5.39a). The procedure for solving $\tilde{c}_m$ is given in **Appendix C**. Finally, the numerical flux is constructed with Eq. (5.34). As will be shown in the following numerical tests, the Roe-type numerical flux works well even for problems with strong discontinuities.

5.3.2 WENO-type numerical flux

For the two-phase two-fluid model, the procedure for constructing the WENO-type numerical flux is the same as the procedure shown in Eq. (5.20) to Eq. (5.25). The difference is that the dimension of vectors and matrices increases from 3 to 6 and the eigenvector matrix $\tilde{\mathbb{K}}$ is replaced with $\tilde{\mathbb{K}}_c$, which is approximated with Eq. (5.38).

5.4 Numerical tests

A numerical solver is developed using the numerical method described in previous sections. As was discussed in **Chapter 4**, the basic two-phase two-fluid model has two complex eigenvalues when the relative velocity is non-zero. From a mathematical point of view, the two complex eigenvalues make the system ill-posed; from a numerical point of view, the numerical solver tends to give non-physical oscillations near discontinuities

when the spatial discretization is fine enough. The numerical tests will show that the interfacial pressure correction helps at least reduce the non-physical oscillations.

For testing purposes, we will use the interfacial pressure correction

$$F_\delta = \phi_p p \frac{\partial \alpha_g}{\partial x} \tag{5.42}$$

where ϕ_p is a dimensionless variable representing the normalized interfacial pressure correction. Because the physical justification for the interfacial pressure correction is difficult, we are unable to tell how large the correction should be. What we can claim is how the numerical solution behaves when a certain interfacial pressure correction is used. In our numerical tests, ϕ_p is evaluated with

$$\phi_p = \max\left\{ \left(\frac{\delta_p^{cr}}{p}\right)_1, \cdots, \left(\frac{\delta_p^{cr}}{p}\right)_N \right\} \tag{5.43}$$

where the maximum value is found over all cells. The value given by Eq. (5.43) ensures that the system is hyperbolic in the whole domain. To test the effect of this regularization on the numerical solution, we will enable or disable this regularization in the numerical tests. To distinguish the difference, we will use the legend 'ROE-IP' (or 'WENO-IP') for the results when the interfacial pressure correction is enabled.

As was discussed in **Chapter 4**, the virtual mass force can also hyperbolize the basic two-phase two-fluid model. But we will not consider the virtual mass force in our numerical tests for two reasons: 1) the addition of virtual mass force changes significantly the eigenvalues of the basic two-phase two-fluid model even for a small relative velocity; 2) the addition of virtual mass force adds extra difficulties to the numerical solver, because it requires constructing two extra upwind numerical fluxes. Unlike the $\partial \alpha_g / \partial x$ term, the discretization of the virtual mass force is non-trivial.

5.4.1 Periodic pipe

This is a periodic problem which is introduced for testing purposes. The problem has initially smooth solution in the whole pipe; after a certain time, discontinuities will be formed. The smooth solution of this problem is used to study the order of accuracy of Roe-type and WENO-type scheme. The source vector is ignored for this problem, i.e. $\mathbf{S} = \mathbf{0}$.

The periodic pipe is filled with water and steam, see Figure 5.3. The length of the pips is $L = 10$ m. Initially, in the whole pipe, the void fraction is $\alpha_g = 0.75$; the velocity of liquid and gas phase are 0; and the

temperature of liquid and gas are 300 K and 700 K. The initial pressure has a sinusoidal profile

$$p(x) = p_0 + p_1 \sin\left(k_0 2\pi \frac{x}{L}\right) \tag{5.44}$$

where $p_0 = 7.5$ MPa, $p_1 = 1.0$ MPa, and $k_0 = 1$. Keeping the void fraction, liquid/gas velocity, and liquid/gas temperature at constants, the solution is completely determined by 3 parameters, p_0, p_1, and k_0.

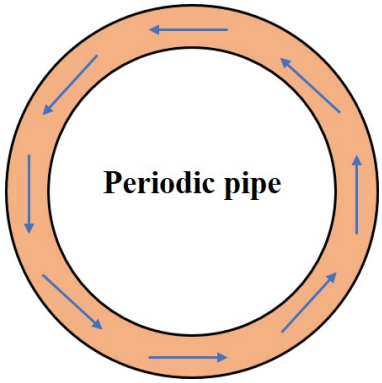

Figure 5.3: Schematic of a periodic pipe

Order of accuracy of Roe-type and WENO-type scheme

This test is to study the order of accuracy of Roe-type and WENO-type scheme. Both Roe-type and WENO-type scheme are run with CFL = 0.8. The numerical solution at $t = 5$ ms is used to calculate the discretization error. Since we do not have an exact solution, the solution from the WENO-type scheme using 6400 cells is used as the reference solution. As will be seen in the results, the WENO-type scheme converges very fast in space and the solution with 6400 cells almost reach the machine precision. We will use the L_2-norm to quantify the discretization error. The L_2-norm of a general function f in the physical domain $[x_1, x_2]$ is calculated by

$$\|\mathrm{DE}_N\|_2 = \sqrt{\frac{1}{x_2 - x_1} \int_{x_1}^{x_2} \left(f_N - f_{\text{reference}}\right)^2 \mathrm{d}x} \tag{5.45}$$

where DE_N denotes the discretization error of a numerical solution using N cells.

Figure 5.4 and Figure 5.5 show the numerical solution at 5 ms and 50 ms, respectively. Though the initial solution is smooth, discontinuities are formed when time goes on. We can find that the solution from WENO-type scheme converges rapidly to the reference solution, even 50 cells are enough to capture the correct profile. In the contrast, the solution from the Roe-type scheme converges slowly. The Roe-type

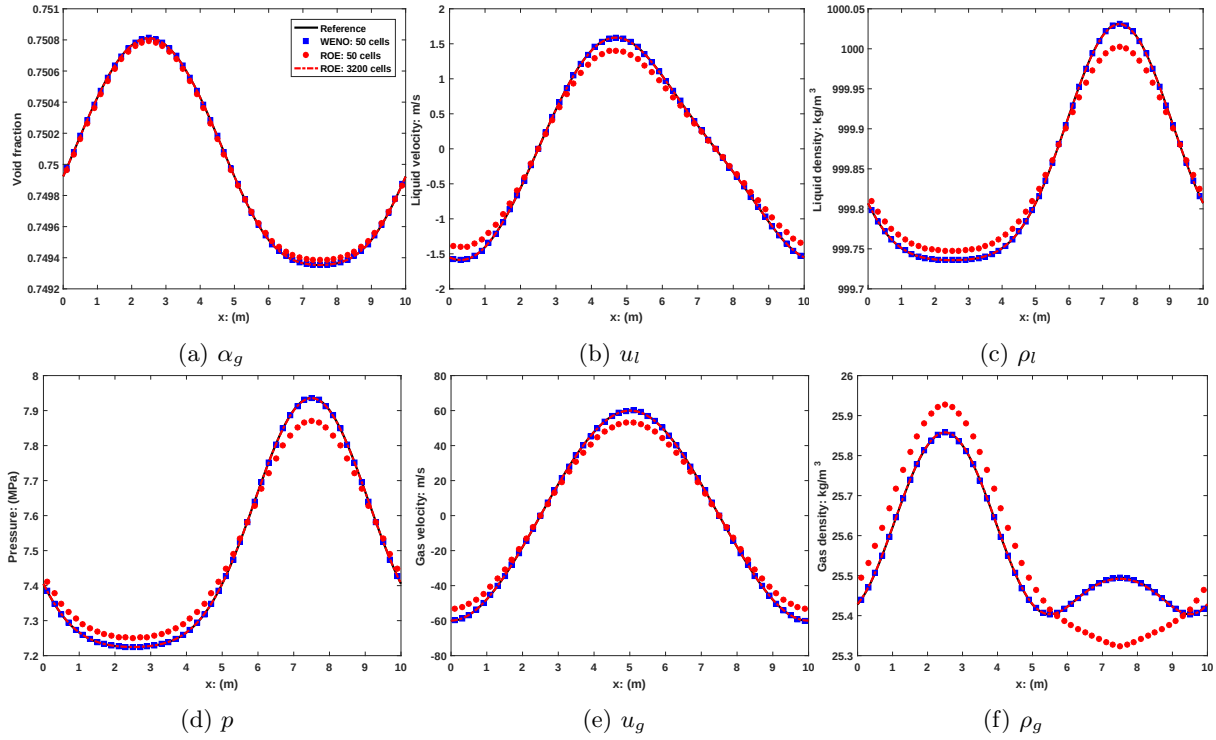

(a) α_g (b) u_l (c) ρ_l

(d) p (e) u_g (f) ρ_g

Figure 5.4: Solution of the periodic pipe problem at 5 ms. The reference solution is obtained with WENO-type scheme using 6400 cells.

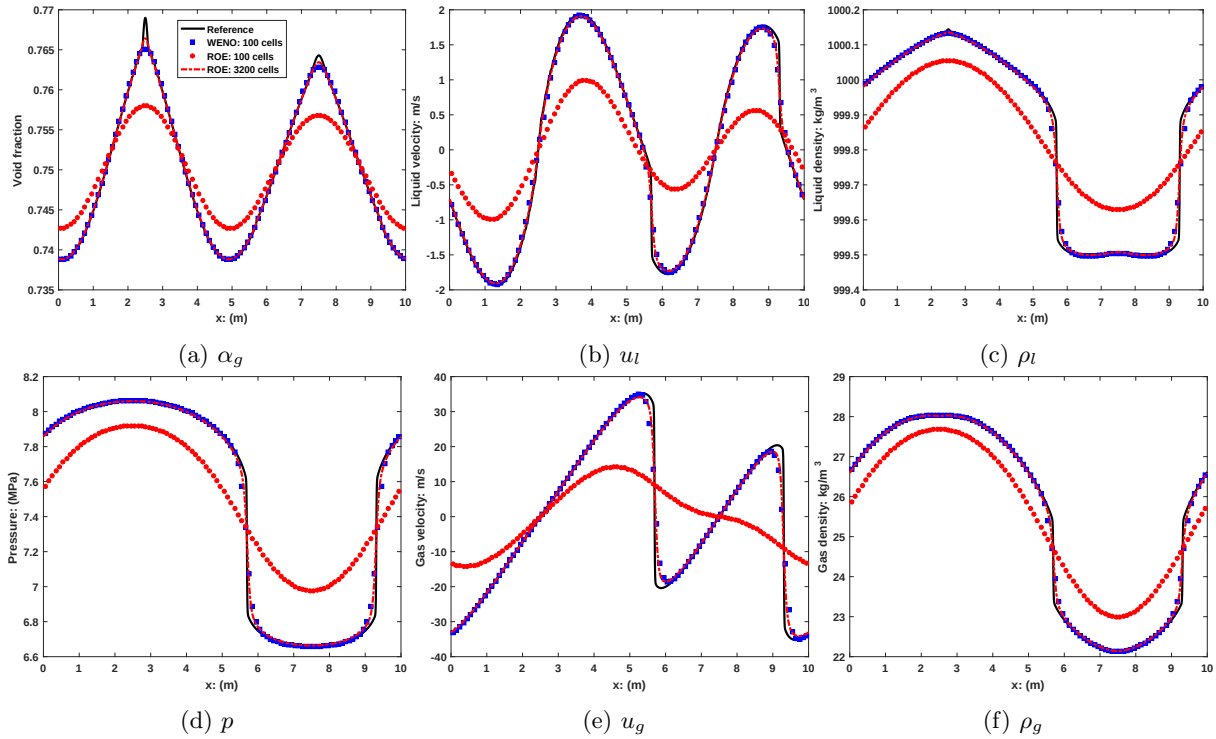

(a) α_g (b) u_l (c) ρ_l

(d) p (e) u_g (f) ρ_g

Figure 5.5: Solution of periodic pipe problem at 50 ms. The reference solution is obtained with WENO-type scheme using 1600 cells.

scheme requires a much finer mesh to capture the correct profile.

Figure 5.6 and Table 5.2 show the L_2-norm and the order of accuracy for the 6 physical variables. The solution at 5 ms is used to obtain the L_2-norm. We see that the order of accuracy of Roe-type scheme and WENO-type scheme are approximately 1 and 3. For the WENO-type scheme, when the mesh is fine enough (larger than 100 cells), L_2-norm of the discretization error does not reduce much when we further refine the mesh, because the numerical solution is so close to the reference solution that the truncation error tends to affect.

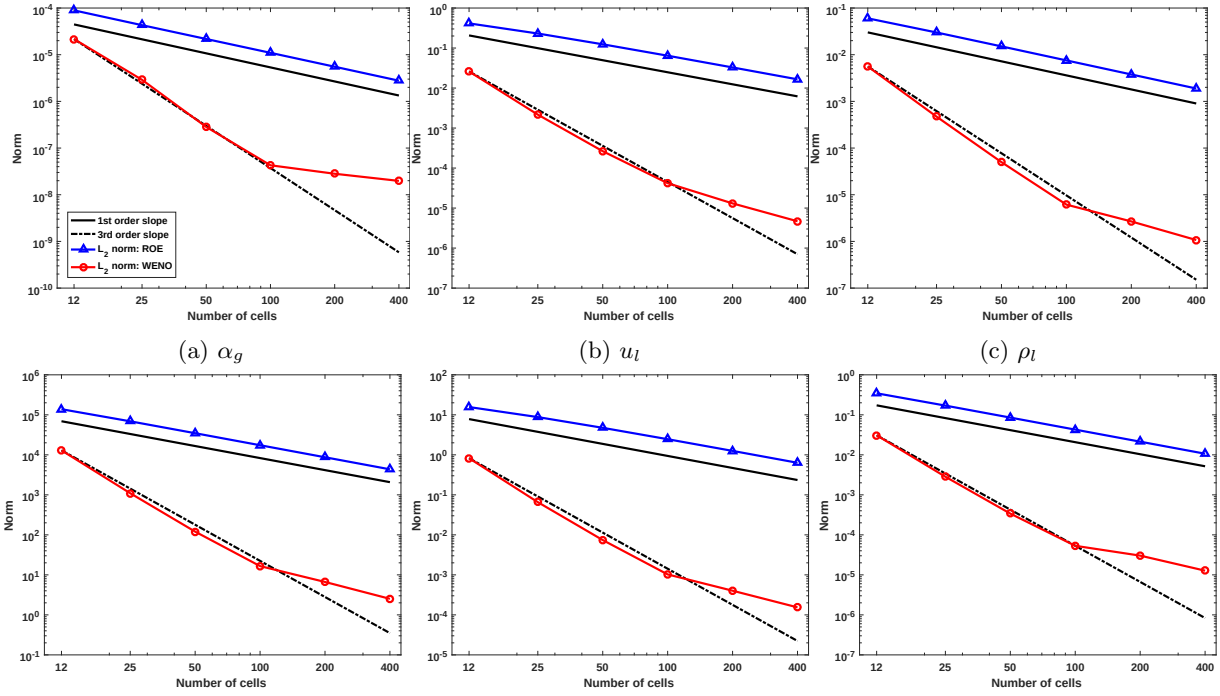

(a) α_g (b) u_l (c) ρ_l

(d) p (e) u_g (f) ρ_g

Figure 5.6: L_2-norm of discretization errors of different variables at 5 ms.

5.4.2 Shock-tube

This problem was originally introduced by Toumi [30]. The objective of this problem is to show that the solver can handle discontinuities and large differences between the two phases. The shock-tube is of 10 m in length and has a diaphragm in the middle ($x = 5$ m), which separates the left and right states. Both ends of the tube are kept closed, see Figure 5.7. The original initial conditions used by Toumi for left and right state pressure are 20 MPa and 10 MPa, which are close to the critical pressure of water/steam mixture. We modify the left and right state pressure to lower values, 15 MPa and 7.5 MPa, to avoid the critical water/steam region. Properties of liquid and gas are obtained from the IAPWS-IF97 formulation [15]. The

Table 5.2: Observed order of accuracy of Roe-type scheme and WENO-type scheme

N	α_g: (L_2, order)		p: (L_2, order)		u_l: (L_2, order)		u_g: (L_2, order)		ρ_l: (L_2, order)		ρ_g: (L_2, order)	
	ROE											
12	8.91E-05	–	1.38E+05	–	4.13E-01	–	1.57E+01	–	6.01E-02	–	3.45E-01	–
25	4.29E-05	1.00	6.89E+04	0.95	2.31E-01	0.79	8.78E+00	0.79	2.99E-02	0.95	1.70E-01	0.97
50	2.17E-05	0.98	3.47E+04	0.99	1.24E-01	0.90	4.74E+00	0.89	1.51E-02	0.99	8.54E-02	0.99
100	1.10E-05	0.98	1.74E+04	1.00	6.43E-02	0.95	2.46E+00	0.94	7.55E-03	1.00	4.27E-02	1.00
200	5.53E-06	0.99	8.70E+03	1.00	3.27E-02	0.97	1.25E+00	0.97	3.78E-03	1.00	2.13E-02	1.00
400	2.77E-06	0.99	4.35E+03	1.00	1.65E-02	0.99	6.33E-01	0.99	1.89E-03	1.00	1.07E-02	1.00
	WENO											
12	2.16E-05	–	1.30E+04	–	2.60E-02	–	8.24E-01	–	5.60E-03	–	3.09E-02	–
25	2.90E-06	2.74	1.10E+03	3.36	2.17E-03	3.38	6.57E-02	3.45	4.72E-04	3.37	2.84E-03	3.25
50	2.83E-07	3.35	1.20E+02	3.19	2.64E-04	3.04	7.42E-03	3.15	4.99E-05	3.24	3.40E-04	3.06
100	4.28E-08	2.73	1.66E+01	2.86	4.19E-05	2.66	1.03E-03	2.85	6.14E-06	3.02	5.33E-05	2.68
200	2.82E-08	0.60	6.65E+00	1.32	1.31E-05	1.68	4.02E-04	1.35	2.68E-06	1.20	3.03E-05	0.82
400	1.98E-08	0.51	2.52E+00	1.40	4.68E-06	1.48	1.54E-04	1.38	1.07E-06	1.32	1.27E-05	1.25

source vector is ignored for this problem, i.e. $\mathbf{S} = \mathbf{0}$.

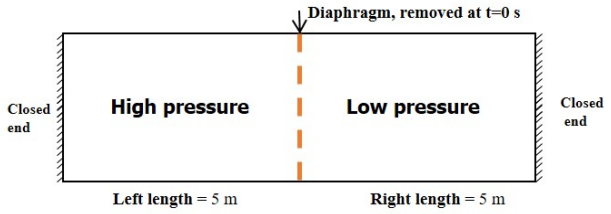

Figure 5.7: Schematic of two-phase shock-tube problem

The initial conditions for this test are listed in Table 5.3. Because the temperature of the two phases are not explicitly shown in this problem, we will report the density of the two phases. Numerical solution at 5 ms will be discussed.

Table 5.3: Initial conditions for two-phase shock-tube problem

Primary variables			Auxiliary variables		
	Left	Right		Left	Right
α_g	0.25	0.1	a_l (m/s)	1526.9	1514.9
p (MPa)	15.0	7.5	a_g (m/s)	576.66	613.83
ρ_l (kg/m^3)	1003.1	999.85	γ_l	1.1629	1.1555
ρ_g (kg/m^3)	57.941	25.527	γ_g	1.2971	1.2944
u_l (m/s)	0.0	0.0	ε_l	154.76	304.8
u_g (m/s)	0.0	0.0	ε_g	-0.01266	-0.01198

Test 1: wave structure

This test is to study the wave structure of the two-phase shock-tube problem and the performance of the numerical solver.

The relative velocity of this problem is not small and the solution contains very strong discontinuities, which make the ill-posedness issue very severe. Without a proper hyperbolicity regularization, we observed numerically that the oscillations near the middle discontinuities are so large that the numerical solver fails (e.g. non-physical void fraction and pressure are produced) for simulations with more than 100 cells. For testing purposes, we bring in the interfacial pressure correction. For this problem, to ensure the system is hyperbolic in the whole tube, the normalized interfacial pressure correction is $\phi_p = 0.126$, which means the interfacial pressure correction is comparable to the phasic pressure.

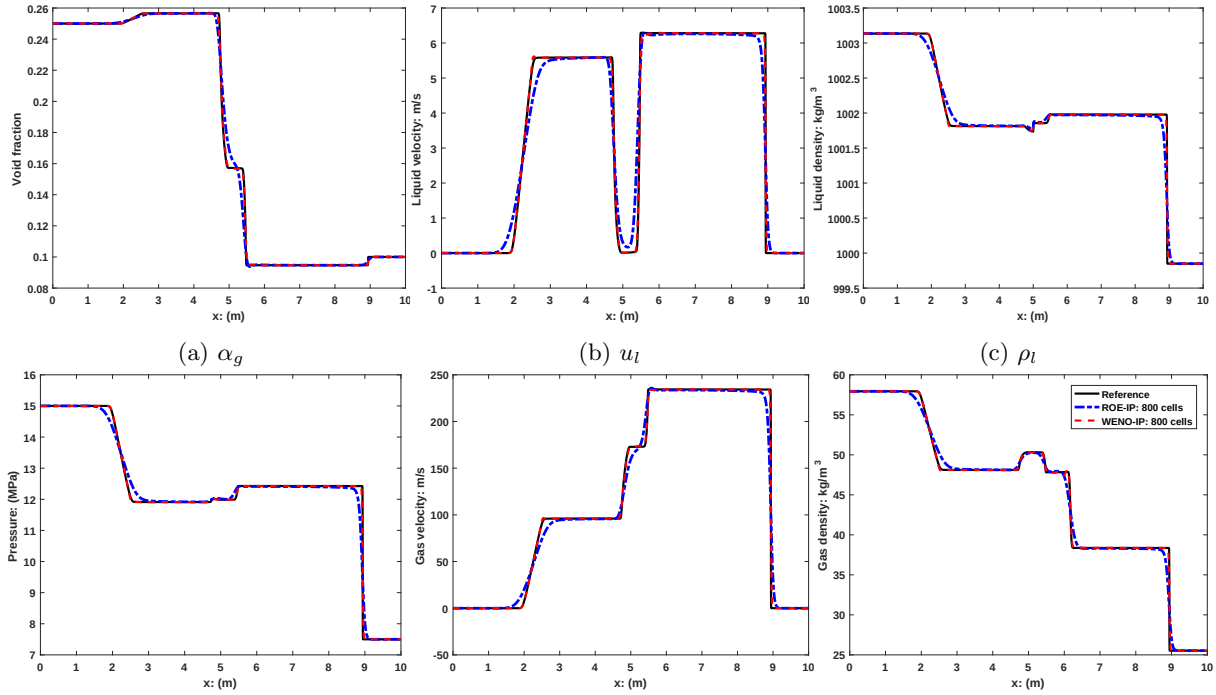

(a) α_g (b) u_l (c) ρ_l

(d) p (e) u_g (f) ρ_g

Figure 5.8: Solution of two-phase shock-tube problem at 5 ms.

Both the Roe-type scheme and the WENO-type scheme are run with CFL = 0.8. For comparison, the numerical solution from Roe-type scheme using 20000 cells is used as the reference solution. Figure 5.8 shows the numerical solution from both schemes at 5 ms. Taking the gas-phase velocity as an example, Figure 5.9 shows the grid convergence of both schemes. We see that both schemes work well. The WENO-type scheme is not oscillation-free near discontinuities, because the WENO-type scheme is only Essentially Non-Oscillatory [36, 37].

For ease of explanation, let λ_m, for $m = 1, \cdots, 6$ be the eigenvalues of the system, which are shown in Figure 5.10. The 6 characteristic waves associated with the eigenvalues are shown in Figure 5.11. λ_1 is a left-moving rarefaction wave with a head and tail speed about -49.78 m/s and -14.81 m/s; λ_2 is a contact

wave with a wave speed about zero, which represents the convection of liquid-phase enthalpy; λ_3 is a right-moving rarefaction wave with a head and tail speed about 101.1 m/s and 88.63 m/s; λ_4 is a left-moving rarefaction wave with head and tail speed about -612.8 m/s and -508.1 m/s; λ_5 is a contact wave with a wave speed about 234.3 m/s, which represents the convection of gas-phase enthalpy; λ_6 is a right-moving shock wave with a shock speed about 788.8 m/s.

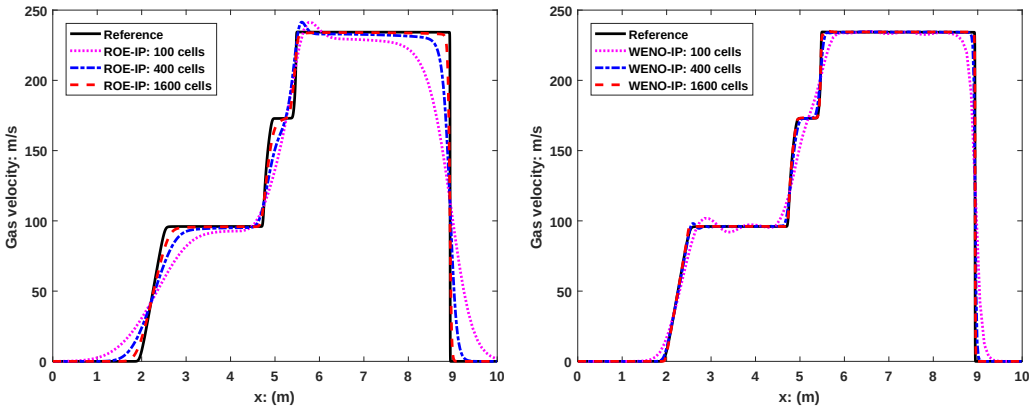

(a) (b)

Figure 5.9: Grid convergence of Roe-type scheme and WENO-type scheme for gas-phase velocity

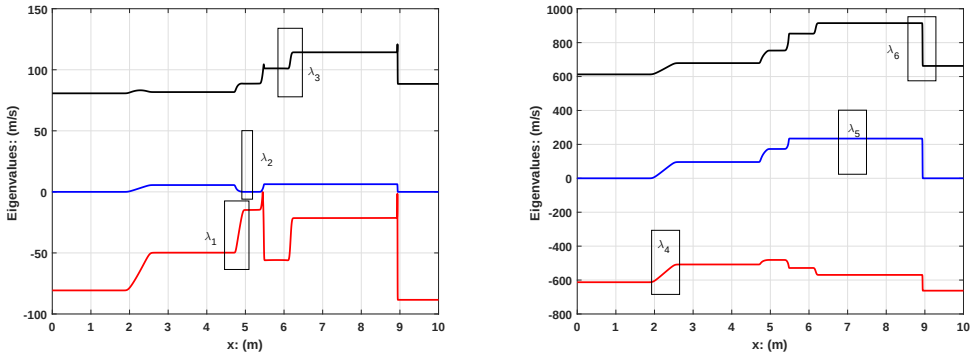

(a) (b)

Figure 5.10: Eigenvalues of the two-phase shock-tube problem. Eigenvalues are obtained with the reference solution

Test 2: two-phase coupling effect and two-phase to single-phase transition

Ignoring the source vector, the two-phase two-fluid model degenerates to the single-phase Euler equation when the void fraction approaches 0 or 1. The solution from the two-phase flow solver should approach the solution from a single-phase flow solver when the void fraction approaches 0 or 1. This test is designed to study the two-phase coupling and the two-phase to single-phase transition behavior. The test setup is

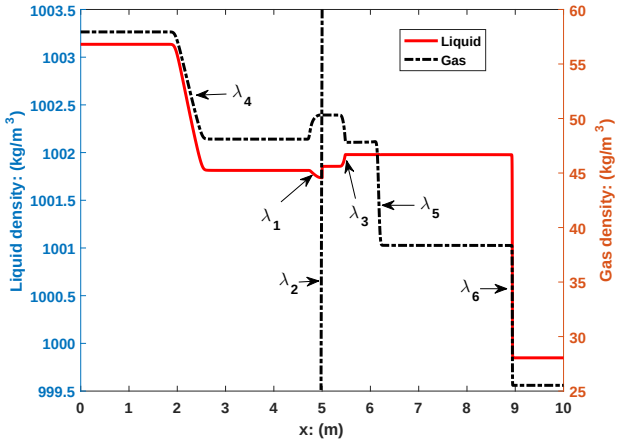

Figure 5.11: Wave structure of the shock-tube problem. Results are obtained with reference solution.

the same as in Test 1, except that the initial void fraction is uniform in the entire tube and is varying to approach 0 (down to 0.0001) or 1 (up to 0.99) for different cases. For comparison, a separate single-phase flow solver is constructed with the Roe-type numerical flux. The details of the single-phase flow solver are omitted here because it is a straightforward simplification of the two-phase flow solver.

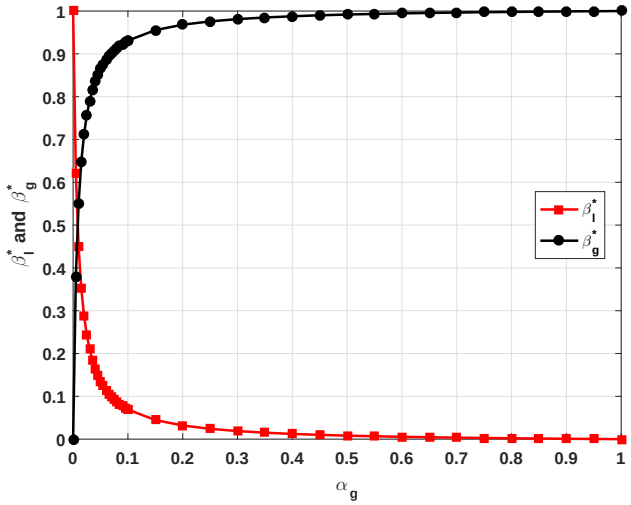

Figure 5.12: Two-phase coupling factors as a function of void fraction

The coupling effect of two phases is more important at a small void fraction, which could be explained by the two-phase coupling factors (β_l^* and β_g^*), which are defined in Eq. (4.48). Figure 5.12 shows the typical profile of the two-phase coupling factors as a function of void fraction. We can see that β_l^* and β_g^* change rapidly when the void fraction increases from 0 to about 0.1.

The Roe-type numerical scheme is run to $t = 5$ ms with CFL $= 0.8$ and 3200 cells. Figure 5.13 shows the gas-phase solution for different cases. When the void fraction approaches 1, the liquid phase has little effect

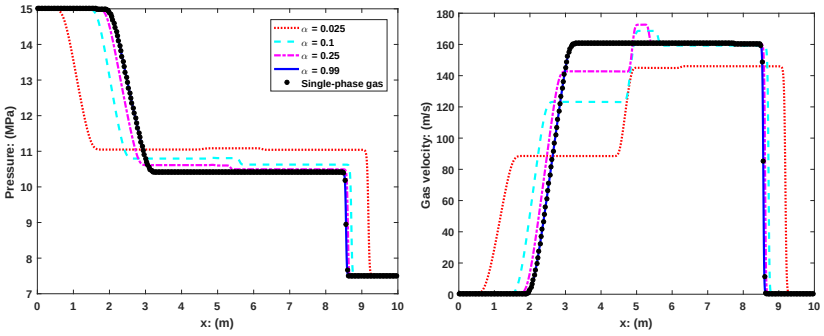

(a) p

(b) u_g

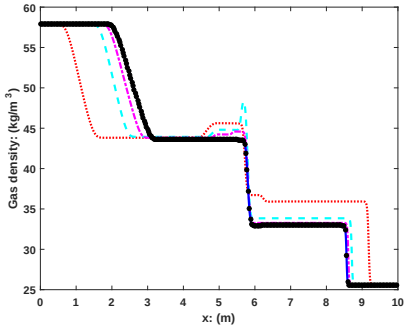

(c) ρ_g

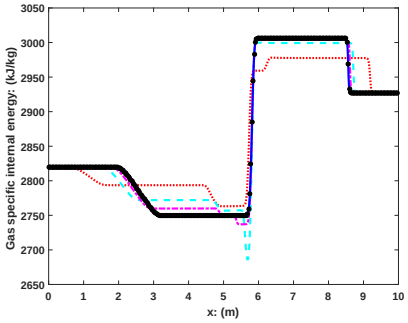

(d) e_g

Figure 5.13: Two-phase to single-phase gas transition.

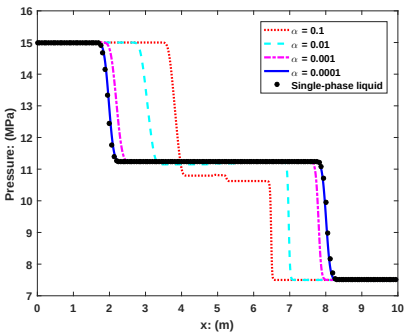

(a) p

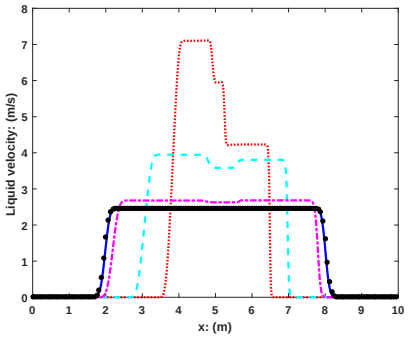

(b) u_l

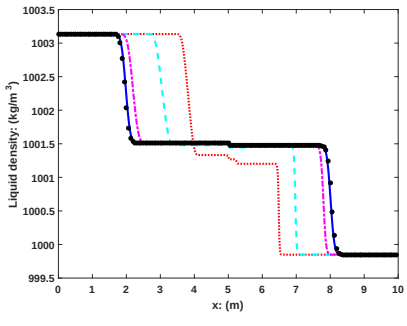

(c) ρ_l

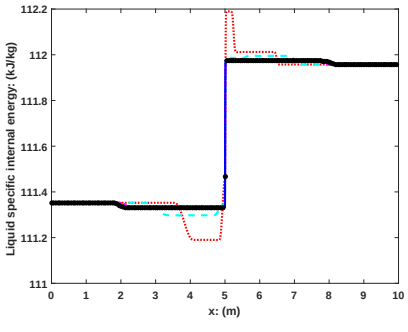

(d) e_l

Figure 5.14: Two-phase to single-phase liquid transition.

on the gas phase and the solution approaches the solution of the single-phase flow solver. The single-phase part is the classical Sod's test problem [25] for a real gas. Figure 5.14 shows the liquid-phase solution for different cases. Because the speed of sound in liquid phase is higher, solution is shown at 2 ms to capture all waves. When the void fraction approaches 0, the solution approaches the solution of the single-phase flow solver. The single-phase part is the classical Sod's test problem for a real liquid. As is expected, our two-phase solver is capable of transiting to a single-phase solver when the void fraction approaches 0 or 1, which gives us more confidence on the numerical solution.

5.4.3 Boiling pipe

A series of electrically heated experiments were performed in the early 1960s to investigate the void fraction profile in vertical tubes. The Christensen Test 15 [50, 18] is used to test the capability of our numerical solver for simulating a practical problem. Figure 5.15 is a schematic of the test facility. The test section was a 1.27 m high rectangular tube with a 1.11 x 4.44 cm cross-section. The tube was heated by passing an electrical current through the tube wall. A series of seven tests were conducted to investigate the void fraction profile based on different inlet conditions. The boundary conditions for Test 15 are: pressure = 5.52 MPa, power = 70 kW, inlet velocity = 1.15 m/s, and inlet subcooling =12.5 K.

The test section is modeled with a 1D vertical pipe. The hydraulic diameter of the pipe is $D = 1.776$ cm. The experimental and initial conditions are shown in Table 5.4. We use a non-zero initial void fraction (0.01) to avoid the phase appearance/disappearance issue. Let i_1 and i_N be the index of the first and last cell in the physical domain. At the inlet, the pressure in the ghost cells are taken to be the values in i_1^{th} cell; all other variables in the ghost cells are kept at inlet values. At the outlet, the pressure in the ghost cells are kept at the outlet values; all other variables in the ghost cells are taken to be the values in the i_N^{th} cell.

Table 5.4: Experiment and initial conditions for Christensen Test 15

Experiment conditions		Initial conditions	
Pipe height	1.27 m	–	–
Hydraulic diameter (D)	1.776 cm	–	–
Heated surface area (a_{wall})	225.225 m^{-1}	Void fraction	0.01
System pressure	5.52 MPa	Pressure	5.52 MPa
Heating power	70 kW	Liquid temperature	530.9 K
Equivalent wall heat flux (q_{wall})	0.49656 MW/m^2	Gas temperature	543.4 K
Inlet mass flux	906.6 $\text{kg/(m}^2\text{s)}$	Liquid velocity	1.15 m/s
Inlet subcooling	12.5 K	Gas velocity	1.15 m/s

Properties of water and steam are obtained from the IAPWS-IF97 formulation. The source vector is

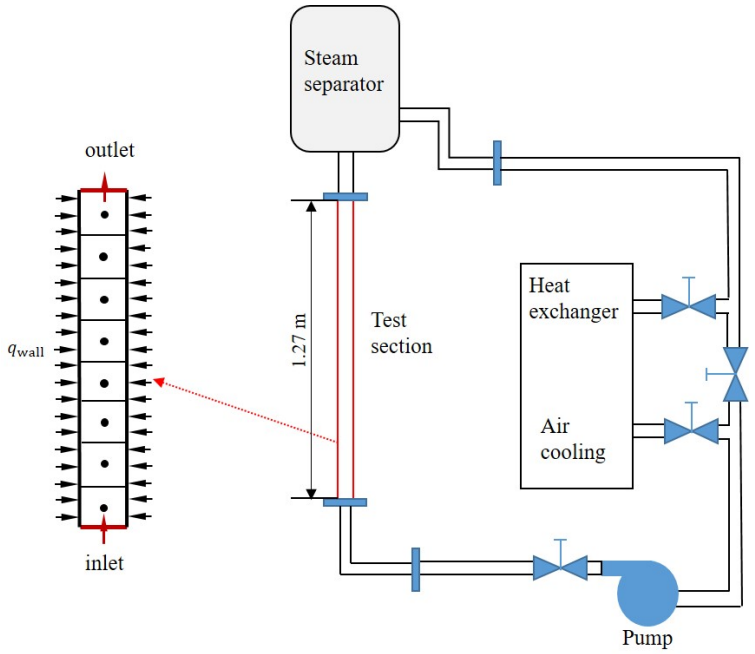

Figure 5.15: Schematic of the Christensen test facility and the simplified 1D problem

modeled as

$$\mathbf{S} = \begin{pmatrix} -\Gamma_g \\ -\alpha_l \rho_l g - f_{wl} + f_i - \Gamma_g u_i \\ Q_{wl} + Q_{il} - \Gamma_w h_l^{'} - \Gamma_{ig} h_l^{*} + \left(f_i - f_{wl} - \alpha_l \rho_l g - \Gamma_g u_i\right) u_l + \Gamma_g \frac{u_l^2}{2} \\ \Gamma_g \\ -\alpha_g \rho_g g - f_{wg} - f_i + \Gamma_g u_i \\ Q_{wg} + Q_{ig} + \Gamma_w h_g^{'} + \Gamma_{ig} h_g^{*} + \left(-f_i - f_{wg} - \alpha_g \rho_g g + \Gamma_g u_i\right) u_g - \Gamma_g \frac{u_g^2}{2} \end{pmatrix} \tag{5.46}$$

where Γ_g is the net vapor generation rate due to wall vapor generation (Γ_w) and bulk vapor generation (Γ_{ig}), u_i is the interface velocity, f_i is the interfacial friction, f_{wk} is the phasic wall friction, Q_{ik} is the phasic interfacial heat flux, Q_{wk} is the phasic wall heat flux, $h_k^{'}$ is the phasic enthalpy carried by the wall vapor generation, and h_k^{*} is the phasic enthalpy carried by the bulk vapor generation. Correlations based on RELAP5-3D code manual [5, 19] are used to model these quantities, see **Sec. 2.4**.

The solver is run to reach steady-state with CFL = 0.8. The finest mesh has 800 cells. Figure 5.16 shows the numerical solution of 6 physical variables. Unlike the shock-tube problem, where the solution contains discontinuities, the solution of this problem is smooth. Considering the simplified correlations for the source vector, we think the solution from our numerical solver is in a good agreement with the measurement data.

The numerical solution from the Roe-type scheme and the WENO-type scheme are consistent with each

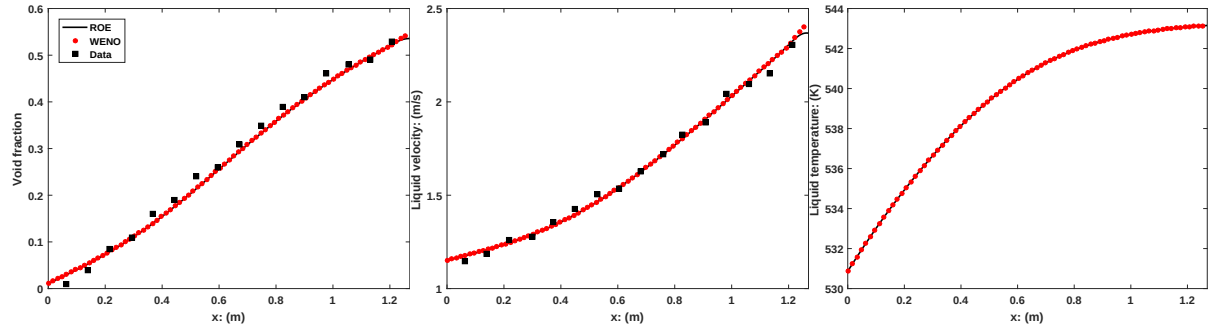

(a) α_g (b) u_l (c) T_l

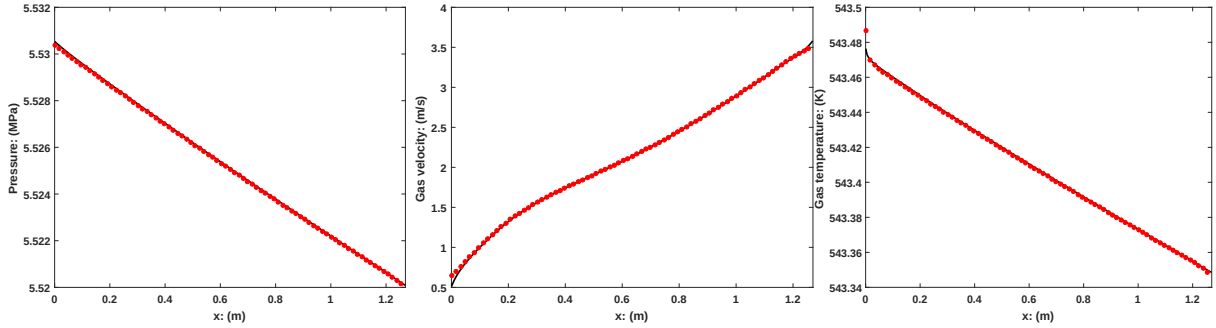

(d) p (e) u_g (f) T_g

Figure 5.16: Solution of Christensen Test 15 at steady-state. 800 cells are used for Roe-type and WENO-type scheme.

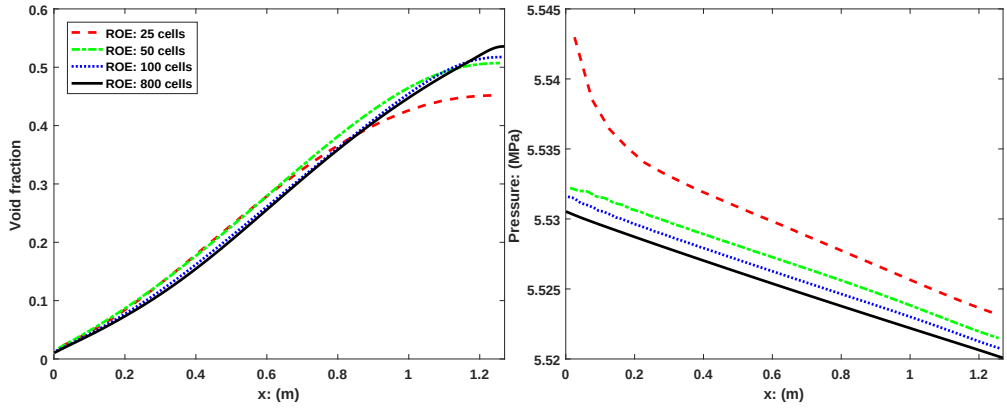

(a) α_g (b) p

Figure 5.17: Mesh convergence of Roe-type scheme for Christensen Test 15

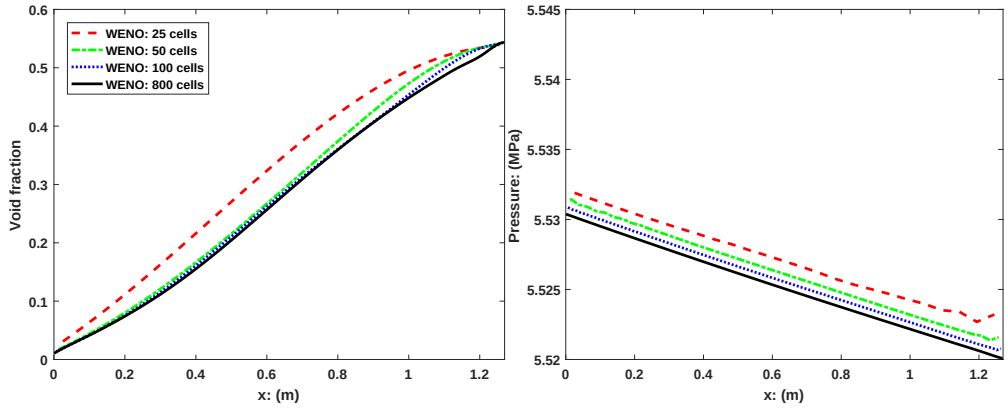

(a) α_g (b) p

Figure 5.18: Mesh convergence of WENO-type scheme for Christensen Test 15

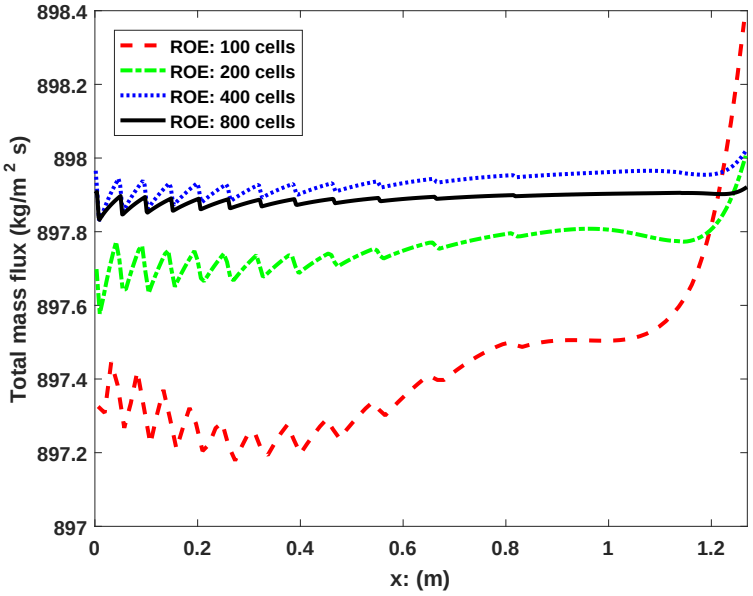

Figure 5.19: Mesh convergence of total mass flux for Christensen Test 15

other, except for the solution near the inlet and outlet boundaries. The treatment of boundary conditions for the WENO-type scheme is complicated. Even for the simpler Euler equation with an ideal EOS, where the characteristics of the system are well known, the treatment of boundary conditions is non-trivial. Existing well-known boundary treatment schemes are mostly based on the characteristics of the system, such as the non-reflecting boundary condition scheme [51, 52] and Inverse Lax-Wendroff boundary condition scheme [48, 49]. Most of these schemes work for problems where the EOS is simple enough and the characteristics of the system are analytically well-known. For the two-phase two-fluid model with a real EOS, a characteristics-based boundary treatment scheme is very complicated and is not the focus of this thesis.

Taking the void fraction and pressure as examples, Figure 5.17 and Figure 5.18 show the grid convergence

of both schemes. We can see that the WENO-type scheme converges faster than the Roe-type scheme. Taking the results from Roe-type scheme as an example, Figure 5.19 shows the mesh convergence of the total mass flux. We see that the total mass flux converges when refining the mesh and the total mass flux is conserved in the pipe for the finest mesh.

5.5 Conclusion

In this chapter, a new forward solver is developed for the two-phase two-fluid model based on two numerical fluxes: a Roe-type numerical flux and a WENO-type numerical flux. Both numerical fluxes are based on the analytical eigenvalues and eigenvectors given in **Chapter 4**.

The new forward solver is tested with a few benchmark problems: periodic pipe, shock-tube, and the Christensen boiling pipe problem. The solver is shown to be stable even for problems that contain discontinuities. The Roe-type scheme is shown to be first-order accurate in space; the WENO-type scheme is shown to be at least second-order accurate in space. Numerically, it is observed that the Roe-type scheme is more robust than the WENO-type scheme, because the boundary conditions for the WENO-type scheme are more difficult to treat. Improvements to the boundary conditions should help improve the robustness of the WENO-type scheme and achieve higher spatial accuracy.

Chapter 6

ADJOINT SENSITIVITY ANALYSIS

6.1 Introduction

An important step in uncertainty analysis is the sensitivity analysis of a response to the uncertain input parameters. Common approach to calculate the sensitivity includes regression-based methods and variance-based methods [11, 12]. However, these methods require solving the system of interest multiple times, sometimes 100s of times, which is very expensive in terms of computational cost. An alternative approach to calculate sensitivities is the adjoint method. The cost of solving an adjoint equation is comparable to the cost of solving the original (forward) equation. However, once the adjoint solution is available, the sensitivity to different parameters can be calculated with little effort, which offers a powerful tool for efficient calculation of sensitivities to a large number of uncertain input parameters.

There is a long history of the use of the adjoint method in optimal control theory. The use of adjoint method for computing sensitivities came up in nuclear science in the 1940s [13]. Later, the adjoint method became popular in computational fluid dynamics [14]. Within the field of aeronautical computational fluid dynamics, the use of adjoint method has been pioneered by Jameson [53, 54, 55, 56]. Adjoint problems arise naturally in the formulation of optimal aerodynamic design and optimal error control [14, 57, 58, 59]. Adjoint solution provides the linear sensitivities of an objective (or response) function (e.g. lift or drag) to a number of design variables. These sensitivities can then be used to drive an optimization procedure. In a sequence of papers, Jameson and co-authors developed the adjoint approach for the potential flow, the Euler equation, and the Navier-Stokes equation [53, 54, 55, 56].

In CFD field, the application of adjoint method to optimal aerodynamic design was very successful. However, to the author's best knowledge, successful application of ajoint method to sensitivity analysis in two-phase flow simulations is rare. Cacuci performed a local adjoint sensitivity analysis to RELAP5/MOD3.2 [13, 60, 61]; this approach is tied to the very specific RELAP5 numerical discretization. An application of Cacuci's approach is illustrated by Petruzzi [62], where the approach is applied to the blowdown of a gas from a pressurized vessel.

In this chapter, an adjoint sensitivity analysis framework is developed for the two-phase two-fluid model. The framework is based on the stable forward numerical solver, which is discussed in the previous chapter.

6.2 Adjoint sensitivity analysis

6.2.1 Adjoint sensitivity analysis: general framework

Let $\boldsymbol{\mathcal{G}}^\dagger$ be the operator that represents the governing equation of the forward problem, e.g. the two-phase two-fluid model. Let $\mathbf{W}$ be the field variables, e.g. the vector of physical variables. For the forward problem, there are usually a few parameters, denoted by $\boldsymbol{\omega}$, that affect the flow field, e.g. the physical model parameters and boundary conditions. Suppose the governing equation is written as

$$\boldsymbol{\mathcal{G}}^\dagger\left(\mathbf{W},\boldsymbol{\omega}\right)=\mathbf{0} \tag{6.1}$$

Let $\mathcal{R}^\dagger$ be the operator that measures the response of interest (R), e.g. the void fraction at certain location. The response could be expressed as

$$R=\mathcal{R}^\dagger\left(\mathbf{W},\boldsymbol{\omega}\right) \tag{6.2}$$

In the following analysis, vectors and matrices are defined such that the multiplications shown in the following equations are the inner product.

Let δ be the variation operator. A change in the parameter ($\delta\boldsymbol{\omega}$) will cause a change in the governing equation

$$\left(\frac{\partial\boldsymbol{\mathcal{G}}^\dagger}{\partial\mathbf{W}}\right)_{\boldsymbol{\omega}}\delta\mathbf{W}+\left(\frac{\partial\boldsymbol{\mathcal{G}}^\dagger}{\partial\boldsymbol{\omega}}\right)_{\mathbf{W}}\delta\boldsymbol{\omega}=\mathbf{0} \tag{6.3}$$

Separately, $\delta\boldsymbol{\omega}$ will also cause a change in the response

$$\delta R=\left(\frac{\partial\mathcal{R}^\dagger}{\partial\mathbf{W}}\right)_{\boldsymbol{\omega}}\delta\mathbf{W}+\left(\frac{\partial\mathcal{R}^\dagger}{\partial\boldsymbol{\omega}}\right)_{\mathbf{W}}\delta\boldsymbol{\omega} \tag{6.4}$$

Note that $\delta R/\delta\boldsymbol{\omega}$ is the sensitivity of interest. From Eq. (6.3), we see that $\delta\boldsymbol{\omega}$ will cause a change $\delta\mathbf{W}$. For the perturbation-based methods, $\delta\mathbf{W}$ needs to be calculated by solving the governing equation, which is usually expensive. For the adjoint method, the idea is to remove the dependency of δR on $\delta\mathbf{W}$ by combining Eq. (6.3) and Eq. (6.4) using the Lagrange multiplier approach.

Let $\boldsymbol{\phi}$ be the vector of Lagrange multiplier, which is a vector of free variables. Multiplying the transpose

of the Lagrange multiplier to Eq. (6.3), we obtain

$$\boldsymbol{\phi}^T \left[\left(\frac{\partial \boldsymbol{\mathcal{G}}^\dagger}{\partial \mathbf{W}} \right)_{\boldsymbol{\omega}} \delta \mathbf{W} + \left(\frac{\partial \boldsymbol{\mathcal{G}}^\dagger}{\partial \boldsymbol{\omega}} \right)_{\mathbf{W}} \delta \boldsymbol{\omega} \right] = 0 \tag{6.5}$$

Since the right-hand side of Eq. (6.5) is zero, we can subtract Eq. (6.5) from Eq. (6.4) without changing the value of δR, i.e.

$$\delta R = \left(\frac{\partial \mathcal{R}^\dagger}{\partial \mathbf{W}} \right)_{\boldsymbol{\omega}} \delta \mathbf{W} + \left(\frac{\partial \mathcal{R}^\dagger}{\partial \boldsymbol{\omega}} \right)_{\mathbf{W}} \delta \boldsymbol{\omega} - \boldsymbol{\phi}^T \left[\left(\frac{\partial \boldsymbol{\mathcal{G}}^\dagger}{\partial \mathbf{W}} \right)_{\boldsymbol{\omega}} \delta \mathbf{W} + \left(\frac{\partial \boldsymbol{\mathcal{G}}^\dagger}{\partial \boldsymbol{\omega}} \right)_{\mathbf{W}} \delta \boldsymbol{\omega} \right] \tag{6.6}$$

We rewrite Eq. (6.6) as

$$\delta R = \left[\left(\frac{\partial \mathcal{R}^\dagger}{\partial \mathbf{W}} \right)_{\boldsymbol{\omega}} - \boldsymbol{\phi}^T \left(\frac{\partial \boldsymbol{\mathcal{G}}^\dagger}{\partial \mathbf{W}} \right)_{\boldsymbol{\omega}} \right] \delta \mathbf{W} + \left[\left(\frac{\partial \mathcal{R}^\dagger}{\partial \boldsymbol{\omega}} \right)_{\mathbf{W}} - \boldsymbol{\phi}^T \left(\frac{\partial \boldsymbol{\mathcal{G}}^\dagger}{\partial \boldsymbol{\omega}} \right)_{\mathbf{W}} \right] \delta \boldsymbol{\omega} \tag{6.7}$$

For simplicity, we will drop the subscripts $\boldsymbol{\omega}$ and $\mathbf{W}$ in the partial derivatives,

$$\delta R = \left(\frac{\partial \mathcal{R}^\dagger}{\partial \mathbf{W}} - \boldsymbol{\phi}^T \frac{\partial \boldsymbol{\mathcal{G}}^\dagger}{\partial \mathbf{W}} \right) \delta \mathbf{W} + \left(\frac{\partial \mathcal{R}^\dagger}{\partial \boldsymbol{\omega}} - \boldsymbol{\phi}^T \frac{\partial \boldsymbol{\mathcal{G}}^\dagger}{\partial \boldsymbol{\omega}} \right) \delta \boldsymbol{\omega} \tag{6.8}$$

Because the Lagrange multiplier ($\boldsymbol{\phi}$) is a vector of free variables, it can be chosen such that

$$\frac{\partial \mathcal{R}^\dagger}{\partial \mathbf{W}} - \boldsymbol{\phi}^T \frac{\partial \boldsymbol{\mathcal{G}}^\dagger}{\partial \mathbf{W}} = \mathbf{0} \tag{6.9}$$

which is the so-called adjoint equation. The Lagrange multiplier ($\boldsymbol{\phi}$) given by Eq. (6.9) is the so-called adjoint solution.

Because of the adjoint equation Eq. (6.9), the change in the response becomes

$$\delta R = \left(\frac{\partial \mathcal{R}^\dagger}{\partial \boldsymbol{\omega}} - \boldsymbol{\phi}^T \frac{\partial \boldsymbol{\mathcal{G}}^\dagger}{\partial \boldsymbol{\omega}} \right) \delta \boldsymbol{\omega} \tag{6.10}$$

The advantage of Eq. (6.10) is that it is independent of $\delta \mathbf{W}$, which means that the sensitivity of the response to an arbitrary number of input parameters can be determined without the need for additional forward calculations.

The adjoint equation Eq. (6.9) and the response equation Eq. (6.10) are problem dependent. There are two fundamental guidelines in formulating the adjoint problem, i.e.

- Rule 1: The adjoint solution (or Lagrange multiplier) is a vector of free variables. The adjoint solution can be chosen to satisfy any conditions to accomplish Rule 2.

- Rule 2: The adjoint problem should be formulated to remove the dependency of change in the response to change in the field variables.

6.2.2 Adjoint sensitivity analysis: two-phase two-fluid model

We will focus on the 1D two-phase two-fluid model. Recall that the two-phase two-fluid model is

$$\frac{\partial \mathbf{U}}{\partial t} + \frac{\partial \mathbf{F}}{\partial x} + \mathbf{P}_{ix}\frac{\partial \alpha_g}{\partial x} + \mathbf{P}_{it}\frac{\partial \alpha_g}{\partial t} - \mathbf{S} = \mathbf{0} \tag{6.11}$$

The $\mathbf{P}_{it}\partial\alpha_g/\partial t$ term makes the notations for adjoint sensitivity analysis very complicated. For simplicity, we will drop the $\mathbf{P}_{it}\partial\alpha_g/\partial t$ term because it can be handled by the matrix $\mathbb{A}_{it}$, which is given in Eq. (4.38) of **Chapter 4**. The derivation starts with

$$\frac{\partial \mathbf{U}}{\partial t} + \frac{\partial \mathbf{F}}{\partial x} + \mathbf{P}_{ix}\frac{\partial \alpha_g}{\partial x} - \mathbf{S} = \mathbf{0} \tag{6.12}$$

Let $\mathbf{W}$ be the vector of physical variables and $\boldsymbol{\omega}$ be the vector of input parameters. The source term is in general a function of $\mathbf{W}$ and $\boldsymbol{\omega}$, i.e.

$$\mathbf{S} = \mathbf{S}\big(\mathbf{W},\boldsymbol{\omega}\big) \tag{6.13}$$

In this thesis, we will study a response R at the time t_1 that can be written as

$$R\big(t_1\big) = \frac{1}{2}\int_{x_0}^{x_1}\big[q\big(t_1\big) - q_d\big(t_1\big)\big]^2 dx \tag{6.14}$$

where q is the quantity of interest and q_d is the design value of q. Thus, R represents the error in the prediction of q. For brevity, we use $\langle * \rangle_x$ to denote the integration in space, $\langle * \rangle_t$ to denote the integration in time, and $\langle * \rangle_{xt}$ to denote the double integration in space and time. The integration in time is from t_0 to time t_1 and the integration in space is from x_0 to x_1.

Following this notation, Eq. (6.14) is transformed into

$$R = \frac{1}{2}\Big\langle \big(q - q_d\big)^2 |^{t_1} \Big\rangle_x \tag{6.15}$$

where $|^{t_1}$ means the integrand is evaluated at the time t_1. Performing the variation operator to the response function, we get

$$\delta R = \Big\langle \big(q - q_d\big)\delta q |^{t_1} \Big\rangle_x \tag{6.16}$$

Let $\boldsymbol{\phi}$ be the Lagrange multiplier. From Eq. (6.12), we obtain

$$\boldsymbol{\phi}^T \delta \left(\frac{\partial \mathbf{U}}{\partial t} + \frac{\partial \mathbf{F}}{\partial x} + \mathbf{P}_{ix} \frac{\partial \alpha_g}{\partial x} - \mathbf{S} \right) = 0 \tag{6.17}$$

which can be transformed into

$$\begin{aligned} &\frac{\partial \boldsymbol{\phi}^T \delta \mathbf{U}}{\partial t} - \frac{\partial \boldsymbol{\phi}^T}{\partial t} \delta \mathbf{U} + \frac{\partial \boldsymbol{\phi}^T \delta \mathbf{F}}{\partial x} - \frac{\partial \boldsymbol{\phi}^T}{\partial x} \delta \mathbf{F} \\ &\quad + \frac{\partial \boldsymbol{\phi}^T \mathbf{P}_{ix} \delta \alpha_g}{\partial x} - \left(\frac{\partial \boldsymbol{\phi}^T}{\partial x} \mathbf{P}_{ix} + \boldsymbol{\phi}^T \frac{\partial \mathbf{P}_{ix}}{\partial x} \right) \delta \alpha_g + \boldsymbol{\phi}^T \frac{\partial \alpha_g}{\partial x} \delta \mathbf{P}_{ix} - \boldsymbol{\phi}^T \delta \mathbf{S} = 0 \end{aligned} \tag{6.18}$$

Integrating Eq. (6.18) over t_0 to t_1 in time and x_0 to x_1 in space, we obtain

$$\begin{aligned} &\left\langle \boldsymbol{\phi}^T \delta \mathbf{U} |^{t_1} - \boldsymbol{\phi}^T \delta \mathbf{U} |^{t_0} \right\rangle_x + \left\langle \boldsymbol{\phi}^T \left(\delta \mathbf{F} + \mathbf{P}_{ix} \delta \alpha_g \right) |^{x_1} - \boldsymbol{\phi}^T \left(\delta \mathbf{F} + \mathbf{P}_{ix} \delta \alpha_g \right) |^{x_0} \right\rangle_t \\ &+ \left\langle - \frac{\partial \boldsymbol{\phi}^T}{\partial t} \delta \mathbf{U} - \frac{\partial \boldsymbol{\phi}^T}{\partial x} \delta \mathbf{F} - \left(\frac{\partial \boldsymbol{\phi}^T}{\partial x} \mathbf{P}_{ix} + \boldsymbol{\phi}^T \frac{\partial \mathbf{P}_{ix}}{\partial x} \right) \delta \alpha_g + \boldsymbol{\phi}^T \frac{\partial \alpha_g}{\partial x} \delta \mathbf{P}_{ix} - \boldsymbol{\phi}^T \delta \mathbf{S} \right\rangle_{xt} = 0 \end{aligned} \tag{6.19}$$

For ease of notations, we define the following vectors and matrices

$$\begin{aligned} \mathbb{A}_0 = \left(\frac{\partial \mathbf{U}}{\partial \mathbf{W}} \right)^T, \mathbb{A}_1 = \left(\frac{\partial \mathbf{F}}{\partial \mathbf{W}} + \mathbf{P}_{ix} \frac{\partial \alpha_g}{\partial \mathbf{W}} \right)^T, \mathbb{A}_2 = \left(\frac{\partial \mathbf{P}_{ix}}{\partial x} \frac{\partial \alpha_g}{\partial \mathbf{W}} - \frac{\partial \mathbf{P}_{ix}}{\partial \mathbf{W}} \frac{\partial \alpha_g}{\partial x} + \frac{\partial \mathbf{S}}{\partial \mathbf{W}} \right)^T \\ \mathbf{Q} = -(q - q_d) \left(\frac{\partial q}{\partial \mathbf{W}} \right)^T \end{aligned} \tag{6.20}$$

The details of the coefficient matrices, $\mathbb{A}_0$, $\mathbb{A}_1$, and $\mathbb{A}_2$, are given in **Appendix E**. Then, Eq. (6.16) and Eq. (6.19) are transformed into

$$\delta R = \left\langle -\mathbf{Q}^T \delta \mathbf{W} |^{t_1} \right\rangle_x \tag{6.21}$$

$$\begin{aligned} &\left\langle \boldsymbol{\phi}^T \mathbb{A}_0^T \delta \mathbf{W} |^{t_1} - \boldsymbol{\phi}^T \mathbb{A}_0^T \delta \mathbf{W} |^{t_0} \right\rangle_x + \left\langle \boldsymbol{\phi}^T \mathbb{A}_1^T \delta \mathbf{W} |^{x_1} - \boldsymbol{\phi}^T \mathbb{A}_1^T \delta \mathbf{W} |^{x_0} \right\rangle_t \\ &\qquad - \left\langle \left(\frac{\partial \boldsymbol{\phi}^T}{\partial t} \mathbb{A}_0^T + \frac{\partial \boldsymbol{\phi}^T}{\partial x} \mathbb{A}_1^T + \boldsymbol{\phi}^T \mathbb{A}_2^T \right) \delta \mathbf{W} \right\rangle_{xt} - \left\langle \boldsymbol{\phi}^T \frac{\partial \mathbf{S}}{\partial \boldsymbol{\omega}} \delta \boldsymbol{\omega} \right\rangle_{xt} = 0 \end{aligned} \tag{6.22}$$

Dividing Eq. (6.22) by $t_1 - t_0$ and subtracting the result from Eq. (6.21), we obtain

$$\begin{aligned} \delta R = &\underbrace{\frac{1}{t_1 - t_0} \left\langle \left(\frac{\partial \boldsymbol{\phi}^T}{\partial t} \mathbb{A}_0^T + \frac{\partial \boldsymbol{\phi}^T}{\partial x} \mathbb{A}_1^T + \boldsymbol{\phi}^T \mathbb{A}_2^T - \mathbf{Q}^T \right) \delta \mathbf{W} \right\rangle_{xt}}_{\mathrm{P}_1} + \underbrace{\frac{1}{t_1 - t_0} \left\langle \boldsymbol{\phi}^T \frac{\partial \mathbf{S}}{\partial \boldsymbol{\omega}} \delta \boldsymbol{\omega} \right\rangle_{xt}}_{\mathrm{P}_2} \\ &+ \underbrace{\frac{1}{t_1 - t_0} \left\langle \boldsymbol{\phi}^T \mathbb{A}_0^T \delta \mathbf{W} |^{t_0} - \boldsymbol{\phi}^T \mathbb{A}_0^T \delta \mathbf{W} |^{t_1} \right\rangle_x}_{\mathrm{P}_3} + \underbrace{\frac{1}{t_1 - t_0} \left\langle \boldsymbol{\phi}^T \mathbb{A}_1^T \delta \mathbf{W} |^{x_0} - \boldsymbol{\phi}^T \mathbb{A}_1^T \delta \mathbf{W} |^{x_1} \right\rangle_t}_{\mathrm{P}_4} \end{aligned} \tag{6.23}$$

For steady-state problems, taking $t_1 \to \infty$, Eq. (6.23) is reduced to

$$\delta R = \underbrace{\left\langle \left(\frac{\partial \boldsymbol{\phi}^T}{\partial x} \mathbb{A}_1^T + \boldsymbol{\phi}^T \mathbb{A}_2^T - \mathbf{Q}^T \right) \delta \mathbf{W} \right\rangle_x}_{\mathrm{P}_1} + \underbrace{\left\langle \boldsymbol{\phi}^T \frac{\partial \mathbf{S}}{\partial \boldsymbol{\omega}} \delta \boldsymbol{\omega} \right\rangle_x}_{\mathrm{P}_2} + \underbrace{\boldsymbol{\phi}^T \mathbb{A}_1^T \delta \mathbf{W}|^{x_0} - \boldsymbol{\phi}^T \mathbb{A}_1^T \delta \mathbf{W}|^{x_1}}_{\mathrm{P}_4} \tag{6.24}$$

As will be discussed in the following section, P_1 will specify the PDE for the adjoint problem, P_2 will specify the contribution of the source vector to the change in the response, P_3 will specify the initial condition of the adjoint problem, and P_4 will specify the boundary condition of the adjoint problem.

Time-dependent problem

For time-dependent problems, the adjoint sensitivity analysis for general boundary conditions is complicated. We will use a simple periodic boundary condition for test purposes. The adjoint problem is determined by the 4 parts in Eq. (6.23): P_1, P_2, P_3, and P_4.

P_1: This part gives the adjoint equation. To remove the dependency of the response on the change in the physical variables, we chose the adjoint solution such that

$$\frac{\partial \boldsymbol{\phi}^T}{\partial t} \mathbb{A}_0^T + \frac{\partial \boldsymbol{\phi}^T}{\partial x} \mathbb{A}_1^T + \boldsymbol{\phi}^T \mathbb{A}_2^T = \mathbf{Q}^T \tag{6.25}$$

Taking the transpose of Eq. (6.25), we obtain the adjoint equation

$$\mathbb{A}_0 \frac{\partial \boldsymbol{\phi}}{\partial t} + \mathbb{A}_1 \frac{\partial \boldsymbol{\phi}}{\partial x} + \mathbb{A}_2 \boldsymbol{\phi} = \mathbf{Q} \tag{6.26}$$

P_2: This part does not depend on the change in the physical variables. It accounts for the change in the response, because the source term is an explicit function of the parameters of interest.

P_3: This part deals with the initial condition of the forward and adjoint equation. To remove the dependency of the response on the change in the physical variables, we chose the adjoint solution at time t_1 to be

$$\boldsymbol{\phi} = 0, \quad \text{at time } t_1 \tag{6.27}$$

Then, P_3 becomes

$$\mathrm{P}_3 = \frac{1}{t_1 - t_0} \left\langle \boldsymbol{\phi}^T \mathbb{A}_0^T \delta \mathbf{W}|^{t_0} \right\rangle_x \tag{6.28}$$

$\delta \mathbf{W}$ at time t_0 is known because it represents the change in the initial conditions of forward problems. Once the adjoint solution at time t_0 is determined, Eq. (6.28) is completely specified.

P_4: This part accounts for the change in the response due to the change in the boundary conditions. This part also determines the appropriate boundary conditions for the adjoint equation. After some algebraic manipulations, we rewrite P4 as

$$\begin{aligned}\mathrm{P}_4 =& \frac{1}{t_1 - t_0} \left\langle \left(B_1 \delta\alpha_g + B_2 \delta p + B_3 \delta T_l + B_4 \delta T_g + B_5 \delta u_l + B_6 \delta u_g\right)|^{x_0} \right\rangle_t \\ & - \frac{1}{t_1 - t_0} \left\langle \left(B_1 \delta\alpha_g + B_2 \delta p + B_3 \delta T_l + B_4 \delta T_g + B_5 \delta u_l + B_6 \delta u_g\right)|^{x_1} \right\rangle_t \end{aligned} \tag{6.29}$$

where B_1 to B_6 are functions of $\boldsymbol{\phi}$ that results from $\boldsymbol{\phi}^T \mathbb{A}_1^T$. We show the details of B_1 to B_6 in **Appendix E**.

For time-dependent adjoint sensitivity analysis, we consider a periodic boundary condition. If we apply a periodic boundary condition to the adjoint equation, i.e.

$$\boldsymbol{\phi}\big(x, t\big) = \boldsymbol{\phi}\big(x + x_1 - x_0, t\big) \tag{6.30}$$

then, we obtain

$$\boldsymbol{\phi}|^{x_0} = \boldsymbol{\phi}|^{x_1} \tag{6.31}$$

and

$$\mathrm{P}_4 = 0, \quad \text{for periodic BC} \tag{6.32}$$

To summarize, for time-dependent problems with a periodic boundary condition, the adjoint problem is specified by

$$\mathbb{A}_0 \frac{\partial \boldsymbol{\phi}}{\partial t} + \mathbb{A}_1 \frac{\partial \boldsymbol{\phi}}{\partial x} + \mathbb{A}_2 \boldsymbol{\phi} = \mathbf{Q} \tag{6.33}$$

with

$$\boldsymbol{\phi}\big(x, t_1\big) = 0, \quad \text{and} \quad \boldsymbol{\phi}\big(x, t\big) = \boldsymbol{\phi}\big(x + x_1 - x_0, t\big) \tag{6.34}$$

The change in the response is reduced to

$$\delta R = \frac{1}{t_1 - t_0} \left\langle \boldsymbol{\phi}^T \frac{\partial \mathbf{S}}{\partial \boldsymbol{\omega}} \delta\boldsymbol{\omega} \right\rangle_{xt} + \frac{1}{t_1 - t_0} \left\langle \boldsymbol{\phi}^T \mathbb{A}_0^T \delta \mathbf{W}|^{t_0} \right\rangle_x \tag{6.35}$$

From Eq. (6.35), we can get the sensitivities of R to different input parameters.

Steady-state problem

For steady-state problems, the adjoint equation is specified by removing the dependency of $\delta\mathbf{W}$ in P_1, i.e.

$$\mathbb{A}_1^{\mathrm{ss}}\frac{\partial\boldsymbol{\phi}}{\partial x}+\mathbb{A}_2^{\mathrm{ss}}\boldsymbol{\phi}=\mathbf{Q}^{\mathrm{ss}} \tag{6.36}$$

where the superscript 'ss' denotes that the quantities are evaluated at steady-state.

We consider the boundary conditions used in the boiling pipe problem: at the inlet ($x = x_0$), void fraction, liquid temperature, gas temperature, liquid velocity, and gas velocity are kept at constant values; at the outlet ($x = x_1$), the pressure is kept at a constant value, i.e.

$$\alpha_g, T_l, T_g, u_l, u_g \quad \text{are constant at } x = x_0 \tag{6.37a}$$

$$p \quad \text{are constant at } x = x_1 \tag{6.37b}$$

When the boundary conditions are changed (i.e. different constant values), we know that

$$\delta\alpha_g, \delta T_l, , \delta T_g, \delta u_l, \delta u_g \quad \text{are known at } x = x_0 \tag{6.38a}$$

$$\delta p \quad \text{is known at } x = x_1 \tag{6.38b}$$

If we apply the following boundary conditions to the adjoint solution

$$B_2^{\mathrm{ss}}\big(\boldsymbol{\phi}\big)=0, \quad \text{for} \quad x=x_0 \tag{6.39a}$$

$$B_1^{\mathrm{ss}}\big(\boldsymbol{\phi}\big)=0, B_3^{\mathrm{ss}}\big(\boldsymbol{\phi}\big)=0, B_4^{\mathrm{ss}}\big(\boldsymbol{\phi}\big)=0, B_5^{\mathrm{ss}}\big(\boldsymbol{\phi}\big)=0, B_6^{\mathrm{ss}}\big(\boldsymbol{\phi}\big)=0, \quad \text{for} \quad x=x_1 \tag{6.39b}$$

then, P_4 is reduced to

$$\mathrm{P}_4=\big(B_1^{\mathrm{ss}}\delta\alpha_g+B_3^{\mathrm{ss}}\delta T_l+B_4^{\mathrm{ss}}\delta T_g+B_5^{\mathrm{ss}}\delta u_l+B_6^{\mathrm{ss}}\delta u_g\big)|^{x_0}-\big(B_2^{\mathrm{ss}}\delta p\big)|^{x_1} \tag{6.40}$$

Once the adjoint solution is known, P_4 is completely specified by Eq. (6.38) and Eq. (6.40).

To summarize, for steady problems with boundary conditions given by Eq. (6.37), the adjoint problem is specified by

$$\mathbb{A}_1^{\mathrm{ss}}\frac{\partial\boldsymbol{\phi}}{\partial x}+\mathbb{A}_2^{\mathrm{ss}}\boldsymbol{\phi}=\mathbf{Q}^{\mathrm{ss}} \tag{6.41}$$

with

$$B_2^{\text{ss}}(\boldsymbol{\phi}) = 0 \quad \text{for} \quad x = x_0 \tag{6.42a}$$

$$B_1^{\text{ss}}(\boldsymbol{\phi}) = 0, B_3^{\text{ss}}(\boldsymbol{\phi}) = 0, B_4^{\text{ss}}(\boldsymbol{\phi}) = 0, B_5^{\text{ss}}(\boldsymbol{\phi}) = 0, B_6^{\text{ss}}(\boldsymbol{\phi}) = 0, \quad \text{for} \quad x = x_1 \tag{6.42b}$$

The change in the response is reduced to

$$\delta R = \left\langle \boldsymbol{\phi}^T \frac{\partial \mathbf{S}}{\partial \boldsymbol{\omega}} \delta \boldsymbol{\omega} \right\rangle_x^{\text{ss}} + \left(B_1^{\text{ss}} \delta \alpha_g + B_3^{\text{ss}} \delta T_l + B_4^{\text{ss}} \delta T_g + B_5^{\text{ss}} \delta u_l + B_6^{\text{ss}} \delta u_g \right)|^{x_0} - \left(B_2^{\text{ss}} \delta p \right)|^{x_1} \tag{6.43}$$

From Eq. (6.43), we can obtain the sensitivities of R to different inut parameters.

6.3 Numerical tests

6.3.1 Time-dependent problem

Problem description

The periodic pipe problem discussed in **Sec. 5.4.1** is used to test the time-dependent adjoint sensitivity analysis framework. Recall that the problem is driven by the following initial pressure

$$p(x) = p_0 + p_1 \sin\left(k_0 \frac{2\pi}{L} x\right) \tag{6.44}$$

Keeping the initial conditions for the other variables (void fraction, liquid/gas temperature, liquid/gas velocity) unchanged, the solution of the system at a certain time is completely determined by 3 parameters, p_0, p_1, and k_0. Let $q_d(t_1)$ be the design solution at time t_1, which corresponds to a design parameter set (p_0^d, p_1^d, k_0^d). The problem is to find the correct parameter set (p_0^d, p_1^d, k_0^d) from an initial guess. In this test, we choose the following parameter set

$$p_0^d = 7.5 \text{ MPa}, p_1^d = 1.0 \text{ MPa}, k_0^d = 1.0 \tag{6.45}$$

The problem could be converted to an equivalent optimization problem: finding the parameter set (p_0^d, p_1^d, k_0^d) that minimizes the following response function

$$R(t_1; p_0, p_1, k_0) = \frac{1}{2} \int_{x_0}^{x_1} \left[q(t_1; p_0, p_1, k_0) - q_d(t_1) \right]^2 dx \tag{6.46}$$

In practice, the optimization could be performed iteratively with

$$p_0^{m+1} = p_0^m - R\big(t_1; p_0^m, p_1^m, k_0^m\big)\left(\frac{\partial R}{\partial p_0}\right)^{-1} \tag{6.47a}$$

$$p_1^{m+1} = p_1^m - R\big(t_1; p_0^m, p_1^m, k_0^m\big)\left(\frac{\partial R}{\partial p_1}\right)^{-1} \tag{6.47b}$$

$$k_0^{m+1} = k_0^m - R\big(t_1; p_0^m, p_1^m, k_0^m\big)\left(\frac{\partial R}{\partial k_0}\right)^{-1} \tag{6.47c}$$

The key point is to evaluate the sensitivities $\partial R/\partial p_0$, $\partial R/\partial p_1$, and $\partial R/\partial k$ efficiently. Recall that the change in the response function is given by

$$\delta R = \frac{1}{t_1 - t_0}\left\langle \boldsymbol{\phi}^T \frac{\partial \mathbf{S}}{\partial \boldsymbol{\omega}} \delta\boldsymbol{\omega} \right\rangle_{xt} + \frac{1}{t_1 - t_0}\left\langle \boldsymbol{\phi}^T \mathbb{A}_0^T \delta\mathbf{W}|^{t_0} \right\rangle_x \tag{6.48}$$

Since the source vector for this problem is zero, Eq. (6.48) is simplified to be

$$\delta R = \frac{1}{t_1 - t_0}\left\langle \boldsymbol{\phi}^T \mathbb{A}_0^T \delta\mathbf{W}|^{t_0} \right\rangle_x \tag{6.49}$$

The perturbation in the initial condition is

$$\begin{aligned} \delta\mathbf{W}|^{t_0} &= \begin{pmatrix} 0 \\ \delta p_0 + \delta p_1 \sin\big(k_0 \frac{2\pi}{L} x\big) + p_1 \cos\big(k_0 \frac{2\pi}{L} x\big) \frac{2\pi}{L} x \delta k_0 \\ 0 \\ 0 \\ 0 \\ 0 \end{pmatrix} \\ &= \left[\delta p_0 + \delta p_1 \sin\big(k_0 \frac{2\pi}{L} x\big) + p_1 \frac{2\pi}{L} x \cos\big(k_0 \frac{2\pi}{L} x\big) \delta k_0\right] \mathbf{e}_2 \end{aligned} \tag{6.50}$$

where $\mathbf{e}_2$ is a column vector whose second component is 1 while other components are 0. Combining Eq. (6.49) and Eq. (6.50), we obtain

$$\frac{\partial R}{\partial p_0} = \frac{1}{t_1 - t_0}\left\langle \boldsymbol{\phi}^T \mathbb{A}_0^T \mathbf{e}_2 \right\rangle_x \tag{6.51a}$$

$$\frac{\partial R}{\partial p_1} = \frac{1}{t_1 - t_0}\left\langle \sin\big(k_0 \frac{2\pi}{L} x\big) \boldsymbol{\phi}^T \mathbb{A}_0^T \mathbf{e}_2 \right\rangle_x \tag{6.51b}$$

$$\frac{\partial R}{\partial k_0} = \frac{1}{t_1 - t_0}\left\langle p_1 \frac{2\pi}{L} x \cos\big(k_0 \frac{2\pi}{L} x\big) \boldsymbol{\phi}^T \mathbb{A}_0^T \mathbf{e}_2 \right\rangle_x \tag{6.51c}$$

Once the adjoint solution at t_0 is known, the sensitivities in Eq. (6.47) are completely specified by Eq. (6.51).

Adjoint solution

Recall that the adjoint equation for the time-dependent problem is

$$\mathbb{A}_0 \frac{\partial \boldsymbol{\phi}}{\partial t} + \mathbb{A}_1 \frac{\partial \boldsymbol{\phi}}{\partial x} + \mathbb{A}_2 \boldsymbol{\phi} = \mathbf{Q} \tag{6.52}$$

In practice, Eq. (6.52) is discretized as

$$\mathbb{A}_{0,i}^n \frac{\boldsymbol{\phi}_i^n - \boldsymbol{\phi}_i^{n-1}}{\Delta t} + \mathbb{A}_{1,i}^n \frac{\boldsymbol{\phi}_{i+1}^n - \boldsymbol{\phi}_{i-1}^n}{2\Delta x} + \mathbb{A}_{2,i}^n \boldsymbol{\phi}_i^n = \mathbf{Q}_i^n \tag{6.53}$$

The adjoint solution is updated in time with

$$\boldsymbol{\phi}_i^{n-1} = \boldsymbol{\phi}_i^n - \Delta t \big(\mathbb{A}_{0,i}^n\big)^{-1} \left(\mathbf{Q}_i^n - \mathbb{A}_{1,i}^n \frac{\boldsymbol{\phi}_{i+1}^n - \boldsymbol{\phi}_{i-1}^n}{2\Delta x} - \mathbb{A}_{2,i}^n \boldsymbol{\phi}_i^n \right) \tag{6.54}$$

One ghost cell on each side of boundaries is used to handle the periodic boundary conditions. Different with the forward equation, the adjoint equation should start from time t_1 and integrate back to time t_0.

A forward simulation is required to prepare the coefficient matrices and source vectors in Eq. (6.52). For this test, we are interested in the solution at $t_1 = 0.001$ s starting from $t_0 = 0$ s. As is discussed in previous chapter, the WENO-type scheme works very well for the periodic pipe problem, which means we can use a coarse mesh to obtain an accurate solution. To save computational resources, we will use the WENO-type scheme to solve the forward problem. The following results could also be obtained with the Roe-type scheme using a much finer mesh. Both the forward and adjoint equation are solved with 400 cells and a constant time step, $\Delta t = 10^{-6}$ s.

The pressure at time t_1 is chosen to evaluate the response function, i.e.

$$R\big(t_1; p_0, p_1, k_0\big) = \frac{1}{2} \int_{x_0}^{x_1} \big[p\big(t_1; p_0, p_1, k_0\big) - p_d\big(t_1\big)\big]^2 dx \tag{6.55}$$

This way, the source vector in Eq. (6.52) is

$$\mathbf{Q} = -\big(p - p_d\big)\mathbf{e}_2 \tag{6.56}$$

Optimization process

Three separate tests are performed to find p_0, p_1, and k_0, respectively. Initial value for p_0 is 8.0 MPa, initial value for p_1 is 1.5 MPa, and initial value for k_0 is 1.5. For each separate test, the values of the uninterested parameters are kept at the design values.

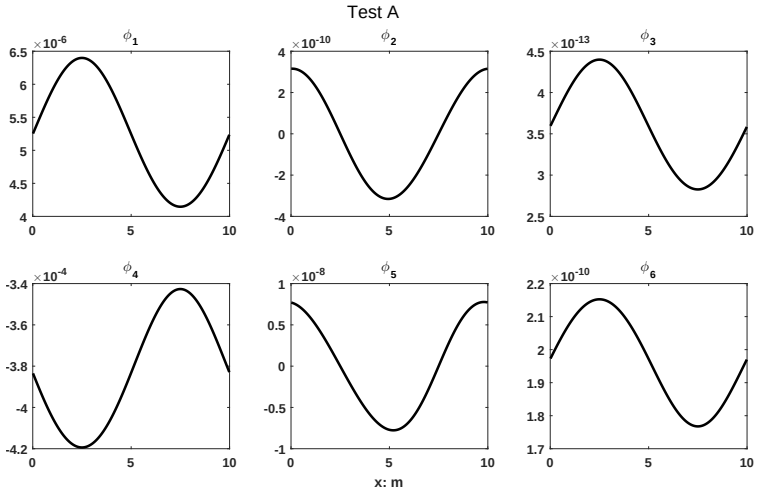

Figure 6.1: Adjoint solution for the first iteration of test A. $p_0 = 8.0$ MPa, $p_1 = 1.0$ MPa, and $k_0 = 1.0$.

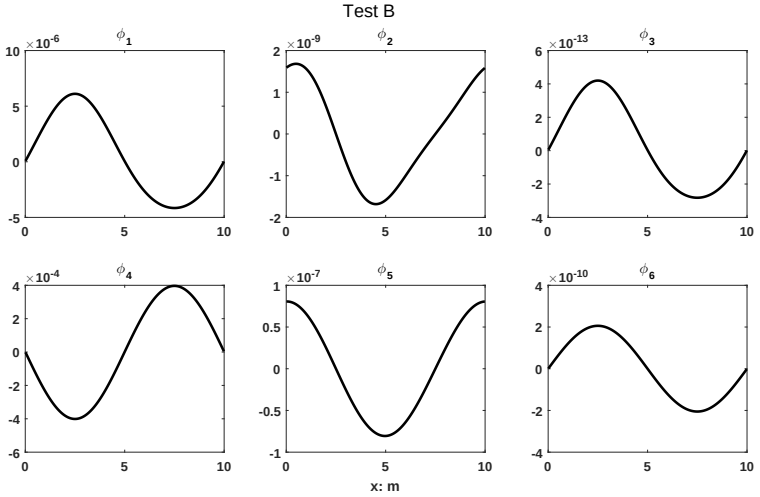

Figure 6.2: Adjoint solution for the first iteration of test B. $p_0 = 7.5$ MPa, $p_1 = 1.5$ MPa, and $k_0 = 1.0$.

For reference, Figure 6.1, Figure 6.2, and Figure 6.3 show the adjoint solution for the first iteration of the three tests. Taking pressure, liquid velocity, and gas velocity as examples, Figure 6.4, Figure 6.5, and Figure 6.6 show the convergence of the numerical solution to the design one as iteration increases. Note that for test A, the numerical solution of liquid and gas velocity changes little when the iteration increases, this is because the liquid and gas velocity are determined by the gradient of initial pressure, which does not

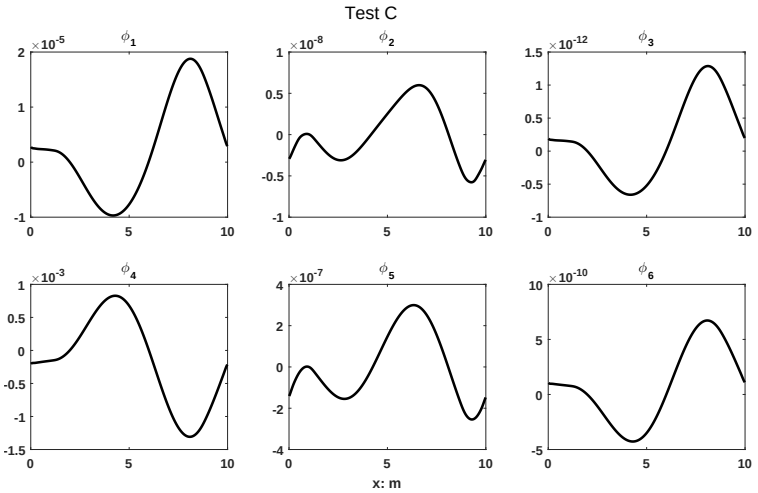

Figure 6.3: Adjoint solution for the first iteration of test C. $p_0 = 7.5$ MPa, $p_1 = 1.0$ MPa, and $k_0 = 1.5$.

depend on p_0. As is expected, the numerical solution converges to the design solution as iteration increases, which verifies the adjoint sensitivity analysis framework.

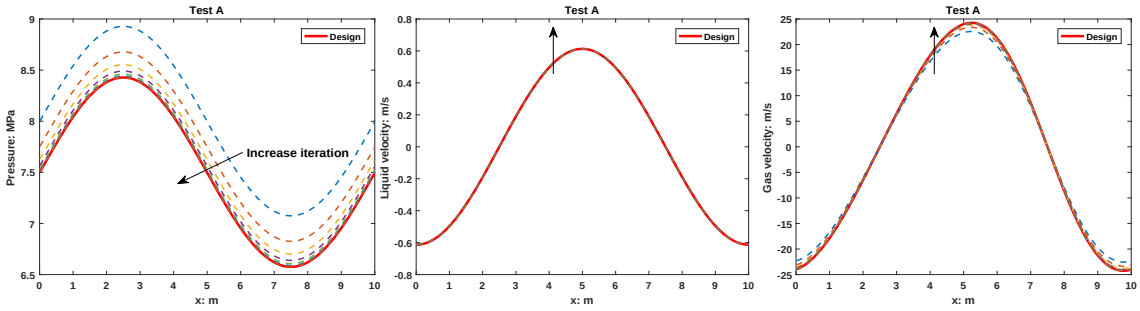

(a) p (b) u_l (c) u_g

Figure 6.4: Convergence of numerical solution for Test A

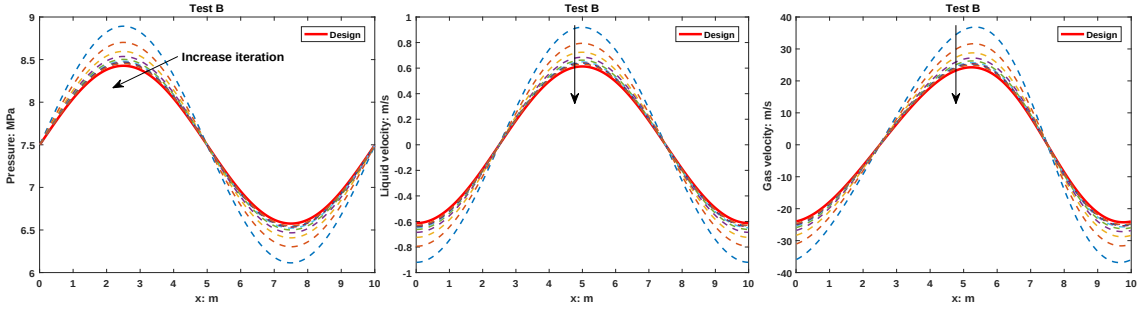

(a) p (b) u_l (c) u_g

Figure 6.5: Convergence of numerical solution for Test B.

The iteration results are given in Table 6.1, Table 6.2, and Table 6.3, respectively. We can see that these three parameters converge to the design values, see the 5^{th} columns. In addition to the optimization results,

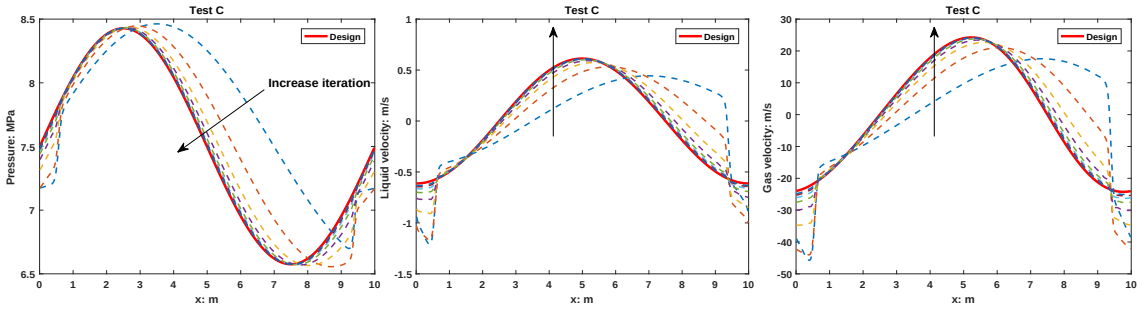

(a) p (b) u_l (c) u_g

Figure 6.6: Convergence of numerical solution for Test C.

the last column in each table gives a verification of the calculated adjoint sensitivities. The verification is based on an important feature of the response function: the design values (p_0, p_1, or k_0) give a local minimum of the response function, see Figure 6.7

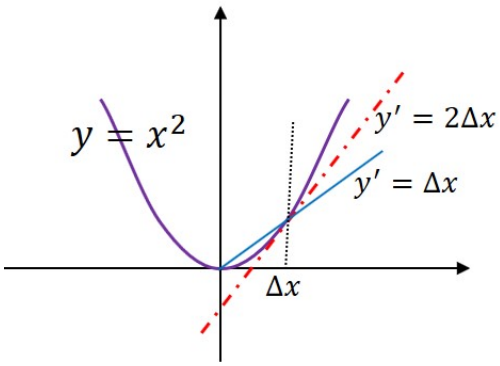

Figure 6.7: Schematic of the response function and the verification scheme

Let ω denotes the parameter of interest, i.e. p_0, p_1, or k_0. Let $\delta\omega$ be the perturbation of the parameter from the design value ω_d. Since ω_d gives a local minimum, we have the following approximation

$$R\big(t_1;\omega_d+\delta\omega\big) \approx R\big(t_1;\omega_d\big) + \frac{1}{2}\left(\frac{\partial^2 R}{\partial\omega^2}\right)_{\omega=\omega_d}\big(\delta\omega\big)^2 \tag{6.57}$$

Taking the first-order derivative of Eq. (6.57) and evaluating the derivative at $\omega = \omega_d + \delta\omega$, we obtain

$$\left(\frac{\partial R}{\partial\omega}\right)_{\omega_d+\delta\omega} \approx \left(\frac{\partial^2 R}{\partial\omega^2}\right)_{\omega=\omega_d}\delta\omega \tag{6.58}$$

Substituting Eq. (6.58) into Eq. (6.57) and canceling the second-order derivative term, we obtain

$$R\big(t_1;\omega_d+\delta\omega\big) \approx R\big(t_1;\omega_d\big) + \frac{1}{2}\left(\frac{\partial R}{\partial\omega}\right)_{\omega_d+\delta\omega}\delta\omega \tag{6.59}$$

Since $R\big(t_1;\omega_d\big)=0$, we have

$$\delta\omega \approx -\frac{2R\big(t_1;\omega_d+\delta\omega\big)}{\big(\frac{\partial R}{\partial\omega}\big)_{\omega_d+\delta\omega}} \tag{6.60}$$

Eq. (6.60) shows that if the sensitivities are correct and the perturbation is small enough, the design parameter could be obtained accurately with 1 iteration, i.e.

$$p_0^d \approx p_0^* = p_0^m - 2R\big(t_1;p_0^m,p_1^m,k_0^m\big)\left(\frac{\partial R}{\partial p_0}\right)^{-1} \tag{6.61a}$$

$$p_1^d \approx p_1^* = p_1^m - 2R\big(t_1;p_0^m,p_1^m,k_0^m\big)\left(\frac{\partial R}{\partial p_1}\right)^{-1} \tag{6.61b}$$

$$k_0^d \approx k_0^* = k_0^m - 2R\big(t_1;p_0^m,p_1^m,k_0^m\big)\left(\frac{\partial R}{\partial k_0}\right)^{-1} \tag{6.61c}$$

The comparison of p_0^*, p_1^*, and k_0^* to the design values provides a good verification scheme to the adjoint sensitivities. As is shown in Table 6.1, Table 6.2, and Table 6.3, p_0^*, p_1^*, and k_0^* are very close to the design values. We have a good confidence in the adjoint sensitivities. Note that in Table 6.3, because the initial guess is too far away from the design value, k_0^* in the first iteration is far away from the design value.

Table 6.1: Results of optimization Test A for finding p_0. p_1 and k_0 are kept at the design values.

Iter. m	R^m	$\big(\partial R/\partial p_0\big)^m$	p_0^m	p_0^{m+1}	p_0^* (verification)
0	1.25E+00	5.01E+00	8.00000	7.75030	7.50061
1	3.13E-01	2.51E+00	7.75030	7.62548	7.50065
2	7.88E-02	1.26E+00	7.62548	7.56309	7.50065
3	1.99E-02	6.38E-01	7.56309	7.53189	7.50067
4	5.09E-03	3.26E-01	7.53189	7.51629	7.50067
5	1.33E-03	1.70E-01	7.51629	7.50849	7.50066
6	3.61E-04	9.20E-02	7.50849	7.50457	7.50063
7	1.06E-04	5.30E-02	7.50457	7.50260	7.50058
8	3.38E-05	3.30E-02	7.50260	7.50158	7.50056
9	1.28E-05	2.30E-02	7.50158	7.50104	7.50046
10	5.41E-06	1.74E-02	7.50104	7.50073	7.50042

Table 6.2: Results of optimization Test B for finding p_1. p_0 and k_0 are kept at the design values.

Iter. m	R^m	$\left(\partial R/\partial p_1\right)^m$	p_1^m	p_1^{m+1}	p_1^* (verification)
0	5.37E-01	2.62E+00	1.50000	1.29525	1.09050
1	1.87E-01	1.65E+00	1.29525	1.18164	1.06792
2	7.08E-02	1.11E+00	1.18164	1.11757	1.05358
3	2.97E-02	8.01E-01	1.11757	1.08054	1.04345
4	1.39E-02	6.24E-01	1.08054	1.05825	1.03595
5	7.28E-03	5.18E-01	1.05825	1.04420	1.03015
6	4.19E-03	4.51E-01	1.04420	1.03491	1.02563
7	2.61E-03	4.07E-01	1.03491	1.02848	1.02208
8	1.74E-03	3.77E-01	1.02848	1.02386	1.01924
9	1.22E-03	3.55E-01	1.02386	1.02042	1.01697
10	8.94E-04	3.38E-01	1.02042	1.01777	1.01513

Table 6.3: Results of optimization Test C for finding k_0. p_0 and p_1 are kept at the design values.

Iter. m	R^m	$\left(\partial R/\partial k_0\right)^m$	k_0^m	k_0^{m+1}	k_0^* (verification)
0	4.01E+00	5.11E+00	1.50000	0.71447	-0.07107
1	1.42E+00	-9.67E+00	0.71447	0.86153	1.00859
2	3.80E-01	-5.34E+00	0.86153	0.93270	1.00388
3	1.02E-01	-3.29E+00	0.93270	0.96360	0.99450
4	3.13E-02	-2.00E+00	0.96360	0.97927	0.99494
5	1.04E-02	-1.24E+00	0.97927	0.98770	0.99613
6	3.73E-03	-7.99E-01	0.98770	0.99237	0.99704
7	1.45E-03	-5.47E-01	0.99237	0.99502	0.99767
8	6.20E-04	-4.00E-01	0.99502	0.99657	0.99811
9	2.95E-04	-3.14E-01	0.99657	0.99751	0.99845
10	1.56E-04	-2.61E-01	0.99751	0.99810	0.99870

6.3.2 Steady-state problem

Problem description

The boiling pipe problem studied in **Sec. 5.4.3** is used to test the adjoint sensitivity analysis framework for steady-state problems. As was mentioned, the source vector is modeled as

$$\mathbf{S} = \begin{pmatrix} -\Gamma_g \\ -\alpha_l\rho_l g - f_{wl} + f_i - \Gamma_g u_i \\ Q_{wl} + Q_{il} - \Gamma_w h_l^{'} - \Gamma_{ig} h_l^* + \left(f_i - f_{wl} - \alpha_l\rho_l g - \Gamma_g u_i\right)u_l + \Gamma_g \frac{u_l^2}{2} \\ \Gamma_g \\ -\alpha_g\rho_g g - f_{wg} - f_i + \Gamma_g u_i \\ Q_{wg} + Q_{ig} + \Gamma_w h_g^{'} + \Gamma_{ig} h_g^* + \left(-f_i - f_{wg} - \alpha_g\rho_g g + \Gamma_g u_i\right)u_g - \Gamma_g \frac{u_g^2}{2} \end{pmatrix} \tag{6.62}$$

The responses of interest for this problem are chosen to be

$$R(q) = \frac{1}{2}\int_{x_0}^{x_1} \left(q^{\text{ss}} - q_d^{\text{ss}}\right)^2 dx, \quad \text{for} \quad q = \alpha_g, p, T_l, T_g, u_l, u_g \tag{6.63}$$

where q_d^{ss} denotes the design solution. Note that different q gives a different response function. q could also be any other quantities that depend on the physical variables, e.g. the total mass flux. Let α_g^{ss}, p^{ss}, T_l^{ss}, T_g^{ss}, u_l^{ss}, and u_g^{ss} be the steady-state solution of the boiling pipe problem. For testing purposes, we choose the following ad-hoc design solution

$$\alpha_{g,d}^{\text{ss}} = \alpha_g^{\text{ss}} + 0.05 \tag{6.64a}$$

$$p_d^{\text{ss}} = p^{\text{ss}} + 10^4 \tag{6.64b}$$

$$T_{l,d}^{\text{ss}} = T_l^{\text{ss}} + 1.0 \tag{6.64c}$$

$$T_{g,d}^{\text{ss}} = T_g^{\text{ss}} + 1.0 \tag{6.64d}$$

$$u_{l,d}^{\text{ss}} = u_l^{\text{ss}} + 0.1 \tag{6.64e}$$

$$u_{g,d}^{\text{ss}} = u_g^{\text{ss}} + 0.1 \tag{6.64f}$$

We are going to study the sensitivities of the response to parameters in the source terms and the boundary conditions.

To perturb the source terms, we introduce the following 8 multiplicative parameters

$$D \leftarrow \omega_D D \tag{6.65a}$$

$$q_{wall} \leftarrow \omega_{qw} q_{wall} \tag{6.65b}$$

$$Q_{wl} \leftarrow q_{wall}\omega_\eta, Q_{wg} \leftarrow q_{wall}(1-\omega_\eta) \tag{6.65c}$$

$$f_i \leftarrow \omega_{fi} f_i \tag{6.65d}$$

$$f_{wl} \leftarrow \omega_{fwl} f_{wl} \tag{6.65e}$$

$$f_{wg} \leftarrow \omega_{fwg} f_{wg} \tag{6.65f}$$

$$H_{il} \leftarrow \omega_{Hil} H_{il} \tag{6.65g}$$

$$H_{ig} \leftarrow \omega_{Hig} H_{ig} \tag{6.65h}$$

Physically, ω_D represents the perturbation in the hydraulic diameter, ω_{qwall} represents the perturbation in the total wall heat flux, ω_η represent the change in the partition of total wall heat flux to liquid and

gas phase, ω_{fi} represents the perturbation in the interfacial friction, ω_{fwl} represents the perturbation in the wall friction to liquid, ω_{fwg} represents the perturbation in the wall friction to gas, ω_{Hil} represents the perturbation in the interface-to-liquid heat transfer coefficient, and ω_{Hig} represents the perturbation in the interface-to-gas heat transfer coefficient. The nominal values for these multiplicative parameters are 1.0.

To perturb the boundary conditions, we introduce the following additive parameters

$$\alpha_{g,\text{inlet}} \leftarrow 0.01 + \delta\alpha_{g,\text{inlet}} \tag{6.66a}$$

$$p_{\text{outlet}} \leftarrow 5.52 \text{ MPa } + \delta p_{\text{outlet}} \tag{6.66b}$$

$$T_{l,\text{inlet}} \leftarrow 530.9 \text{ K } + \delta T_{l,\text{inlet}} \tag{6.66c}$$

$$u_{l,\text{inlet}} \leftarrow 1.15 \text{ m/s } + \delta u_{l,\text{inlet}} \tag{6.66d}$$

Physically, $\delta\alpha_{g,\text{inlet}}$ represents the perturbation in the inlet void fraction, δp_{outlet} represents the perturbation in the outlet pressure, $\delta T_{l,\text{inlet}}$ represents the perturbation in the inlet subcooling, and $\delta u_{l,\text{inlet}}$ represents the perturbation in the inlet mass flux. The nominal values for the perturbations are 0.0.

Let ω be the parameter of interest. We are interested in quantifying the following sensitivities related to the source terms

$$\frac{\partial R(q)}{\partial \omega}, \quad \text{for} \quad q = \alpha_g, p, T_l, T_g, u_l, u_g \quad \text{and} \quad \omega = \omega_D, \omega_{qw}, \omega_\eta, \omega_{fi}, \omega_{fwl}, \omega_{fwg}, \omega_{Hil}, \omega_{Hig} \tag{6.67}$$

and the following sensitivities related to the boundary conditions

$$\frac{\partial R(q)}{\partial \omega}, \quad \text{for} \quad q = \alpha_g, p, T_l, T_g, u_l, u_g \quad \text{and} \quad \omega = \alpha_{g,\text{inlet}}, p_{\text{outlet}}, T_{l,\text{inlet}}, u_{l,\text{inlet}} \tag{6.68}$$

Forward sensitivity analysis

To provide reference values to the adjoint sensitivities, we perform a forward sensitivity analysis. The forward sensitivity analysis is performed by simulating the boiling pipe problem with the Roe-type scheme multiple times with perturbed parameters (multiplicative or additive parameters). Table 6.4 lists the test matrix for the forward simulations. For each parameter, the problem is simulated twice with the given lower and upper bounds of the corresponding parameter. A total of 25 forward simulations (1 base case and 2 for each of 12 parameters) are required.

Taking the void fraction (α_g) and liquid velocity (u_l) as two examples, Figure 6.8 and Figure 6.9 show the results of the forward simulations. The perturbation in the void fraction and the liquid velocity are reported

Table 6.4: Test matrix for the forward sensitivity analysis

Source parameters			Boundary condition parameters		
Case name	parameters	lower/upper bound	Case name	parameters	lower/upper bound
S1	ω_D	0.95, 1.05	BC1	$\alpha_{g,\text{inlet}}$	0.008, 0.012
S2	ω_{qw}	0.95, 1.05	BC2	p_{outlet} : MPa	5.519, 5.521
S3	ω_η	0.98, 1.00	BC3	$T_{l,\text{inlet}}$: K	530.4, 531.4
S4	ω_{fi}	0.95, 1.05	BC4	$u_{l,\text{inlet}}$: m/s	1.10, 1.20
S5	ω_{fwl}	0.95, 1.05			
S6	ω_{fwg}	0.95, 1.05			
S7	ω_{Hil}	0.95, 1.05			
S8	ω_{Hig}	0.75, 1.25			

in Figure 6.8 and Figure 6.9. The forward sensitivities are calculated with a finite difference method, i.e.

$$\frac{\partial R(q)}{\partial \omega} \approx \frac{R(q;\omega_{\text{upper}}) - R(q;\omega_{\text{lower}})}{\omega_{\text{upper}} - \omega_{\text{lower}}} \tag{6.69}$$

The calculated forward sensitivities are shown in Table 6.5 to compare with the adjoint sensitivities.

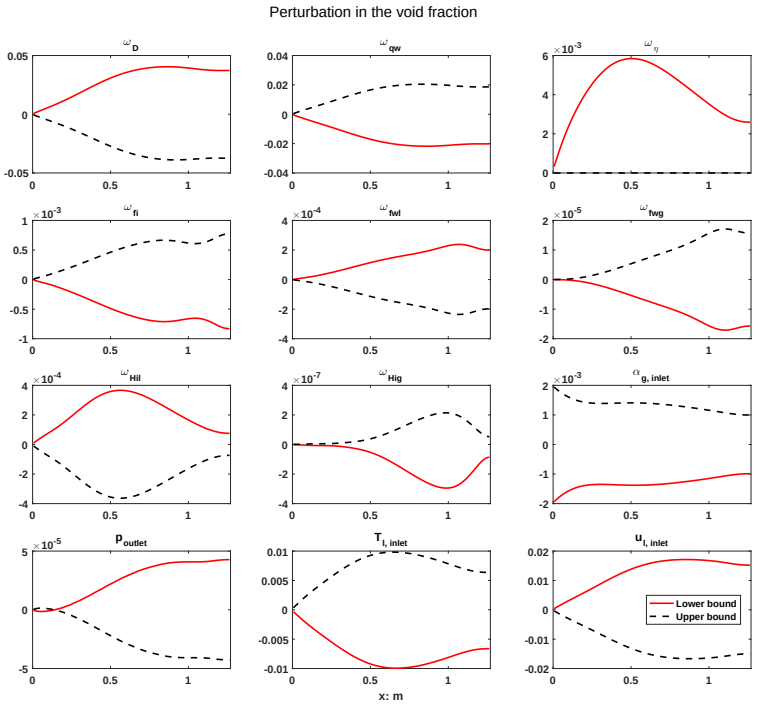

Figure 6.8: Perturbation in the void fraction due to the perturbation in source terms and boundary conditions. Each subfigure represents perturbation in the void fraction due to the corresponding parameter of interest.

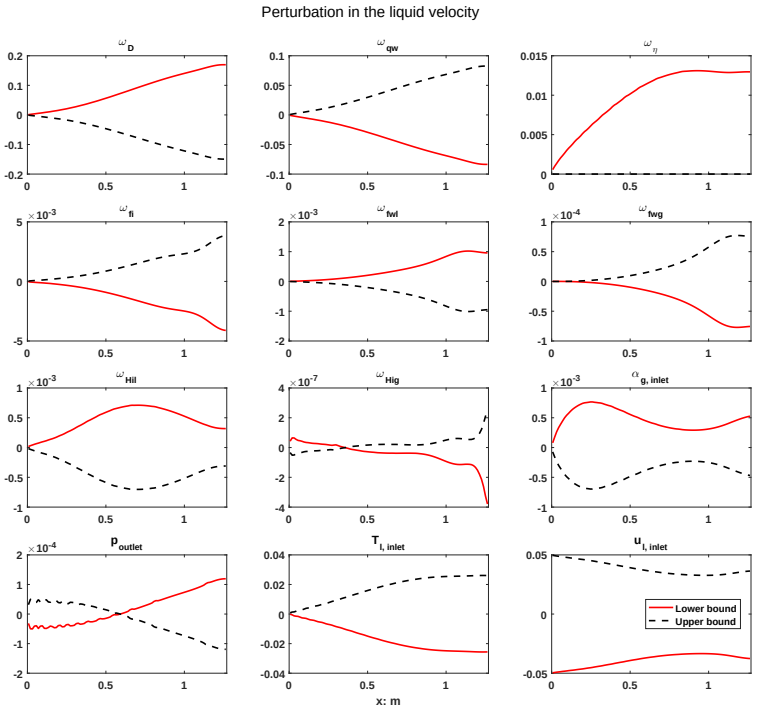

Figure 6.9: Perturbation in the liquid velocity due to the perturbation in source terms and boundary conditions. Each subfigure represents perturbation in the liquid velocity due to the corresponding parameter of interest.

Adjoint sensitivity analysis

The adjoint equation given in Eq. (6.41) is solved to obtain the adjoint solution $\boldsymbol{\phi}$. To solve for the adjoint solution $\boldsymbol{\phi}$, we need to prepare the coefficient matrices and vectors, including $\mathbb{A}_1^{\text{ss}}$, $\mathbb{A}_2^{\text{ss}}$, and $\mathbf{Q}^{\text{ss}}$. These matrices and vectors are obtained with the nominal steady-state solution. Once these matrices and vectors are available, Eq. (6.41) can be solved easily since it is a linear equation. In practice, Eq. (6.41) is discretized as

$$\mathbb{A}_{1,i}^{\text{ss}} \frac{\boldsymbol{\phi}_{i+1} - \boldsymbol{\phi}_{i-1}}{2\Delta x} + \mathbb{A}_{2,i}^{\text{ss}} \boldsymbol{\phi}_i = \mathbf{Q}_i^{\text{ss}} \tag{6.70}$$

Eq. (6.70) is then assembled to form a system of linear equations for solving $\boldsymbol{\phi}$. For each q, e.g. $q = \alpha_g$, there is one set of adjoint solution. Let ϕ_m, $m = 1, \cdots, 6$, be the m^{th} component of the adjoint solution vector $\boldsymbol{\phi}$. Taking the void fraction ($q = \alpha_g$) and the liquid velocity ($q = u_l$) as two examples, Figure 6.10 and Figure 6.11 show the adjoint solution for these two responses. Note that there is a non-smooth region, around $x = 0.15$ m, in the adjoint solution. This non-smooth solution is caused by the change of sign in the relative velocity. The relative velocity is important in calculating the source terms, because it is used in modeling the average bubble diameter and the interfacial area concentration. As an example, Figure 6.12 shows the profile of the liquid velocity, gas velocity, $\partial\Gamma_g/\partial u_g$ (used in the adjoint equation), and ϕ_5 in the

pipe. From Figure 6.12, we can see that the non-smooth solution happens in the location where the relative velocity changes its sign.

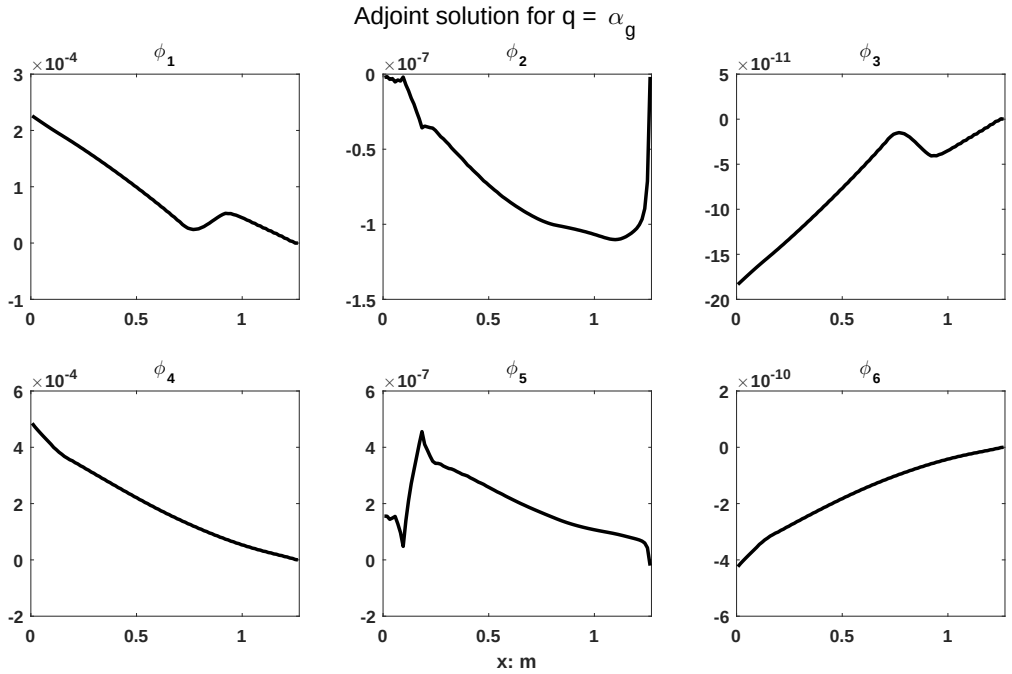

Figure 6.10: Adjoint solution for $q = \alpha_g$.

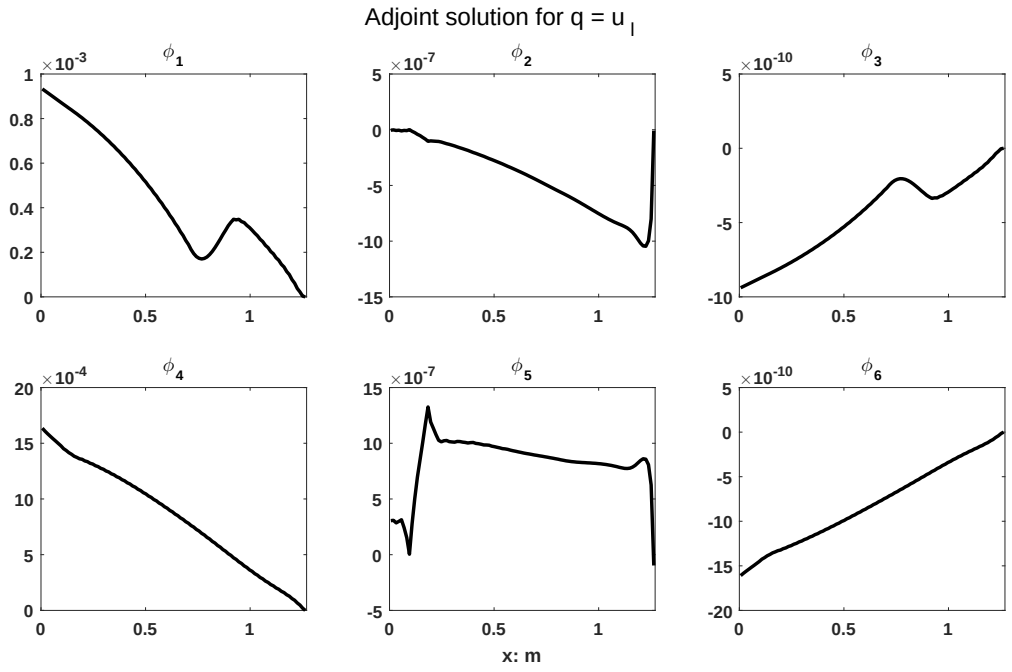

Figure 6.11: Adjoint solution for $q = u_l$.

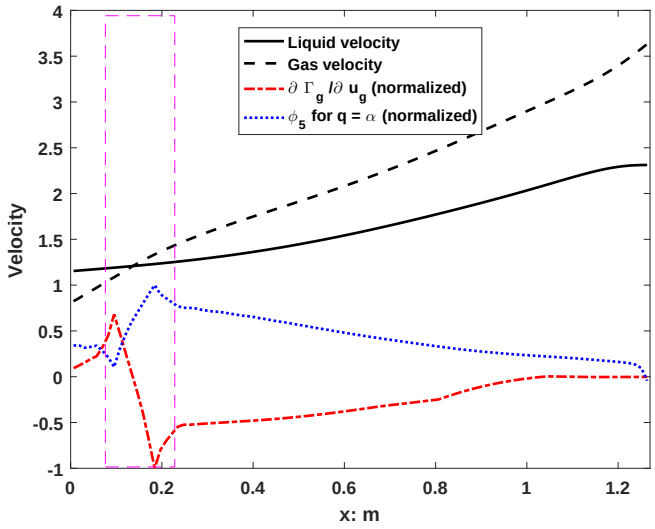

Figure 6.12: Cause of the non-smooth adjoint solution. The magnitude of $\partial\Gamma_g/\partial u_g$ and ϕ_5 are normalized for comparison.

After obtaining the adjoint solution, the adjoint sensitivities are calculated with Eq. (6.43), i.e.

$$\frac{\partial R(q)}{\partial \omega} = \left\langle \boldsymbol{\phi}^T \frac{\partial \mathbf{S}}{\partial \omega} \right\rangle_x^{\text{ss}}, \quad \text{for} \quad \omega = \omega_D, \omega_{qw}, \omega_\eta, \omega_{fi}, \omega_{fwl}, \omega_{fwg}, \omega_{Hil}, \omega_{Hig} \tag{6.71}$$

and

$$\frac{\partial R(q)}{\partial \alpha_{g,\text{inlet}}} = B_1^{\text{ss}} \tag{6.72a}$$

$$\frac{\partial R(q)}{\partial p_{\text{outlet}}} = -B_2^{\text{ss}} \tag{6.72b}$$

$$\frac{\partial R(q)}{\partial T_{l,\text{inlet}}} = B_3^{\text{ss}} \tag{6.72c}$$

$$\frac{\partial R(q)}{\partial u_{l,\text{inlet}}} = B_5^{\text{ss}} \tag{6.72d}$$

The adjoint sensitivities are given in Table 6.5, which also includes the forward sensitivities. Comparison of adjoint sensitivities to the forward sensitivities is also shown in Figure 6.13, where the magnitude of forward sensitivities and adjoint sensitivities are compared. For most cases, the adjoint sensitivities match the forward sensitivities very well, which verifies the adjoint sensitivity analysis framework. However, when the response is not sensitive to the parameters of interest, the adjoint sensitivities do not match the forward sensitivities well. This is reasonable. If the response is not sensitive to the parameters, the perturbation in the response is negligible and the numerical noise dominates both the forward sensitivities and the adjoint

Table 6.5: Comparison of sensitivities from forward sensitivity analysis and adjoint sensitivity analysis

Parameters	Method	$q = \alpha_g$	$q = p$	$q = T_l$	$q = T_g$	$q = u_l$	$q = u_g$
ω_D	Forward	3.28E-02	2.09E-06	3.10E-05	8.47E-09	1.83E-01	3.04E-01
	Adjoint	3.41E-02	1.47E-06	2.66E-05	2.05E-07	1.79E-01	2.56E-01
ω_{qw}	Forward	-1.55E-02	-7.90E-07	-1.80E-05	-3.17E-09	-8.95E-02	-1.39E-01
	Adjoint	-1.94E-02	-3.94E-07	-1.00E-05	-5.69E-08	-1.06E-01	-1.66E-01
ω_η	Forward	1.25E-02	2.97E-08	-3.08E-05	1.86E-05	4.93E-02	8.63E-02
	Adjoint	1.20E-02	1.68E-08	-2.96E-05	-1.96E-04	5.85E-02	9.23E-02
ω_{fi}	Forward	-6.48E-04	-7.43E-08	3.60E-08	-3.45E-10	-3.84E-03	7.41E-03
	Adjoint	-6.01E-04	3.37E-09	3.72E-08	2.22E-10	-3.86E-03	8.01E-03
ω_{fwl}	Forward	1.61E-04	-4.27E-07	-4.38E-08	-1.80E-09	1.02E-03	-1.87E-03
	Adjoint	1.66E-04	-4.50E-07	-4.22E-08	-6.11E-08	1.07E-03	-1.74E-03
ω_{fwg}	Forward	-9.95E-06	-2.68E-08	-1.61E-09	-1.28E-10	-6.97E-05	1.37E-04
	Adjoint	-1.02E-05	-2.65E-08	-1.70E-09	-3.91E-09	-7.13E-05	1.48E-04
ω_{Hil}	Forward	3.11E-04	1.01E-09	-7.91E-07	-1.77E-12	1.30E-03	2.23E-03
	Adjoint	2.59E-04	-4.99E-09	-7.02E-07	-6.30E-10	1.11E-03	1.87E-03
ω_{Hig}	Forward	-1.65E-10	1.25E-14	-1.11E-13	-4.61E-11	-8.21E-10	-3.12E-09
	Adjoint	-2.53E-08	3.47E-12	4.41E-12	-5.83E-10	-1.69E-08	-1.64E-07
$\alpha_{g,\text{inlet}}$	Forward	-3.40E-02	2.40E-06	-1.40E-05	1.02E-08	4.52E-02	-1.60E-02
	Adjoint	-4.04E-02	2.76E-06	-1.33E-05	3.90E-07	2.78E-02	-1.75E-02
p_{outlet}	Forward	1.15E-08	-3.75E-10	-2.71E-11	-1.75E-12	5.48E-08	2.14E-08
	Adjoint	1.56E-09	-3.79E-10	-4.98E-11	-5.18E-11	2.64E-09	1.53E-08
$T_{l,\text{inlet}}$	Forward	-8.50E-04	-1.92E-08	-1.98E-06	-7.00E-11	-3.93E-03	-6.58E-03
	Adjoint	-8.90E-04	1.51E-09	-1.83E-06	-4.53E-11	-4.24E-03	-7.01E-03
$u_{l,\text{inlet}}$	Forward	1.52E-02	-2.27E-06	9.92E-06	-9.53E-09	-9.54E-02	-4.32E-02
	Adjoint	1.53E-02	-1.15E-06	8.99E-06	-1.52E-07	-9.72E-02	-3.03E-02

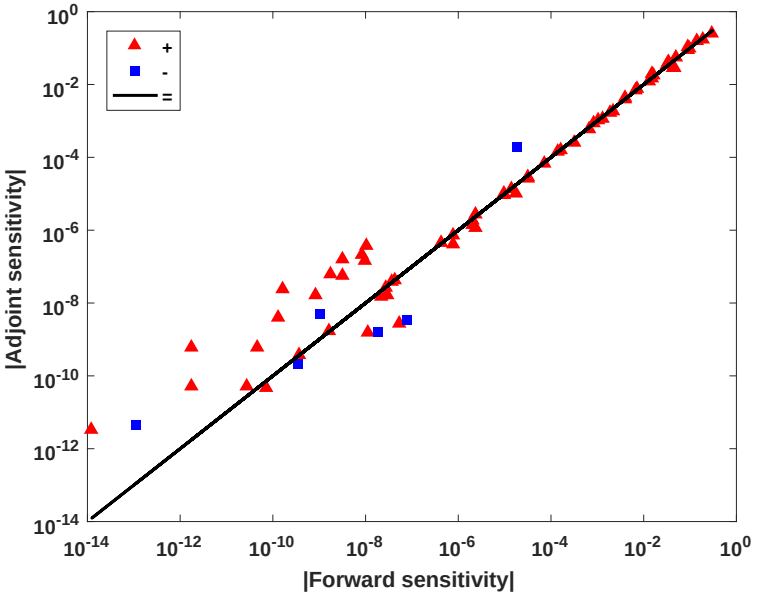

Figure 6.13: Comparison of forward sensitivities to adjoint sensitivities. Absolute values of forward and adjoint sensitivities are plotted. ▲ represent cases where the forward and adjoint sensitivities have the same sign; ■ represent cases where the forward and adjoint sensitivities have different sign; straight line denotes that the forward sensitivities are equal to the adjoint sensitivities.

sensitivities, especially when the sensitivity value is below 10^{-7}. Column-wise, for $q = p$, the adjoint sensitivities to the source parameters ($\omega_{fi}, \omega_{Hil}$, and ω_{Hig}) do not match the forward sensitivities well, because the pressure depends weakly on these three parameters. The same issue happen with $q = T_g$, because the gas temperature is at the saturation temperature of local pressure and depends weakly on the parameters of interest. Row-wise, the same issue happens with the source parameters ω_{Hig}.

The response is in general sensitive to the boundary conditions but not sensitive to several the physical model parameters, e.g. interfacial heat transfer coefficients. These sensitivities represent the multi-dimensional gradients of the response function to the parameters of interest. If high-quality measurement data is available, the adjoint sensitivities can be used to improve the physical models, e.g. with a calibration method. Another application of the adjoint sensitivities is to propagate the uncertainty in the parameters of interest to the response function. Because the adjoint sensitivities to all parameters are obtained with 1 forward simulation, a significant amount of computational time will be saved.

6.4 Conclusion

In this chapter, an adjoint sensitivity analysis framework is developed for the two-phase two-fluid model. The adjoint sensitivity analysis framework is based on the forward numerical solver developed in **Chapter 5**.

The adjoint sensitivity analysis framework is divided into two parts corresponding to time-dependent problems and the steady-state problems. In this thesis, the time-dependent adjoint sensitivity analysis is used for testing purposes. For simplicity, the time-dependent adjoint sensitivity analysis is derived with periodic boundary conditions. The steady-state adjoint sensitivity analysis is derived with practical boundary conditions.

The time-dependent adjoint sensitivity analysis is tested with the periodic pipe problem to find the design parameters. The steady-state adjoint sensitivity analysis is tested with the boiling pipe problem to calculate sensitivities of responses to several input parameters, including physical model parameters and boundary conditions. For both tests, the adjoint sensitivities are shown to match very well with either analytical sensitivities or forward sensitivities, which verifies the current adjoint sensitivity analysis framework.

Chapter 7

SUMMARY AND FUTURE WORK

7.1 Summary

In this thesis, a new shock-capturing upwind numerical solver and an adjoint sensitivity analysis framework for the two-phase two-fluid model are developed. Both the forward solver and the adjoint sensitivity analysis are verified extensively with several benchmark problems.

The forward solver is based on analytical eigenvalues and eigenvectors of the two-fluid model. The treatment of arbitrary EOS is essential to perform an analytical analysis to the two-phase two-fluid model. The challenge in the analytical analysis (due to the arbitrary EOS) is overcome by introducing a few auxiliary variables. Through thermodynamic and algebraic transformations, the Jacobian matrix of the system is simplified to a simple and well-structured form, which is convenient for the analytical analysis. Approximate eigenvalues and eigenvectors of the conservative part are obtained by exploiting the difference in the thermodynamic properties of liquid and gas phases. The eigenvalues and eigenvectors are essential for constructing the forward numerical solver, because they provide accurate upwind information of the system.

Based on the analytical eigenvalues and eigenvectors, a Roe-type and a WENO-type numerical flux are constructed to provide appropriate upwind numerical flux to the forward solver. The solver is tested with three benchmark problems: a periodic problem, the two-phase shock-tube problem, and the Christensen boiling pipe problem. Because of the analytical eigenvalues and eigenvectors, the solver is algebraically very simple. The results show that the solver is stable, accurate, and robust. The grid convergence study shows that the Roe-type scheme is first-order accurate in space and the WENO-type solver is at least second-order accurate in space.

The basic two-phase two-fluid model assumes all pressure terms are equal. In this case, the two-phase system has two complex eigenvalues when the relative velocity is non-zero. From mathematical point of view, the two complex eigenvalues make the system ill-posed; from numerical point of view, when the spatial discretization is fine enough to distinguish the characteristic waves related to the two complex eigenvalues, the numerical solver tends to give non-physical oscillations. This issue is more severe when the absolute

value of relative velocity is comparable to the speed of sound, because the magnitude of the imaginary part of the two complex eigenvalues becomes too large. Numerically, it is found that the regularization using the interfacial pressure correction helps at least reduce the non-physical oscillations near discontinuities.

A critical and unique feature of the forward solver is that the formulation does not depend on the form of EOS, which ensures that the solver is applicable to practical two-phase problems, such as a boiling pipe. The successful application of the new solver to a boiling pipe is very encouraging, because it opens up the possibility of applying many other advanced methods (e.g. WENO, DG-FEM, etc) to nuclear reactor thermal-hydraulic simulations.

An adjoint sensitivity analysis framework for the two-phase flow problems is developed based on the new forward solver. The adjoint sensitivity analysis is formulated for both time-dependent and steady-state problems. The adjoint sensitivity analysis framework for both time-dependent and steady-state problems is verified. The adjoint sensitivities to different parameters of interest are verified by either analytical sensitivities or forward sensitivities. The key feature of the current adjoint sensitivity analysis framework is that it is based on the continuous form of the forward equation and is algebraically very simple. The connection between the forward problem and the adjoint problem is through the coefficient matrices. The application of this method to other two-phase flow problems should be straightforward.

7.2 Future work

7.2.1 Issues and future work in forward solver

The current forward solver provides the essential framework for developing a mathematically consistent, algebraically simple, and numerically accurate and robust solver for realistic thermal-hydraulic simulations. However, there are some issues in the current forward solver:

1. The current solver uses very small time step because of the CFL condition, it is not suitable for long time transient simulations in the real-world reactor safety analysis. The current solver is not very robust. It is based on an explicit method and the stiffness of the source terms has not been considered, which might cause an issue.

2. Though second-order spatial accuracy is achieved with the WENO-type numerical flux, the WENO-type scheme is not as robust as the Roe-type scheme.

3. The current solver works for two-phase flows only. It is not capable of simulating the appearance and disappearance of either phase.

4. The current solver uses a simple boundary condition treatment, it might affect the numerical solution and degrade the accuracy of the solver.

These issues have to be solved in the future. Here are potential solutions to these issues:

1. A fully-implicit scheme is recommended to avoid the time step limit and improve the robustness of the current explicit scheme. The fully implicit scheme is recommended to be solved with a Jacobian-Free Newton-Krylov (JFNK) method. Fully implicit schemes for two-phase flows have been proposed and studied by many researchers. Recently, the JFNK method becomes popular as a nonlinear solver. Mousseau [63] did the pioneering work to apply the JFNK method to two-phase flows. Applications of the JFNK method to two-phase flows can be seen in [64, 65, 8, 66, 9]. Encouraging and promising results have been shown by Zou and his coworkers [8, 66, 9], where the fully implicit scheme is used to solve realistic two-phase flow problems.

2. To achieve a high-order accuracy, it is recommended to explore numerical procedures for converting the first-order Roe-type numerical flux to a high-order one. Because the current solver has a direct link, i.e. a Roe-type numerical flux, to the existing schemes for single-phase flows, it is recommended to seek for a mature high-resolution scheme in single-phase flows and extend it to two-phase flows. Mature high-resolution schemes are not rare for single-phase flows. A through review of these schemes can be found in [67, 68]. Among these high-resolution schemes, the Monotone Upstream Scheme for Conservation Laws (MUSCL) of Van Leer [34], the Total-Variation-Diminishing (TVD) scheme of Harten [69], and the Essentially Non-Oscillatory (ENO) scheme of Harten and Osher [46] are the most well known. Among these schemes, the TVD scheme of Harten [69] seems a natural choice since it requires little extra work given a working forward solver and a robust Roe-type numerical flux.

3. Phase appearance and disappearance issue is a major challenge in two-phase flow simulations. The discontinuity in the void fraction due to the appearance and disappearance of one phase puts a strict requirement on the robustness of the numerical scheme. It is recommended to explore a numerical treatment, such as truncating the void fraction numerically, to solve this issue. However, the numerical treatment might not be optimal and more analytical work on the numerical scheme is required to solve this issue.

4. It is recommended to implement a characteristics-based boundary condition treatment to the forward solver. The approximate eigenvalues and eigenvectors might be used to treat the boundary conditions in the characteristic space.

In addition to solve the previous issues, there are some important and valuable extension to the current forward solver:

1. It is recommended to explore the possibility of solving the two-phase two-fluid model with the auxiliary form of the governing equations, e.g. the enthalpy equation. The current forward solver is based on a conservative form of the two-phase two-fluid model, which might not be appropriate for simulating problems when the change in the temperature of the liquid/gas phases is significantly smaller than the change in the velocity of liquid/gas phases. Analytical work on the change in the eigenvalues, eigenvectors, and numerical fluxes is required.

2. It is recommended to explore the possibility of solving the 2D or 3D two-phase two-fluid model within the current framework. The eigenvalues and eigenvectors of the 2D or 3D model are similar to the 1D model. There are three difficulties. The first difficulty lies in providing the closure correlations for the 2D or 3D model, e.g. the multi-dimensional interfacial friction model and multi-dimensional interfacial heat flux model. The second difficulty lies in the numerical treatment of the high-dimensional geometry, which changes significantly the data structure in the forward solver. The third difficulty lies in extending the 1D numerical flux to 2D or 3D, which is non-trivial.

3. It is recommended to extend the current solver for real-world reactor safety analysis. Adding the capability of simulating more complex two-phase flow problems requires extensive extra numerical work to the current solver.

7.2.2 Issues and future work in adjoint sensitivity analysis

There are also some issues in the current adjoint sensitivity analysis framework. The issues are listed below:

1. The current adjoint sensitivity analysis relies on numerical coefficient matrices. The effect of the truncation error to the adjoint sensitivities is not fully studied.

2. The current adjoint sensitivity analysis works with a specific form of the response function, which measures the quantify of interest in the whole domain. The local (e.g. in a certain location) information of the quantity of interest is not considered.

3. The current adjoint sensitivity analysis for time-dependent problems is only valid for problems with periodic boundary conditions. It can not be applied directly to the real-world transient simulations in reactor safety analysis. Effect of the time-dependent boundary conditions to the system has not been studied.

4. The current adjoint equation is solved with a basic finite difference method, which might not be robust enough for applications to more complex problems.

These issues have to be solved in the future. Here are potential solutions to these issues:

1. It is recommended to obtain analytical coefficient matrices. For realistic problems where the source terms are modeled with complicated closure correlations, it is recommended to provide approximate coefficient matrices instead. This is non-trivial but important, because the analytical coefficient matrices can also be used in the forward solver when an implicit method is used.

2. It is recommended to develop an adjoint sensitivity analysis framework that is general for other kinds of response function. Besides the method used in the current adjoint sensitivity analysis, it is valuable to explore the possibility of applying the discrete adjoint method [70] to two-phase flow simulations.

3. It is recommended to study the effect of the time-dependent boundary conditions to the two-phase system using the adjoint method.

4. It is recommended to explore the possibility of solving the adjoint equation with a more robust method, e.g. an implicit method. This study is recommended to do only after a robust forward implicit solver is available.

Appendix A

DERIVATIONS OF JACOBIAN MATRIX

Recall that the Jacobian matrix of the system is defined as

$$\mathbb{A} = \left(\mathbb{I} + \mathbb{A}_{it,nc}\right)^{-1}\left(\mathbb{A}_c + \mathbb{A}_{ix,nc}\right) \tag{A.1}$$

with

$$\mathbb{A}_c \equiv \frac{\partial \mathbf{F}}{\partial \mathbf{U}}, \mathbb{A}_{ix,nc} \equiv \mathbf{P}_{ix}\frac{\partial \alpha_g}{\partial \mathbf{U}}, \mathbb{A}_{ix,nc} \equiv \mathbf{P}_{it}\frac{\partial \alpha_g}{\partial \mathbf{U}} \tag{A.2}$$

Recall that $\mathbf{U}$ is the vector of conservative variables, $\mathbf{F}$ is the vector of fluxes, $\mathbf{P}_{ix}$ and $\mathbf{P}_{it}$ are the vectors related to the averaged interfacial pressure. The vectors in Eq. (A.2) are

$$\mathbf{U} \equiv \begin{pmatrix} \alpha_l\rho_l \\ \alpha_l\rho_l u_l \\ \alpha_l\rho_l E_l \\ \alpha_g\rho_g \\ \alpha_g\rho_g u_g \\ \alpha_g\rho_g E_g \end{pmatrix}, \mathbf{F} \equiv \begin{pmatrix} \alpha_l\rho_l u_l \\ \alpha_l\rho_l u_l^2 + \alpha_l p \\ \alpha_l\rho_l E_l u_l + \alpha_l p u_l \\ \alpha_g\rho_g u_g \\ \alpha_g\rho_g u_g^2 + \alpha_g p \\ \alpha_g\rho_g E_g u_g + \alpha_g p u_g \end{pmatrix}, \mathbf{P}_{ix} \equiv \begin{pmatrix} 0 \\ p_i \\ 0 \\ 0 \\ -p_i \\ 0 \end{pmatrix}, \mathbf{P}_{it} \equiv \begin{pmatrix} 0 \\ 0 \\ -p_i \\ 0 \\ 0 \\ p_i \end{pmatrix} \tag{A.3}$$

For ease of notations, we write $\mathbf{U}$ and $\mathbf{F}$ as

$$\mathbf{U} \equiv \begin{pmatrix} x_1 \\ x_2 \\ x_3 \\ x_4 \\ x_5 \\ x_6 \end{pmatrix} = \begin{pmatrix} \alpha_l\rho_l \\ \alpha_l\rho_l u_l \\ \alpha_l\rho_l E_l \\ \alpha_g\rho_g \\ \alpha_g\rho_g u_g \\ \alpha_g\rho_g E_g \end{pmatrix}, \mathbf{F} \equiv \begin{pmatrix} y_1 \\ y_2 \\ y_3 \\ y_4 \\ y_5 \\ y_6 \end{pmatrix} = \begin{pmatrix} \alpha_l\rho_l u_l \\ \alpha_l\rho_l u_l^2 + \alpha_l p \\ \alpha_l\rho_l E_l u_l + \alpha_l p u_l \\ \alpha_g\rho_g u_g \\ \alpha_g\rho_g u_g^2 + \alpha_g p \\ \alpha_g\rho_g E_g u_g + \alpha_g p u_g \end{pmatrix} \tag{A.4}$$

Then,

$$\mathbb{A}_c \equiv \begin{pmatrix} \frac{\partial y_1}{\partial x_1} & \frac{\partial y_1}{\partial x_2} & \frac{\partial y_1}{\partial x_3} & \frac{\partial y_1}{\partial x_4} & \frac{\partial y_1}{\partial x_5} & \frac{\partial y_1}{\partial x_6} \\ \frac{\partial y_2}{\partial x_1} & \frac{\partial y_2}{\partial x_2} & \frac{\partial y_2}{\partial x_3} & \frac{\partial y_2}{\partial x_4} & \frac{\partial y_2}{\partial x_5} & \frac{\partial y_2}{\partial x_6} \\ \frac{\partial y_3}{\partial x_1} & \frac{\partial y_3}{\partial x_2} & \frac{\partial y_3}{\partial x_3} & \frac{\partial y_3}{\partial x_4} & \frac{\partial y_3}{\partial x_5} & \frac{\partial y_3}{\partial x_6} \\ \frac{\partial y_4}{\partial x_1} & \frac{\partial y_4}{\partial x_2} & \frac{\partial y_4}{\partial x_3} & \frac{\partial y_4}{\partial x_4} & \frac{\partial y_4}{\partial x_5} & \frac{\partial y_4}{\partial x_6} \\ \frac{\partial y_5}{\partial x_1} & \frac{\partial y_5}{\partial x_2} & \frac{\partial y_5}{\partial x_3} & \frac{\partial y_5}{\partial x_4} & \frac{\partial y_5}{\partial x_5} & \frac{\partial y_5}{\partial x_6} \\ \frac{\partial y_6}{\partial x_1} & \frac{\partial y_6}{\partial x_2} & \frac{\partial y_6}{\partial x_3} & \frac{\partial y_6}{\partial x_4} & \frac{\partial y_6}{\partial x_5} & \frac{\partial y_6}{\partial x_6} \end{pmatrix} \tag{A.5}$$

$$\mathbb{A}_{ix,nc} \equiv \begin{pmatrix} 0 & 0 & 0 & 0 & 0 & 0 \\ p_i \frac{\partial \alpha_g}{\partial x_1} & p_i \frac{\partial \alpha_g}{\partial x_2} & p_i \frac{\partial \alpha_g}{\partial x_3} & p_i \frac{\partial \alpha_g}{\partial x_4} & p_i \frac{\partial \alpha_g}{\partial x_5} & p_i \frac{\partial \alpha_g}{\partial x_6} \\ 0 & 0 & 0 & 0 & 0 & 0 \\ 0 & 0 & 0 & 0 & 0 & 0 \\ -p_i \frac{\partial \alpha_g}{\partial x_1} & -p_i \frac{\partial \alpha_g}{\partial x_2} & -p_i \frac{\partial \alpha_g}{\partial x_3} & -p_i \frac{\partial \alpha_g}{\partial x_4} & -p_i \frac{\partial \alpha_g}{\partial x_5} & -p_i \frac{\partial \alpha_g}{\partial x_6} \\ 0 & 0 & 0 & 0 & 0 & 0 \end{pmatrix} \tag{A.6}$$

$$\mathbb{A}_{it,nc} \equiv \begin{pmatrix} 0 & 0 & 0 & 0 & 0 & 0 \\ 0 & 0 & 0 & 0 & 0 & 0 \\ -p_i \frac{\partial \alpha_g}{\partial x_1} & -p_i \frac{\partial \alpha_g}{\partial x_2} & -p_i \frac{\partial \alpha_g}{\partial x_3} & -p_i \frac{\partial \alpha_g}{\partial x_4} & -p_i \frac{\partial \alpha_g}{\partial x_5} & -p_i \frac{\partial \alpha_g}{\partial x_6} \\ 0 & 0 & 0 & 0 & 0 & 0 \\ 0 & 0 & 0 & 0 & 0 & 0 \\ p_i \frac{\partial \alpha_g}{\partial x_1} & p_i \frac{\partial \alpha_g}{\partial x_2} & p_i \frac{\partial \alpha_g}{\partial x_3} & p_i \frac{\partial \alpha_g}{\partial x_4} & p_i \frac{\partial \alpha_g}{\partial x_5} & p_i \frac{\partial \alpha_g}{\partial x_6} \end{pmatrix} \tag{A.7}$$

The difficulty lies in deriving these partial derivatives with arbitrary EOS and simplifying them to suitable forms. Taking a close look at these partial derivatives, we find that the following partial derivatives are essential

$$\frac{\partial p}{\partial x_m}, \frac{\partial \alpha_g}{\partial x_m}, \text{ for } m = 1, \cdots, 6 \tag{A.8}$$

Because x_m's contain the density and specific internal energy, which are related to pressure through the EOS, we know that the EOS has to be used in deriving $\frac{\partial p}{\partial x_m}$ and $\frac{\partial \alpha_g}{\partial x_m}$.

Let Δ denotes the operator for the change in variables. Note that in the derivations, Δ will also denote the infinitesimal change, which is often denoted with operator 'd'. The derivations start with

$$\begin{aligned} \Delta x_1 &= \Delta(\alpha_l \rho_l) = \alpha_l \Delta \rho_l - \rho_l \Delta \alpha_g = \alpha_l \left(\frac{\partial \rho_l}{\partial p} \Delta p + \frac{\partial \rho_l}{\partial e_l} \Delta e_l \right) - \rho_l \Delta \alpha_g \\ \Delta x_4 &= \Delta(\alpha_g \rho_g) = \alpha_g \Delta \rho_g + \rho_g \Delta \alpha_g = \alpha_g \left(\frac{\partial \rho_g}{\partial p} \Delta p + \frac{\partial \rho_g}{\partial e_g} \Delta e_g \right) + \rho_g \Delta \alpha_g \end{aligned} \tag{A.9}$$

Solving for Δp and $\Delta\alpha_g$ from Eq. (A.9), we get

$$\begin{aligned}\Delta p &= \frac{\rho_l \Delta x_4 + \rho_g \Delta x_1 - \left(\alpha_g \rho_l \frac{\partial \rho_g}{\partial e_g}\Delta e_g + \alpha_l \rho_g \frac{\partial \rho_l}{\partial e_l}\Delta e_l\right)}{\alpha_g \rho_l \frac{\partial \rho_g}{\partial p} + \alpha_l \rho_g \frac{\partial \rho_l}{\partial p}} \\ \Delta\alpha_g &= \frac{\alpha_l \frac{\partial \rho_l}{\partial p}\Delta x_4 - \alpha_g \frac{\partial \rho_g}{\partial p}\Delta x_1 - \alpha_g\alpha_l\left(\frac{\partial \rho_l}{\partial p}\frac{\partial \rho_g}{\partial e_g}\Delta e_g - \frac{\partial \rho_g}{\partial p}\frac{\partial \rho_l}{\partial e_l}\Delta e_l\right)}{\alpha_g \rho_l \frac{\partial \rho_g}{\partial p} + \alpha_l \rho_g \frac{\partial \rho_l}{\partial p}}\end{aligned} \tag{A.10}$$

Taking Δp as an example, we show the process of simplifications. Multiplying $\frac{\partial p}{\partial \rho_l}\frac{\partial p}{\partial \rho_g}$ to the nominator and denominator of Δp in Eq. (A.10) and using the mathematical relations

$$\frac{\partial p}{\partial \rho_l}\frac{\partial \rho_l}{\partial p} = 1, \text{ and } \frac{\partial p}{\partial \rho_g}\frac{\partial \rho_g}{\partial p} = 1 \tag{A.11}$$

we get

$$\Delta p = \frac{\frac{\partial p}{\partial \rho_l}\frac{\partial p}{\partial \rho_g}\left[\rho_l \Delta x_4 + \rho_g \Delta x_1 - \left(\alpha_g \rho_l \frac{\partial \rho_g}{\partial e_g}\Delta e_g + \alpha_l \rho_g \frac{\partial \rho_l}{\partial e_l}\Delta e_l\right)\right]}{\alpha_g \rho_l \frac{\partial p}{\partial \rho_l} + \alpha_l \rho_g \frac{\partial p}{\partial \rho_g}} \tag{A.12}$$

By using the mathematical relations

$$\begin{aligned}\frac{\partial p}{\partial e_g} &= -\frac{\partial p}{\partial \rho_g}\frac{\partial \rho_g}{\partial e_g} \\ \frac{\partial p}{\partial e_l} &= -\frac{\partial p}{\partial \rho_l}\frac{\partial \rho_l}{\partial e_l}\end{aligned} \tag{A.13}$$

Eq. (A.12) is further transformed into

$$\begin{aligned}\Delta p &= \frac{\frac{\partial p}{\partial \rho_l}\frac{\partial p}{\partial \rho_g}\left[\rho_l \Delta x_4 + \rho_g \Delta x_1\right] + \alpha_g \rho_l \frac{\partial p}{\partial \rho_l}\frac{\partial p}{\partial e_g}\Delta e_g + \alpha_l \rho_g \frac{\partial p}{\partial \rho_g}\frac{\partial p}{\partial e_l}\Delta e_l}{\alpha_g \rho_l \frac{\partial p}{\partial \rho_l} + \alpha_l \rho_g \frac{\partial p}{\partial \rho_g}} \\ &= c_1 \Delta x_1 + c_2 \Delta x_4 + c_3 \Delta e_l + c_4 \Delta e_g\end{aligned} \tag{A.14}$$

where c_1, c_2, c_3, and c_4 are auxiliary variables used for ease of notations , they are defined as

$$\begin{aligned}c_1 &\equiv \frac{\rho_g \frac{\partial p}{\partial \rho_l}\frac{\partial p}{\partial \rho_g}}{\alpha_g \rho_l \frac{\partial p}{\partial \rho_l} + \alpha_l \rho_g \frac{\partial p}{\partial \rho_g}} \\ c_2 &\equiv \frac{\rho_l \frac{\partial p}{\partial \rho_l}\frac{\partial p}{\partial \rho_g}}{\alpha_g \rho_l \frac{\partial p}{\partial \rho_l} + \alpha_l \rho_g \frac{\partial p}{\partial \rho_g}} \\ c_3 &\equiv \frac{\alpha_l \rho_g \frac{\partial p}{\partial \rho_g}\frac{\partial p}{\partial e_l}}{\alpha_g \rho_l \frac{\partial p}{\partial \rho_l} + \alpha_l \rho_g \frac{\partial p}{\partial \rho_g}} \\ c_4 &\equiv \frac{\alpha_g \rho_l \frac{\partial p}{\partial \rho_l}\frac{\partial p}{\partial e_g}}{\alpha_g \rho_l \frac{\partial p}{\partial \rho_l} + \alpha_l \rho_g \frac{\partial p}{\partial \rho_g}}\end{aligned} \tag{A.15}$$

The partial derivatives $\frac{\partial p}{\partial \rho_l}$, $\frac{\partial p}{\partial \rho_g}$, $\frac{\partial p}{\partial e_l}$, and $\frac{\partial p}{\partial e_g}$ in Eq. (A.15) are not very informative and will make the matrices in Eq. (A.5), Eq. (A.6), and Eq. (A.7) very complicated. For simplifications, we replace $\frac{\partial p}{\partial \rho_l}$, $\frac{\partial p}{\partial \rho_g}$, $\frac{\partial p}{\partial e_l}$, and $\frac{\partial p}{\partial e_g}$ with

$$\frac{\partial p}{\partial e_l} = \rho_l\big(\gamma_l - 1\big) \tag{A.16a}$$

$$\frac{\partial p}{\partial \rho_l} = a_l^2 - \frac{p}{\rho_l}\big(\gamma_l - 1\big) \tag{A.16b}$$

$$\frac{\partial p}{\partial e_g} = \rho_g\big(\gamma_g - 1\big) \tag{A.16c}$$

$$\frac{\partial p}{\partial \rho_g} = a_g^2 - \frac{p}{\rho_g}\big(\gamma_g - 1\big) \tag{A.16d}$$

which is derived in Eq. (3.13) of **Chapter 3** for general EOS. Then, Eq. (A.15) is further transformed into

$$\begin{aligned}
c_1 &= \frac{1}{\rho_l}\frac{\big[\rho_l a_l^2 - p\big(\gamma_l - 1\big)\big]\big[\rho_g a_g^2 - p\big(\gamma_g - 1\big)\big]}{\alpha_g\big[\rho_l a_l^2 - p\big(\gamma_l - 1\big)\big] + \alpha_l\big[\rho_g a_g^2 - p\big(\gamma_g - 1\big)\big]} \\
c_2 &= \frac{1}{\rho_g}\frac{\big[\rho_l a_l^2 - p\big(\gamma_l - 1\big)\big]\big[\rho_g a_g^2 - p\big(\gamma_g - 1\big)\big]}{\alpha_g\big[\rho_l a_l^2 - p\big(\gamma_l - 1\big)\big] + \alpha_l\big[\rho_g a_g^2 - p\big(\gamma_g - 1\big)\big]} \\
c_3 &= \frac{\alpha_l\rho_l\big(\gamma_l - 1\big)\big[\rho_g a_g^2 - p\big(\gamma_g - 1\big)\big]}{\alpha_g\big[\rho_l a_l^2 - p\big(\gamma_l - 1\big)\big] + \alpha_l\big[\rho_g a_g^2 - p\big(\gamma_g - 1\big)\big]} \\
c_4 &= \frac{\alpha_g\rho_g\big(\gamma_g - 1\big)\big[\rho_l a_l^2 - p\big(\gamma_l - 1\big)\big]}{\alpha_g\big[\rho_l a_l^2 - p\big(\gamma_l - 1\big)\big] + \alpha_l\big[\rho_g a_g^2 - p\big(\gamma_g - 1\big)\big]}
\end{aligned} \tag{A.17}$$

Dividing the nominator and denominator in Eq. (A.17) by p and using the definitions of ε_l and ε_g, Eq. (A.17) is further transformed into

$$\begin{aligned}
c_1 &= \frac{\Big[a_l^2 - \frac{p}{\rho_l}\big(\gamma_l - 1\big)\Big]\big(1 + \varepsilon_g\big)}{1 + \alpha_g\varepsilon_l + \alpha_l\varepsilon_g} \\
c_2 &= \frac{\Big[a_g^2 - \frac{p}{\rho_g}\big(\gamma_g - 1\big)\Big]\big(1 + \varepsilon_l\big)}{1 + \alpha_g\varepsilon_l + \alpha_l\varepsilon_g} \\
c_3 &= \frac{\alpha_l\rho_l\big(\gamma_l - 1\big)\big(1 + \varepsilon_g\big)}{1 + \alpha_g\varepsilon_l + \alpha_l\varepsilon_g} \\
c_4 &= \frac{\alpha_g\rho_g\big(\gamma_g - 1\big)\big(1 + \varepsilon_l\big)}{1 + \alpha_g\varepsilon_l + \alpha_l\varepsilon_g}
\end{aligned} \tag{A.18}$$

In short, for arbitrary EOS, we can obtain

$$\begin{aligned}
\Delta p = &\frac{\Big[a_l^2 - \frac{p}{\rho_l}\big(\gamma_l - 1\big)\Big]\big(1 + \varepsilon_g\big)}{1 + \alpha_g\varepsilon_l + \alpha_l\varepsilon_g}\Delta x_1 + \frac{\Big[a_g^2 - \frac{p}{\rho_g}\big(\gamma_g - 1\big)\Big]\big(1 + \varepsilon_l\big)}{1 + \alpha_g\varepsilon_l + \alpha_l\varepsilon_g}\Delta x_4 \\
&+ \frac{\alpha_l\rho_l\big(\gamma_l - 1\big)\big(1 + \varepsilon_g\big)}{1 + \alpha_g\varepsilon_l + \alpha_l\varepsilon_g}\Delta e_l + \frac{\alpha_g\rho_g\big(\gamma_g - 1\big)\big(1 + \varepsilon_l\big)}{1 + \alpha_g\varepsilon_l + \alpha_l\varepsilon_g}\Delta e_g
\end{aligned} \tag{A.19}$$

Eq. (A.19) tells that once we obtain the relations of Δe_l and Δe_g to the change in the conservative variables, i.e. Δx_m, we can get the required partial derivatives $\frac{\partial p}{\partial x_m}$ easily.

We will take $\frac{\partial p}{\partial x_1}$ as an example to show the derivation process. When Δx_1 is the only changing variable while other conservative variables are kept constant, we have

$$\begin{aligned}
\Delta x_1 &= \Delta x_1 \\
\Delta x_2 &= \Delta\big(x_1 u_l\big) = \Delta x_1 u_l + x_1 \Delta u_l = 0 \\
\Delta x_3 &= \Delta\big(x_1 E_l\big) = \Delta x_1 E_l + x_1\big(\Delta e_l + u_l \Delta u_l\big) = 0 \\
\Delta x_4 &= 0 \\
\Delta x_5 &= \Delta\big(x_4 u_g\big) = \Delta x_4 u_g + x_4 \Delta u_g = 0 \\
\Delta x_6 &= \Delta\big(x_4 E_g\big) = \Delta x_4 E_g + x_4\big(\Delta e_g + u_g \Delta u_g\big) = 0
\end{aligned} \tag{A.20}$$

which gives

$$\begin{aligned}
\Delta x_1 &= \Delta x_1 \\
\Delta x_4 &= 0 \\
\Delta e_l &= \big(u_l^2 - E_l\big)\frac{\Delta x_1}{x_1} \\
\Delta e_g &= 0
\end{aligned} \tag{A.21}$$

Replacing Eq. (A.21) back into Eq. (A.19), we get

$$\begin{aligned}
\Delta p &= \frac{\Big[a_l^2 - \frac{p}{\rho_l}\big(\gamma_l - 1\big)\Big]\big(1 + \varepsilon_g\big)}{1 + \alpha_g\varepsilon_l + \alpha_l\varepsilon_g}\Delta x_1 + \frac{\alpha_l\rho_l\big(\gamma_l - 1\big)\big(1 + \varepsilon_g\big)}{1 + \alpha_g\varepsilon_l + \alpha_l\varepsilon_g}\big(u_l^2 - E_l\big)\frac{\Delta x_1}{x_1} \\
&= \frac{\big(1 + \varepsilon_g\big)}{1 + \alpha_g\varepsilon_l + \alpha_l\varepsilon_g}\Big[a_l^2 + \big(\gamma_l - 1\big)\big(u_l^2 - H_l\big)\Big]\Delta x_1
\end{aligned} \tag{A.22}$$

Thus, we get

$$\frac{\partial p}{\partial x_1} = \frac{\big(1 + \varepsilon_g\big)}{1 + \alpha_g\varepsilon_l + \alpha_l\varepsilon_g}\Big[a_l^2 + \big(\gamma_l - 1\big)\big(u_l^2 - H_l\big)\Big] \tag{A.23}$$

Following the same process, we can get

$$\frac{\partial \alpha_g}{\partial x_1} = -\frac{1}{p}\frac{\alpha_g}{1 + \alpha_g\varepsilon_l + \alpha_l\varepsilon_g}\Big[a_l^2 + \big(\gamma_l - 1\big)\big(u_l^2 - H_l\big)\Big] \tag{A.24}$$

When the other conservative variables are taken to be the changing variables, the partial derivatives $\frac{\partial p}{\partial x_m}$, $\frac{\partial \alpha_g}{\partial x_m}$

for $m = 2, 3, 4, 5, 6$ can be obtained similarly. They are found to be

$$\frac{\partial p}{\partial x_1} = \frac{\big(1+\varepsilon_g\big)}{1+\alpha_g\varepsilon_l+\alpha_l\varepsilon_g}\Big[a_l^2+\big(\gamma_l-1\big)\big(u_l^2-H_l\big)\Big] \tag{A.25a}$$

$$\frac{\partial p}{\partial x_2} = -\frac{\big(1+\varepsilon_g\big)}{1+\alpha_g\varepsilon_l+\alpha_l\varepsilon_g}\Big[\big(\gamma_l-1\big)u_l\Big] \tag{A.25b}$$

$$\frac{\partial p}{\partial x_3} = \frac{\big(1+\varepsilon_g\big)}{1+\alpha_g\varepsilon_l+\alpha_l\varepsilon_g}\Big[\big(\gamma_l-1\big)\Big] \tag{A.25c}$$

$$\frac{\partial p}{\partial x_4} = \frac{\big(1+\varepsilon_l\big)}{1+\alpha_g\varepsilon_l+\alpha_l\varepsilon_g}\Big[a_g^2+\big(\gamma_g-1\big)\big(u_g^2-H_g\big)\Big] \tag{A.25d}$$

$$\frac{\partial p}{\partial x_5} = -\frac{\big(1+\varepsilon_l\big)}{1+\alpha_g\varepsilon_l+\alpha_l\varepsilon_g}\Big[\big(\gamma_g-1\big)u_g\Big] \tag{A.25e}$$

$$\frac{\partial p}{\partial x_6} = \frac{\big(1+\varepsilon_l\big)}{1+\alpha_g\varepsilon_l+\alpha_l\varepsilon_g}\Big[\big(\gamma_g-1\big)\Big] \tag{A.25f}$$

and

$$\frac{\partial \alpha_g}{\partial x_1} = -\frac{1}{p}\frac{\alpha_g}{1+\alpha_g\varepsilon_l+\alpha_l\varepsilon_g}\Big[a_l^2+\big(\gamma_l-1\big)\big(u_l^2-H_l\big)\Big] \tag{A.26a}$$

$$\frac{\partial \alpha_g}{\partial x_2} = -\frac{1}{p}\frac{-\alpha_g}{1+\alpha_g\varepsilon_l+\alpha_l\varepsilon_g}\Big[\big(\gamma_l-1\big)u_l\Big] \tag{A.26b}$$

$$\frac{\partial \alpha_g}{\partial x_3} = -\frac{1}{p}\frac{\alpha_g}{1+\alpha_g\varepsilon_l+\alpha_l\varepsilon_g}\Big[\big(\gamma_l-1\big)\Big] \tag{A.26c}$$

$$\frac{\partial \alpha_g}{\partial x_4} = \frac{1}{p}\frac{\alpha_l}{1+\alpha_g\varepsilon_l+\alpha_l\varepsilon_g}\Big[a_l^2+\big(\gamma_l-1\big)\big(u_l^2-H_l\big)\Big] \tag{A.26d}$$

$$\frac{\partial \alpha_g}{\partial x_5} = \frac{1}{p}\frac{-\alpha_l}{1+\alpha_g\varepsilon_l+\alpha_l\varepsilon_g}\Big[\big(\gamma_l-1\big)u_l\Big] \tag{A.26e}$$

$$\frac{\partial \alpha_g}{\partial x_6} = \frac{1}{p}\frac{\alpha_l}{1+\alpha_g\varepsilon_l+\alpha_l\varepsilon_g}\Big[\big(\gamma_l-1\big)\Big] \tag{A.26f}$$

The two matrices, $\mathbb{A}_{ix,nc}$ and $\mathbb{A}_{it,nc}$, are completely specified by Eq. (A.26).

As for the matrix $\mathbb{A}_c$, we will take $\frac{\partial y_2}{\partial x_1}$ as an example to show the derivation process. Following previous process, we have

$$\begin{aligned}\Delta y_2 &= \Delta\big(\alpha_l\rho_l u_l^2+\alpha_l p\big) = \Delta\big(x_1 u_l^2\big)+\alpha_l\Delta p + p\Delta\alpha_l \\ &= u_l^2\Delta x_1 + 2x_1u_l\Delta u_l + \alpha_l\Delta p - p\Delta\alpha_g\end{aligned} \tag{A.27}$$

From Eq. (A.20), we get

$$\Delta u_l = -\frac{\Delta x_1}{x_1}u_l \tag{A.28}$$

Replacing Eq. (A.28) to Eq. (A.27), we get

$$\Delta y_2 = -u_l^2 \Delta x_1 + \alpha_l \Delta p - p \Delta \alpha_g \tag{A.29}$$

Thus we get

$$\begin{aligned} \frac{\partial y_2}{\partial x_1} &= -u_l^2 + \alpha_l \frac{\partial p}{\partial x_1} - p \frac{\partial \alpha_g}{\partial x_1} \\ &= -u_l^2 + \frac{1 + \alpha_l \varepsilon_g}{1 + \alpha_g \varepsilon_l + \alpha_l \varepsilon_g} \Big[a_l^2 + \big(\gamma_l - 1\big)\big(u_l^2 - H_l\big) \Big] \end{aligned} \tag{A.30}$$

Following similar derivations, we can get all partial derivatives in $\mathbb{A}_c$.

In practice, for simplification purpose, we define the following auxiliary variables

$$c_l^h \equiv a_l^2 + \big(\gamma_l - 1\big)\big(u_l^2 - H_l\big); \quad c_g^h \equiv a_g^2 + \big(\gamma_g - 1\big)\big(u_g^2 - H_g\big) \tag{A.31a}$$

$$c_l^u \equiv \big(\gamma_l - 1\big) u_l; \quad c_g^u \equiv \big(\gamma_g - 1\big) u_g \tag{A.31b}$$

$$c_l^1 \equiv \gamma_l - 1; \quad c_g^1 \equiv \gamma_g - 1 \tag{A.31c}$$

$$\beta_l \equiv \frac{1 + \alpha_l \varepsilon_g}{1 + \alpha_g \varepsilon_l + \alpha_l \varepsilon_g}; \quad \beta_g \equiv \frac{1 + \alpha_g \varepsilon_l}{1 + \alpha_g \varepsilon_l + \alpha_l \varepsilon_g} \tag{A.31d}$$

$$\sigma_l \equiv \frac{\alpha_l \varepsilon_l}{1 + \alpha_g \varepsilon_l + \alpha_l \varepsilon_g}; \quad \sigma_g \equiv \frac{\alpha_g \varepsilon_g}{1 + \alpha_g \varepsilon_l + \alpha_l \varepsilon_g} \tag{A.31e}$$

$$\tau_l \equiv \frac{p_i}{p} \frac{1}{1 + \alpha_g \varepsilon_l + \alpha_l \varepsilon_g}; \quad \tau_g \equiv \frac{p_i}{p} \frac{1}{1 + \alpha_g \varepsilon_l + \alpha_l \varepsilon_g} \tag{A.31f}$$

Then the matrices, $\mathbb{A}_c$, $\mathbb{A}_{ix,nc}$, and $\mathbb{A}_{it,nc}$, are found to be

$$\mathbb{A}_c = \begin{pmatrix} 0 & 1 & 0 & 0 & 0 & 0 \\ -u_l^2 + \beta_l c_l^h & 2u_l - \beta_l c_l^u & \beta_l c_l^1 & \sigma_l c_g^h & -\sigma_l c_g^u & \sigma_l c_g^1 \\ -u_l H_l + u_l \beta_l c_l^h & H_l - u_l \beta_l c_l^u & u_l + u_l \beta_l c_l^1 & \sigma_l u_l c_g^h & -\sigma_l u_l c_g^u & \sigma_l u_l c_g^1 \\ 0 & 0 & 0 & 0 & 1 & 0 \\ \sigma_g c_l^h & -\sigma_g c_l^u & \sigma_g c_l^1 & -u_g^2 + \beta_g c_g^h & 2u_g - \beta_g c_g^u & \beta_g c_g^1 \\ \sigma_g u_g c_l^h & -\sigma_g u_g c_l^u & \sigma_g u_g c_l^1 & -u_g H_g + u_g \beta_g c_g^h & H_g - u_g \beta_g c_g^u & u_g + u_g \beta_g c_g^1 \end{pmatrix} \tag{A.32}$$

$$\mathbb{A}_{ix,nc} = \begin{pmatrix} 0 & 0 & 0 & 0 & 0 & 0 \\ -\alpha_g\tau_l c_l^h & \alpha_g\tau_l c_l^u & -\alpha_g\tau_l c_l^1 & \alpha_l\tau_g c_g^h & -\alpha_l\tau_g c_g^u & \alpha_l\tau_g c_g^1 \\ 0 & 0 & 0 & 0 & 0 & 0 \\ 0 & 0 & 0 & 0 & 0 & 0 \\ \alpha_g\tau_l c_l^h & -\alpha_g\tau_l c_l^u & \alpha_g\tau_l c_l^1 & -\alpha_l\tau_g c_g^h & \alpha_l\tau_g c_g^u & -\alpha_l\tau_g c_g^1 \\ 0 & 0 & 0 & 0 & 0 & 0 \end{pmatrix} \tag{A.33}$$

$$\mathbb{A}_{it,nc} = \begin{pmatrix} 0 & 0 & 0 & 0 & 0 & 0 \\ 0 & 0 & 0 & 0 & 0 & 0 \\ \alpha_g\tau_l c_l^h & -\alpha_g\tau_l c_l^u & \alpha_g\tau_l c_l^1 & -\alpha_l\tau_g c_g^h & \alpha_l\tau_g c_g^u & -\alpha_l\tau_g c_g^1 \\ 0 & 0 & 0 & 0 & 0 & 0 \\ 0 & 0 & 0 & 0 & 0 & 0 \\ -\alpha_g\tau_l c_l^h & \alpha_g\tau_l c_l^u & -\alpha_g\tau_l c_l^1 & \alpha_l\tau_g c_g^h & -\alpha_l\tau_g c_g^u & \alpha_l\tau_g c_g^1 \end{pmatrix} \tag{A.34}$$

The remaining task is to obtain the Jacobian matrix of the system, i.e. $\mathbb{A}$. Since the matrices $\mathbb{A}_c$, $\mathbb{A}_{ix,nc}$, and $\mathbb{A}_{it,nc}$ have been obtained, the Jacobian matrix $\mathbb{A}$ is obtained by the symbolic calculation software Mathematica. The Jacobian matrix is found to be

$$\mathbb{A} = \begin{pmatrix} 0 & 1 & 0 & 0 & 0 & 0 \\ -u_l^2 + \beta_l^s c_l^h & 2u_l - \beta_l^s c_l^u & \beta_l^s c_l^1 & \sigma_l^s c_g^h & -\sigma_l^s c_g^u & \sigma_l^s c_g^1 \\ a_{31} & a_{32} & a_{33} & a_{34} & a_{35} & a_{36} \\ 0 & 0 & 0 & 0 & 1 & 0 \\ \sigma_g^s c_l^h & -\sigma_g^s c_l^u & \sigma_g^s c_l^1 & -u_g^2 + \beta_g^s c_g^h & 2u_g - \beta_g^s c_g^u & \beta_g^s c_g^1 \\ a_{61} & a_{62} & a_{63} & a_{64} & a_{65} & a_{66} \end{pmatrix} \tag{A.35}$$

with

$$
\begin{aligned}
a_{31} &= \frac{1}{\Delta_{nc}}\Big[\big(1+\alpha_l c_l^1\tau_g\big)\big(\beta_l u_l c_l^h - u_l H_l\big) + \alpha_g\tau_l\big(\beta_l^s c_l^u c_l^h - c_l^u u_l^2\big) + \alpha_l\tau_l c_l^h\big(c_g^1\sigma_g u_g - \sigma_g^s c_g^u\big)\Big]\\
a_{32} &= \frac{1}{\Delta_{nc}}\Big[\big(1+\alpha_l c_l^1\tau_g\big)\big(H_l - \beta_l c_l^u u_l\big) + \alpha_g\tau_l\big(2c_l^u u_l - \beta_l^s c_l^u c_l^u - c_l^h\big) - \alpha_l\tau_l c_l^u\big(c_g^1\sigma_g u_g - \sigma_g^s c_g^u\big)\Big]\\
a_{33} &= \frac{1}{\Delta_{nc}}\Big[\big(1+\alpha_l c_l^1\tau_g\big)\big(u_l + \beta_l c_l^1 u_l\big) + \alpha_g\tau_l\big(c_l^1 c_l^u\beta_l^s\big) + \alpha_l\tau_l c_l^1\big(c_g^1\sigma_g u_g - \sigma_g^s c_g^u\big)\Big]\\
a_{34} &= \frac{1}{\Delta_{nc}}\Big\{\big(1+\alpha_l c_l^1\tau_g\big)\big(\sigma_l u_l c_g^h\big) + \alpha_g\tau_l\big(\sigma_l^s c_l^u c_g^h\big) + \alpha_l\tau_l\big[c_g^1 u_g\big(\beta_g c_g^h - H_g\big) - c_g^u\big(\beta_g^s c_g^h - u_g^2\big)\big]\Big\}\\
a_{35} &= -\frac{1}{\Delta_{nc}}\Big\{\big(1+\alpha_l c_l^1\tau_g\big)\big(\sigma_l u_l c_g^u\big) + \alpha_g\tau_l\big(\sigma_l^s c_l^u c_g^u\big) + \alpha_l\tau_l\big[c_g^u\big(2u_g - \beta_g^s u_g\big) - c_g^1\big(H_g - \beta_g c_g^u u_g\big) - c_g^h\big]\Big\}\\
a_{36} &= \frac{1}{\Delta_{nc}}\Big\{\big(1+\alpha_l c_l^1\tau_g\big)\big(\sigma_l u_l c_g^1\big) + \alpha_g\tau_l\big(\sigma_l^s c_l^u c_g^1\big) + \alpha_l\tau_l\big[c_g^1\big(u_g + \beta_g c_g^1 u_g\big) - c_g^1\beta_g^s c_g^u\big]\Big\}
\end{aligned}
\tag{A.36}
$$

and

$$
\begin{aligned}
a_{61} &= \frac{1}{\Delta_{nc}}\Big\{\big(1+\alpha_g c_g^1\tau_l\big)\big(\sigma_g u_g c_l^h\big) + \alpha_l\tau_g\big(\sigma_g^s c_g^u c_l^h\big) + \alpha_g\tau_g\big[c_l^1 u_l\big(\beta_l c_l^h - H_l\big) - c_l^u\big(\beta_l^s c_l^h - u_l^2\big)\big]\Big\}\\
a_{62} &= -\frac{1}{\Delta_{nc}}\Big\{\big(1+\alpha_g c_g^1\tau_l\big)\big(\sigma_g u_g c_l^u\big) + \alpha_l\tau_g\big(\sigma_g^s c_g^u c_l^u\big) + \alpha_g\tau_g\big[c_l^u\big(2u_l - \beta_l^s u_l\big) - c_l^1\big(H_l - \beta_l c_l^u u_l\big) - c_l^h\big]\Big\}\\
a_{63} &= \frac{1}{\Delta_{nc}}\Big\{\big(1+\alpha_g c_g^1\tau_l\big)\big(\sigma_g u_g c_l^1\big) + \alpha_l\tau_g\big(\sigma_g^s c_g^u c_l^1\big) + \alpha_g\tau_g\big[c_l^1\big(u_l + \beta_l c_l^1 u_l\big) - c_l^1\beta_l^s c_l^u\big]\Big\}\\
a_{64} &= \frac{1}{\Delta_{nc}}\Big[\big(1+\alpha_g c_g^1\tau_l\big)\big(\beta_g u_g c_g^h - u_g H_g\big) + \alpha_l\tau_g\big(\beta_g^s c_g^u c_g^h - c_g^u u_g^2\big) + \alpha_g\tau_g c_g^h\big(c_l^1\sigma_l u_l - \sigma_l^s c_l^u\big)\Big]\\
a_{65} &= \frac{1}{\Delta_{nc}}\Big[\big(1+\alpha_g c_g^1\tau_l\big)\big(H_g - \beta_g c_g^u u_g\big) + \alpha_l\tau_g\big(2c_g^u u_g - \beta_g^s c_g^u c_g^u - c_g^h\big) - \alpha_g\tau_g c_g^u\big(c_l^1\sigma_l u_l - \sigma_l^s c_l^u\big)\Big]\\
a_{66} &= \frac{1}{\Delta_{nc}}\Big[\big(1+\alpha_g c_g^1\tau_l\big)\big(u_g + \beta_g c_g^1 u_g\big) + \alpha_l\tau_g\big(c_g^1 c_g^u\beta_g^s\big) + \alpha_g\tau_g c_g^1\big(c_l^1\sigma_l u_l - \sigma_l^s c_l^u\big)\Big]
\end{aligned}
\tag{A.37}
$$

where the following auxiliary variables are used

$$
\begin{aligned}
\Delta_{nc} &= 1 + \alpha_g\big(\gamma_l - 1\big)\tau_l + \alpha_g\big(\gamma_g - 1\big)\tau_g\\
\beta_l^s &= \beta_l - \alpha_g\tau_l;\ \beta_g^s = \beta_g - \alpha_l\tau_g\\
\sigma_l^s &= \sigma_l + \alpha_l\tau_g;\ \sigma_g^s = \sigma_g + \alpha_g\tau_l
\end{aligned}
\tag{A.38}
$$

Appendix B

ROE-PIKE INTERMEDIATE STATE FOR SINGLE-PHASE SYSTEM

The fundamental requirement to the Roe-Pike intermediate state is

$$\mathbf{U}_R - \mathbf{U}_L = \sum_{m=1}^{3} \tilde{c}_m \tilde{\mathbf{K}}_m \tag{B.1a}$$

$$\mathbf{F}_R - \mathbf{F}_L = \sum_{m=1}^{3} \tilde{c}_m \tilde{\lambda}_m \tilde{\mathbf{K}}_m \tag{B.1b}$$

where λ_m and $\mathbf{K}_m$ are the eigenvalues and eigenvectors of the Jacobian matrix of Euler system. Before seeking the intermediate state for two general states $\mathbf{U}_L$, $\mathbf{U}_R$, we at first study two close states.

Decomposition of two close states $\mathbf{U}_L$, $\mathbf{U}_R$

Consider two states $\mathbf{U}_L$, $\mathbf{U}_R$ (left and right) that are close and seek c_1, c_2, c_3, such that

$$\Delta\mathbf{U} = \sum_{m=1}^{3} c_m \mathbf{K}_m \tag{B.2}$$

to within $O(\Delta^2)$, where $\Delta(\cdot) = (\cdot)_R - (\cdot)_L$. Writing Eq. (B.2) in full we have

$$\Delta\rho = c_1 + c_2 + c_3 \tag{B.3a}$$

$$\Delta(\rho u) = c_1(u - a) + c_2 u + c_3(u + a) \tag{B.3b}$$

$$\Delta(\rho E) = c_1(H - ua) + c_2(H - \gamma^* a^2) + c_3(H + ua) \tag{B.3c}$$

Solving for c_1, c_2, c_3 from Eq. (B.3), we get

$$c_1 = \frac{1}{2\gamma^* a^2}\left\{\left[u(u + \gamma^* a) - (H - \gamma^* a^2)\right]\Delta\rho - (u + \gamma^* a)\Delta(\rho u) + \Delta(\rho E)\right\} \tag{B.4a}$$

$$c_2 = \frac{1}{\gamma^* a^2}\left[(H - u^2)\Delta\rho - u\Delta(\rho u) - \Delta(\rho E)\right] \tag{B.4b}$$

$$c_3 = \frac{1}{2\gamma^* a^2}\left\{\left[u(u - \gamma^* a) - (H - \gamma^* a^2)\right]\Delta\rho - (u - \gamma^* a)\Delta(\rho u) + \Delta(\rho E)\right\} \tag{B.4c}$$

Within $O(\Delta^2)$, for two close states $\mathbf{U}_L$, $\mathbf{U}_R$, we have

$$\Delta(\rho u) = u\Delta\rho + \rho\Delta u \tag{B.5a}$$

$$\Delta(\rho E) = E\Delta\rho + \rho\Delta e + \rho u\Delta u \tag{B.5b}$$

Recall from **Chapter 3** that the definitions of a and γ give

$$\left(\frac{\partial p}{\partial e}\right)_\rho = \rho(\gamma - 1) \tag{B.6a}$$

$$\left(\frac{\partial p}{\partial \rho}\right)_e = a^2 - \frac{p}{\rho}(\gamma - 1) \tag{B.6b}$$

which gives

$$\Delta p = \left[a^2 - \frac{p}{\rho}(\gamma - 1)\right]\Delta\rho + \rho(\gamma - 1)\Delta e \tag{B.7}$$

Replacing Eq. (B.5) and Eq. (B.6) back to Eq. (B.3), we get to

$$c_1 = \frac{1}{2a^2}(\Delta p - \rho a\Delta u) \tag{B.8a}$$

$$c_2 = \Delta\rho - \Delta p/a^2 \tag{B.8b}$$

$$c_3 = \frac{1}{2a^2}(\Delta p + \rho a\Delta u) \tag{B.8c}$$

Note that Eq. (B.8) are consistent with Glaister's result [45] though we took different ways in representing the Jacobian matrix and eigenvectors. And to within $O(\Delta^2)$, we can check that

$$\Delta\mathbf{F} = \sum_{m=1}^{3} c_m\lambda_m\mathbf{K}_m \tag{B.9}$$

Thus, for two close states, we have found c_1, c_2, c_3 as in Eq. (B.8) for a general EOS such that

$$\Delta\mathbf{U} = \sum_{m=1}^{3} c_m\mathbf{K}_m \tag{B.10a}$$

$$\Delta\mathbf{F} = \sum_{m=1}^{3} c_m\lambda_m\mathbf{K}_m \tag{B.10b}$$

to within $O(\Delta^2)$.

Decomposition of two general states $\mathbf{U}_L$, $\mathbf{U}_R$

For two general states, $\mathbf{U}_L$ and $\mathbf{U}_R$, that are not necessarily close, we would like to seek the intermediate values of $\tilde{\rho}, \tilde{u}, \tilde{H}, \tilde{a}, \tilde{\gamma}$ such that Eq. (B.1) holds. Let

$$\mathbf{U}_R - \mathbf{U}_L = \begin{pmatrix} \Delta\rho \\ \Delta(\rho u) \\ \Delta(\rho E) \end{pmatrix} = \begin{pmatrix} \rho_R - \rho_L \\ \rho_R u_R - \rho_L u_L \\ \rho_R E_R - \rho_L E_L \end{pmatrix} \tag{B.11a}$$

$$\mathbf{F}_R - \mathbf{F}_L = \begin{pmatrix} \Delta(\rho u) \\ \Delta(\rho u^2 + p) \\ \Delta(\rho u H) \end{pmatrix} = \begin{pmatrix} \rho_R u_R - \rho_L u_L \\ \rho_R u_R^2 - \rho_L u_L^2 + p_R - p_L \\ \rho_R H_R u_R - \rho_L H_L u_L \end{pmatrix} \tag{B.11b}$$

Expanding the requirement in Eq. (B.1) in full, we get

$$\Delta\rho = \tilde{c}_1 + \tilde{c}_2 + \tilde{c}_3 \tag{B.12a}$$

$$\Delta(\rho u) = \tilde{c}_1(\tilde{u} - \tilde{a}) + \tilde{c}_2\tilde{u} + \tilde{c}_3(\tilde{u} + \tilde{a}) \tag{B.12b}$$

$$\Delta(\rho E) = \tilde{c}_1(\tilde{H} - \tilde{u}\tilde{a}) + \tilde{c}_2(\tilde{H} - \tilde{\gamma}^*\tilde{a}^2) + \tilde{c}_3(\tilde{H} + \tilde{u}\tilde{a}) \tag{B.12c}$$

$$\Delta(\rho u) = \tilde{c}_1(\tilde{u} - \tilde{a}) + \tilde{c}_2\tilde{u} + \tilde{c}_3(\tilde{u} + \tilde{a}) \tag{B.12d}$$

$$\Delta(\rho u^2 + p) = \tilde{c}_1(\tilde{u} - \tilde{a})^2 + \tilde{c}_2\tilde{u}^2 + \tilde{c}_3(\tilde{u} + \tilde{a})^2 \tag{B.12e}$$

$$\Delta(\rho u H) = \tilde{c}_1(\tilde{H} - \tilde{u}\tilde{a})(\tilde{u} - \tilde{a}) + \tilde{c}_2(\tilde{H} - \tilde{\gamma}^*\tilde{a}^2)\tilde{u} + \tilde{c}_3(\tilde{H} + \tilde{u}\tilde{a})(\tilde{u} + \tilde{a}) \tag{B.12f}$$

with

$$\tilde{c}_1 = \frac{1}{2\tilde{a}^2}(\Delta p - \tilde{\rho}\tilde{a}\Delta u) \tag{B.13a}$$

$$\tilde{c}_2 = \Delta\rho - \Delta p/\tilde{a}^2 \tag{B.13b}$$

$$\tilde{c}_3 = \frac{1}{2\tilde{a}^2}(\Delta p + \tilde{\rho}\tilde{a}\Delta u) \tag{B.13c}$$

To be clear, note that $\Delta\rho = \rho_R - \rho_L$, $\Delta p = p_R - p_L$, and $\Delta u = u_R - u_L$ might not be small. With Eq. (B.12a), Eq. (B.12b), and Eq. (B.12c), we have

$$\Delta\rho = \tilde{c}_1 + \tilde{c}_2 + \tilde{c}_3 \tag{B.14a}$$

$$\Delta p = \tilde{a}^2\big(\tilde{c}_1 + \tilde{c}_3\big) \tag{B.14b}$$

$$\Delta u = \frac{\tilde{a}}{\tilde{\rho}}\big(\tilde{c}_3 - \tilde{c}_1\big) \tag{B.14c}$$

Eq. (B.12a) is satisfied because of Eq. (B.14a); while Eq. (B.12b) is the same as Eq. (B.12d). Thus the intermediate state must make sure Eq. (B.12c) to Eq. (B.12f) are satisfied. From Eq. (B.12d) and Eq. (B.14), we obtain

$$\begin{aligned} \Delta\big(\rho u\big) &= \tilde{u}\big(\tilde{c}_1 + \tilde{c}_2 + \tilde{c}_3\big) + \tilde{a}\big(\tilde{c}_3 - \tilde{c}_1\big) \\ \Rightarrow \Delta\big(\rho u\big) &= \tilde{u}\Delta\rho + \tilde{\rho}\Delta u \end{aligned} \tag{B.15}$$

From Eq. (B.12e) and Eq. (B.14), we obtain

$$\begin{aligned} \Delta\big(\rho u^2\big) + \Delta p &= \tilde{u}^2\big(\tilde{c}_1 + \tilde{c}_2 + \tilde{c}_3\big) + 2\tilde{u}\tilde{a}\big(\tilde{c}_3 - \tilde{c}_1\big) + \tilde{a}^2\big(\tilde{c}_3 + \tilde{c}_1\big) \\ &= \tilde{u}^2\Delta\rho + 2\tilde{\rho}\tilde{u}\Delta u + \Delta p \\ \Rightarrow \Delta\big(\rho u^2\big) &= \tilde{u}^2\Delta\rho + 2\tilde{\rho}\tilde{u}\Delta u \end{aligned} \tag{B.16}$$

Substituting $\tilde{\rho}$ from Eq. (B.16) into Eq. (B.15), we get a quadratic equation for $\tilde{u}$

$$\tilde{u}^2\Delta\rho - 2\tilde{u}\Delta\big(\rho u\big) + \Delta\big(\rho u^2\big) = 0 \tag{B.17}$$

Only one solution of $\tilde{u}$ from Eq. (B.17) is productive, that is

$$\tilde{u} = \frac{\Delta\big(\rho u\big) - \sqrt{\big[\Delta\big(\rho u\big)\big]^2 - \Delta\rho\Delta\big(\rho u^2\big)}}{\Delta\rho} \tag{B.18}$$

which gives

$$\tilde{u} = \frac{\sqrt{\rho_L}u_L + \sqrt{\rho_R}u_R}{\sqrt{\rho_L} + \sqrt{\rho_R}} \tag{B.19}$$

Substituting $\tilde{u}$ back into Eq. (B.15), we get

$$\tilde{\rho} = \sqrt{\rho_L\rho_R} \tag{B.20}$$

With Eq. (B.19) and Eq. (B.20), we can obtain the following mathematical identity

$$\Delta\big(\rho u\phi\big) = \tilde{u}\Delta\big(\rho\phi\big) + \tilde{\rho}\Delta u\frac{\sqrt{\rho_L}\phi_L + \sqrt{\rho_R}\phi_R}{\sqrt{\rho_L} + \sqrt{\rho_R}} \tag{B.21}$$

where ϕ could be any quantity. Now we need to determine the remaining variables $\tilde{H}$, $\tilde{a}$, and $\tilde{\gamma}$. Using Eq. (B.14), we rewrite Eq. (B.12c) and Eq. (B.12f) as

$$\Delta\big(\rho E\big) = \big(\tilde{H} - \tilde{\gamma}^*\tilde{a}^2\big)\Delta\rho + \tilde{u}\tilde{\rho}\Delta u + \tilde{\gamma}^*\Delta p \tag{B.22a}$$

$$\Delta\big(\rho u H\big) = \tilde{u}\big(\tilde{H} - \tilde{\gamma}^*\tilde{a}^2\big)\Delta\rho + \big(\tilde{H} + \tilde{u}^2\big)\tilde{\rho}\Delta u + \tilde{u}\big(1 + \tilde{\gamma}^*\big)\Delta p \tag{B.22b}$$

Substituting $\phi = H$ into Eq. (B.21), we obtain

$$\begin{aligned}\Delta\big(\rho u H\big) &= \tilde{u}\Delta\big(\rho H\big) + \tilde{\rho}\Delta u\frac{\sqrt{\rho_L}H_L + \sqrt{\rho_R}H_R}{\sqrt{\rho_L} + \sqrt{\rho_R}} \\ &= \tilde{u}\Delta\big(\rho E\big) + \tilde{u}\Delta p + \tilde{\rho}\Delta u\frac{\sqrt{\rho_L}H_L + \sqrt{\rho_R}H_R}{\sqrt{\rho_L} + \sqrt{\rho_R}}\end{aligned} \tag{B.23}$$

Substituting Eq. (B.22a) into Eq. (B.23) and then comparing Eq. (B.23) with Eq. (B.22b), we get

$$\tilde{H}\tilde{\rho}\Delta u = \tilde{\rho}\Delta u\frac{\sqrt{\rho_L}H_L + \sqrt{\rho_R}H_R}{\sqrt{\rho_L} + \sqrt{\rho_R}} \tag{B.24}$$

which gives

$$\tilde{H} = \frac{\sqrt{\rho_L}H_L + \sqrt{\rho_R}H_R}{\sqrt{\rho_L} + \sqrt{\rho_R}} \tag{B.25}$$

which means if $\tilde{H}$ is given by Eq. (B.25), Eq. (B.22b) and Eq. (B.12f) are satisfied.

We have one more equation, Eq. (B.22a), to satisfy. Replacing $\Delta\big(\rho u^2\big) = \tilde{u}^2\Delta\rho + 2\tilde{\rho}\tilde{u}\Delta u$ into Eq. (B.22a), we get

$$\Delta\big(\rho e\big) = \big(\tilde{H} - \frac{1}{2}\tilde{u}^2 - \tilde{\gamma}^*\tilde{a}^2\big)\Delta\rho + \tilde{\gamma}^*\Delta p \tag{B.26}$$

Noting that $h = e + p/\rho$, Eq. (B.26) is equivalent to

$$\Delta\big(\rho h\big) = \Delta\big(\rho e\big) + \Delta p = \big(\tilde{H} - \frac{1}{2}\tilde{u}^2 - \tilde{\gamma}^*\tilde{a}^2\big)\Delta\rho + \tilde{\gamma}^*\Delta p + \Delta p \tag{B.27}$$

By taking the choice that

$$\tilde{h} = \frac{\sqrt{\rho_L}h_L + \sqrt{\rho_R}h_R}{\sqrt{\rho_L} + \sqrt{\rho_R}} \tag{B.28}$$

We get

$$\Delta\big(\rho h\big) = \tilde{\rho}\Delta h + \tilde{h}\Delta\rho \tag{B.29}$$

and Eq. (B.27) is simplified to

$$\Delta p = \frac{\tilde{\gamma}-1}{\tilde{\gamma}}\tilde{\rho}\Delta h + \frac{\tilde{a}^2}{\tilde{\gamma}}\Delta\rho \tag{B.30}$$

which is consistent with the definitions of a and γ as the two states are close, as is seen in Eq. (3.13a) and Eq. (3.13b) of **Chapter 3**. We transform Eq. (B.30) into

$$\Delta\rho = \frac{\tilde{\gamma}}{\tilde{a}^2}\Delta p - \frac{\tilde{\gamma}-1}{\tilde{a}^2}\tilde{\rho}\Delta h \tag{B.31}$$

which gives that relation of the change in density to the change in pressure and specific enthalpy (or temperature) that the intermediate state has to satisfy. From **Chapter 3**, especially Figure 3.4, we know that γ is almost a linear function of pressure and temperature (or enthalpy), thus to be consistent with other intermediate variables, we take

$$\tilde{\gamma} = \frac{\sqrt{\rho_L}\gamma_L + \sqrt{\rho_R}\gamma_R}{\sqrt{\rho_L}+\sqrt{\rho_R}} \tag{B.32}$$

And then $\tilde{a}$ is determined by

$$\tilde{a} = \left[\frac{\Delta\rho}{\tilde{\gamma}\Delta p - \big(\tilde{\gamma}-1\big)\tilde{\rho}\Delta h}\right]^{-1/2} \tag{B.33}$$

In case $\Delta p = 0$ and $\Delta h = 0$, we have

$$\tilde{a} = a_L = a_R, \quad \text{and} \quad \tilde{\gamma} = \gamma_L = \gamma_R \tag{B.34}$$

To conclude, by taking the following intermediate state

$$\tilde{\rho} = \sqrt{\rho_L\rho_R} \tag{B.35a}$$

$$\tilde{u} = \omega_L u_L + \omega_R u_R \tag{B.35b}$$

$$\tilde{H} = \omega_L H_L + \omega_R H_R \tag{B.35c}$$

$$\tilde{h} = \omega_L h_L + \omega_R h_R \tag{B.35d}$$

$$\tilde{\gamma} = \omega_L\gamma_L + \omega_R\gamma_R \tag{B.35e}$$

$$\tilde{a} = \omega_L a_L + \omega_R a_R, \qquad \text{if} \quad \Delta p = 0 \text{ and } \Delta h = 0 \tag{B.35f}$$

$$= \left[\frac{\Delta\rho}{\tilde{\gamma}\Delta p - \big(\tilde{\gamma}-1\big)\tilde{\rho}\Delta h}\right]^{-1/2}, \quad \text{otherwise}$$

with ω_L and ω_R being the weights defined as

$$\omega_L = \frac{\sqrt{\rho_L}}{\sqrt{\rho_L} + \sqrt{\rho_R}}, \quad \omega_R = \frac{\sqrt{\rho_R}}{\sqrt{\rho_L} + \sqrt{\rho_R}} \tag{B.36}$$

we can show that the fundamental requirement in Eq. (B.1) is satisfied with coefficients

$$\tilde{c}_1 = \frac{1}{2\tilde{a}^2}\left(\Delta p - \tilde{\rho}\tilde{a}\Delta u\right) \tag{B.37a}$$

$$\tilde{c}_2 = \Delta\rho - \Delta p/\tilde{a}^2 \tag{B.37b}$$

$$\tilde{c}_3 = \frac{1}{2\tilde{a}^2}\left(\Delta p + \tilde{\rho}\tilde{a}\Delta u\right) \tag{B.37c}$$

where $\Delta\rho = \rho_R - \rho_L$, $\Delta u = u_R - u_L$, and $\Delta p = p_R - p_L$.

Appendix C

ROE-PIKE INTERMEDIATE STATE FOR TWO-PHASE SYSTEM

Recall that the Roe-type numerical flux for the two-phase system is

$$\hat{\mathbf{F}}^{\text{Roe}}_{i+\frac{1}{2}} = \frac{1}{2}\big(\mathbf{F}^n_i + \mathbf{F}^n_{i+1}\big) - \frac{1}{2}|\tilde{\mathbb{A}}_c|\big(\mathbf{U}^n_{i+1} - \mathbf{U}^n_i\big) \tag{C.1}$$

Or equivalently,

$$\hat{\mathbf{F}}^{\text{Roe}}_{i+\frac{1}{2}} = \frac{1}{2}\big(\mathbf{F}^n_i + \mathbf{F}^n_{i+1}\big) - \frac{1}{2}\sum_{m=1}^{6} \tilde{c}_m|\tilde{\lambda}_{c,m}|\tilde{\mathbf{K}}_{c,m} \tag{C.2}$$

where $\lambda_{c,m}$ and $\mathbf{K}_{c,m}$ is the m-th eigenvalue and eigenvector of the matrix $\mathbb{A}_c$. As discussed in previous chapter, we are not able to obtain analytically the exact eigenvalues and eigenvectors of $\mathbb{A}_c$. In practice, we use the approximations made in Eq. (4.42) and Eq. (4.43), i.e.

$$\lambda_{c,1} \approx u_l - \sqrt{\beta_l}a_l; \lambda_{c,2} = u_l; \lambda_{c,3} \approx u_l + \sqrt{\beta_l}a_l \tag{C.3a}$$

$$\lambda_{c,4} \approx u_g - \sqrt{\beta_g}a_g; \lambda_{c,5} = u_g; \lambda_{c,6} \approx u_g + \sqrt{\beta_g}a_g \tag{C.3b}$$

and the right eigenvectors are approximated with

$$\begin{gathered}
\mathbf{K}_{1,c} \approx \begin{pmatrix} 1 \\ u_l - \sqrt{\beta_l} a_l \\ H_l - \sqrt{\beta_l} a_l u_l \\ 0 \\ 0 \\ 0 \end{pmatrix}, \mathbf{K}_{2,c} \approx \begin{pmatrix} 1 \\ u_l \\ H_l - \gamma_l^* a_l^2 \\ 0 \\ 0 \\ 0 \end{pmatrix}, \mathbf{K}_{3,c} \approx \begin{pmatrix} 1 \\ u_l + \sqrt{\beta_l} a_l \\ H_l + \sqrt{\beta_l} a_l u_l \\ 0 \\ 0 \\ 0 \end{pmatrix} \\
\mathbf{K}_{4,c} \approx \begin{pmatrix} q_4 \\ q_4 \lambda_{c,4} \\ q_4 \big[H_l - u_l^2 + u_l \lambda_{c,4} \big] \\ 1 \\ u_g - \sqrt{\beta_g} a_g \\ H_g - \sqrt{\beta_g} a_g u_g \end{pmatrix}, \mathbf{K}_{5,c} \approx \begin{pmatrix} 0 \\ 0 \\ 0 \\ 1 \\ u_g \\ H_g - \gamma_g^* a_g^2 \end{pmatrix}, \mathbf{K}_{6,c} \approx \begin{pmatrix} q_6 \\ q_6 \lambda_{c,6} \\ q_6 \big[H_l - u_l^2 + u_l \lambda_{c,6} \big] \\ 1 \\ u_g + \sqrt{\beta_g} a_g \\ H_g + \sqrt{\beta_g} a_g u_g \end{pmatrix}
\end{gathered} \tag{C.4}$$

where $\gamma_l^* = 1/\big(\gamma_l - 1\big)$ and $\gamma_g^* = 1/\big(\gamma_g - 1\big)$. And q_4 and q_6 are two auxiliary variables defined as

$$q_4 \equiv \frac{\sigma_l a_g^2}{\big(\lambda_{c,4} - \lambda_{c,1}\big)\big(\lambda_{c,4} - \lambda_{c,3}\big)}; \quad q_6 \equiv \frac{\sigma_l a_g^2}{\big(\lambda_{c,6} - \lambda_{c,1}\big)\big(\lambda_{c,6} - \lambda_{c,3}\big)} \tag{C.5}$$

As is required in single-phase system, the fundamental requirement to the Roe-Pike intermediate state is

$$\mathbf{U}_R - \mathbf{U}_L = \sum_{m=1}^{6} \tilde{c}_m \tilde{\mathbf{K}}_{c,m} \tag{C.6a}$$

$$\mathbf{F}_R - \mathbf{F}_L = \sum_{m=1}^{6} \tilde{c}_m \tilde{\lambda}_{c,m} \tilde{\mathbf{K}}_{c,m} \tag{C.6b}$$

Expanding the requirement in Eq. (C.6) in full, we get

$$\Delta(\alpha_l\rho_l) = \tilde{c}_1 + \tilde{c}_2 + \tilde{c}_3 + \tilde{c}_4\tilde{q}_4 + \tilde{c}_6\tilde{q}_6 \tag{C.7a}$$

$$\Delta(\alpha_l\rho_l u_l) = \tilde{c}_1(\tilde{u}_l - \sqrt{\tilde{\beta}_l}\tilde{a}_l) + \tilde{c}_2\tilde{u}_l + \tilde{c}_3(\tilde{u}_l + \sqrt{\tilde{\beta}_l}\tilde{a}_l) + \tilde{c}_4\tilde{q}_4(\tilde{u}_g - \sqrt{\tilde{\beta}_g}\tilde{a}_g) + \tilde{c}_6\tilde{q}_6(\tilde{u}_g + \sqrt{\tilde{\beta}_g}\tilde{a}_g) \tag{C.7b}$$

$$\begin{aligned}\Delta(\alpha_l\rho_l E_l) = {} & \tilde{c}_1(\tilde{H}_l - \sqrt{\tilde{\beta}_l}\tilde{u}_l\tilde{a}_l) + \tilde{c}_2(\tilde{H}_l - \tilde{\gamma}_l^*\tilde{a}_l^2) + \tilde{c}_3(\tilde{H}_l + \sqrt{\tilde{\beta}_l}\tilde{u}_l\tilde{a}_l) \\ & + \tilde{c}_4\tilde{q}_4[\tilde{H}_l - \tilde{u}_l^2 + \tilde{u}_l(\tilde{u}_g - \sqrt{\tilde{\beta}_g}\tilde{a}_g)] + \tilde{c}_6\tilde{q}_6[\tilde{H}_l - \tilde{u}_l^2 + \tilde{u}_l(\tilde{u}_g + \sqrt{\tilde{\beta}_g}\tilde{a}_g)]\end{aligned} \tag{C.7c}$$

$$\Delta(\alpha_g\rho_g) = \tilde{c}_4 + \tilde{c}_5 + \tilde{c}_6 \tag{C.7d}$$

$$\Delta(\alpha_g\rho_g u_g) = \tilde{c}_4(\tilde{u}_g - \sqrt{\tilde{\beta}_g}\tilde{a}_g) + \tilde{c}_5\tilde{u}_g + \tilde{c}_6(\tilde{u}_g + \sqrt{\tilde{\beta}_g}\tilde{a}_g) \tag{C.7e}$$

$$\Delta(\alpha_g\rho_g E_g) = \tilde{c}_4(\tilde{H}_g - \sqrt{\tilde{\beta}_g}\tilde{u}_g\tilde{a}_g) + \tilde{c}_5(\tilde{H}_g - \tilde{\gamma}_g^*\tilde{a}_g^2) + \tilde{c}_6(\tilde{H}_g + \sqrt{\tilde{\beta}_g}\tilde{u}_g\tilde{a}_g) \tag{C.7f}$$

and

$$\Delta(\alpha_l\rho_l u_l) = \tilde{c}_1(\tilde{u}_l - \sqrt{\tilde{\beta}_l}\tilde{a}_l) + \tilde{c}_2\tilde{u}_l + \tilde{c}_3(\tilde{u}_l + \sqrt{\tilde{\beta}_l}\tilde{a}_l) + \tilde{c}_4\tilde{q}_4(\tilde{u}_g - \sqrt{\tilde{\beta}_g}\tilde{a}_g) + \tilde{c}_6\tilde{q}_6(\tilde{u}_g + \sqrt{\tilde{\beta}_g}\tilde{a}_g) \tag{C.8a}$$

$$\Delta(\alpha_l\rho_l u_l^2 + \alpha_l p) = \tilde{c}_1(\tilde{u}_l - \sqrt{\tilde{\beta}_l}\tilde{a}_l)^2 + \tilde{c}_2\tilde{u}_l^2 + \tilde{c}_3(\tilde{u}_l + \sqrt{\tilde{\beta}_l}\tilde{a}_l)^2 \tag{C.8b}$$

$$\begin{aligned}\Delta(\alpha_l\rho_l u_l H_l) = {} & \tilde{c}_1(\tilde{H}_l - \sqrt{\tilde{\beta}_l}\tilde{u}_l\tilde{a}_l)(\tilde{u}_l - \sqrt{\tilde{\beta}_l}\tilde{a}_l) + \tilde{c}_2(\tilde{H}_l - \tilde{\gamma}_l^*\tilde{a}_l^2)\tilde{u}_l \\ & + \tilde{c}_3(\tilde{H}_l + \sqrt{\tilde{\beta}_l}\tilde{u}_l\tilde{a}_l)(\tilde{u}_l + \sqrt{\tilde{\beta}_l}\tilde{a}_l) \\ & + \tilde{c}_4\tilde{q}_4[\tilde{H}_l - \tilde{a}_l^2 + \tilde{u}_l(\tilde{u}_g - \sqrt{\tilde{\beta}_g}\tilde{a}_g)](\tilde{u}_l - \sqrt{\tilde{\beta}_l}\tilde{a}_l) \\ & + \tilde{c}_6\tilde{q}_6[\tilde{H}_l - \tilde{a}_l^2 + \tilde{u}_l(\tilde{u}_g + \sqrt{\tilde{\beta}_g}\tilde{a}_g)](\tilde{u}_l + \sqrt{\tilde{\beta}_l}\tilde{a}_l)\end{aligned} \tag{C.8c}$$

$$\Delta(\alpha_g\rho_g u_g) = \tilde{c}_4(\tilde{u}_g - \sqrt{\tilde{\beta}_g}\tilde{a}_g) + \tilde{c}_5\tilde{u}_g + \tilde{c}_6(\tilde{u}_g + \sqrt{\tilde{\beta}_g}\tilde{a}_g) \tag{C.8d}$$

$$\Delta(\alpha_g\rho_g u_g^2 + \alpha_g p) = \tilde{c}_4(\tilde{u}_g - \sqrt{\tilde{\beta}_g}\tilde{a}_g)^2 + \tilde{c}_5\tilde{u}_g^2 + \tilde{c}_6(\tilde{u}_g + \sqrt{\tilde{\beta}_g}\tilde{a}_g)^2 \tag{C.8e}$$

$$\begin{aligned}\Delta(\alpha_g\rho_g u_g H_g) = {} & \tilde{c}_4(\tilde{H}_g - \sqrt{\tilde{\beta}_g}\tilde{u}_g\tilde{a}_g)(\tilde{u}_g - \sqrt{\tilde{\beta}_g}\tilde{a}_g) + \tilde{c}_5(\tilde{H}_g - \tilde{\gamma}_g^*\tilde{a}_g^2)\tilde{u}_g \\ & + \tilde{c}_6(\tilde{H}_g + \sqrt{\tilde{\beta}_g}\tilde{u}_g\tilde{a}_g)(\tilde{u}_g + \sqrt{\tilde{\beta}_g}\tilde{a}_g)\end{aligned} \tag{C.8f}$$

Finding exactly the intermediate state from Eq. (C.7) and Eq. (C.8) is difficult. And, because the eigenvalues and eigenvectors are only approximated values, finding exactly the intermediate state does not gains much. We propose to use approximate intermediate state.

Taking a close look at Eq. (C.7), Eq. (C.8), and Eq. (B.12), we observe that, except for the additional void fraction α_k and coupling factors β_k, there are great similarities among them. For example, Eq. (B.12a) has the same form as Eq. (C.7d), Eq. (B.12b) has the same form as Eq. (C.7e), and Eq. (B.12c) has

the same form as Eq. (C.7f). Because of the similarities, we would expect that the intermediate state for two-phase system should have a similar form as the intermediate state for the single-phase system. Thus, we propose to use the following intermediate variables

$$\tilde{\phi}_k = \omega_{k,L}\phi_{k,L} + \omega_{k,R}\phi_{k,R}, \text{ for } k = l, g \text{ and } \phi = u, H, a, \gamma, \beta, \sigma \tag{C.9}$$

with

$$\omega_{k,L} = \frac{\sqrt{\alpha_{k,L}\rho_{k,L}}}{\sqrt{\alpha_{k,L}\rho_{k,L}} + \sqrt{\alpha_{k,R}\rho_{k,R}}}, \omega_{k,R} = \frac{\sqrt{\alpha_{k,R}\rho_{k,R}}}{\sqrt{\alpha_{k,L}\rho_{k,L}} + \sqrt{\alpha_{k,R}\rho_{k,R}}}, \text{ for } k = l, g \tag{C.10}$$

Once the intermediate variables are specified by Eq. (C.9), we can solve for the coefficients $\tilde{c}_m$ from Eq. (C.7). The expression for the coefficients $\tilde{c}_m$ is messy to write explicitly. We provide the procedure for calculating them.

The procedure start with

$$\begin{aligned}
\Delta u_4 &= \alpha_{g,R}\rho_{g,R} - \alpha_{g,L}\rho_{g,L} \\
\Delta u_5 &= \alpha_{g,R}\rho_{g,R}u_{g,R} - \alpha_{g,L}\rho_{g,L}u_{g,L} \\
\Delta u_6 &= \alpha_{g,R}\rho_{g,R}E_{g,R} - \alpha_{g,L}\rho_{g,L}E_{g,L} \\
\Delta u_{54} &= \Delta u_5 - \big(\tilde{u}_g - \sqrt{\tilde{\beta}_g}\tilde{a}_g\big)\Delta u_4 \\
\Delta u_{64} &= \Delta u_6 - \big(\tilde{H}_g - \sqrt{\tilde{\beta}_g}\tilde{u}_g\tilde{a}_g\big)\Delta u_4
\end{aligned} \tag{C.11}$$

Substituting Eq. (C.11) into Eq. (C.7d), Eq. (C.7e), and Eq. (C.7f) , we get

$$\begin{aligned}
\tilde{c}_5 &= \big(\tilde{\gamma}_g - 1\big)\frac{\tilde{u}_g\Delta u_{54} - \Delta u_{64}}{\tilde{a}_g^2} \\
\tilde{c}_6 &= \frac{\Delta u_{54}}{2\tilde{\beta}_g\tilde{a}_g} - \frac{\tilde{c}_5}{2} \\
\tilde{c}_4 &= \Delta u_4 - \tilde{c}_6 - \tilde{c}_5
\end{aligned} \tag{C.12}$$

Since $\tilde{c}_4$, $\tilde{c}_5$, and $\tilde{c}_6$ are found, we can substitute them back into Eq. (C.7a), Eq. (C.7b), and Eq. (C.7c) to

solve for $\tilde{c}_1$, $\tilde{c}_2$, and $\tilde{c}_3$. Let

$$
\begin{aligned}
\Delta u_1 &= \alpha_{l,R}\rho_{l,R} - \alpha_{l,L}\rho_{l,L} - \tilde{c}_4\tilde{q}_4 - \tilde{c}_6\tilde{q}_6 \\
\Delta u_2 &= \alpha_{l,R}\rho_{l,R}u_{l,R} - \alpha_{l,L}\rho_{l,L}u_{l,L} - \tilde{c}_4\tilde{q}_4\big(\tilde{u}_g - \sqrt{\tilde{\beta}_g}\tilde{a}_g\big) - \tilde{c}_6\tilde{q}_6\big(\tilde{u}_g + \sqrt{\tilde{\beta}_g}\tilde{a}_g\big) \\
\Delta u_3 &= \alpha_{l,R}\rho_{l,R}E_{l,R} - \alpha_{l,L}\rho_{l,L}E_{l,L} - \tilde{c}_4\tilde{q}_4\big[\tilde{H}_l - \tilde{u}_l^2 + \tilde{u}_l\big(\tilde{u}_g - \sqrt{\tilde{\beta}_g}\tilde{a}_g\big)\big] - \tilde{c}_6\tilde{q}_6\big[\tilde{H}_l - \tilde{u}_l^2 + \tilde{u}_l\big(\tilde{u}_g + \sqrt{\tilde{\beta}_g}\tilde{a}_g\big)\big] \\
\Delta u_{21} &= \Delta u_2 - \big(\tilde{u}_l - \sqrt{\tilde{\beta}_l}\tilde{a}_l\big)\Delta u_1 \\
\Delta u_{31} &= \Delta u_3 - \big(\tilde{H}_l - \sqrt{\tilde{\beta}_l}\tilde{u}_l\tilde{a}_l\big)\Delta u_1
\end{aligned}
\tag{C.13}
$$

Substituting Eq. (C.13) to Eq. (C.7a), Eq. (C.7b), and Eq. (C.7c), we get

$$
\begin{aligned}
\tilde{c}_2 &= \big(\tilde{\gamma}_l - 1\big)\frac{\tilde{u}_l\Delta u_{21} - \Delta u_{31}}{\tilde{a}_l^2} \\
\tilde{c}_3 &= \frac{\Delta u_{21}}{2\tilde{\beta}_l\tilde{a}_l} - \frac{\tilde{c}_2}{2} \\
\tilde{c}_1 &= \Delta u_1 - \tilde{c}_3 - \tilde{c}_2
\end{aligned}
\tag{C.14}
$$

Finally, the Roe-type numerical flux is completely specified by Eq. (C.2) using the respective variables given in Eq. (C.9), Eq. (C.12), and Eq. (C.14).

Appendix D

U-W TRANSFORM

Recall that $\mathbf{U}$ is the vector of conservative variables and $\mathbf{W}$ is the vector of primitive/physical variables

$$\mathbf{U} = \begin{pmatrix} \alpha_l\rho_l \\ \alpha_l\rho_l u_l \\ \alpha_l\rho_l E_l \\ \alpha_g\rho_g \\ \alpha_g\rho_g u_g \\ \alpha_g\rho_g E_g \end{pmatrix}, \mathbf{W} = \begin{pmatrix} \alpha_g \\ p \\ T_l \\ T_g \\ u_l \\ u_g \end{pmatrix} \tag{D.1}$$

The small changes in $\mathbf{U}$ and $\mathbf{W}$ are related by

$$\Delta\mathbf{U} = \mathbb{A}_{\mathrm{w}}\Delta\mathbf{W}, \text{ with } \mathbb{A}_{\mathrm{w}} \equiv \frac{\partial\mathbf{U}}{\partial\mathbf{W}} \tag{D.2}$$

The derivation of $\mathbb{A}_{\mathrm{w}}$ matrix is straightforward, which we omit for brevity. Let

$$x_{11} = \left(\frac{\partial\rho_l}{\partial p}\right)_{T_l}, \quad x_{12} = \left(\frac{\partial\rho_l}{\partial T_l}\right)_p \tag{D.3a}$$

$$x_{21} = \left(\frac{\partial\rho_g}{\partial p}\right)_{T_g}, \quad x_{22} = \left(\frac{\partial\rho_g}{\partial T_g}\right)_p \tag{D.3b}$$

$$y_{11} = \left(\frac{\partial e_l}{\partial p}\right)_{T_l}, \quad y_{12} = \left(\frac{\partial e_l}{\partial T_l}\right)_p \tag{D.3c}$$

$$y_{21} = \left(\frac{\partial e_g}{\partial p}\right)_{T_g}, \quad y_{22} = \left(\frac{\partial e_g}{\partial T_g}\right)_p \tag{D.3d}$$

The $\mathbb{A}_{\mathrm{w}}$ matrix is obtained to be

$$\mathbb{A}_{\mathrm{w}} = \begin{pmatrix} -\rho_l & \alpha_l x_{11} & \alpha_l x_{12} & 0 & 0 & 0 \\ -\rho_l u_l & \alpha_l u_l x_{11} & \alpha_l u_l x_{12} & 0 & \alpha_l \rho_l & 0 \\ -\rho_l E_l & \alpha_l (E_l x_{11} + \rho_l y_{11}) & \alpha_l (E_l x_{12} + \rho_l y_{12}) & 0 & \alpha_l \rho_l u_l & 0 \\ \rho_g & \alpha_g x_{21} & 0 & \alpha_g x_{22} & 0 & 0 \\ \rho_g u_g & \alpha_g u_g x_{21} & 0 & \alpha_g u_g x_{22} & 0 & \alpha_g \rho_g \\ \rho_g E_g & \alpha_g (E_g x_{21} + \rho_g y_{21}) & 0 & \alpha_g (E_g x_{22} + \rho_g y_{22}) & 0 & \alpha_g \rho_g u_g \end{pmatrix} \tag{D.4}$$

In practice, the inverse of $\mathbb{A}_{\mathrm{w}}$ is required to obtain $\mathbf{\Delta W}$ with

$$\mathbf{\Delta W} = \mathbb{A}_{\mathrm{w}}^{-1} \mathbf{\Delta U} \tag{D.5}$$

The inverse matrix $\mathbb{A}_{\mathrm{w}}^{-1}$ is found with Mathematica to be

$$\mathbb{A}_{\mathrm{w}}^{-1} = \begin{pmatrix} a_{11} & a_{12} & a_{13} & a_{14} & a_{15} & a_{16} \\ a_{21} & a_{22} & a_{23} & a_{24} & a_{25} & a_{26} \\ a_{31} & a_{32} & a_{33} & a_{34} & a_{35} & a_{36} \\ a_{41} & a_{42} & a_{43} & a_{44} & a_{45} & a_{46} \\ -\frac{u_l}{\alpha_l \rho_l} & \frac{1}{\alpha_l \rho_l} & 0 & 0 & 0 & 0 \\ 0 & 0 & 0 & -\frac{u_g}{\alpha_g \rho_g} & \frac{1}{\alpha_g \rho_g} & 0 \end{pmatrix} \tag{D.6}$$

with

$$
\begin{aligned}
a_{11} &= -\frac{\alpha_g\big[\big(E_l-u_l^2\big)x_{12}+\rho_l y_{12}\big]t_2}{\rho_l C}, a_{12} = -\frac{\alpha_g u_l x_{12} t_2}{\rho_l C}, a_{13} = \frac{\alpha_g x_{12} t_2}{\rho_l C} \\
a_{14} &= \frac{\alpha_l\big[\big(E_g-u_g^2\big)x_{22}+\rho_g y_{22}\big]t_1}{\rho_g C}, a_{15} = \frac{\alpha_l u_g x_{22} t_1}{\rho_g C}, a_{16} = -\frac{\alpha_l x_{22} t_1}{\rho_g C} \\
a_{21} &= -\frac{\rho_g\big[\big(E_l-u_l^2\big)x_{12}+\rho_l y_{12}\big]y_{22}}{\rho_l C}, a_{22} = -\frac{\rho_g u_l x_{12} y_{22}}{\rho_l C}, a_{23} = \frac{\rho_g x_{12} y_{22}}{\rho_l C} \\
a_{24} &= -\frac{\rho_l\big[\big(E_g-u_g^2\big)x_{22}+\rho_g y_{22}\big]y_{12}}{\rho_g C}, a_{25} = -\frac{\rho_l u_g x_{22} y_{12}}{\rho_g C}, a_{26} = \frac{\rho_l x_{22} y_{12}}{\rho_g C} \\
a_{31} &= \frac{\alpha_l\rho_g\big[\big(E_l-u_l^2\big)x_{11}+\rho_l y_{11}\big]y_{22}-\alpha_g\rho_l\big(E_l-u_l^2\big)t_2}{\alpha_l\rho_l C}, a_{32} = \frac{u_l\big(\alpha_l\rho_g x_{11} y_{22}-\alpha_g\rho_l t_2\big)}{\alpha_l\rho_l C} \\
a_{33} &= -\frac{\alpha_l\rho_g x_{11} y_{22}-\alpha_g\rho_l t_2}{\alpha_l\rho_l C} \\
a_{34} &= \frac{\rho_l\big[\big(E_g-u_g^2\big)x_{22}+\rho_g y_{22}\big]y_{11}}{\rho_g C}, a_{35} = \frac{\rho_l u_g x_{22} y_{11}}{\rho_g C}, a_{36} = -\frac{\rho_l x_{22} y_{11}}{\rho_g C} \\
a_{41} &= \frac{\rho_g\big[\big(E_l-u_l^2\big)x_{12}+\rho_l y_{12}\big]y_{21}}{\rho_l C}, a_{42} = \frac{\rho_g u_l x_{12} y_{21}}{\rho_l C}, a_{43} = -\frac{\rho_g x_{12} y_{21}}{\rho_l C} \\
a_{44} &= \frac{\alpha_g\rho_l\big[\big(E_g-u_g^2\big)x_{21}+\rho_g y_{21}\big]y_{12}-\alpha_l\rho_g\big(E_g-u_g^2\big)t_1}{\alpha_g\rho_g C}, a_{45} = \frac{u_g\big(\alpha_g\rho_l x_{21} y_{12}-\alpha_l\rho_g t_1\big)}{\alpha_g\rho_g C} \\
a_{46} &= -\frac{\alpha_g\rho_l x_{21} y_{12}-\alpha_l\rho_g t_1}{\alpha_g\rho_g C}
\end{aligned}
\tag{D.7}
$$

where t_1, t_2, and C are auxiliary variables used for ease of notations. They are defined as

$$
\begin{aligned}
t_1 &= x_{12}y_{11} - x_{11}y_{12} \\
t_2 &= x_{22}y_{21} - x_{21}y_{22} \\
C &= \alpha_l\rho_g t_1 y_{22} + \alpha_g\rho_l t_2 y_{12}
\end{aligned}
\tag{D.8}
$$

Appendix E

COEFFICIENT MATRICES

The coefficient matrix $\mathbb{A}_0$ and its inverse in the adjoint equation is

$$\mathbb{A}_0 \equiv \left(\frac{\partial \mathbf{U}}{\partial \mathbf{W}}\right)^T = \mathbb{A}_{\mathrm{w}}^T \tag{E.1}$$

$$\mathbb{A}_0^{-1} = \left(\mathbb{A}_{\mathrm{w}}^{-1}\right)^T \tag{E.2}$$

where $\mathbb{A}_{\mathrm{w}}$ and $\mathbb{A}_{\mathrm{w}}^{-1}$ are given in **Appendix D**.

The coefficient matrix $\mathbb{A}_1$ in the adjoint equation is

$$\mathbb{A}_1 \equiv \left(\frac{\partial \mathbf{F}}{\partial \mathbf{W}} + \mathbf{P}_{ix}\frac{\partial \alpha_g}{\partial \mathbf{W}}\right)^T = \begin{pmatrix} -\rho_l u_l & -\rho_l u_l^2 - p + p_i & -\rho_l u_l H_l & \rho_g u_g & \rho_g u_g^2 + p - p_i & \rho_g u_g H_g \\ \alpha_l u_l x_{11} & \alpha_l\left(1 + u_l^2 x_{11}\right) & \alpha_l u_l\left(E_l x_{11} + \rho_l y_{11} + 1\right) & \alpha_g u_g x_{21} & \alpha_g\left(1 + u_g^2 x_{21}\right) & \alpha_g u_g\left(E_g x_{21} + \rho_g y_{21} + 1\right) \\ \alpha_l u_l x_{12} & \alpha_l u_l^2 x_{22} & \alpha_l u_l\left(E_l x_{12} + \rho_l y_{12}\right) & 0 & 0 & 0 \\ 0 & 0 & 0 & \alpha_g u_g x_{22} & \alpha_g u_g^2 x_{22} & \alpha_g u_g\left(E_g x_{22} + \rho_g y_{22}\right) \\ \alpha_l \rho_l & 2\alpha_l \rho_l u_l & \alpha_l \rho_l\left(H_l + u_l^2\right) & 0 & 0 & 0 \\ 0 & 0 & 0 & \alpha_g \rho_g & 2\alpha_g \rho_g u_g & \alpha_g \rho_g\left(H_g + u_g^2\right) \end{pmatrix} \tag{E.3}$$

where $x_{11}, x_{12}, x_{21}, x_{22}, y_{11}, y_{12}, y_{21}$, and y_{22} are variables defined in **Appendix D**.

The coefficient matrix $\mathbb{A}_2$ in the adjoint equation is

$$\begin{aligned} \mathbb{A}_2 &\equiv \left(\frac{\partial \mathbf{P}_{ix}}{\partial x}\frac{\partial \alpha_g}{\partial \mathbf{W}} - \frac{\partial \mathbf{P}_{ix}}{\partial \mathbf{W}}\frac{\partial \alpha_g}{\partial x} + \frac{\partial \mathbf{S}}{\partial \mathbf{W}}\right)^T \\ &= \frac{p_i}{p}\begin{pmatrix} 0 & \frac{\partial p}{\partial x} & 0 & 0 & -\frac{\partial p}{\partial x} & 0 \\ 0 & -\frac{\partial \alpha_g}{\partial x} & 0 & 0 & \frac{\partial \alpha_g}{\partial x} & 0 \\ 0 & 0 & 0 & 0 & 0 & 0 \\ 0 & 0 & 0 & 0 & 0 & 0 \\ 0 & 0 & 0 & 0 & 0 & 0 \\ 0 & 0 & 0 & 0 & 0 & 0 \end{pmatrix} + \begin{pmatrix} \frac{\partial S_l^c}{\partial \alpha_g} & \frac{\partial S_l^m}{\partial \alpha_g} & \frac{\partial S_e^c}{\partial \alpha_g} & \frac{\partial S_g^c}{\partial \alpha_g} & \frac{\partial S_g^m}{\partial \alpha_g} & \frac{\partial S_g^e}{\partial \alpha_g} \\ \frac{\partial S_l^c}{\partial p} & \frac{\partial S_l^m}{\partial p} & \frac{\partial S_e^c}{\partial p} & \frac{\partial S_g^c}{\partial p} & \frac{\partial S_g^m}{\partial p} & \frac{\partial S_g^e}{\partial p} \\ \frac{\partial S_l^c}{\partial T_l} & \frac{\partial S_l^m}{\partial T_l} & \frac{\partial S_e^c}{\partial T_l} & \frac{\partial S_g^c}{\partial T_l} & \frac{\partial S_g^m}{\partial T_l} & \frac{\partial S_g^e}{\partial T_l} \\ \frac{\partial S_l^c}{\partial T_g} & \frac{\partial S_l^m}{\partial T_g} & \frac{\partial S_e^c}{\partial T_g} & \frac{\partial S_g^c}{\partial T_g} & \frac{\partial S_g^m}{\partial T_g} & \frac{\partial S_g^e}{\partial T_g} \\ \frac{\partial S_l^c}{\partial u_l} & \frac{\partial S_l^m}{\partial u_l} & \frac{\partial S_e^c}{\partial u_l} & \frac{\partial S_g^c}{\partial u_l} & \frac{\partial S_g^m}{\partial u_l} & \frac{\partial S_g^e}{\partial u_l} \\ \frac{\partial S_l^c}{\partial u_g} & \frac{\partial S_l^m}{\partial u_g} & \frac{\partial S_e^c}{\partial u_g} & \frac{\partial S_g^c}{\partial u_g} & \frac{\partial S_g^m}{\partial u_g} & \frac{\partial S_g^e}{\partial u_g} \end{pmatrix} \end{aligned} \tag{E.4}$$

The functions $B_1(\boldsymbol{\phi})$ to $B_6(\boldsymbol{\phi})$ are

$$
\begin{aligned}
B_1(\boldsymbol{\phi}) &= -\rho_l u_l \phi_1 - \big(\rho_l u_l^2 + p - p_i\big)\phi_2 - \rho_l u_l H_l \phi_3 + \rho_g u_g \phi_4 + \big(\rho_g u_g^2 + p - p_i\big)\phi_5 + \rho_g u_g H_g \phi_6 \\
B_2(\boldsymbol{\phi}) &= \alpha_l u_l x_{11} \phi_1 + \alpha_l \big(1 + u_l^2 x_{11}\big)\phi_2 + \alpha_l u_l \big(E_l x_{11} + \rho_l y_{11} + 1\big)\phi_3 \\
&\quad + \alpha_g u_g x_{21} \phi_4 + \alpha_g \big(1 + u_g^2 x_{21}\big)\phi_5 + \alpha_g u_g \big(E_g x_{21} + \rho_g y_{21} + 1\big)\phi_6 \\
B_3(\boldsymbol{\phi}) &= \alpha_l u_l x_{12} \phi_1 + \alpha_l u_l^2 x_{12} \phi_2 + \alpha_l u_l \big(E_l x_{12} + \rho_l y_{12}\big)\phi_3 \\
B_4(\boldsymbol{\phi}) &= \alpha_g u_g x_{22} \phi_4 + \alpha_g u_g^2 x_{22} \phi_5 + \alpha_g u_g \big(E_g x_{22} + \rho_g y_{22}\big)\phi_6 \\
B_5(\boldsymbol{\phi}) &= \alpha_l \rho_l \phi_1 + 2\alpha_l \rho_l u_l \phi_2 + \alpha_l \rho_l \big(H_l + u_l^2\big)\phi_3 \\
B_6(\boldsymbol{\phi}) &= \alpha_g \rho_g \phi_4 + 2\alpha_g \rho_g u_g \phi_5 + \alpha_g \rho_g \big(H_g + u_g^2\big)\phi_3
\end{aligned}
\tag{E.5}
$$

where $x_{11}, x_{12}, x_{21}, x_{22}, y_{11}, y_{12}, y_{21}$, and y_{22} are variables defined in **Appendix D**.

References

[1] M. Ishii and T. Hibiki, *Thermo-fluid dynamics of two-phase flow*. Springer Science & Business Media, 2010.

[2] A.-L. Shieh, R. Krishnamurthy, and V. Ransom, "Stability, accuracy, and convergence of the numerical methods in relap5/mod3," *Nuclear science and engineering*, vol. 116, no. 4, pp. 227–244, 1994.

[3] D. R. Liles and J. Mahaffy, "Trac-pf1/mod1: an advanced best-estimate computer program for pressurized water reactor thermal-hydraulic analysis," tech. rep., Los Alamos National Lab., NM (USA). Safety Code Development Group, 1986.

[4] S. Bajorek *et al.*, "Trace v5. 0 theory manual, field equations, solution methods and physical models," *United States Nuclear Regulatory Commission*, 2008.

[5] INL, *RELAP5-3D Code Manual Volume I: Code Structure, System Models and Solution Methods*. INL-EXT-98-00834-V1, Revision 4.0, Idaho National Laboratory, 2012.

[6] J. H. Mahaffy, "A stability-enhancing two-step method for fluid flow calculations," *Journal of Computational Physics*, vol. 46, no. 3, pp. 329–341, 1982.

[7] A. S. Rabie Abdullah, *Two-Phase Two-Fluid Model Solver Based on A High-Resolution Total Variation Diminishing Scheme*. PhD thesis, University of Illinois at Urbana-Champaign, 2014.

[8] L. Zou, H. Zhao, and H. Zhang, "Applications of high-resolution spatial discretization scheme and Jacobian-free Newton-Krylov method in two-phase flow problems," *Annals of Nuclear Energy*, vol. 83, pp. 101–107, 2015.

[9] L. Zou, H. Zhao, and H. Zhang, "Application of Jacobian-free Newton-Krylov method in implicitly solving two-fluid six-equation two-phase flow problems: Implementation, validation and benchmark," *Nuclear Engineering and Design*, vol. 300, pp. 268–281, 2016.

[10] W. L. Oberkampf and C. J. Roy, *Verification and validation in scientific computing*. Cambridge University Press, 2010.

[11] A. Saltelli, M. Ratto, T. Andres, F. Campolongo, J. Cariboni, D. Gatelli, M. Saisana, and S. Tarantola, *Global sensitivity analysis: the primer*. John Wiley & Sons, 2008.

[12] X. Wu, *Metamodel-based inverse uncertainty quantification of nuclear reactor simulators under the Bayesian framework*. PhD thesis, University of Illinois at Urbana-Champaign, 2017.

[13] D. G. Cacuci and E. Wacholder, "Adjoint Sensitivity Analysis for Transient Two-Phase Flow," *Nuclear Science and Engineering*, vol. 82, no. 4, pp. 461–468, 1982.

[14] M. Giles and N. Pierce, "On the properties of solutions of the adjoint Euler equations," *Numerical Methods for Fluid Dynamics VI. ICFD*, pp. 1–16, 1998.

[15] W. Wagner and A. Kruse, "The industrial standard iapws-if97 for the thermodynamic properties and supplementary equations for other properties," *Properties of Water and Steam, Springer*, pp. 1–354, 1998.

[16] T. Dinh, R. Nourgaliev, and T. Theofanous, "Understanding the ill-posed two-fluid model," in *Proceedings of the 10th international topical meeting on nuclear reactor thermal-hydraulics (NURETH03)*, 2003.

[17] INL, *RELAP5-3D Code Manual Volume II: Users Guide and Input Requirements.* INL-EXT-98-00834-V2, Revision 4.0, Idaho National Laboratory, 2012.

[18] INL, *RELAP5-3D Code Manual Volume III: Developmental Assessment.* INL-EXT-98-00834-V3, Revision 4.0, Idaho National Laboratory, 2012.

[19] INL, *RELAP5-3D Code Manual Volume IV: Models and Correlations.* INL-EXT-98-00834-V4, Revision 4.0, Idaho National Laboratory, 2012.

[20] R. Lahey, "A mechanistic subcooled boiling model," in *Proceedings of the 6th International Heat Transfer Conference*, vol. 1, pp. 293–297, 1978.

[21] P. Saha and N. Zuber, "Point of net vapor generation and vapor void fraction in subcooled boiling," in *Heat transfer, 1974. Vol. 4*, 1974.

[22] B. Chexal and G. Lellouche, "A full range drift-flux correlation for vertical flows, epri," tech. rep., NP-3989-SR, Revision 1, September 1986, 1985.

[23] D. Groeneveld, S. Cheng, and T. Doan, "1986 aecl-uo critical heat flux lookup table," *Heat Transfer Engineering*, vol. 7, no. 1-2, pp. 46–62, 1986.

[24] W. Greiner, L. Neise, and H. Stöcker, *Thermodynamics and statistical mechanics.* Springer Science & Business Media, 2012.

[25] E. F. Toro, *Riemann solvers and numerical methods for fluid dynamics: a practical introduction.* Springer Science & Business Media, 2013.

[26] H. Pokharna, M. Mori, and V. H. Ransom, "Regularization of Two-Phase Flow Models: A Comparison of Numerical and Differential Approaches," *Journal of Computational Physics*, vol. 134, no. 2, pp. 282–295, 1997.

[27] W. Mathematica, "Wolfram research," *Inc., Champaign, Illinois*, 2009.

[28] J. Stuhmiller, "The influence of interfacial pressure forces on the character of two-phase flow model equations," *International Journal of Multiphase Flow*, vol. 3, no. 6, pp. 551–560, 1977.

[29] D. Bestion, "The physical closure laws in the cathare code," *Nuclear Engineering and Design*, vol. 124, no. 3, pp. 229–245, 1990.

[30] I. Toumi, A. Kumbaro, and H. Paillere, *Approximate Riemann solvers and flux vector splitting schemes for two-phase flow.* CEA Saclay, Direction de l'information scientifique et technique, 1999.

[31] F. Barre and M. Bernard, "The cathare code strategy and assessment," *Nuclear engineering and design*, vol. 124, no. 3, pp. 257–284, 1990.

[32] S. K. Godunov, "A difference method for numerical calculation of discontinuous solutions of the equations of hydrodynamics," *Matematicheskii Sbornik*, vol. 89, no. 3, pp. 271–306, 1959.

[33] P. L. Roe, "Approximate riemann solvers, parameter vectors, and difference schemes," *Journal of computational physics*, vol. 43, no. 2, pp. 357–372, 1981.

[34] B. Van Leer, "Towards the ultimate conservative difference scheme," *Journal of Computational Physics*, vol. 135, no. 2, pp. 229–248, 1997.

[35] S. Osher and F. Solomon, "Upwind difference schemes for hyperbolic systems of conservation laws," *Mathematics of computation*, vol. 38, no. 158, pp. 339–374, 1982.

[36] C.-W. Shu and S. Osher, "Efficient implementation of essentially non-oscillatory shock-capturing schemes," *Journal of Computational Physics*, vol. 77, no. 2, pp. 439–471, 1988.

[37] C.-W. Shu and S. Osher, "Efficient implementation of essentially non-oscillatory shock-capturing schemes, ii," in *Upwind and High-Resolution Schemes*, pp. 328–374, Springer, 1989.

[38] G.-S. Jiang and C.-W. Shu, "Efficient Implementation of Weighted ENO Schemes," *Journal of Computational Physics*, vol. 126, no. 126, pp. 202–228, 1995.

[39] D. S. Balsara and C.-W. Shu, "Monotonicity Preserving Weighted Essentially Non-oscillatory Schemes with Increasingly High Order of Accuracy," *Journal of Computational Physics*, vol. 160, pp. 405–452, 2000.

[40] X. Zhang and C. W. Shu, "Positivity-preserving high order discontinuous Galerkin schemes for compressible Euler equations with source terms," *Journal of Computational Physics*, vol. 230, no. 4, pp. 1238–1248, 2011.

[41] M. T. Henry de Frahan, S. Varadan, and E. Johnsen, "A new limiting procedure for discontinuous Galerkin methods applied to compressible multiphase flows with shocks and interfaces," *Journal of Computational Physics*, vol. 280, pp. 89–509, 2015.

[42] X. Zhong and C. W. Shu, "A simple weighted essentially nonoscillatory limiter for Runge-Kutta discontinuous Galerkin methods," *Journal of Computational Physics*, vol. 232, no. 1, pp. 397–415, 2013.

[43] G.-S. Yeom and K.-S. Chang, "Numerical simulation of two-fluid two-phase flows by hll scheme using an approximate jacobian matrix," *Numerical Heat Transfer, Part B: Fundamentals*, vol. 49, no. 2, pp. 155–177, 2006.

[44] C.-H. Chang and M.-S. Liou, "A new approach to the simulation of compressible multifluid flows with ausm+ scheme," in *16th AIAA Computational Fluid Dynamics Conference*, p. 4107, 2003.

[45] P. Glaister, "An approximate linearised riemann solver for the euler equations for real gases," *Journal of Computational Physics*, vol. 74, no. 2, pp. 382–408, 1988.

[46] A. Harten and S. Osher, "Uniformly high-order accurate nonoscillatory schemes. i," *SIAM Journal on Numerical Analysis*, vol. 24, no. 2, pp. 279–309, 1987.

[47] X.-D. Liu, S. Osher, and T. Chan, "Weighted essentially non-oscillatory schemes," *Journal of computational physics*, vol. 115, no. 1, pp. 200–212, 1994.

[48] S. Tan, C. Wang, C. W. Shu, and J. Ning, "Efficient implementation of high order inverse Lax-Wendroff boundary treatment for conservation laws," *Journal of Computational Physics*, vol. 231, no. 6, pp. 2510–2527, 2012.

[49] J. Lu, J. Fang, S. Tan, C. W. Shu, and M. Zhang, "Inverse Lax-Wendroff procedure for numerical boundary conditions of convection-diffusion equations," *Journal of Computational Physics*, vol. 317, no. 21, pp. 276–300, 2016.

[50] H. Christensen, "Power-to-void transfer functions," tech. rep., Argonne National Lab., Ill., 1961.

[51] M. Giles, "Non-reflecting boundary conditions for the Euler equations," *AIAA Journal*, vol. 28, no. February, pp. 2050–2058, 1990.

[52] J. B. Keller and D. Givoli, "Exact non-reflecting boundary conditions," *Journal of Computational Physics*, vol. 82, no. 1, pp. 172–192, 1989.

[53] A. Jameson, "Aerodynamic design via control theory," *Journal of Scientific Computing*, vol. 3, no. 3, pp. 233–260, 1988.

[54] A. Jameson, "Optimum Aerodynamic Design via Boundary Control," *AGARD-VKI Lecture Series, Optimum Design Methods in Aerodynamics*, 1994.

[55] A. Jameson, L. Martinelli, and N. Pierce, "Optimum Aerodynamic Design Using the Navier-Stokes Equations," *Theoretical and Computational Fluid Dynamics*, vol. 10, no. 1-4, pp. 213–237, 1998.

[56] S. K. Nadarajah and A. Jameson, "A Comparison of the Continuous and Discrete Adjoint Approach To Automatic Aerodynamic Optimization," *Aiaa*, 2000.

[57] M. B. Giles and N. A. Pierce, "An Introduction to the Adjoint Approach to Design," *Flow, Turbulence and Combustion*, vol. 65, no. 3, pp. 393–415, 2000.

[58] M. B. Giles and N. A. Pierce, "Analytic adjoint solutions for the quasi-one-dimensional Euler equations," *Journal of Fluid Mechanics*, vol. 426, pp. 327–345, 2001.

[59] M. B. Giles, M. C. Duta, J.-D. Muller, and N. A. Pierce, "Algorithm Developments for Discrete Adjoint Methods," *AIAA Journal*, vol. 41, no. 2, pp. 198–205, 2003.

[60] D. G. Cacuci and M. Ionescu-Bujor, "Adjoint sensitivity analysis of the RELAP5/MOD3.2 two-fluid thermal-hydraulic code system-I: theory," *Nuclear Science and Engineering*, vol. 136, no. 1, pp. 59–84, 2000.

[61] D. G. Cacuci and M. Ionescu-Bujor, "Adjoint Sensitivity Analysis of the RELAP5 / MOD3 . 2 Two-Fluid Thermal-Hydraulic Code System II : Applications," *Nuclear Science and Engineering*, vol. 136, pp. 85–121, 2000.

[62] A. Petruzzi, *Development and application of methodologies for sensitivity analysis and uncertainty evaluation of the results of the best estimate system codes applied in nuclear technology.* PhD thesis, Universit di Pisa, 2008.

[63] V. A. Mousseau, "Implicitly balanced solution of the two-phase flow equations coupled to nonlinear heat conduction," *Journal of computational physics*, vol. 200, no. 1, pp. 104–132, 2004.

[64] A. Ashrafizadeh, C. Devaud, and N. Aydemir, "A jacobian-free newton–krylov method for thermalhydraulics simulations," *International Journal for Numerical Methods in Fluids*, vol. 77, no. 10, pp. 590–615, 2015.

[65] R. A. Abu Saleem, T. Kozlowski, and R. Shrestha, "A solver for the two-phase two-fluid model based on high-resolution total variation diminishing scheme," *Nuclear Engineering and Design*, vol. 301, pp. 255–263, 2016.

[66] L. Zou, H. Zhao, and H. Zhang, "Implicitly solving phase appearance and disappearance problems using two-fluid six-equation model," *Progress in Nuclear Energy*, vol. 88, pp. 198–210, 2016.

[67] B. Van Leer, "Upwind and high-resolution methods for compressible flow: From donor cell to residual-distribution schemes," *Communications in Computational Physics*, vol. 1, no. 192-206, p. 138, 2006.

[68] M. Y. Hussaini, B. van Leer, and J. Van Rosendale, *Upwind and high-resolution schemes.* Springer Science & Business Media, 2012.

[69] A. Harten, "High resolution schemes for hyperbolic conservation laws," *Journal of Computational Physics*, vol. 49, no. 3, pp. 357–393, 1983.

[70] G. Marchuk, *Adjoint equations and analysis of complex systems.* Springer-Science, 1995.